



HAL
open science

The ultrastrong coupling regime as a resource for the generation of nonclassical states of light

Sergueï Fedortchenko

► **To cite this version:**

Sergueï Fedortchenko. The ultrastrong coupling regime as a resource for the generation of nonclassical states of light. Physics [physics]. Université Sorbonne Paris Cité, 2017. English. NNT : 2017USPCC279 . tel-02178858

HAL Id: tel-02178858

<https://theses.hal.science/tel-02178858>

Submitted on 10 Jul 2019

HAL is a multi-disciplinary open access archive for the deposit and dissemination of scientific research documents, whether they are published or not. The documents may come from teaching and research institutions in France or abroad, or from public or private research centers.

L'archive ouverte pluridisciplinaire **HAL**, est destinée au dépôt et à la diffusion de documents scientifiques de niveau recherche, publiés ou non, émanant des établissements d'enseignement et de recherche français ou étrangers, des laboratoires publics ou privés.

Thèse de Doctorat

Spécialité: Physique Quantique

The ultrastrong coupling regime as a resource
for the generation of nonclassical states of light

Le couplage ultrafort, une ressource pour la
génération d'états non-classiques de la lumière

présentée par

Sergueï Fedortchenko

afin d'obtenir le grade de

Docteur de l'Université Paris Diderot

sous la direction de Pérola Milman et de Thomas Coudreau

Soutenue le 28 septembre 2017

devant le jury composé de

M.	Robin Kaiser	Rapporteur
M.	Enrique Solano	Rapporteur
M.	Mazyar Mirrahimi	Président du jury
M.	Christophe Mora	Examineur
Mme.	Pérola Milman	Directrice de thèse
M.	Thomas Coudreau	Co-directeur de thèse

Abstract

Since the advent of quantum mechanics, the study of light-matter interactions at the quantum level has been greatly developed as a research field. For instance, surprising theoretical predictions gave rise to experiments with unprecedented interaction strengths between matter, and terahertz and microwave radiations. These results correspond to the so-called ultrastrong coupling regime, that is reached when the interaction energy becomes comparable to the typical energies of the light and matter when they are not interacting. In this regime, intriguing properties can be found such as the presence of photons even when no energy is given to the system. However, these photons cannot, a priori, be emitted from the system to the outside world in order to be measured and therefore demonstrate these properties.

In this thesis, we studied these intriguing properties and proposed several means to access them experimentally. We relied on several physical platforms which are good candidates for such studies, and for each one of these systems we devised a model that can evidence these properties one way or another. By doing so, we explored the link between the ultrastrong coupling regime and the generation of nonclassical states of light. Additionally, as an outlook we showed that the light-matter interactions in one of these platforms could be used to design quantum communication protocols. On top of showing fundamental interest, our results fit in the line of developing applications for quantum technologies using different experimentally available systems.

key words: light-matter interactions, ultrastrong coupling regime, nonclassical states of light, squeezed states of light, quantum entanglement, quantum communication, intersubbands devices, superconducting circuits, optomechanics

Résumé

Depuis l'avènement de la mécanique quantique, l'étude des interactions lumière-matière à l'échelle quantique s'est énormément développée en tant que domaine de recherche. Par exemple, grâce à des prédictions théoriques surprenantes, des interactions d'une force sans précédent ont été démontrées entre de la matière et des radiations terahertz et microonde. Ces résultats correspondent à un régime dit de couplage ultrafort, atteint lorsque l'énergie d'interaction devient comparable aux énergies propres de la lumière et de la matière lorsque celles-ci n'interagissent pas. Dans ce régime, des propriétés intrigantes peuvent subsister telles que la présence de photons même lorsqu'aucune énergie n'est fournie au système. Cependant, ces photons ne peuvent, a priori, être émis du système vers l'extérieur de manière à pouvoir être mesurés et par conséquent démontrer ces propriétés.

Dans cette thèse, nous avons étudié ces propriétés intrigantes et proposé plusieurs moyens permettant d'y accéder expérimentalement. Nous nous sommes appuyés sur plusieurs plate-formes physiques qui sont de bon candidats pour ces études, et pour chacun de ces systèmes nous avons mis au point un modèle mettant en évidence ces propriétés d'une manière ou d'une autre. De cette façon, nous avons exploré le lien entre le régime de couplage ultrafort et la génération d'états non-classiques de la lumière. En outre, dans une étude plus ouverte nous avons montré que les interactions lumière-matière dans l'une de ces plate-formes peuvent être utilisées pour concevoir des protocoles de communication quantique. En plus de montrer un intérêt fondamental, nos résultats s'inscrivent dans une optique de développement d'applications pour les technologies quantiques en utilisant différents systèmes expérimentaux disponibles actuellement.

mots clefs: interactions lumière-matière, régime de couplage ultrafort, états non-classiques de la lumière, états comprimés de la lumière, intrication quantique, communication quantique, dispositifs intersousbandes, circuits supraconducteurs, optomécanique

Résumé substantiel

Dans cette thèse nous avons souhaité explorer plusieurs facettes des interactions lumière-matière dans le régime de couplage ultrafort entre deux champs bosoniques, en étudiant la manière dont ce régime est relié à des états non-classiques de la lumière, en particulier à des états comprimés, et s'il est possible d'une manière ou d'une autre d'extraire des propriétés de l'état fondamental de ce régime. Premièrement, nous avons conçu un modèle dans lequel un nouveau type de couplage ultrafort est introduit, appelé *régime de couplage ultrafort dispersif*. Principalement, nous avons introduit de nouveaux ingrédients qui modifient le régime de couplage ultrafort déjà connu et atteint expérimentalement dans des matériaux semi-conducteurs confinés dans des cavités résonantes dans les fréquences terahertz ou dans le moyen-infrarouge, qui ont été les premiers systèmes à démontrer des telles forces de couplage [Günter09, Todorov09, Anappara09]. Nous avons exploré une situation où le couplage lumière-matière est dépendent du temps, prouvé d'être requis pour permettre d'extraire des particules d'un système non pompé [De Liberato07]. Avec ces outils, nous avons montré qu'il était possible pour la cavité d'émettre des photons dans un état comprimé [Fedortchenko16], même si le Hamiltonien du système ne contient pas d'interaction de compression pour un mode bosonique. Nous avons continué d'examiner la génération d'états comprimés à l'aide du régime de couplage ultrafort, en proposant un modèle basé sur une autre plate-forme physique constituée de circuits supraconducteurs, une technologie qui a rapidement progressé ces dernières années jusqu'à devenir l'un des candidats les plus prometteurs pour l'étude des interactions lumière-matière à l'échelle quantique [Schoelkopf08], l'optique quantique pour des gammes de fréquences alternatives [You11], la simulation quantique [Houck12], ou encore l'information [Devoret13] et le calcul [Ladd10] quantique. En utilisant la versatilité de ces systèmes et leur haut degré de contrôle, nous avons conçu un modèle où le régime de couplage ultrafort peut être simulé entre deux résonateurs microonde. La nature particulière de l'interaction physique dans ce système le rend semblable à une interaction ultraforte standard, mais dans un référentiel bien particulier. De plus, les prédictions de ce modèle prévoient l'émission d'une radiation comprimée. Cependant, ici les deux résonateurs microonde émettent des photons au même moment, ce qui permet d'étudier les corrélations quantiques entre eux. Ces corrélations ont été démontrées comme étant de même nature que les corrélations présentes dans l'état fondamental d'une interaction ultraforte bosonique [Fedortchenko17]. Ainsi, nous avons conçu une plate-forme basée sur une technologie actuelle permettant d'explorer expérimentalement la nature de l'état fondamental d'un tel régime. De plus, nous avons obtenu des résultats préliminaires dans un modèle que nous avons basé sur une interaction optomécanique [Aspelmeyer14]. Ces résultats montrent qu'il est possible dans ce modèle de générer des états quantiques de la lumière ayant les mêmes corrélations quantiques et les mêmes caractéristiques spectrales que dans la simulation quantique du couplage ultrafort que nous avons évoqué précédemment. Cela montre que ce modèle optomécanique, même s'il possède un Hamiltonien très différent comparé au Hamiltonien d'un régime de couplage ultrafort, est d'une certaine manière lié à ce régime et mérite une étude plus approfondie. En outre, nous avons utilisé cette interaction optomécanique pour explorer des phénomènes au-delà du cadre initial de cette thèse, en montrant qu'en

plus d'être lié au régime de couplage ultrafort, ce modèle peut être aussi un bon candidat pour l'établissement d'un réseau de communication quantique, une étape cruciale pour un but à long terme, la mise en place de *l'Internet quantique* [Pirandola16]. En particulier, nous avons montré comment effectuer deux protocoles de communication quantique entre deux parties, où chaque partie est constituée d'un dispositif optomécanique correspondant à notre modèle [Felicetti17a].

Le plan de ce manuscrit se décrit comme suit. Dans le chapitre I nous présentons les concepts de base ainsi que les outils nécessaires pour la compréhension des résultats de cette thèse présentés plus loin. Nous commençons par une brève vue d'ensemble des différents régimes d'interaction lumière-matière. Ensuite, nous nous concentrons sur les états quantiques de la lumière en présentant leur description dans l'espace des phases, suivie par une introduction de certains de ces états, avec des efforts plus marqués sur la description des états comprimés.

Dans le chapitre II, nous présentons nos résultats sur la génération d'états comprimés à un mode en utilisant le régime de couplage ultrafort dispersif. Nous commençons par introduire la plate-forme physique sur laquelle se base notre modèle, consistant d'un puits quantique semi-conducteur confiné dans une cavité terahertz ou moyen-infrarouge. Nous montrons brièvement comment le Hamiltonien initial fermionique peut être réécrit en termes d'opérateurs bosoniques seulement, puis nous utilisons cette forme bosonique du Hamiltonien pour introduire notre modèle spécifique. Nous montrons comment dans notre modèle un effet rappelant l'effet Casimir dynamique [Moore70, Kardar99] est à l'origine de la génération de photons comprimés.

Dans le chapitre III, nous présentons notre simulation quantique du régime de couplage ultrafort avec des circuits supraconducteurs. Nous commençons par brièvement introduire les circuits supraconducteurs et l'interaction physique dans un dispositif appelé mixer de Josephson, utilisé dans notre simulation quantique. Nous présentons ensuite notre modèle, en montrant comment en partant du Hamiltonien physique dans le référentiel du laboratoire nous pouvons obtenir un Hamiltonien effectif dans un référentiel tournant ayant la même forme que le Hamiltonien du régime de couplage ultrafort standard.

Dans le chapitre IV, nous présentons nos résultats sur notre modèle basé sur un système optomécanique. Après une introduction de l'interaction optomécanique décrite dans la théorie quantique, nous présentons notre modèle constitué d'un interféromètre, avec ces avantages en comparaison avec un système optomécanique standard. Puis, nous exposons des résultats préliminaires sur le lien entre notre modèle et la simulation quantique du couplage ultrafort abordée dans le chapitre III. Enfin, nous montrons comment le modèle développé dans ce chapitre peut être utilisé en tant que nœud d'un réseau quantique. En particulier, nous montrons comment il est possible d'implémenter deux protocoles de communication quantique entre deux de ces nœuds et évaluons leur succès.

Finalement, une conclusion générale présente quelques remarques finales ainsi que des perspectives.

Remerciements

C'est à présent le bon moment pour remercier les personnes que j'ai pu côtoyer pendant ces trois années de thèse et qui ont pu contribuer de prêt ou de loin à l'aboutissement de mon doctorat.

J'aimerais tout d'abord remercier les membres de mon jury, qui ont accepté la tâche de lire mon manuscrit, de m'écouter pendant ma soutenance de thèse et enfin de m'avoir attribué le grade de docteur de l'Université Paris Diderot. Merci à Christophe Mora, merci à Mazyar Mirrahimi pour avoir également accepté d'être le président du jury, et merci à Robin Kaiser et Enrique Solano pour avoir également accepté d'être les rapporteurs de mon manuscrit.

Merci à toi Pérola d'avoir été ma directrice de thèse pendant ces trois ans, d'avoir toujours été disponible pour discuter et me guider. Dans les moments difficiles de cette thèse, ta capacité à toujours rebondir sur de nouvelles idées m'ont très souvent remonté le moral pendant nos sessions de brainstorming ! Merci également à Thomas et Arne, que j'ai toujours vu comme mes co-encadrants pendant mon doctorat, vous m'avez également beaucoup apporté pendant mon temps au labo. A vous trois, je pense que vous vous complétez extrêmement bien pour encadrer des étudiants, vous formez un trio de choc !

Il est maintenant temps de dire quelques mots sur l'équipe. Je me souviens encore de ce début de mois d'octobre 2013 où j'ai pu rencontrer toute l'équipe au cours de l'une des premières réunions de press review d'Andreas (je n'avais pas compris grand chose, et dans mon souvenir Andreas non plus ;)). Merci à Andreas et Tom, les doyens de l'équipe en ce qui concerne les thésards. C'est en partie grâce au toi Tom que j'ai voulu faire un stage dans l'équipe, car le jour où j'ai visité le labo en tant que jeune étudiant de M2, c'était toi qui m'avais expliqué les qualités de Pérola, de Thomas et de Arne. Andreas, effectivement on était loin d'être d'accord sur pas mal de films, mais nous avons pu avoir des débats très sympa ! ;) Merci à toi Adrien, arrivé en même temps que moi dans l'équipe, nous avons pu affronter les difficultés d'une thèse en parallèle. Je te souhaite de t'épanouir dans le machine learning ! Merci à toute la partie brésilienne de l'équipe, c'est à dire Alexandre, Cleidson, Mariana, Romeu (dommage de ne pas avoir eu le temps d'organiser ce paintball finalement ;)) et bien sûr Saulo, qui est longtemps resté le seul représentant brésilien avec Pérola ! Merci à toi Jean-François et tes good vibes venues tout droit de Belgique, merci à toi Aurianne et ta bonne humeur, merci à toi Guillaume arrivé dans l'équipe puis parti puis revenu (un peu comme un quantum walk ?), et merci à toi Ibrahim (souvent en retard, comme moi ;)), je te souhaite tout le meilleur pour la suite ! Merci à toi Simone pour ta disponibilité et ta rigueur scientifique, cela à été un vrai plaisir de travailler avec toi (j'ai encore toutes les photos du tableau blanc de la cafet, rempli d'équations suite à une de nos séances de brainstorming et de calculs ;)). Merci à toi Louis et pour ces discussions sur des sujets de la plus haute importance comme Doctor Who ou encore Game of Thrones ! Merci également et la plus jeune génération de l'équipe, à Sébastien qui maintenant vis la belle vie en Suisse, à Gaël le militant, à Nicolas et à Peregrine. Et merci bien sûr à toutes les autres personnes du labo que j'ai pu oublier !

Laissez-moi également remercier les autres personnes avec qui j'ai eu la chance de

collaborer pendant cette thèse. Merci à Simon, à Angela, à Cristiano, à Yanko, à Carlo, mais également merci à Sara et à Ivan, et bien sûr merci à Danijela, à Sébastien et à Benjamin !

Enfin, merci à ma famille et à mes amis, et surtout merci à toi Déborah de m'avoir soutenu au quotidien pendant cette thèse !

Contents

General Introduction	15
I Light-matter interactions and quantum states of light	19
I.1 Light-matter interactions	19
I.1.1 From the photoelectric effect to cavity quantum electrodynamics	19
I.1.2 A simple light-matter coupling	20
I.1.2.1 The Hamiltonian	20
I.1.2.2 The rotating wave approximation	21
I.1.2.3 Beyond cavity quantum electrodynamics	22
I.1.3 The weak coupling limit	23
I.1.4 The strong coupling regime	24
I.1.5 The ultrastrong coupling regime	26
I.1.6 The deep strong coupling regime	28
I.2 Quantum states of light	30
I.2.1 From the birth of a revolutionary description of light to modern quantum optics	30
I.2.2 Phase space description of light	31
I.2.3 Coherent states, or the essential basis for describing light in phase-space	32
I.2.4 Introducing the quasiprobability distributions	34
I.2.5 The Glauber-Sudarshan P representation	35
I.2.6 The Husimi- Q representation and heterodyne detection	36
I.2.7 The Wigner representation and homodyne detection	39
I.2.8 Thermal states	41
I.2.9 Squeezed states	41
I.2.9.1 Single-mode squeezed states	42
I.2.9.2 Two-mode squeezed states	45
I.2.10 Some examples of other nonclassical states	49
I.3 Conclusion	50
II Dispersive ultrastrong coupling regime in intersubband devices	53
II.1 Many-body properties of intersubband devices	53
II.2 General light-matter Hamiltonian in the Power-Zinai-Wooley representation	55
II.3 From a fermionic to a bosonic description of electronic excitations	56
II.4 Simplified Hamiltonian in the Power-Zinai-Wooley representation	56
II.5 Renormalization of the many-body excitation frequencies: the intersubband plasmons	57

II.6	Two-level quantum well	58
II.6.1	The need for a time-modulated coupling	58
II.6.2	Model of a dispersive ultrastrong coupling regime	59
II.6.3	Noise spectra	61
II.6.4	Influence of the temperature	63
II.6.5	Influence of the modulation frequency	63
II.7	Three-level quantum well	65
II.7.1	An additional diagonalization	65
II.7.2	Dispersive USC with multisubband plasmons	67
II.7.3	Noise spectra	67
II.7.4	Influence of the temperature	68
II.7.5	Influence of the modulation frequency	69
II.8	Experimental implementation	69
II.9	Conclusion	70
III	Quantum simulated ultrastrong coupling regime in superconducting circuits	71
III.1	Superconducting circuits as tools for quantum information and quantum optics	71
III.1.1	The Josephson junction	72
III.1.2	The quantum LC circuit	72
III.1.3	The Josephson ring modulator	73
III.2	Basics of a quantum simulation	74
III.3	Modeling a quantum simulation in a Josephson mixer	75
III.3.1	Motivation for a quantum simulation of the USC regime	75
III.3.2	The model	76
III.4	Results	77
III.4.1	Noise spectra	78
III.4.2	Influence of the red pump intensity	81
III.4.3	Influence of the red pump frequency	82
III.5	Link with the USC ground state correlations	83
III.5.1	Ground state squeezing	84
III.5.2	Discussion	85
III.6	Comments on the experimental implementation	86
III.7	Conclusion	88
IV	Light-matter interactions and quantum communications in optomechanics	89
IV.1	Introduction to quantum optomechanics	89
IV.1.1	Old and recent achievements	89
IV.1.2	Modeling the quantum optomechanical interaction	91
IV.2	Interferometric model with a double-sided moving mirror	92
IV.3	Results in the continuous regime	94
IV.3.1	Validity of the effective Hamiltonian	94
IV.3.2	Squeezing generation	95
IV.3.3	Comparison with the quantum simulation of the USC regime	97
IV.3.4	Stability in the continuous regime	99
IV.4	Results in the pulsed regime	100
IV.4.1	State swap	101

IV.4.2 EPR state generation	101
IV.4.3 Protocols	103
IV.4.3.1 Teleportation	104
IV.4.3.2 Implementation in physical systems	104
IV.4.3.3 Remote state transfer	107
IV.4.4 Implementation in physical systems	109
IV.5 Conclusion	109
General conclusion	111
A Deriving the equations of motion with input-output theory	113
B Evaluating the output squeezing from a degenerate optical parametric oscillator with input-output theory	117
C Evaluating the output two-squeezing and logarithmic negativity from a non-degenerate optical parametric oscillator with input-output theory	121
D Evaluating the output squeezing in the dispersive ultrastrong coupling regime	125
E Derivation of the effective Hamiltonian	127
F Validity of the diagonalization	129
G Derivation of the system's Hamiltonian and coupling to the baths	131
H Teleportation between two distant mechanical resonators	133
H.0.1 EPR state generation	133
H.0.2 State-swap, or beam splitter-type interaction	136
H.0.3 Measurement and classical channel	138
I Remote quantum state transfer between two distant mechanical resonators	141
Bibliography	143

General Introduction

Among the many contributions brought to physics by the advent of the quantum theory, the new tools it gave for the study and understanding of light-matter interactions at a microscopic level is outstanding. Before the quantum theory, examples of phenomena involving microscopic bodies and evidenced as consequences of light and matter occupying the same space and interacting were not many. For systems at macroscopic scales, a particularly important example of light-matter interactions is worth mentioning, as it plays a crucial role in this manuscript. Demonstrated early in the twentieth century [Lebedew01, Nichols01], it is the fact that when light is shined on an object made of matter, this light could exercise a force on the matter coming from a pressure, called the *radiation pressure*. The consequence of this remarkable result nowadays is the rapid development of a research field called quantum optomechanics that explores fundamental as well as practical topics due to this interaction.

Going back to the twentieth century, a crucial result is the understanding of the photoelectric effect [Einstein05] (for a translation in English, see [Arons65]), as the first illustration of the particle character of light. This article laid the foundations leading to a proper definition of the quantum theory. Rapidly after its advent, quantum physics could be used to bring a whole new description of light, with the definition of a theory describing its quantization [Dirac27, Fermi32]. Later, great effort was devoted to a better description of the quantum states of light [Glauber63a, Glauber63b, Glauber63c]. The characterization of the possible states of light allowed to better understand in what ways some states are nonclassical. One instance of such states is of particular interest for this thesis, namely states that allow to reduce the uncertainty on the number of photons present in the state below this uncertainty for vacuum. First presented as a theoretical object, these states, called squeezed states [Gardiner04, Walls08], were successfully experimentally produced over the last thirty years with photons in a variety of frequency ranges [Slusher85, Shelby86, Wu86, Yurke88, Castellanos-Beltran08, Mallet11].

Another type of quantum states relevant for this manuscript comes from a notion introduced in the early days of the quantum theory. It concerns a particular kind of influence between two systems that is only possible in the realm of quantum physics, also called "spooky action at a distance" at the time [Einstein35a]. This phenomenon, called *entanglement*, was intensely studied in the years that followed, and is still a topic of great theoretical and experimental interest nowadays. Similarly as for the squeezed states mentioned above, entangled states were experimentally achieved with many different systems in the last three decades. For instance, entanglement between photons, that can be seen as a form of squeezing, was successfully demonstrated in many experiments [Silberhorn01, Bowen02, Josse04, Eichler11, Flurin12]. However, this type of entanglement is not the only one to be experimentally explored, since entanglement between light and matter was already tackled since few decades [Raimond01].

In fact, entangling light and matter is the harvest of many years in studying light

and matter interaction. Indeed, in the fifties the development of optical pumping [Kastler50] was crucial for the creation of both the maser [Gordon54, Gordon55] and the laser [Schawlow58, Maiman60]. This led to the development of cavity quantum electrodynamics in the seventies and the eighties (cavity QED) [Goy83, Heinzen87], which deeply explored different regimes of light-matter interactions.

In addition to the so-called weak coupling and strong coupling regimes tackled in cavity QED in the last thirty years, another regime is the focus of this thesis, called the ultrastrong coupling (USC) regime. Theoretically predicted much more recently than the other two [Ciuti05], this regime pushes further the interaction between light and matter, such that even in the ground state, the system is predicted to contain virtual particles, that share entanglement. This ground state being fundamentally different from the one in the weak or the strong coupling regimes, it has been the subject of studies proposing to experimentally demonstrate its properties [Lolli15, Peropadre13a, Cirio16]. However, although some features of the USC regime have been demonstrated in different physical platforms and for different frequency ranges for light [Günter09, Todorov09, Anappara09, Niemczyk10, Forn-Díaz10], its peculiar ground state nature was not one of them.

In this thesis, we wished to explore various facets of light-matter interactions in the USC regime between two bosonic fields, by studying how this regime is related to nonclassical states of light, in particular to squeezed states, and whether it is possible to somehow extract the ground state properties of this regime. First, we designed a model where a novel type of USC interaction is introduced, called the *dispersive USC regime*. Essentially, we introduced new ingredients which slightly modified the USC regime already achieved in semiconductors confined in terahertz or mid-infrared cavities, which were the first ones to achieve such coupling strength [Günter09, Todorov09, Anappara09]. We explored a situation where the light-matter coupling is time-dependent, already proven to be a prerequisite for extracting particles from a non-driven system [De Liberato07]. With these tools, we showed that it is possible for the cavity mode to emit squeezed photons [Fedortchenko16], even if the Hamiltonian for the system does not contain a single-mode squeezing interaction. We continued to investigate the generation of squeezed states with the USC regime by proposing a model based on another physical platform this time made of superconducting circuits, a technology that rapidly matured during the last two decades and even became one of the most promising candidates for studying light-matter interactions at the quantum level [Schoelkopf08], quantum optics at alternative frequency ranges [You11], quantum simulation [Houck12], or quantum information [Devoret13] and quantum computing [Ladd10]. Using the versatility of these systems and their high degree of control, we designed a model where the USC regime could be simulated between two microwave resonators. The particular nature of the physical interaction in the system we used makes it look like a standard USC interaction in a particular referential frame, and additionally, the system is also predicted to emit a squeezed radiation. However, here both microwave resonators emit photons at the same time, which allow us to study the correlations between them. These correlations were found to be of the same nature than the ones present in the ground state of a bosonic USC interaction [Fedortchenko17]. Thus, we designed a platform using current technology that allow to experimentally explore the nature of the ground state of such a regime. Additionally, we obtained preliminary

results in a model we designed based on optomechanical interactions [Aspelmeyer14]. These results showed that it is possible in this model to generate quantum states of photons that have the same type of quantum correlations and the same spectral features as in the quantum simulation we studied with superconducting circuits. This shows that this optomechanical model, although with a very different Hamiltonian than in the USC regime, is somehow connected to this regime and deserves a deeper study. As an outlook, we used this optomechanical interaction to explore phenomena beyond the initial scope of this thesis, by showing that is not only linked to the USC regime, but that it can also be a good candidate for building a quantum communication network, which is a crucial step in the long standing goal called *quantum Internet* [Pirandola16]. In particular, we showed how to perform two quantum communication protocols between two parties where each one is made of the optomechanical device we designed [Felicetti17a].

The outline of this thesis is the following. In chapter I, we present the basic concepts and tools crucial for the understanding of our results presented later. We begin with a brief overview of the different kinds of light-matter interactions. Then, we focus on quantum states of light by presenting their description in phase-space, followed by an introduction of some of these states, distinctly focusing our efforts on squeezed states.

In chapter II, we present our results regarding the generation of single-mode squeezing using the dispersive USC regime. We first introduce the experimental platform on which we based our model, which consists of a semiconductor quantum well confined in a terahertz or mid-infrared cavity. We briefly show how the initial fermionic Hamiltonian can be rewritten in terms of bosonic operators only, and we then use this bosonic form to introduce our specific model. We show how in our model an effect reminiscent of the dynamical Casimir effect [Moore70, Kardar99] is at the origin of the generation of squeezed photons.

In chapter III, we present our quantum simulation of the USC regime with superconducting circuits. We start by briefly introducing superconducting circuits and the physical interaction in the so-called Josephson mixer, that we use in the quantum simulation. We then present our model, by showing how from the physical Hamiltonian of the system in the laboratory frame we can derive an effective Hamiltonian in a rotating frame that has the same form as the Hamiltonian in the USC regime. We show how the quantum simulation results in an emission of a two-mode radiation which shows the same type of properties as in the ground state of the USC regime.

In chapter IV, we present our results based on our model in an optomechanical platform. After an introduction of an optomechanical interaction described in quantum theory, we present our interferometric model and its advantages with respect to a common optomechanical set-up. Then, we show preliminary results on the link between this model and a quantum simulation of the USC regime. Afterwards, we show how this model can be used as a node in a quantum network. In particular, we show how to implement two quantum communication protocols between such two nodes and benchmark their success.

Finally, a general conclusion includes some final remarks and perspectives.

I Light-matter interactions and quantum states of light

The goal of this chapter is to present the basic concepts and tools used throughout the manuscript, with occasional references to indicative, but not exhaustive material from the literature. We do not yet present the original results found during this thesis, that will be extensively developed in the next chapters, but rather focus on the essential theoretical background needed to apprehend these results. The prerequisites for the present chapter are an understanding of the basics of quantum mechanics [Cohen-Tannoudji77], a grasp of both the quantization of the electromagnetic field [Dirac27, Fermi32, Scully97] and of the second quantization in general [Negele98], namely, being accustomed to the use of annihilation and creation operators to describe both light and matter particles. First, we review the different regimes of light-matter interactions that can be achieved in a laboratory. Second, although both concepts are linked, we will independently introduce quantum states of light of interest for this thesis, their theoretical description, and have a glimpse at the possible applications for such states.

I.1 Light-matter interactions

I.1.1 From the photoelectric effect to cavity quantum electrodynamics

The fact that light could in some way influence the behavior of matter, or vice versa, due to quantum effects, is a more than one hundred years old idea. Even before the proper definition of a quantum theory, the particle character of light, and the consequences of its interaction with electrons from the surface of a solid have been predicted [Einstein05] (for a translation in English, see [Arons65]). After additional theoretical progress, such as the discovery of stimulated emission [Einstein16, Einstein17] (for a translation in English, see [Einstein97]), later in the century, important advances of artificial control of atoms in their quantum levels were made, such as optical pumping [Kastler50], or the creation of both the maser [Gordon54, Gordon55] and the laser [Schawlow58, Maiman60]. These selected breakthroughs, among others not shown here for the sake of succinctness, laid the foundations of cavity quantum electrodynamics (or cavity QED) [Goy83, Heinzen87], a field that aims at studying the interaction of atoms with a radiation field confined inside a cavity. Although the study of light-matter interactions naturally occurring in our world, such as the first example evoked here, is a fascinating topic, in the rest of the thesis we shall focus on interactions achieved artificially with the light confined in cavity modes.

Cavity QED can be seen as the precursor of recent subfields that study light-matter interactions in different physical systems, yet with the observation of analog phenomena. These recent subfields cover quantum wells in microcavities [Weisbuch92, Rapaport00], circuits quantum electrodynamics [Blais04, Chiorescu04, Wallraff04], and to some extent

cavity quantum optomechanics [Fabre94, Aspelmeyer14]. These topics are to be tackled in the next Chapters, and here we wish to use the framework of cavity QED as an illustration board for concepts and phenomena that will be needed later.

1.1.2 A simple light-matter coupling

1.1.2.1 The Hamiltonian

In order to illustrate the quantum description of light-matter interactions, let us briefly present the most basic coupling that can occur between a two-level atom and a cavity mode. The atom's accessible quantum states are $|g\rangle$, the ground state, and $|e\rangle$, an excited state, forming its Hilbert space. Essentially, in cavity QED such an interaction is of electric-dipole nature, with the form $-\hat{\mathbf{D}} \cdot \hat{\mathbf{E}}$.¹ $\hat{\mathbf{D}} = q\hat{\mathbf{R}}$ is the atomic dipole operator associated with the transition between the two states $|g\rangle$ and $|e\rangle$, and although it is written in the same form as the classical electric dipole moment where the charge q multiplies a displacement vector pointing from the negative to the positive charge, here $\hat{\mathbf{R}}$ is a quantum operator. Another way to express $\hat{\mathbf{D}}$ and to see that it acts as a transition between the two levels is the following form

$$\hat{\mathbf{D}} = q(\langle g|\hat{\mathbf{R}}|e\rangle |g\rangle\langle e| + \langle e|\hat{\mathbf{R}}|g\rangle |e\rangle\langle g|), \quad (\text{I.1})$$

where the operators $|e\rangle\langle g|$ and $|g\rangle\langle e|$ represent such transitions. $\hat{\mathbf{E}}$ is an electric field coupled to the two-level system, and assuming that only one mode interacts with the atom, we have

$$\hat{\mathbf{E}} = i\mathcal{E}(\boldsymbol{\epsilon}_a^* \hat{a} - \boldsymbol{\epsilon}_a \hat{a}^\dagger), \quad (\text{I.2})$$

where \mathcal{E} is a normalization factor and $\boldsymbol{\epsilon}$ is the polarization vector of the field. Note that no spatial dependence of the field mode appears here, since $\hat{\mathbf{E}} = \hat{\mathbf{E}}_{\text{tot}}(\mathbf{0})$ is the field at $\mathbf{r} = \mathbf{0}$. This comes from the fact that the interaction $-\hat{\mathbf{D}} \cdot \hat{\mathbf{E}}$ we study here is only valid in the electric-dipole approximation. In fact, $-\hat{\mathbf{D}} \cdot \hat{\mathbf{E}}_{\text{tot}}(\mathbf{0})$ is derived from the expression of the modified kinetic energy operator of the atomic charge q , due to its interaction with a radiation field, written as $(\hat{\mathbf{P}} - q\hat{\mathbf{A}}(\hat{\mathbf{R}}))^2/2m$ (no additional term is present when the magnetic interaction can be neglected and the total Hamiltonian is written in the Coulomb gauge), where $\hat{\mathbf{P}}$ is the momentum of the charge and $\hat{\mathbf{A}}(\hat{\mathbf{R}})$ is the vector potential of the field at the position described by the operator $\hat{\mathbf{R}}$. Using such an approximation means that the characteristic size of the atom is much smaller than the wavelength of the electromagnetic field, a very common and widely used approximation.²

Now we can write the Hamiltonian of the system,

$$\hat{H} = \omega_a \hat{a}^\dagger \hat{a} + \omega_{eg} |e\rangle\langle e| + (d^* \boldsymbol{\epsilon}_d^* |g\rangle\langle e| + d \boldsymbol{\epsilon}_d |e\rangle\langle g|) (i\mathcal{E} \boldsymbol{\epsilon}_a^* \hat{a} - i\mathcal{E} \boldsymbol{\epsilon}_a \hat{a}^\dagger), \quad (\text{I.3})$$

where we introduced d as the dipole matrix element of the atomic transition and $\boldsymbol{\epsilon}_d$ as the unit vector describing the atomic transition polarization, with $q\langle e|\hat{\mathbf{R}}|g\rangle = d\boldsymbol{\epsilon}_d$.

¹Note that here and in the rest of the manuscript, a symbol with a hat describes a quantum operator, while a symbol written in bold stands for a vector. Accordingly, in the case of $\hat{\mathbf{D}}$ and $\hat{\mathbf{E}}$, they are both.

²For more details on the electric-dipole approximation, see [Haroche06].

Eq. (I.3) can be written in a more practical form

$$\hat{H} = \hbar\omega_a \hat{a}^\dagger \hat{a} + \hbar\omega_{eg} \sigma_+ \sigma_- + i\hbar G (\sigma_- + \sigma_+) (\hat{a} - \hat{a}^\dagger), \quad (\text{I.4})$$

where

$$G = -\frac{\mathcal{E}d\epsilon_d \cdot \epsilon_a^*}{\hbar} \quad (\text{I.5})$$

is the Rabi frequency [Haroche06] introduced in Eq. (I.4) by assuming that G is real, without loss of generality. In this new expression of the Hamiltonian, we also introduced the ladder operators $\sigma_+ = |e\rangle\langle g| = (\sigma_-)^\dagger$ and $\sigma_- = |g\rangle\langle e| = (\sigma_+)^\dagger$, defined from the Pauli matrices [Pauli27]

$$\sigma_x = |g\rangle\langle e| + |e\rangle\langle g|, \quad (\text{I.6})$$

$$\sigma_y = i|g\rangle\langle e| - i|e\rangle\langle g|, \quad (\text{I.7})$$

$$\sigma_z = |e\rangle\langle e| - |g\rangle\langle g|. \quad (\text{I.8})$$

These matrices are very useful for the description of two level systems such as spins 1/2, or qubits.³

Note that here we established the zero of energy at the ground state, such that in the Hamiltonian (I.4), the energy of the excited state $|e\rangle$ is $\hbar\omega_{eq} = \hbar(\omega_e - \omega_g)$, the difference between the true energies of the states. An alternative choice commonly used in the literature is the zero of energy being in the middle of the two levels [Haroche06]. In that case, the free evolution Hamiltonian of the atom would be $\hbar\omega_{eg}\sigma_z/2$ instead of $\hbar\omega_{eg}\sigma_+\sigma_-$. Herewith, a definition for the Rabi frequency often associated with this other energy origin is $2\mathcal{E}d\epsilon_d \cdot \epsilon_a^*/\hbar$.

The Hamiltonian (I.4) that we just presented is the quantum counterpart of the so-called Rabi model. In 1936, Rabi introduced a model where an atom possessing a nuclear spin, described quantum mechanically as a two-level system, interacts with a rapidly varying weak magnetic field, described as a classical object [Rabi36]. In short, it was a semi-classical approximation, and it is only three decades later that Jaynes and Cummings introduces a fully quantum model [Jaynes63], in order to clarify the relationship between the semiclassical theory and a theory where the radiation field is quantized as well. Historically, even if the fully quantum model was first presented by Jaynes and Cummings, Eq. (I.4) is most usually called the quantum Rabi model. However, their seminal paper from 1963 was used to define what is called the Jaynes-Cummings model, that we describe hereafter.

I.1.2.2 The rotating wave approximation

The interaction shown in Eq. (I.4) can be simplified, depending on how large the Rabi frequency G is compared to the oscillation frequencies ω_a and ω_{eg} . This can be done by writing the Hamiltonian in a rotating frame,

$$\hat{H}' = i\frac{d\hat{U}_0^\dagger(t)}{dt}\hat{U}_0(t) + \hat{U}_0^\dagger(t)\hat{H}\hat{U}_0(t). \quad (\text{I.9})$$

³A qubit is the quantum mechanical counterpart of a bit, an object that spans a two dimensional Hilbert space and uses it to carry information [Nielsen00].

We are making a change of reference frame, by going from the laboratory frame to a frame that is defined by the expression of $\hat{U}_0(t)$. Here, $\hat{U}_0(t) = e^{-i\hat{H}_0 t}$, with

$$\hat{H}_0 = \hbar\omega_a \hat{a}^\dagger \hat{a} + \hbar\omega_{eg} \sigma_+ \sigma_- . \quad (\text{I.10})$$

The Hamiltonian (I.9) is said to be in the interaction picture, and now writes⁴

$$\hat{H}' = i\hbar G (\sigma_- e^{-i\hbar\omega_{eg} t} + \sigma_+ e^{i\hbar\omega_{eg} t}) (\hat{a} e^{-i\hbar\omega_a t} - \hat{a}^\dagger e^{i\hbar\omega_a t}), \quad (\text{I.11})$$

where one can distinguish two type of terms. The first type are the two terms that oscillate at $\omega_a - \omega_{eg}$. They represent the exchange of energy quanta between light and matter; for each annihilated photon a matter excitation is created, and vice versa. These terms are commonly called resonant terms or rotating terms, because when $\omega_a = \omega_{eg}$, these terms are time-independent in Eq. (I.11) and are resonant with the rotating frame. The second type are the two terms that oscillate at $\omega_a + \omega_{eg}$. They represent the creation of both a quantum of light and a quantum on matter, or the destruction of both quanta. This process is fundamentally different from the energy exchange seen above, and now the energy is not conserved throughout the dynamics. If ω_a and ω_{eg} are physical, thus positive frequencies, these terms cannot be resonant in the interaction picture. Therefore, they are called anti-resonant or counter-rotating terms.

If one has

$$|G| \ll \omega_{a, eg}, \quad (\text{I.12})$$

$$|\omega_a - \omega_{eg}| \ll (\omega_a + \omega_{eg}), \quad (\text{I.13})$$

then the coupling frequency is weak compared to the free frequencies, and the anti-resonant terms are rapidly oscillating compared to the resonant ones. In that case, one can neglect the counter rotating terms, and Eq. (I.11) becomes

$$\hat{H}' = i\hbar G (\sigma_+ \hat{a} e^{-i\hbar(\omega_a - \omega_{eg})t} - \sigma_- \hat{a}^\dagger e^{i\hbar(\omega_a - \omega_{eg})t}). \quad (\text{I.14})$$

In Eq. (I.14) we have performed what is called a rotating wave approximation (or RWA). By coming back into the laboratory frame, we are left with the following Hamiltonian

$$\hat{H}_{\text{RWA}} = \hbar\omega_a \hat{a}^\dagger \hat{a} + \hbar\omega_{eg} \sigma_+ \sigma_- + i\hbar G (\sigma_+ \hat{a} - \sigma_- \hat{a}^\dagger). \quad (\text{I.15})$$

The form seen in Eq. (I.15) of the quantum Rabi model is called the Jaynes-Cummings model, introduced by Jaynes and Cummings in 1963 [Jaynes63]. Since then, this model has been widely studied, both theoretically and experimentally, for a variety of physical systems.

I.1.2.3 Beyond cavity quantum electrodynamics

So far, we used the framework of a two-level atom interacting with a cavity to introduce the quantum description of light-matter interactions. However, not only the quantum

⁴In order to obtain the expression for the operators in the rotating frame, one may find very useful the Baker-Campbell-Hausdorff formula for quantum operators: $e^{\hat{A}} \hat{B} e^{-\hat{A}} = \hat{B} + [\hat{A}, \hat{B}] + \frac{1}{2!} [\hat{A}, [\hat{A}, \hat{B}]] + \frac{1}{3!} [\hat{A}, [\hat{A}, [\hat{A}, \hat{B}]]] + \dots$.

Rabi model and the Jaynes-Cummings model can be studied in others physical systems, but the same type of interaction can be found in systems where the matter excitations are (or can be approximated by) bosonic degrees of freedom. Thus, the use of $\hbar\omega_{eg}\sigma_+\sigma_-$ for the atom's free Hamiltonian instead of the more commonly used $\hbar\omega_{eg}\sigma_z/2$ had the purpose of introducing the general interaction Hamiltonian

$$\hat{H} = \hbar\omega_a\hat{a}^\dagger\hat{a} + \hbar\omega_A\hat{A}^\dagger\hat{A} + i\hbar G(\hat{A} + \hat{A}^\dagger)(\hat{a} - \hat{a}^\dagger), \quad (\text{I.16})$$

with $\hat{A} \in \{\sigma_-, \hat{b}\}$ and $\hat{A}^\dagger \in \{\sigma_+, \hat{b}^\dagger\}$, and where \hat{b} (\hat{b}^\dagger) is a bosonic annihilation (creation) operator. Accordingly, the index A in ω_A stands for either eg or b . Eq. (I.16) shows us that whether the matter is a fermion or a boson, the same form for the interaction can be used, and the previous discussion about the RWA still applies here. However, it is important to note that on the one hand, the bosonic case is described by bosonic creation and annihilation operators. On the other hand, the fermionic case is not described by fermionic creation and annihilation operators, but Pauli operators, which represent transitions between two quantum states and not the creation or annihilation of particles. In what follows, we will use Eq. (I.16) to introduce the different regimes of light-matter interaction.

I.1.3 The weak coupling limit

Historically, the first regime of quantum light-matter interactions achieved was the weak coupling regime or the weak coupling limit. Usually in this limit, the coupling frequency is weak with respect to the free frequencies, $|G| \ll \omega_{a,A}$, hence the RWA can be used,

$$\hat{H}_{\text{RWA}} = \hbar\omega_a\hat{a}^\dagger\hat{a} + \hbar\omega_A\hat{A}^\dagger\hat{A} + i\hbar G(\hat{A}^\dagger\hat{a} - \hat{A}\hat{a}^\dagger). \quad (\text{I.17})$$

However, the crucial criterion of this regime is the coupling being weak compared to the dissipation rates of both systems,

$$|G| \ll \gamma_{a,A}. \quad (\text{I.18})$$

These dissipation rates are defined such that $1/\gamma_{a,A}$ represent the coherence times of the light and matter respectively. Note that for a cavity, the dissipation rate is used to define its quality factor,

$$\gamma_a = \omega_a/Q_a. \quad (\text{I.19})$$

Naturally, the more the cavity can confine the electromagnetic field without losing photons to the outside, the lower is its dissipation rate γ_a , and the higher is its quality factor Q_a . Eq. (I.18) tells us that the interaction and specifically the exchange of quanta expressed in Eq. (I.17) does not have the time to occur periodically before the system decays towards thermal equilibrium with its environment. Nevertheless, this regime can be used to study interesting phenomena such as the Purcell effect. This phenomenon is the modification of the spontaneous emission rate of a quantum system interacting with a cavity mode. Originally, the system, say an atom, is coupled to its environment, a continuum of vacuum modes of the electromagnetic field. Its coupling to a confined electromagnetic mode of a certain volume can enhance, or inhibit its spontaneous emission rate. In particular, the effect depends on whether the cavity is resonant or not with the

atom, on the quality factor of the cavity and on the volume of its mode. First reported by Purcell *et al.* in 1946 [Purcell46], the effect became popular with the advent of experimental cavity QED. It has been first demonstrated with dye molecules deposited on a thin dielectric layer over a metal substrate [Drexhage74], in atomic physics with microwaves [Goy83] and optical [Heinzen87] frequencies, in the cyclotron motion of a single electron [Gabrielse85], as well as in doped solid-state heterostructures [Yablonovitch88]. Later, it has also been observed in other physical platforms, such as in superconducting circuits for instance [Houck08].

1.1.4 The strong coupling regime

The strong coupling regime is the next step in the study of light-matter interactions. In this case, the coupling G can also be very weak compared to the free oscillation frequencies, just as in section I.1.3. Thus, the Hamiltonian (I.17) can be used again to describe the interaction. However, the important condition for the strong coupling regime is the following,

$$|G| \gg \gamma_{a,A}. \quad (\text{I.20})$$

Essentially, it means that the time scale for the light-matter interaction is now shorter than the time scale for the relaxation of the system. Thus, the exchange of energy mentioned in section I.1.2.2 can now take place, and even occur several times if the coupling G is larger than the dissipations rates $\gamma_{a,A}$ by more than a factor of two. If the matter system is a spin, i.e., if $\hat{A} = \sigma_-$ in Eq. (I.17), then a particular oscillation phenomenon can be witnessed, called the Rabi oscillations. These correspond to the transition of the spin back and forth between its two quantum states, and occurs at the Rabi frequency G . Thus, before either the cavity or the spin had the time to completely relax, the transition is repeated over time, following this cycle: an emission then an absorption of a photon.

This behavior is illustrated in Fig. I.1 where are depicted experimental results taken from early demonstrations of Rabi oscillations. In Fig. I.1(a), Rydberg atoms, a nice example of two-level systems, are sent through a microwave cavity, interact with its field during the time they spend inside it, and are measured after they left the cavity, which provides information about their state [Kaluzny83]. However, in this work the quality factor of the cavity was not high enough to allow a single atom to be strongly coupled to the cavity field, so the trick was to increase the number of atoms present inside the cavity at the same time. In this way, the total light-matter Rabi frequency scales as the square root of the number of atoms, and is expressed as $G\sqrt{N}$ [Agarwal84]. Thus, in Fig. I.1(a), as the number of atoms N is increased, one can see that the Rabi oscillations become more and more distinguishable, but also last longer in time, and with a decrease in the oscillation period. In Fig. I.1(b), the same technique of many atoms was used in order to reach the strong coupling regime, and in this work sodium atoms are sent through an optical cavity [Brecha95]. The shown results are not direct measurements of the atoms upper state population, but rather the number of photons that escape the cavity after the interaction. However, the oscillations of these output photons are in fact a direct evidence of the Rabi oscillations, since the atoms periodically absorb and emits photons when they are inside the cavity.

An important property of a strongly coupled light-matter system, this time regard-

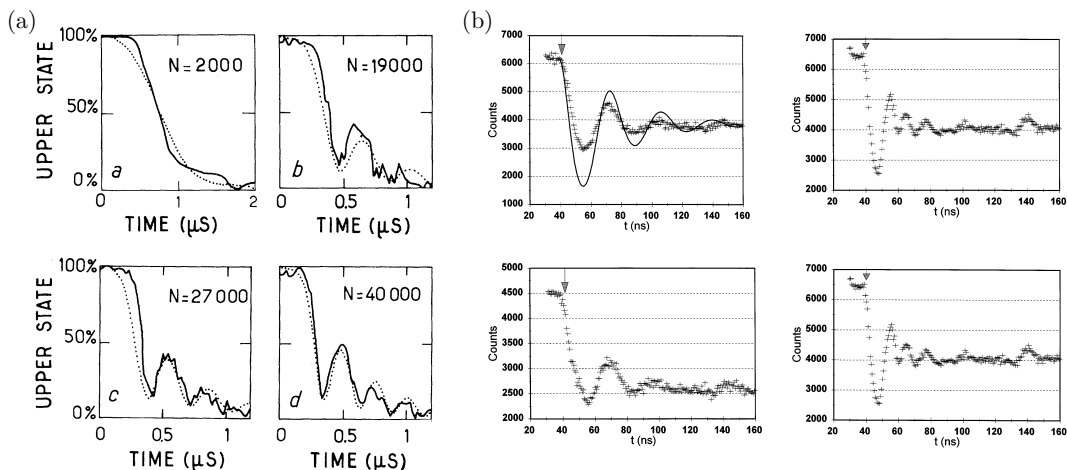


Figure I.1: Experimental evidence of Rabi oscillations occurring in atoms-light coupling. (a) Measurement of the population of sodium Rydberg atoms interacting with a microwave cavity. The single atom coupling being weak, strong coupling is achieved by increasing the number of atoms present at the same time inside the cavity. Taken from [Kaluzny83]. (b) Measured counts of emitted photons from an optical cavity interacting with sodium atoms. Here the strong coupling regime is also reached with the presence of many atoms. Taken from [Brecha95].

less whether the matter is described as two-level systems or as quantum harmonic oscillators, is the Rabi splitting, which is the normal-mode splitting of the light-matter system resonances. This comes from the fact that when the coupling is sufficiently strong to beat any dissipation process, the system hybridizes, and light and matter can no longer be described separately. When the interaction takes place in a resonant cavity, its transmission spectrum shows the new eigenfrequencies split around the original resonance frequency, the one that correspond to the empty cavity case. Fig. I.2 shows the measured Rabi splittings for two different physical systems. Note that the distance between the two peaks is $2G\sqrt{N}$ in Fig. I.2(a) the coupling is enhanced by the number of atoms. In Fig. I.2(b) however, this distance is equal to $2G$, since in this work one superconducting qubit is coupled to a microwave transmission line resonator (playing the role of the cavity).

This regime has first been reached in a case where many atoms were coupled to a microwave cavity field [Kaluzny83], and only after, a single-atom strong coupling has been reached [Meschede85]. Later, it has also been realized beyond the realm of cavity QED, such as with quantum wells in semiconductors [Weisbuch92, Rapaport00], superconducting circuits [Chiorescu04, Wallraff04] (sometimes called circuit QED, analogously to cavity QED), single quantum dots embedded in various kinds of photonic resonators [Reithmaier04, Yoshie04, Peter05], optomechanics [Thompson08a], electromechanics [Teufel11], or ion Coulomb crystals [Herskind09]. Additionally to the demonstration of core properties of this regime such as the Rabi oscillations [Kaluzny83], or the Rabi splitting [Raizen89], note that strong light-matter coupling can be a useful tool for the exploration of further important questions in quantum physics, regard-

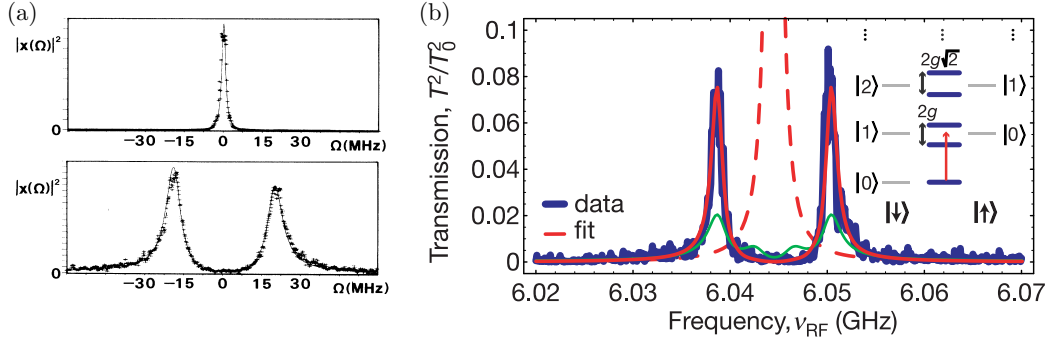


Figure I.2: Experimental evidence of Rabi splitting in light-matter coupling. (a) Transmission spectra versus the probed frequency expressed as the detuning from the carrier frequency, in an experiment where sodium atoms are sent through an optical cavity. The upper panel stands for an empty cavity, while the lower panel is for the case where N , the number of interacting atoms is such that $20 \leq N \leq 600$. Taken from [Raizen89]. (b) Measured transmission versus the microwave probe frequency, for a single superconducting qubit coupled to an on-chip superconducting cavity, a transmission line resonator. The dashed red line stands for the transmission when there is no coupling. Taken from [Wallraff04].

ing the quantum-classical boundary [Bertet01], quantum entanglement [Raimond01], nondestructive measurement [Nogues99], or coherent state transfer [Palomaki13a] for instance.

I.1.5 The ultrastrong coupling regime

The last regime of light-matter interactions reviewed here is the ultrastrong coupling (or USC) regime. It is reached when the Rabi frequency becomes a significant fraction of the free oscillation frequencies of the system, typically when

$$|G| \gtrsim 0.1\omega_{a,A}. \quad (\text{I.21})$$

One can notice that this condition immediately violates the condition (I.12), and hence, the RWA is no longer valid here. Instead, the system is described by the full interaction Hamiltonian reported in Eq. (I.16), where the counter-rotating terms are present. In the USC regime these terms play a significant role, in particular due to the fact that now the number of excitations in the system is not conserved throughout the dynamics. There is a common phenomenon both in the strong coupling and in the USC regime. As explained in section I.1.4, light and matter hybridize in the strong coupling regime, and they naturally hybridize in the USC regime as well. As a matter of fact, this hybridization goes even further in the USC regime, as it modifies the nature of the system's ground state. Indeed, in the strong coupling regime the ground state is simply an absence of any excitation, in both photonic and matter degrees of freedom. In the USC regime however, the ground state cannot be the vacuum, as it contains a finite number of both photonic and matter excitations. This can be rapidly understood in the following example when one considers a bosonic matter excitation, i.e., if $\hat{A} = \hat{b}$ in

Eq. (I.16). In that case, we have the Hamiltonian of two quantum harmonic oscillators coupled by their position (if one defines the position operator as $\hat{X}_b = (\hat{b} + \hat{b}^\dagger)/\sqrt{2}$ for instance)

$$\hat{H} = \hbar\omega_a\hat{a}^\dagger\hat{a} + \hbar\omega_b\hat{b}^\dagger\hat{b} + i\hbar G(\hat{b} + \hat{b}^\dagger)(\hat{a} - \hat{a}^\dagger), \quad (\text{I.22})$$

which can be easily diagonalized. The Hamiltonian (I.22) can then be expressed in terms of its independent normal modes,

$$\hat{H} = \hbar\omega_1\hat{p}_1^\dagger\hat{p}_1 + \hbar\omega_2\hat{p}_2^\dagger\hat{p}_2, \quad (\text{I.23})$$

where the energies of these normal modes are $\omega_{1,2} = \sqrt{\omega_a(\omega_a \pm 2G)}$ (if $\omega_b = \omega_a$). The annihilation operators of these modes are expressed as

$$\hat{p}_{1,2} = t_{1,2}\hat{a} + u_{1,2}\hat{b} + v_{1,2}\hat{a}^\dagger + w_{1,2}\hat{b}^\dagger, \quad (\text{I.24})$$

where the coefficients $\vec{p}_{1,2} = \{t_{1,2}, u_{1,2}, v_{1,2}, w_{1,2}\}$ are obtained by diagonalizing the Hopfield matrix for our system [Hopfield58]. This matrix is obtained from the relation $[\hat{p}_{1,2}, \hat{H}] = \omega_{1,2}\hat{p}_{1,2}$, which is the definition of our eigenvalue problem. Note that in order to fulfill the Bose commutation rule for the normal modes, their coefficients have to be normalized such that $|t_{1,2}|^2 + |u_{1,2}|^2 - |v_{1,2}|^2 - |w_{1,2}|^2 = 1$ is satisfied. The ground state of the Hamiltonian (I.23) is the absence of any excitation in the normal modes \hat{p}_1 and \hat{p}_2 , that we write as $|\tilde{0}\rangle$, to distinguish it from the true vacuum $|0\rangle$. Thereby, it is defined such that $\hat{p}_{1,2}|\tilde{0}\rangle = 0$. However, one might wonder what happens for $\hat{a}|\tilde{0}\rangle$, or $\hat{b}|\tilde{0}\rangle$? As a matter of fact, these operators do have non-zero eigenvalues applied to the ground state, which can be understood by inverting Eq. (I.24),

$$\hat{a} = \tilde{t}_1\hat{p}_1 + \tilde{u}_1\hat{p}_2 + \tilde{v}_1\hat{p}_1^\dagger + \tilde{w}_1\hat{p}_2^\dagger, \quad (\text{I.25})$$

$$\hat{b} = \tilde{t}_2\hat{p}_1 + \tilde{u}_2\hat{p}_2 + \tilde{v}_2\hat{p}_1^\dagger + \tilde{w}_2\hat{p}_2^\dagger. \quad (\text{I.26})$$

From Eqs. (I.25) and (I.26) we can immediately deduce that

$$\langle\tilde{0}|\hat{a}^\dagger\hat{a}|\tilde{0}\rangle = |\tilde{v}_1|^2 + |\tilde{w}_1|^2, \quad (\text{I.27})$$

$$\langle\tilde{0}|\hat{b}^\dagger\hat{b}|\tilde{0}\rangle = |\tilde{v}_2|^2 + |\tilde{w}_2|^2, \quad (\text{I.28})$$

which gives us a clear expression for the number of both the photons and the matter excitations in the ground state. When the USC regime was first predicted and named in 2005 [Ciuti05], the authors pointed out the fact that not only the ground state contained excitations, but that these excitations must exhibit quantum correlations, or entanglement, since expectation values such as $\langle\tilde{0}|\hat{a}^\dagger\hat{b}|\tilde{0}\rangle$ or $\langle\tilde{0}|\hat{b}\hat{a}|\tilde{0}\rangle$ are non vanishing.

Note that this first prediction of the USC regime occurred much later than the first theoretical studies on the weak and the strong couplings regimes. One reason is that for atoms coupled to cavities, there is no way to increase further the coupling strength beyond a certain point, due to the natural possibilities of these platforms. In particular, the key parameter to tune the interaction that can be changed in those systems is the dissipation rate of the cavity, which comes from a better and better engineering of the cavity mirrors, and could only bring again a strong coupling, with the resonances of the Rabi splitting being more sharply defined. What the authors illustrated

in Ref. [Ciuti05], is that for bringing the Rabi frequency at the same order of magnitude than the free oscillation frequencies, one can no longer rely on natural systems, and needs an ingenious artificial platform where the parameters involved in the light-matter coupling strength could be directly tuned in an experiment. Therefore, the system pictured in their work is a semiconductor quantum well where electrons interact with light, and where the Rabi frequency depends in particular on the density of electrons and on the number of superimposed quantum wells in the sample. These parameters can be increased either during fabrication or by injecting more electrons in the system, which can lead to the USC regime.

Only few years later this regime has been experimentally reached in those systems [Günter09, Todorov09, Anappara09]. Shortly after, it was reported in another kind of fully controllable and rapidly progressing engineered devices, namely artificial atoms coupled to on-chip resonators, all made of superconducting circuits [Niemczyk10, Forn-Díaz10]. Impressively, this was only few years after these circuit QED systems reached the strong coupling regime in the first place, as mentioned in section I.1.4. Note that recently it has also been demonstrated in other types of systems, such as various kinds of molecular degrees of freedom coupled to light [Schwartz11, Kéna-Cohen13, George16]. The results of various experiments with the USC regime can be appreciated in Fig. I.3.

Besides the peculiar ground states properties present in the USC regime, there are others worth studying phenomena occurring when one breaks the RWA. One example is the Bloch-Siegert shift [Bloch40], which is a shift in the system's energy-levels due to the fast time-oscillating terms that are usually dropped, and it had been already observed in an experiment with the USC regime [Forn-Díaz10] (see Fig. I.3(c)). Quantum phase transitions can arise in this particular regime of light-matter interactions, and have been studied in a case with many two-levels systems coupled to a bosonic field [Nataf10], as in the Dicke model for instance [Dicke54]. Other applications of the USC regime have been considered, such as its study in the frame of quantum memories [Kyaw15], parity-dependent state engineering and tomography [Felicetti15], or its effect in a photon blockade scenario [Ridolfo12]. Note that some studies explored the USC regime as a tool for the preparation of nonclassical states [Ashhab10, Stassi16], and some analyzed or suggested manners to access its ground state properties [Peropadre13a, Lollo15, Cirio16]. However, a clear picture of the link between the two was not yet formed, particularly in a case where both matter and light are described by quantum harmonic oscillators, as opposed to the case treated in the references mentioned just above where the matter is described as a two-level system.

I.1.6 The deep strong coupling regime

Before moving to the second major part of this chapter, let us conclude this overview by briefly mentioning a last regime of light-matter interactions. Very recently suggested [Casanova10] and called the deep strong coupling (DSC) regime, it occurs when

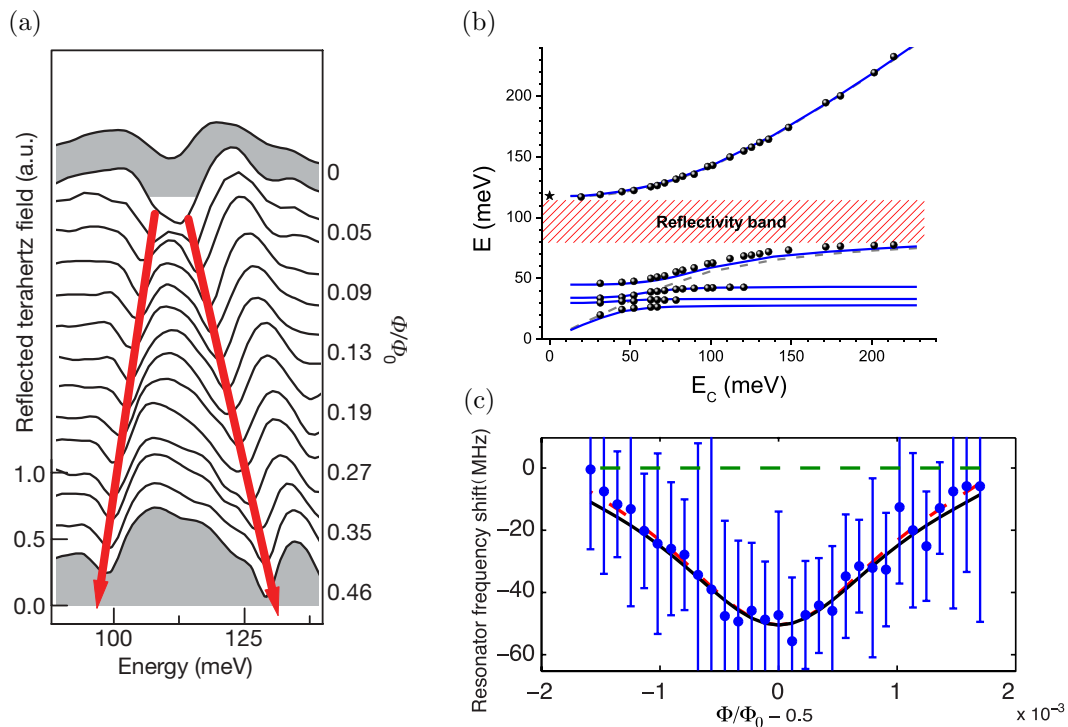


Figure I.3: Experimental evidence of the USC regime. (a) Reflectance spectra as a function of the probed frequency (113 meV = 27 THz) from a sample made of quantum wells confined in a THz cavity, obtained by shining a THz probe on the system. Another THz field, a control pulse, is sent on the system to activate the electronic transitions that couple to the cavity field, and that are then evidenced in the probe field. From top to bottom, the figure essentially shows the reflectance from weaker to stronger light-matter coupling. Here the coupling-over-frequency ratio is above 0.1. Taken from [Günter09]. (b) Eigenenergies of a light-matter system as a function of the cavity free frequency (100 meV = 24 THz), measured in a solid-state sample made of quantum wells confined in a cavity. Here the coupling-over-frequency ratio is 0.73 (between the highest curves). Taken from [Askenazi14]. (c) Bloch-Siegert shift of an LC resonator (the boson coupled to the qubit), as a function of the external magnetic flux applied to the qubit. Taken from [Forn-Díaz10].

the coupling strength G becomes comparable or greater than the system's free oscillation frequencies

$$|G| \gtrsim \omega_{a,A}, \quad (\text{I.29})$$

thus being described by the Hamiltonian (I.16) as the USC regime. Theoretically, it has been proven to induce non-trivial features [Casanova10, Barberena17], and non-intuitive phenomena such as the breakdown of the Purcell effect [De Liberato14]. Additionally, with the rapid progress of superconducting circuits, the DSC regime has been achieved in those systems very recently [Yoshihara17b, Yoshihara17a].

I.2 Quantum states of light

I.2.1 From the birth of a revolutionary description of light to modern quantum optics

An important topic in quantum physics closely linked to light-matter interactions is the study of light itself, from its general description to the various states in which it can be found. In particular, an essential question in the previous century was about whether light needed the tools of quantum physics for its description at all or whether a classical treatment was sufficient. The first step towards a quantum description of light was made by Einstein in 1905 regarding the photoelectric effect, as it is the very first characterization of light in terms of quanta [Einstein05] (although Planck already described radiation as elementary units of energy but without having any corpuscular picture of light in mind [Planck01]), each one carrying a finite amount of energy directly proportional to the frequency of the radiation, used at the time only to describe its wave nature. Both his works on the photoelectric effect and the stimulated emission [Einstein16, Einstein17] strongly contributed to the formation of a quantized understanding of light. It was later Dirac that formalized this understanding with his quantum theory of radiation [Dirac27, Fermi32]. However, even though in the following decades the wave-particle duality of light became quite assimilated by the physics community, its quantum nature had little impact on the understanding of experiments that were finely characterized by classical theory at the time. This came from the experimental difficulty in resolving the corpuscular nature of light on the one hand, and a lack of concrete features and phenomena that would be only described by a quantum theory and could be observed even with intense beams. Such issues were greatly dealt by Glauber, who wrote crucial contributions towards quantum optics in his works on quantum optical coherence [Glauber63a, Glauber63b, Glauber63c]. This helped to clarify where the difference between a classical and a quantum description of light must be drawn, and in particular what features can only be described by the quantum theory. One of those features is the detailed characterization of optical coherence and a method on how to observe it experimentally. First briefly exposed in a letter [Glauber63a], this method uses the so-called $g^{(n)}$ correlation functions, whose definition was thoroughly detailed few months after [Glauber63b], and that are widely used now our days. Another feature mentioned in his work is the Heisenberg uncertainty principle [Heisenberg27] between the two conjugate variables describing the light in phase-space [Glauber63c]. Note that an interest in this principle has led to the study of the so-called standard quantum limit (SQL), which is a saturation of the Heisenberg principle [Stoler70]. In particular, the possibility of going beyond that principle has been studied, eventually called squeezing [Lu71, Yuen75, Milburn81]. With the rapid development of experimental techniques, as in nonlinear optics or instance [Wang65, Giordmaine65], squeezed states of light have eventually been generated [Slusher85, Shelby86, Wu86]. Shortly before that, preliminary experiments produced non classical states through antibunching [Kimble77] and sub-Poissonian photon number statistics [Short83, Teich85]. Later, experimental advances allowed the observation of other nonclassical states of light, such as photon Fock states [Varcoe00, Nogues00, Lvovsky01, Bertet02, Hofheinz08] or Schrödinger cat states [Brune96, Ourjoumtsev07, Deléglise08]. Very recently, even more exotic version of these cat states were generated [Kirchmair13, Wang16].

In what remains of this chapter we shall briefly introduce the concepts needed to describe the quantum states of light using the tools of quantum physics, and give examples of some of those states. In particular, we focus on the definition of squeezed states, since these are the nonclassical states of interest for the next chapter of this thesis.

I.2.2 Phase space description of light

When one wants to describe a quantum system, one way to get all the possible information about its quantum state is to use the so-called density matrix $\hat{\rho}$ of this system. For describing systems with a small Hilbert space [Cohen-Tannoudji77], namely the space that contains all the possible states available for the system, the density matrix is surely the most adequate approach. It can be obtained experimentally with quantum tomography for few interacting qubits for instance. However, when the Hilbert space is very large, if not infinite, it becomes rather difficult to use the density matrix formalism. As opposed to qubits, for a Hilbert space with infinite dimension, the quantum tomography is out of the question. The density matrix can still be practical in few cases where the dimension of the system is *a priori* too large, for instance when an anharmonicity is introduced in the harmonic ladder of an oscillator for instance, such that one of the low transitions is detuned enough to approximate the Hilbert space made only of the states below this transition [Blais04]. If no anharmonicity is possible, then truncating the Hilbert space after some cutoff value in the density matrix method could still be a reasonable approximation, if one is sure the system will not populate states beyond the truncation [Restrepo14a, Felicetti15]. However, if no anharmonicity nor practical cutoff are feasible, then one needs an alternate yet fully equivalent method for describing the quantum state under study, a method that would allow both a practical theoretical description for systems whose Hilbert space is infinite dimension, and their experimental characterization. In the case of a quantum harmonic oscillator, a framework analogous to the study of motion of an object in classical mechanics, called phase-space. Essentially, for a one dimensional classical motion of an object of mass m , the phase-space is a two-dimensional plane whose coordinates are the position x and the momentum $p = m\dot{x}$ [Landau76]. This plane can thus contain all the information about the trajectory of the object, and accordingly, about its dynamics. For a quantum harmonic oscillator however, there is no such thing as a deterministic trajectory.⁵ Nevertheless, starting from the standard Hamiltonian for a quantized harmonic oscillator describing a single mode of the electromagnetic field

$$\hat{H} = \hbar\omega(\hat{a}^\dagger\hat{a} + 1/2), \quad (\text{I.30})$$

one can define operators analogous to the classical position and momentum, such that Hamiltonian becomes

$$\hat{H} = \frac{\hat{\mathcal{P}}^2}{2m} + \frac{m\omega^2\hat{\mathcal{X}}^2}{2}, \quad (\text{I.31})$$

⁵At least not in the Copenhagen interpretation we use throughout the manuscript. For a deterministic interpretation of quantum mechanics, see for instance [Bohm52].

where $\hat{\mathcal{X}}$ and $\hat{\mathcal{P}}$ are related to the creation and annihilation operator of the electromagnetic field in the following way

$$\hat{\mathcal{X}} = \sqrt{\frac{\hbar}{2m\omega}}(\hat{a} + \hat{a}^\dagger), \quad (\text{I.32})$$

$$\hat{\mathcal{P}} = \sqrt{\frac{\hbar m\omega}{2}}i(\hat{a}^\dagger - \hat{a}). \quad (\text{I.33})$$

Here of course the mass m does not correspond to a real mass since we are dealing with an electromagnetic field, and only kept it to highlight the analogy with classical mechanics. One way to link the position and momentum operators $\hat{\mathcal{X}}$ and $\hat{\mathcal{P}}$, also called field quadratures, to a physical picture for the electromagnetic field can easily be found by rewriting the Hamiltonian in terms of the electric field $\hat{\mathbf{E}}$ and the magnetic field $\hat{\mathbf{B}}$

$$\hat{H} = \int \left(\frac{\epsilon_0}{2} \hat{\mathbf{E}}^2 + \frac{1}{2\mu_0} \hat{\mathbf{B}}^2 \right) d\mathbf{r}, \quad (\text{I.34})$$

where ϵ_0 and μ_0 are respectively the vacuum permittivity and the vacuum permeability. By comparing both Eqs. (I.31) and (I.34) and remembering the typical expression of the electric field given by Eq. (I.2), we can see that for a quantized electromagnetic field the analogs for position and momentum are simply the electric and the magnetic components of the field [Lu71]. Note that in the remainder of the manuscript we work with the following dimensionless version of the field quadratures

$$\hat{X} = \sqrt{\frac{m\omega}{\hbar}} \hat{\mathcal{X}} = \frac{\hat{a} + \hat{a}^\dagger}{\sqrt{2}}, \quad (\text{I.35})$$

$$\hat{Y} = \sqrt{\frac{1}{\hbar m\omega}} \hat{\mathcal{P}} = i \frac{\hat{a}^\dagger - \hat{a}}{\sqrt{2}}, \quad (\text{I.36})$$

and define the axes of the phase-space, which is a complex plane, since \hat{X} and \hat{Y} are simply the real and imaginary parts of $\hat{a} = (\hat{X} + i\hat{Y})/\sqrt{2}$. Sometimes it may be appropriate to rotate the axes by an angle ϕ such that

$$\hat{X}_\phi = \frac{\hat{a}e^{-i\phi} + \hat{a}^\dagger e^{i\phi}}{\sqrt{2}}, \quad (\text{I.37})$$

and consider the pair of conjugate variables \hat{X}_ϕ and $\hat{X}_{\phi+\pi/2}$ instead of \hat{X} and \hat{Y} .⁶

1.2.3 Coherent states, or the essential basis for describing light in phase-space

Before showing how the conjugate variables can be of use in the phase-space representation of light, let us first introduce a basic but very states often encountered in quantum optics. In particular, these states form a basis that is essential for the phase-space description of light, as we will see in later sections. These states are called coherent states, and for the sake of clarity, let us first remind two types of states that are needed

⁶Note that following the definition in Eq. (I.37) we have $\hat{Y} = \hat{X}_{\pi/2}$.

to introduce them. The first one is the vacuum state, and by definition, for light the vacuum state is the state that contains zero photons. It is represented as $|0\rangle$, and is most commonly the ground state of the electromagnetic field⁷

$$\hat{a}|0\rangle = 0. \quad (\text{I.38})$$

Note that usually in the presence of several modes in vacuum, for compactness we use $|0\rangle \otimes |0\rangle \otimes |0\rangle \otimes \dots \otimes |0\rangle = |0\rangle$.

The second ones are the Fock states, or number states, represented as

$$|n\rangle = \frac{(\hat{a}^\dagger)^n}{\sqrt{n!}}|0\rangle, \quad (\text{I.39})$$

where n is the number of photons in the Fock state, and where we have

$$\hat{a}|n\rangle = \sqrt{n}|n-1\rangle, \quad (\text{I.40})$$

$$\hat{a}^\dagger|n\rangle = \sqrt{n+1}|n+1\rangle. \quad (\text{I.41})$$

Now we can introduce the coherent states, commonly noted $|\alpha\rangle$ [Glauber63a], that are defined as the eigenvectors of the annihilation operator

$$\hat{a}|\alpha\rangle = \alpha|\alpha\rangle, \quad (\text{I.42})$$

with the eigenvalue α , which may also be referred as the size of the coherent state. Indeed, $\langle\alpha|\hat{n}|\alpha\rangle = |\alpha|^2$, with $\hat{n} = \hat{a}^\dagger\hat{a}$. α is in general a complex number, and following the definition in Eq. (I.37), we have

$$\mathbf{Re}\{\alpha\} = \frac{\langle\alpha|\hat{X}|\alpha\rangle}{\sqrt{2}}, \quad (\text{I.43})$$

$$\mathbf{Im}\{\alpha\} = \frac{\langle\alpha|\hat{Y}|\alpha\rangle}{\sqrt{2}}. \quad (\text{I.44})$$

These states form a basis, since⁸

$$\int d^2\alpha |\alpha\rangle\langle\alpha| = \hat{\mathbb{1}}, \quad (\text{I.45})$$

where $d^2\alpha = d(\mathbf{Re}\{\alpha\})d(\mathbf{Im}\{\alpha\})$ and $\hat{\mathbb{1}}$ is the identity operator. However, the basis is overcomplete due to the fact that the coherent states are not orthogonal

$$\langle\alpha|\beta\rangle = e^{-|\alpha|^2/2-|\beta|^2/2+\alpha^*\beta}. \quad (\text{I.46})$$

By looking at the magnitude of the scalar product $|\langle\alpha|\beta\rangle|^2 = e^{-|\alpha-\beta|^2}$, one can see that the orthogonality is a limit where the difference between α and β tends to infinity. Let

⁷Note that this statement is not true anymore in the ultrastrong and deep strong regimes of light-matter interactions (see sections I.1.5 and I.1.6).

⁸Note that here and in the rest of manuscript, we use $f \equiv \int_{-\infty}^{+\infty}$, unless specified otherwise.

us finally give the expression of a coherent state in the Fock basis⁹

$$|\alpha\rangle = e^{-\frac{1}{2}|\alpha|^2} \sum_{n=0}^{\infty} \frac{\alpha^n}{n!} |n\rangle, \quad (\text{I.47})$$

where we can clearly see that for $\alpha = 0$, we retrieve the vacuum state. This is due to the fact that a coherent state is essentially a vacuum state displaced in phase-space. Thus, the coherent states have the same noise as the vacuum state, namely, they both saturate the Heisenberg uncertainty relation¹⁰

$$\langle \Delta \hat{X} \rangle \langle \Delta \hat{Y} \rangle = 1/2, \quad (\text{I.48})$$

where

$$\langle \Delta \hat{X} \rangle = \langle \Delta \hat{Y} \rangle = 1/\sqrt{2}, \quad (\text{I.49})$$

where the variance for any operator \hat{S} is $\langle \Delta \hat{S} \rangle^2 = \langle \hat{S}^2 \rangle - \langle \hat{S} \rangle^2$. Formally, the right hand side in Eq. (I.48) is $\hbar/2$, however, we work with the adimensioned field quadratures defined in Eqs. (I.35) and (I.36), which is equivalent here to work with the $\hbar \equiv 1$ units. Note that Eqs. (I.48) and (I.49) also apply to the vacuum state. Using the phase-space description developed in the next sections, a coherent state is a vacuum state displaced in phase-space, thus it keeps the same variances. These coherent states have been briefly introduced in a short letter [Glauber63a], and a more detailed definition have been exposed few months later [Glauber63c] with all the appropriate demonstrations. They are often referred to be the most classical states in quantum optics since they are minimal uncertainty states. Quoting Glauber, a coherent state "represents as close an approach to classical localization as is possible" [Glauber63c].

I.2.4 Introducing the quasiprobability distributions

Now that we have defined the phase-space, a relevant question is how to represent a quantum state using the quadratures defined in Eqs. (I.35) and (I.36)? To do this one needs to somehow write the density matrix ρ of the state as a function of the quadratures. As a matter of fact, one would not directly plot ρ in phase-space, but rather extract some information, if not all of it, from ρ , and plot this information in the plane $\{X, Y\}$. This information is characterized by a function, called a distribution, spanning all phase-space, and defined in a particular manner using ρ . There exist different distributions, which are also called representations, and the difference between them is the ordering in which they return expectation values of annihilation and creation operators. To illustrate this point let us express the average of the number operator $\hat{a}^\dagger \hat{a}$ for a state ρ using some distribution that we do not specify at the moment,

$$\langle \hat{a}^\dagger \hat{a} \rangle_k = \text{Tr}\{\rho(\hat{a}^\dagger \hat{a})_k\} = \int f_k(\alpha) |\alpha|^2 d^2\alpha. \quad (\text{I.50})$$

⁹For a detailed derivation, see [Glauber63c].

¹⁰Note that this is true as long as the coherent state remains pure. The saturation in Eq. (I.48) does not hold if the state is mixed (see section I.2.8).

Here, $f_k(\alpha)$ is the phase-space distribution used to compute the expectation value $\langle \hat{a}^\dagger \hat{a} \rangle_k$. However, note that $\langle \hat{a}^\dagger \hat{a} \rangle_k$ is not necessarily equal to $\langle \hat{a}^\dagger \hat{a} \rangle$. Indeed, the index k is very important, as it stands for the type of distribution chosen here. Choosing a particular distribution will actually influence the formal expression of $\langle \hat{a}^\dagger \hat{a} \rangle_k$, namely its ordering. An ordering is a specific way annihilation and creation operators are positioned in a product, which is important because of the non-commutativity of the operators \hat{a} and \hat{a}^\dagger . There are three orderings that are most commonly used, and each one of them has a different distribution associated to them. In the normal ordering for instance, the product of some creation and annihilation operators is rewritten such that creation operators appear on the right and annihilation operators appear on the left, e.g., $((\hat{a}^\dagger)^m \hat{a}^n)_{\mathcal{N}} = ((\hat{a}^\dagger)^m \hat{a}^n)$. Conversely, in the anti-normal ordering, the product is rewritten such that the annihilation operators appear on the left and the creation ones on the right, e.g., $((\hat{a}^\dagger)^m \hat{a}^n)_{\mathcal{A}} = (\hat{a}^n (\hat{a}^\dagger)^m)$. The last one is the symmetric ordering, where the operators are symmetrized in the product. It is basically a sum over all possible symmetric combinations of the initial product. For instance, when $m = n = 1$ it goes as $(\hat{a}^\dagger \hat{a})_{\mathcal{S}} = (\hat{a}^\dagger \hat{a} + \hat{a} \hat{a}^\dagger)/2$. Now we can rewrite Eq. (I.50) and introduce the three commonly used distributions (or functions)

$$\langle \hat{a}^\dagger \hat{a} \rangle = \langle \hat{a}^\dagger \hat{a} \rangle_{\mathcal{N}} = \int P(\alpha) |\alpha|^2 d^2\alpha, \quad (\text{I.51})$$

$$\langle \hat{a} \hat{a}^\dagger \rangle = \langle \hat{a} \hat{a}^\dagger \rangle_{\mathcal{A}} = \int Q(\alpha) |\alpha|^2 d^2\alpha, \quad (\text{I.52})$$

$$\frac{\langle \hat{a}^\dagger \hat{a} + \hat{a} \hat{a}^\dagger \rangle}{2} = \langle \hat{a}^\dagger \hat{a} \rangle_{\mathcal{S}} = \int W(\alpha) |\alpha|^2 d^2\alpha, \quad (\text{I.53})$$

Where the function $P(\alpha)$ stands for the Glauber-Sudarshan P representation [Sudarshan63, Glauber63c], the function $Q(\alpha)$ stands for the Husimi- Q representation [Husimi40], and the function $W(\alpha)$ stands for the Wigner representation [Wigner32]. We can notice that although the right hand side in Eqs. (I.51), (I.52), and (I.53) is the same, the left hand side clearly shows that we are computing different expectation values. Note also that these equations express expectation values in a form clearly analogous to classical statistical physics. However, in classical physics one will use a *probability* distribution in Eqs. (I.51), (I.52), and (I.53) instead of $P(\alpha)$, $Q(\alpha)$, and $W(\alpha)$, since those are not necessarily ones.

1.2.5 The Glauber-Sudarshan P representation

Historically, although the Wigner function and the Husimi- Q functions were introduced much earlier, the first such function used in the framework of modern quantum optics was the P function [Sudarshan63, Glauber63c]. In the seminal works by Sudarshan and Glauber, it was found by diagonally expressing the density operator ρ for a state of light in the coherent states basis

$$\hat{\rho} = \int P(\alpha) |\alpha\rangle \langle \alpha| d^2\alpha, \quad (\text{I.54})$$

This diagonal representation is only possible because this basis is overcomplete [Carmichael99], since two coherent states are not orthogonal (see section I.2.3).

Note that this already indicates that $P(\alpha)$ cannot be thought of as a probability distribution. Indeed, if one expresses ρ on some complete basis $\{|l\rangle\}$, then each diagonal term $\langle l|\rho|l\rangle$ is a true probability, with $\sum_l \langle l|\rho|l\rangle = 1$, yet ρ may contain non-zero off-diagonal terms $\langle l|\rho|k\rangle$. However, for the P distribution the sum over all possible α s also gives 1,

$$\int P(\alpha)d^2\alpha = 1, \quad (\text{I.55})$$

and hence, conversely to $\langle l|\rho|l\rangle$, here $P(\alpha)d^2\alpha$ cannot be a probability because of the diagonal form of ρ in Eq. (I.54). $P(\alpha)$ is rather called a *quasiprobability* distribution. Note also that Eq. (I.54) shows that $P(\alpha)$ is naturally in the normal order, since writing $\text{Tr}\{\rho\hat{a}^\dagger\hat{a}\}$ using Eq. (I.54) directly leads to Eq. (I.51).¹¹ Moreover, for some states $P(\alpha)$ can even take negative values [Carmichael99]. It can be useful to describe some states, but can also be very unpractical for describing very simple ones, such as a coherent state.¹² Mostly used theoretically, it is not the distribution experimentalist commonly aim at reconstructing.

1.2.6 The Husimi- Q representation and heterodyne detection

The Husimi- Q function on its side can be expressed as the overlap between the state of interest ρ and a coherent state

$$Q(\alpha) = \frac{1}{\pi} \langle \alpha|\rho|\alpha\rangle, \quad (\text{I.56})$$

and therefore is a true probability. The Q function is also normalized, as $\int Q(\alpha)d^2\alpha = 1$. This distribution is used not only in theory but also in experiments, and is especially practical when one uses heterodyne measurements. The most standard example of a heterodyne measurement consists in measuring the signal of interest by mixing it with a signal of another frequency, called local oscillator (LO). This is accomplished by sending the signal and the LO through a device whose function is to perform the mixing. When the signals are mixed, the new signal has a component that oscillate at the sum of the frequencies, and another component that oscillates at the difference $\Delta\omega$ between them (see Fig. I.4(a)). The important point is that $\Delta\omega$ is low enough to be processed by electronics, typically being in the radio frequency region.

In such a measurement scheme, both conjugate variables \hat{X} and \hat{Y} are recorded at the same time [Yamamoto86]. However, knowing that $\langle \Delta\hat{X}\rangle\langle \Delta\hat{Y}\rangle \geq \hbar/2$, that simultaneous measurement comes at the price of an additional noise added to the shot noise of the standard Heisenberg principle. It was shown five decades ago that by using two detectors measuring two non-commuting variables is possible, where one detector measures the quadrature \hat{X} , while the other measures the conjugate quadrature \hat{Y} [Arthurs65]. In this first model, an interaction Hamiltonian was introduced, that couples \hat{X} to some quadrature \hat{Y}_1 of detector 1, while coupling \hat{Y} to some quadrature \hat{Y}_2 of detector 2. Thus, we have two independent quantum operators \hat{Y}_1 and \hat{Y}_2 , that commute, while each of them contains information about \hat{X} and \hat{Y} respectively. By recording the values

¹¹The equivalence shown in Eq. (I.51) is actually called the *optical equivalence theorem* [Mandel95].

¹²Indeed, the P function for a coherent state $|\beta\rangle$ is a double Dirac delta $P(\alpha) = \delta(\text{Re}\{\alpha\} - \text{Re}\{\beta\})\delta(\text{Im}\{\alpha\} - \text{Im}\{\beta\})$.

of \hat{Y}_1 and \hat{Y}_2 for many runs of an experiment with the same initial conditions, one can construct a joint probability distribution $p(Y_1, Y_2)$ for the variables \hat{Y}_1 and \hat{Y}_2 . It is known for quite some time that such a joint probability distribution can actually correspond to the Husimi- Q function [Arthurs65, Braunstein91, Stenholm92]

$$p(Y_1, Y_2) = \frac{1}{2}Q(Y_1, Y_2), \quad (\text{I.57})$$

where the right hand side is actually $Q(\alpha)/2$ as in Eq. (I.56), simply by recalling $\alpha = Y_1 + iY_2$. It thus means that the expectation values measured in terms of \hat{Y}_1 and \hat{Y}_2 by the detectors correspond to anti-normally ordered averages in terms of \hat{X} and \hat{Y} for the system of interest (see Eq. (I.52)). While for the detailed derivation of Eq. (I.57) we invite the reader to examine Refs. [Braunstein91, Stenholm92] in details, we nevertheless give an intuitive picture of the previous sentence in what comes next, with a simple illustration. We hereafter show how this measurement scheme with two detectors, each measuring a different complementary variable, correspond to anti-normal ordered expectation values [Müller16]. This is a simplified example whose purpose is only to give a grasp at the principle of heterodyne detection.

The two detectors are independent, and thus, after the system-detectors interaction their conjugated variables $\{\hat{X}_1(t), \hat{Y}_1(t)\}$ and $\{\hat{X}_2(t), \hat{Y}_2(t)\}$ obey

$$[\hat{X}_i(t), \hat{Y}_j(t)] = i\hbar\delta_{ij}. \quad (\text{I.58})$$

However, we know that they contain information about the system's quadratures $\{\hat{X}, \hat{Y}\}$. In fact, we can write the detector operators as follows¹³

$$\hat{X}_1(t) = \hat{X}(0) + \hat{\Lambda}(0), \quad (\text{I.59})$$

$$\hat{X}_2(t) = \hat{Y}(0) + \hat{\Gamma}(0), \quad (\text{I.60})$$

where t stands for the moment after the interaction with the detectors, while $t = 0$ stands for prior to this interaction. Consequently $[\hat{\Gamma}(0), \hat{\Lambda}(0)] = i\hbar$ since $[\hat{X}(0), \hat{Y}(0)] = i\hbar$. $\hat{\Gamma}$ and $\hat{\Lambda}$ are introduced as detectors operators

$$\hat{\Lambda}(0) = \hat{X}_1(0) + \frac{\hat{Y}_2(0)}{2}, \quad (\text{I.61})$$

$$\hat{\Gamma}(0) = \hat{X}_2(0) - \frac{\hat{Y}_1(0)}{2}. \quad (\text{I.62})$$

¹³The following is formally demonstrated in Ref. [Stenholm92].

Then, let us shift to a description in terms of creation and annihilation operators

$$\hat{\nu} = \frac{\hat{X}_1 + i\hat{X}_2}{\sqrt{2}}, \quad (\text{I.63})$$

$$\hat{a} = \frac{\hat{X} + i\hat{Y}}{\sqrt{2}}, \quad (\text{I.64})$$

$$\hat{A} = \frac{\hat{\Gamma} + i\hat{\Lambda}}{\sqrt{2}}, \quad (\text{I.65})$$

$$(\text{I.66})$$

Instead of Eqs. (I.59) and (I.60), we can use

$$\hat{\nu}(t) = \hat{a} + i\hat{A}^\dagger, \quad (\text{I.67})$$

in order to define a θ ordered expectation value

$$\langle \hat{a}^\dagger \hat{a} \rangle_\theta = \langle \sin^2 \theta \hat{a} \hat{a}^\dagger + \cos^2 \theta \hat{a}^\dagger \hat{a} \rangle. \quad (\text{I.68})$$

Now, Eq. (I.67) represents an annihilation operator $\hat{\nu}(t)$ for the signal that is recorded, which is a superposition between the annihilation operator \hat{a} describing the quantum state of the signal of interest and the creation operator \hat{A}^\dagger describing the quantum state of a detector used to record the signal. In this manner, the whole scheme can be seen as a simultaneous measurement of both quadratures $\hat{X}(0)$ and $\hat{Y}(0)$ using only one detector whose quadratures are $\hat{\Gamma}(0)$ and $\hat{\Lambda}(0)$. By using Eq. (I.67), we can rewrite Eq. (I.68)

$$\begin{aligned} \langle \hat{a}^\dagger \hat{a} \rangle_\theta &= (\cos^2 \theta + \sin^2 \theta) |\nu|^2 + \cos^2 \theta \langle \hat{A} \hat{A}^\dagger \rangle + \sin^2 \theta \langle \hat{A}^\dagger \hat{A} \rangle \\ &= |\nu|^2 + \frac{1}{2} \langle \hat{A} \hat{A}^\dagger + \hat{A}^\dagger \hat{A} \rangle + \frac{\cos 2\theta}{2} \langle [\hat{A}, \hat{A}^\dagger] \rangle \\ &= |\nu|^2 + \langle \hat{A}^\dagger \hat{A} \rangle + \frac{1}{2} + \frac{\cos 2\theta}{2}. \end{aligned} \quad (\text{I.69})$$

where $|\nu|^2$ is the average of the operator $\hat{\nu}^\dagger \hat{\nu}$ found by measuring the variables \hat{X}_1 (\hat{X}_2) and constructing their joint probability distribution $p(X_1, X_2)$ shown in Eq. (I.57). Since \hat{A} corresponds to the initial state of the detector, $\langle \hat{A}^\dagger \hat{A} \rangle$ indicates the initial population of this the state. If $\langle \hat{A}^\dagger \hat{A} \rangle = 0$ the detector is in its ground state, and the Eq. (I.69) thus simplifies to

$$\langle \hat{a}^\dagger \hat{a} \rangle_\theta = |\nu|^2 + \frac{1}{2} + \frac{\cos 2\theta}{2} \quad (\text{I.70})$$

now, by choosing $\theta = \pi/2$, we $\langle \hat{a}^\dagger \hat{a} \rangle_{\pi/2} = |\nu|^2$, where now, given Eq. (I.68), the measured average correspond to the following expectation value

$$\langle \hat{a} \hat{a}^\dagger \rangle = |\nu|^2. \quad (\text{I.71})$$

Thus, such a measurement scheme using two detectors 1 and 2, that can be seen as one detector in its ground state naturally leads to anti-normally ordered expectation values. Note that in actual experiments the measurement scheme does not necessarily

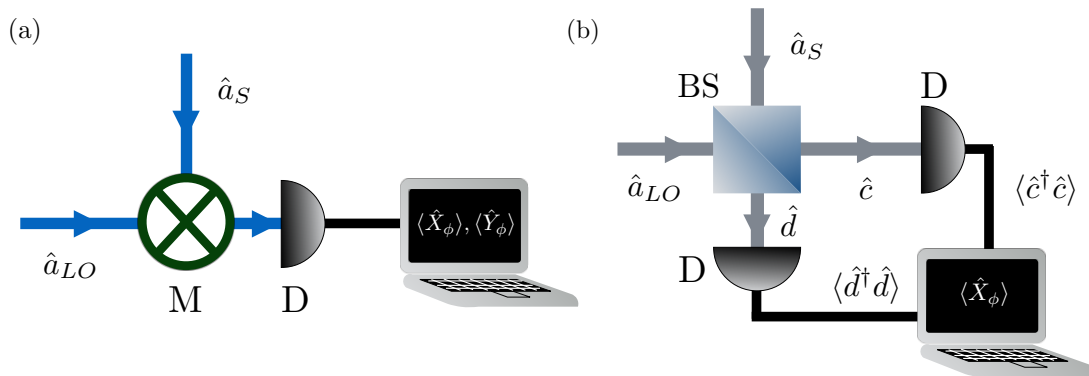


Figure I.4: Sketches for heterodyne and homodyne detections. M: mixer; D: detector; BS: 50:50 beam-splitter. (a) Heterodyne detection at microwave frequencies. A mixer M combines the signal \hat{a}_S with a local oscillator \hat{a}_{LO} , with the LO being detuned by an amount $\Delta\omega = \omega_{LO} - \omega_S$ from the signal. In what comes out from the mixer, the component oscillating at $\omega_{LO} + \omega_S$ is filtered out in the detection apparatus D, while the component oscillating at $\Delta\omega$ can be processed by the electronic circuit. Indeed, for instance the time-oscillating voltage $V(t)$ can be measured and demodulated such that the averages $\langle \hat{X}_\phi \rangle$ and $\langle \hat{Y}_\phi \rangle$ of the field quadratures are retrieved. (b) Balanced homodyne detection at optical frequencies. The optical signal \hat{a}_S is combined on a 50:50 beam-splitter with the local oscillator \hat{a}_{LO} , were both are initially derived from the same source and thus have the same central frequency. After the beam-splitter, the intensity $\langle \hat{c}^\dagger \hat{c} \rangle$ $\langle \hat{d}^\dagger \hat{d} \rangle$ are measured and subtracted in order to retrieve $\langle \hat{X}_\phi \rangle$.

involve two detectors. Indeed, in heterodyne detection the purpose is to shift the signal of interest to a frequency region that is low enough for the time oscillation of the electric field to be detected. Eventually, the measured electric field or voltage is recorded and demodulated such that both measured quadratures are retrieved.¹⁴

1.2.7 The Wigner representation and homodyne detection

The Wigner function can be linked to off-diagonal elements of ρ , taken in the position basis $\{|X\rangle\}$, through the integral

$$W(X, Y) = \frac{1}{2\pi} \int \langle X + \lambda/2 | \rho | X - \lambda/2 \rangle e^{-i\lambda Y} d\lambda, \quad (\text{I.72})$$

where the factor 2 may change position depending on the convention used to define \hat{X} and \hat{Y} [Mandel95, Haroche06, Lvovsky09]. The Wigner function is normalized as $\int W(\alpha) d^2\alpha = 1$. As $P(\alpha)$, and conversely to $Q(\alpha)$, $W(\alpha)$ can take negative values and thus is not a probability distribution. Experimentally, the Wigner representation is widely adopted by the quantum optics community, as the components needed for

¹⁴If the signal of interest is initially in the optical region, then only intensities are detected. However, there are still ways for measuring both quadratures simultaneously. One of them for instance involve two simultaneous homodyne detections right after combining the signal with vacuum at a beam-splitter (see section 1.2.7 for a description of homodyne detection).

its reconstruction are naturally obtained with homodyne detection. As heterodyne detection, its homodyne counterpart aims at detecting an electromagnetic signal by mixing with an LO. However, here the LO have to be derived from the same source as the one used to generate the signal of interest. Thus, the signal is measured at its true frequency. Essentially, a signal characterized by the operator \hat{a}_S is mixed on a beam splitter (BS) with the LO characterized by the operator \hat{a}_{LO} . If the beam splitter is 50/50, i.e., if its reflexion and transmission coefficients are the same, then the fields outgoing from the BS are expressed as

$$\hat{c} = \frac{\hat{a}_S + \hat{a}_{LO}}{\sqrt{2}}, \quad (\text{I.73})$$

$$\hat{d} = \frac{\hat{a}_S - \hat{a}_{LO}}{\sqrt{2}}. \quad (\text{I.74})$$

After the mixing, one measures the intensities $n_c = \langle \hat{c}^\dagger \hat{c} \rangle$ and $n_d = \langle \hat{d}^\dagger \hat{d} \rangle$, and then computes their difference. It yields $n_c - n_d = \langle \hat{a}_S^\dagger \hat{a}_{LO} + \hat{a}_S \hat{a}_{LO}^\dagger \rangle$, noting that \hat{a}_S and \hat{a}_{LO} are not correlated although they come initially from the same source. Since we are interested in measuring a difference between two output signals, this scheme is called *balanced* homodyne detection [Collett87]. If the stiff pump approximation can be made so that the LO is considered to be a classical field, then $\hat{a}_{LO} \approx \alpha_{LO} e^{i\phi}$, where α_{LO} is a complex number. If α_{LO} is real however, then we have $n_c - n_d \approx \alpha_{LO} \langle \hat{a}_S^\dagger e^{i\phi} + \hat{a}_S e^{-i\phi} \rangle = \sqrt{2} \alpha_{LO} \langle \hat{X}_\phi \rangle$. Thus, measuring the difference in the intensities after the BS gives us the expectation value of a signal's quadrature \hat{X}_ϕ with angle ϕ (see Fig. I.4(b)). Performing such measurements, one can statistically reconstruct the probability distribution for this quadrature, and by changing experimentally ϕ , one can access such distributions for all possible angles and thus span all the quadratures in phase-space. The link with the Wigner function is revealed in what follows: for each angle ϕ , the probability distribution is actually a marginal of the Wigner function [Vogel89], namely

$$p(X_\phi) = \langle X_\phi | \rho | X_\phi \rangle = \int W(X_\phi, Y_\phi) dY_\phi. \quad (\text{I.75})$$

Subsequently, once the probability distributions $p(X_\phi)$ are constructed for enough ϕ s, one can reconstruct the Wigner function of the state by using what is called an inverse Radon transform [Smithey93]. Notice that here, conversely to heterodyne measurement, one cannot obtain both the amplitude and phase information in once, but only the amplitude information by detecting the energy of the photons impinging on the detectors. However, accessing the information of only one quadrature dispense us from the extra noise added on the measurement. See Fig. I.5 for the representation of Wigner functions for common quantum states.

Note that apart from Eqs. (I.54), (I.56) and (I.72), there are other ways in linking ρ with $P(\alpha)$, $Q(\alpha)$ and $W(\alpha)$.¹⁵ Note also that these three representations are not the only existing ones. For instance, another version of the P representation exists that abolished any negativities, by doubling the number of degrees of freedom of the

¹⁵For instance, by using the so-called characteristic functions $C_N(\alpha) = \text{Tr}\{\rho e^{\alpha \hat{a}^\dagger} e^{-\alpha^* \hat{a}}\}$, $C_A(\alpha) = \text{Tr}\{\rho e^{-\alpha^* \hat{a}} e^{\alpha \hat{a}^\dagger}\}$, and $C_W(\alpha) = \text{Tr}\{\rho e^{\alpha \hat{a}^\dagger - \alpha^* \hat{a}}\}$ [Carmichael99, Haroche06].

system [Drummond80].

I.2.8 Thermal states

In section I.2.3 we only dealt with pure states, which can always be expressed as a *ket* and thus do not require a density matrix formalism. However, in real experiments the states that one creates and manipulates are never pure but mixed, and thus the density matrix is needed to describe those states. The simplest example of mixed states are thermal states, that correspond to the radiation emitted by a black body for instance. It is a thermal distribution (or Boltzmann, or Gibbs distribution), and in the Fock basis, these states are expressed as

$$\hat{\rho} = \sum_{n=0}^{\infty} \frac{n_{\text{th}}^n}{(n_{\text{th}} + 1)^{n+1}} |n\rangle\langle n|, \quad (\text{I.76})$$

where $n_{\text{th}} = 1/(e^{\hbar\omega/k_{\text{B}}T} - 1)$ is the Bose-Einstein distribution corresponding to the thermal photon number. Its representation in the coherent state basis is

$$\hat{\rho} = \int \frac{1}{\pi n_{\text{th}}} e^{-|\alpha|^2/n_{\text{th}}} |\alpha\rangle\langle\alpha| d^2\alpha, \quad (\text{I.77})$$

by using Eq. (I.54) and the expression of the Glauber-Sudarshan P distribution for a thermal state [Mandel95]. It is also worthwhile to take a look at its Wigner function [Haroche06]

$$W_{\text{th}}(\alpha) = \frac{2}{\pi} \frac{1}{2n_{\text{th}} + 1} e^{\frac{-2|\alpha|^2}{2n_{\text{th}} + 1}}, \quad (\text{I.78})$$

represented in Fig. I.5(b) and in particular to compare it to the Wigner function for vacuum $W_{\text{vac}}(\alpha) = (2/\pi)e^{-2|\alpha|^2}$ (see Fig. I.5(a)). Essentially in the thermal state the width of the Gaussian is larger, such that conversely to the vacuum state that saturates the Heisenberg principle, the thermal state do not

$$\langle\Delta\hat{X}\rangle\langle\Delta\hat{Y}\rangle = (n_{\text{th}} + 1/2). \quad (\text{I.79})$$

So the higher the temperature, the larger is n_{th} , and the further is the state from a minimal uncertainty state. In quantum optics, these states are not generated intentionally in the laboratory, however, in particular in the microwave region, the quantum states might be coherent, yet with some mixedness depending on the value of n_{th} . For a very low temperature, n_{th} is just a perturbation that may not substantially affect the outcome of the experiment.

I.2.9 Squeezed states

If one takes the coherent states as being the closest analog for classical states, then squeezed states may be thought of the simplest example of a truly quantum state. Indeed, their main property cannot be explained by any classical model, namely the fact that in those states the noise of one field quadrature is lower than the noise in vacuum. The absence of light is then more noisy than the light in a squeezed state, a surprisingly non-intuitive feature. Thus, the noise of one quadrature is less than

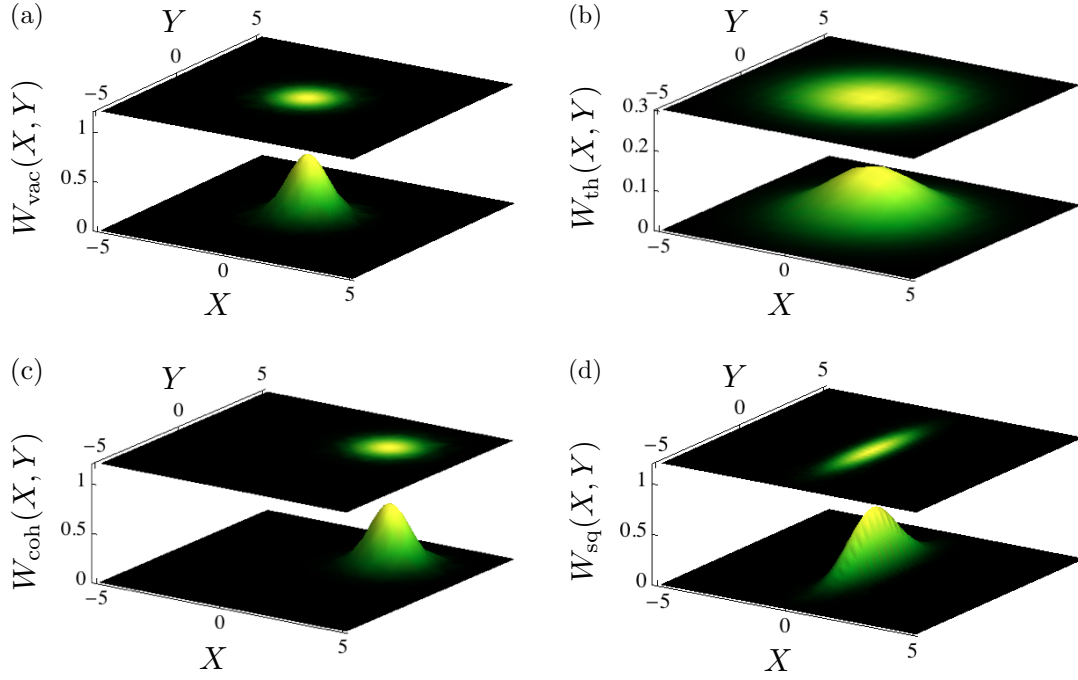


Figure I.5: Wigner functions for common quantum states. (a) Vacuum state. (b) Thermal state with $n_{\text{th}} = 2$. (c) Coherent state with $\langle \hat{X} \rangle = 2$ and $\langle Y \rangle = 2$. (d) Squeezed vacuum state with $\langle \Delta \hat{X} \rangle = e^{-\zeta}/\sqrt{2}$, $\langle \Delta \hat{Y} \rangle = e^{\zeta}/\sqrt{2}$ and $\zeta = 0.7$, corresponding to -6 dB of squeezing using Eq. (I.80).

$1/\sqrt{2}$ (see Eq. (I.49)). However, due to the Heisenberg principle for vacuum, as in Eq. (I.48), this noise reduction comes at the price of an increase in the noise for the conjugated quadrature. If the squeezed state is not pure but mixed, as introduced in the section I.2.8, the Heisenberg principle has the general expression $\langle \Delta \hat{X} \rangle \langle \Delta \hat{Y} \rangle \geq 1/2$, yet the state may still be called squeezed as long as one can find an angle ϕ such that $\langle \Delta \hat{X}_\phi \rangle < 1/\sqrt{2}$. Squeezing may be quantified with the following logarithmic scale

$$S_\phi = 10 \log_{10} \left(\frac{\langle \Delta \hat{X}_\phi^2 \rangle}{\langle \Delta \hat{X}_{\text{vac}}^2 \rangle} \right). \quad (\text{I.80})$$

For a vacuum or a coherent state we have $S_\phi^{\text{vac}} = 0$, which defines the SQL. A mixed state, such as a thermal state, gives $S_\phi^{\text{mixed}} > 0$. There are two types of squeezed states, single-mode and two-mode ones. They are described in the two following sections.

I.2.9.1 Single-mode squeezed states

A single-mode squeezed state, as its name suggest refer to the state of one mode of the electromagnetic field. In short, this mode is a quantum mechanical object described by the annihilation (creation) operator \hat{a} (\hat{a}^\dagger),¹⁶ or by its conjugate variables \hat{X}_a and \hat{Y}_a . A one-mode or a single-mode squeezed state is defined as a state where one can find an

¹⁶For a more rigorous and more detailed definition of a mode, see [Grynberg10].

angle ϕ such that

$$\langle \Delta \hat{X}_{a,\phi} \rangle < 1/\sqrt{2}, \quad (\text{I.81})$$

while satisfying

$$\langle \Delta \hat{X}_{a,\phi} \rangle \langle \Delta \hat{Y}_{a,\phi} \rangle \leq 1/2. \quad (\text{I.82})$$

The operator $\hat{X}_{a,\phi}$ is defined as in Eq. (I.37), and we have $\hat{Y}_{a,\phi} = \hat{X}_{a,\phi+\pi/2}$. Thus, as for the vacuum and for a coherent state, its Wigner function is Gaussian, yet with a different asymmetric shape (see Fig. I.5(d)). Without yet detailing its nature, note that there is an operator, called the *squeezing operator*, which gives a squeezed state,

$$S(z) = e^{\frac{1}{2}(z^* \hat{a} \hat{a} - z \hat{a}^\dagger \hat{a}^\dagger)}, \quad (\text{I.83})$$

when applied on the vacuum state or on a coherent state.

Although their final designation came in the eighties [Milburn81], squeezed states, and in particular single-mode squeezed states were first discovered in 1927 [Kennard27]. In his paper, Kennard studied the motion of a quantum harmonic oscillator and derived expressions for $\langle \Delta \hat{X}_{a,\phi} \rangle$ and $\langle \Delta \hat{Y}_{a,\phi} \rangle$ that were oscillating and where one variance could be reduced at the expense of increasing the other, while still satisfying the Heisenberg principle for a coherent state (see Eq. (I.48)).¹⁷ The study of these states restarted only in the seventies [Lu71], where their link to the squeezing operator in Eq. (I.83) was established [Stoler70, Stoler71]. It was not possible to experimentally generate those states back then, yet experimental proposals emerged [Stoler74, Yuen75, Milburn81]. The first experimental demonstrations did not clearly involve squeezing, but rather photon-antibunching [Kimble77] and sub-Poissonian photon statistics [Short83, Teich85], that are both related forms of correlations between photons. Later in the eighties experimental generation of squeezed states has been finally reached [Slusher85], with experimental techniques that are widely used now our days, such as four wave mixing [Shelby86], or parametric down conversion in optical parametric oscillators [Wu86]. Fig. I.6 show the squeezing obtained in two of the very first squeezing experiments in the eighties. Note that although this research field was mainly focused on squeezing light at optical frequencies, even at the early days of the experimental realization of squeezing, a contribution was brought at microwave frequencies [Yurke88], followed by others in recent years [Castellanos-Beltran08, Mallet11].

Squeezed states have applications in various domains. In the early days before their experimental demonstration, Caves proposed to use it as a tool to improve the detection of gravitational waves [Caves81], which was later shown to be true [Grote13]. In general, they can be used to improve the precision in many quantum measurement schemes [Giovannetti04]. Another important application of those states is in continuous-variable quantum information, where they represent one of its most basic resources [Cerf01, Braunstein05].

Before moving to two-mode squeezed states in the next section, let us give an example of a scheme where single-mode squeezed are generated, and describe how one can treat this scheme theoretically. Such an example is a degenerate parametric down conversion achieved in a optical parametric oscillator (OPO). In short, the device (such as a nonlinear crystal inside an optical cavity for instance [Wu86]), is driven by an electromagnetic

¹⁷For a more detailed story on their discovery, see [Nieto97].

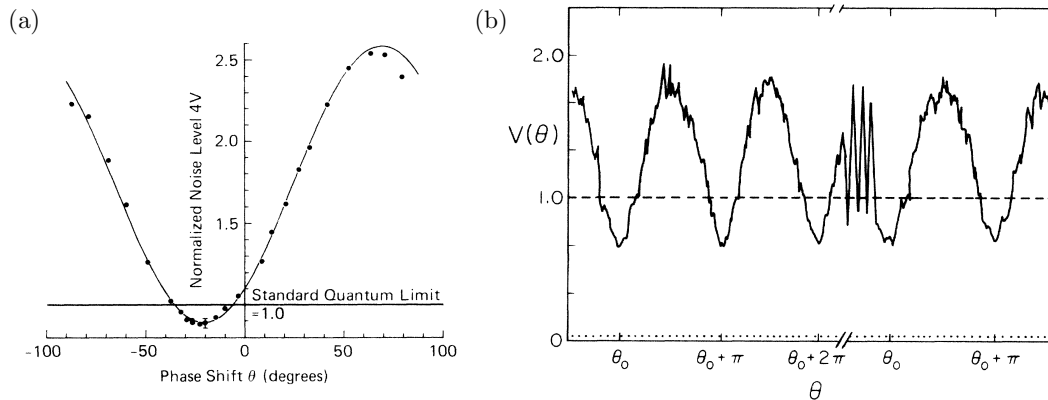


Figure I.6: Squeezing obtained in two of the very first squeezing experiments. (a) Variance of one quadrature of the radiation coming out of a four-wave-mixing experiment, as a function of the phase of the quadrature. The horizontal solid line stands for the SQL, *i.e.*, the minimal noise found in vacuum. Taken from [Shelby86]. (b) Variance of one quadrature of the radiation coming out of a degenerate parametric down conversion experiment, as a function of the phase of the quadrature. The horizontal dashed line stands for the SQL. Taken from [Wu86].

field \hat{c} , called the pump, and oscillating at ω_c . Inside the OPO, a nonlinear interaction takes place between the pump mode, and two other modes, called signal and idler. In principle, the signal and idler are distinct modes \hat{a}_s and \hat{a}_i . However, in a *degenerate* OPO they have the same frequency $\omega_a = \omega_s = \omega_i$, and thus can be treated as being the same mode $\hat{a} = \hat{a}_s = \hat{a}_i$. In the interaction picture, the Hamiltonian of this process can be written as

$$\hat{H}_{\text{dOPO}} = i \frac{\hbar g}{2} (\hat{c}(\hat{a}^\dagger)^2 - \hat{c}^\dagger \hat{a}^2), \quad (\text{I.84})$$

where g is the coupling between the modes. The interaction picture was derived using the same method as in Eq. (I.9), and here the free Hamiltonian is $\hat{H}_0 = \hbar\omega_a \hat{a}^\dagger \hat{a} + \hbar\omega_c \hat{c}^\dagger \hat{c}$. The meaning of Eq. (I.84) is that each time a photon from the pump is destroyed at the frequency ω_c , two photons are created at a frequency $\omega_a = \omega_c/2$. This way the energy is conserved in this quantum process. If the stiff pump approximation can be made, thus considering the pump as undepleted, the pump operator \hat{c} can be replaced by a complex number being the complex amplitude of the pump field, $\alpha_c = \langle \hat{c} \rangle$. If α_c is real¹⁸, Eq. (I.84) becomes

$$\hat{H}_{\text{dOPO}} = i \frac{\hbar g \alpha_c}{2} ((\hat{a}^\dagger)^2 - \hat{a}^2). \quad (\text{I.85})$$

Eq. (I.85) is the form most commonly used to introduce a squeezing Hamiltonian [Scully97].

Experimentally, this squeezing is measured on the light that escapes the system after some time. An important question now is how to compute this escaping squeezing from the Hamiltonian (I.85), a crucial point in this thesis. Computing the time evolution

¹⁸This assumption is only made for the sake of simplicity, and does not change the physics of the problem but only the angle of the maximally squeezed quadrature.

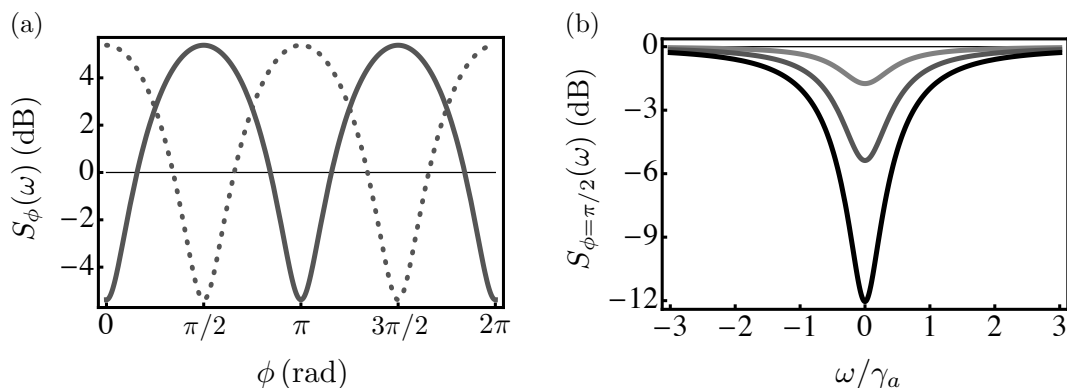


Figure I.7: Noise spectra in decibels for the degenerate parametric oscillator derived by applying input-output theory to the Hamiltonian (I.85). For the derivation of the equation of motion for \hat{a} using input-output theory, see the appendix A; for the derivation of these noise spectra using input-output theory, see the appendix B. (a) $S_\phi(\omega)$ (dashed curve) and $S_{\phi+\pi/2}(\omega)$ (solid curve), respectively for quadratures \hat{X}_ϕ and $\hat{X}_{\phi+\pi/2}$, shown as functions of ϕ . Here $g\alpha_c = 0.15\gamma_a$, $\omega = 0$ (origin of the rotating frame, that rotates at $\omega_c/2$). (b) $S_{\phi=\pi/2}(\omega)$, namely the noise spectrum for the quadrature \hat{Y} , as a function of ω (the measurement frequency in the rotating frame). From top to bottom, $g\alpha_c = 0.05\gamma_a$; $0.15\gamma_a$, $0.3\gamma_a$. For $g\alpha_c = 0.5\gamma_a$, $S_{\phi=\pi/2}(\omega)$ is infinitely squeezed (not shown here). In both plots the solid horizontal line indicates the SQL.

of the density matrix for the system using a master equation is a solution difficult to implement when one treats intense fields, as we do not want to put any restriction on the field amplitude α_c . Therefore, this method is not really appropriate. A more convenient method is the one called input-output theory [Gardiner04]. Developed in the eighties [Yurke84, Gardiner85], this theory aims at formulating interactions between quantum systems as a set of coupled equations of motions, and to extract a transformation matrix between the initial states (the inputs) and the final states (the outputs) once the equations have been linearized. To understand how to go from the Hamiltonian in Eq. (I.85) to an equation of motion for the operator \hat{a} , see the appendix A. For a derivation of the noise spectra of the output radiation \hat{a}_{out} from the equation of motion, and using input-output theory, see the appendix B. The results from this appendix were used to plot the noise spectra shown in Fig. I.7, where one can observe the same oscillatory behavior for the squeezing than in Fig. I.6, by varying the phase ϕ .

I.2.9.2 Two-mode squeezed states

A priori, two-mode squeezed states do not satisfy the inequality in Eq. (I.81), meaning that each mode taken independently is not squeezed.¹⁹ However, in these states squeezing appears as a quantum correlation between the two modes. Indeed, one can define a

¹⁹We will see in chapter III that there are situations where this statement is not true, and where a two-mode squeezed state can also be squeezed in the single-mode picture.

collective quadrature [Duan00]

$$\hat{u}_{\phi_a, \phi_b}^{\pm} = \frac{\hat{X}_{a, \phi_a} \pm \hat{X}_{b, \phi_b}}{\sqrt{2}}, \quad (\text{I.86})$$

where \hat{X}_{a, ϕ_a} is a quadrature for a mode \hat{a} with angle ϕ_a defined in Eq. (I.37), and where with same definition \hat{X}_{b, ϕ_b} is a quadrature for a mode \hat{b} with angle ϕ_b . If this quadrature satisfies

$$\langle \Delta \hat{u}_{\phi_a, \phi_b}^{\pm} \rangle^2 < 1/2, \quad (\text{I.87})$$

then the state is said to be two-mode squeezed. An intuitive picture for understanding those states can be made with the following example. If ϕ_a and ϕ_b are chosen so that \hat{X}_{a, ϕ_a} and \hat{X}_{b, ϕ_b} are the amplitudes of both fields, and if Eq. (I.87) is satisfied for $\hat{u}_{\phi_a, \phi_b}^{-}$, then the number of photons can be measured with less noise than the vacuum if one looks at the difference between the amplitudes of both modes, instead of looking at the amplitudes separately. Two-mode squeezing has first been analyzed in [McNeil83], where the authors studied the squeezing in a linear combination of the signal and idler fields in a non-degenerate OPO.

A concept directly linked to two-mode squeezing is quantum entanglement. First highlighted in 1935 by Einstein, Podolsky and Rosen [Einstein35b] with their "spooky action at a distance", and by Schrödinger with his famous cat thought experiment [Schrödinger35], quantum entanglement is the fact that two systems (or even more) cannot be described separately, even if they are spatially distant. In mathematical terms, it means that if we call $\rho_{a,b}$ the density matrix describing two entangled electromagnetic field modes \hat{a} and \hat{b} , then we have

$$\hat{\rho}_{a,b} \neq \hat{\rho}_a \otimes \hat{\rho}_b, \quad (\text{I.88})$$

where $\hat{\rho}_a$ is a density matrix in the Hilbert space of mode \hat{a} , and $\hat{\rho}_b$ a density matrix in the Hilbert space of mode \hat{b} , with a tensorial product between them. Eq. (I.88) thus defines the inseparability between modes \hat{a} and \hat{b} . For continuous variables quantum systems²⁰ there are criteria that allow to detect entanglement or even quantify it. However, those criteria were formally demonstrated at the very end of the previous millennium, yet two-mode squeezing was theoretically studied [McNeil83, Reynaud87, Reid88] and experimentally demonstrated [Reynaud87, Ou92] years before that. Therefore, back then, instead of studying entanglement, the trend was to disprove the so-called Einstein-Podolsky-Rosen (EPR) paradox [Einstein35b]. For continuous variables systems, it was shown to be directly linked to two-mode squeezing, and the paradox is said to be realized when the following inequality is satisfied [Reid89, Ou92]

$$\langle \Delta \hat{u}_{\phi_a, \phi_b}^{+} \rangle^2 \langle \Delta \hat{u}_{\phi_a + \pi/2, \phi_b + \pi/2}^{-} \rangle^2 < 1/4, \quad (\text{I.89})$$

where it may be rewritten as $\langle \Delta(\hat{X}_a + \hat{X}_b) \rangle^2 \langle \Delta(\hat{Y}_a - \hat{Y}_b) \rangle^2 < 1$, in the instance $\phi_a =$

²⁰Namely quantum systems whose state is described in a Hilbert space of infinite dimension, such as when the electromagnetic field is described in phase space. The opposite kind of systems is called discrete variables quantum systems, where the Hilbert space has a finite size, such as for qubits for instance.

$\phi_b = 0$.

Concerning the other criteria demonstrated later and mentioned above, the first one is an entanglement witness, that can be written as [Duan00]

$$\langle \Delta \hat{u}_{\phi_a, \phi_b}^+ \rangle^2 + \langle \Delta \hat{u}_{\phi_a + \pi/2, \phi_b + \pi/2}^- \rangle^2 < 1, \quad (\text{I.90})$$

For instance, if $\phi_a = \phi_b = 0$, Eq. (I.90) may be written as $\langle \Delta(\hat{X}_a + \hat{X}_b) \rangle^2 + \langle \Delta(\hat{Y}_a - \hat{Y}_b) \rangle^2 < 2$. This quantity is an entanglement witness, therefore the inequality (I.90), when satisfied, tells us that we have an entangled state, but does not quantify the amount of entanglement since it is only a sufficient condition for entanglement. Furthermore, in general it is only a sufficient criterion, meaning that if the inequality is not satisfied, we do not know if the state is separable or entangled. However, for Gaussian states,²¹ it is a necessary and sufficient criterion, and thus, states that do not satisfy Eq. (I.90) are necessarily separable. Another criterion widely used is the one based on the covariance matrix \mathcal{V} . If one defines the vector $\hat{\mathcal{X}} = \{\hat{X}_a, \hat{Y}_a, \hat{X}_b, \hat{Y}_b\}$, then the elements of \mathcal{V} are defined as [Serafini04]

$$\mathcal{V}_{ij} = \frac{1}{2} \langle \hat{\mathcal{X}}_i \hat{\mathcal{X}}_j + \hat{\mathcal{X}}_j \hat{\mathcal{X}}_i \rangle - \langle \hat{\mathcal{X}}_i \rangle \langle \hat{\mathcal{X}}_j \rangle. \quad (\text{I.91})$$

This matrix contains all the possible correlations between modes \hat{a} and \hat{b} , and can be used to define a Peres-Horodecki separability criterion for continuous variables [Simon00]. As in the discrete variable case [Peres96, Horodecki96, Horodecki97], it is the non-positivity of the partial transpose of the density matrix $\hat{\rho}_{a,b}$ that is used to show that a state is entangled, and a negativity can also be defined that will in a sense quantify the entanglement. To define it, let us write the covariance matrix \mathcal{V} in terms of 2×2 matrices $\boldsymbol{\alpha}$, $\boldsymbol{\beta}$ and $\boldsymbol{\gamma}$

$$\mathcal{V} = \begin{pmatrix} \boldsymbol{\alpha} & \boldsymbol{\gamma} \\ \boldsymbol{\gamma}^T & \boldsymbol{\beta} \end{pmatrix}, \quad (\text{I.92})$$

where $\boldsymbol{\gamma}^T$ is the transpose of $\boldsymbol{\gamma}$. In order to obtain our criterion we first must compute the symplectic eigenvalues $\tilde{\nu}_{\pm}$ of the partially transposed covariance matrix $\tilde{\mathcal{V}}$ [Adesso05]

$$\tilde{\nu}_{\pm} = \sqrt{\frac{\Delta(\tilde{\mathcal{V}}) \pm \sqrt{\Delta^2(\tilde{\mathcal{V}}) - 4 \det \mathcal{V}}}{2}}, \quad (\text{I.93})$$

where $\Delta(\tilde{\mathcal{V}}) = \det \boldsymbol{\alpha} + \det \boldsymbol{\beta} - 2 \det \boldsymbol{\gamma}$. The smallest symplectic eigenvalue $\tilde{\nu}_-$ can then be used to compute the logarithmic negativity for the state $\hat{\rho}_{a,b}$ ²²

$$E_{\mathcal{N}}(\hat{\rho}_{a,b}) = \max\left(0, -\log(2\tilde{\nu}_-)\right), \quad (\text{I.94})$$

which quantifies the amount of entanglement between modes \hat{a} and \hat{b} , and is an upper

²¹States whose Wigner function is Gaussian.

²²Note that with our definition for the field quadratures in Eq. (I.37), we have $\tilde{\nu}_{\pm} \leq 1/2$. Thus, with a different definition we may have $\tilde{\nu}_{\pm} \leq 1$ as in [Adesso05], the logarithmic negativity will be $E_{\mathcal{N}}(\hat{\rho}_{a,b}) = \max(0, -\log \tilde{\nu}_-)$

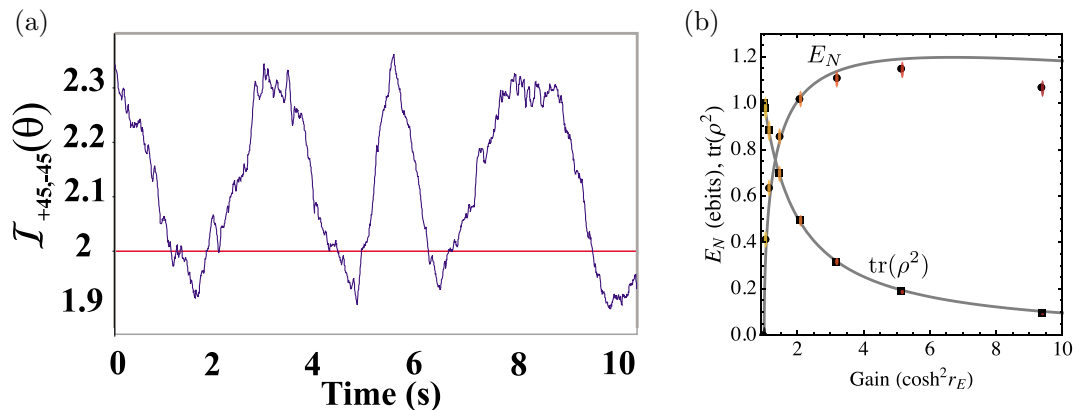


Figure I.8: Experimental demonstrations of bipartite continuous variable entanglement (a) Entanglement witness (I.90) as a function of time, generated by light interacting with cold atoms. When $\mathcal{I}_{+45,-45}(\theta) < 2$, the two light beams at optical frequencies are entangled. Taken from [Josse04]. (b) Logarithmic negativity (I.94) as a function of the gain in a three-wave mixing process at microwave frequencies. r_E is a squeezing parameter that may be defined here as $\langle \Delta \hat{X}_{\text{sq}} \rangle = e^{-r_E} / \sqrt{2}$, where \hat{X}_{sq} is the squeezed quadrature. Taken from [Flurin12].

bound to the distillable entanglement²³ present in the state $\hat{\rho}_{a,b}$ [Adesso05].

In recent years, these entanglement criteria have been applied in various experiments, at optical [Silberhorn01, Bowen02, Josse04] as well at microwave [Eichler11, Flurin12] frequencies. In Fig. I.8 one can see experimental demonstrations of two-mode squeezing and the applications of both the entanglement witness (I.90) and the logarithmic negativity (I.8). Two-modes squeezed states are of great use for the study of fundamental properties of quantum mechanics such as non-locality [Chen02], but are also an essential resource in quantum information and communications protocols [Braunstein05], such as in a quantum teleportation protocol for instance [Braunstein98, Furusawa98].

The last part of the present section is devoted to show how to compute the two-mode squeezing for an experimental scheme. We are again interested in the interaction taking place in an OPO, as it is the most common set-up to achieve two-mode squeezing. Yet, here we are interested in the non-degenerate OPO, whose interaction Hamiltonian is

$$\hat{H}_{\text{OPO}} = i \frac{\hbar g \alpha_c}{2} (\hat{a}_s^\dagger \hat{a}_i^\dagger - \hat{a}_s \hat{a}_i), \quad (\text{I.95})$$

where \hat{a}_s and \hat{a}_i stand for the signal and the idler modes, and where we already applied the stiff pump approximation, as we did in Eq. (I.85). Here again we can use the input-output theory in order to study the noise properties of the output radiation, we we did in section I.2.9.1. For a derivation of the input-output relations for both modes and of the covariance matrix, see appendix C. In Fig. I.9 we show some noise properties of the output radiation coming from a non-degenerate OPO. Essentially, Figs. I.9(a) and I.9(b) show that while two collective quadratures are squeezed below the SQL, the noises of

²³The distillation of entanglement is a process where l copies of some entangled state are used to produce k copies of maximally entangled states [Bennett96].

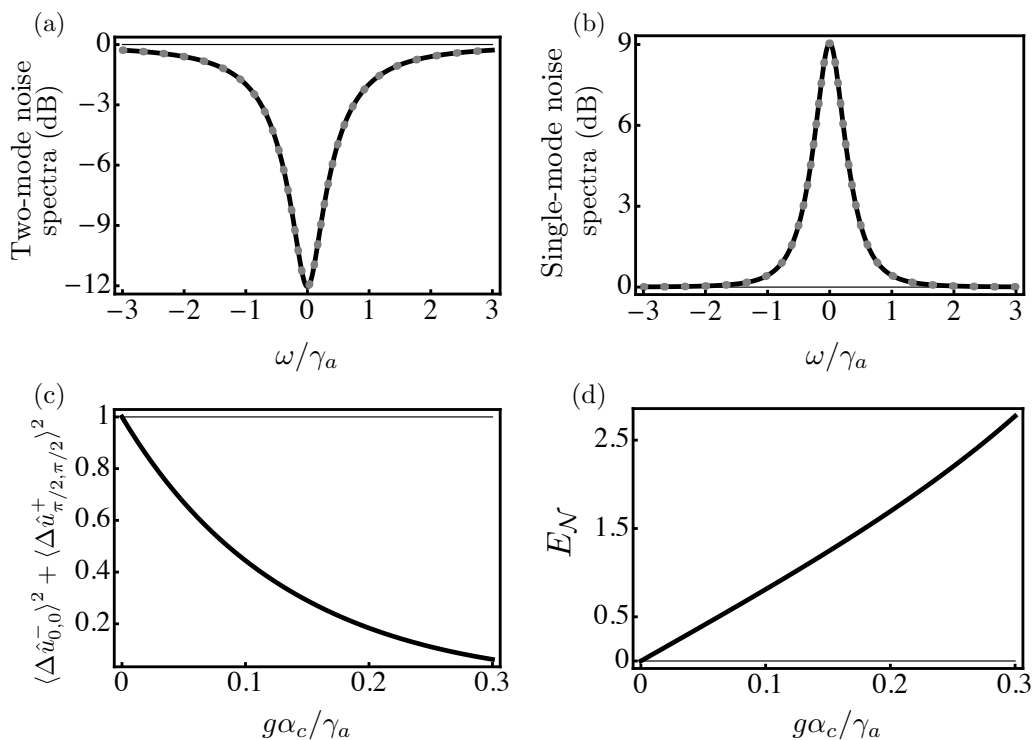


Figure I.9: Noise spectra in decibels, entanglement witness and logarithmic negativity for the non-degenerate parametric oscillator derived by applying input-output theory to the Hamiltonian (I.95). For the derivation of these noise spectra using input-output theory, see the appendix C. (a) Noise spectra for the two-mode quadratures $\hat{u}_{0,0}^- = (\hat{X}_s - \hat{X}_i)/\sqrt{2}$ (gray dashed curve) and $\hat{u}_{\pi/2, \pi/2}^+ = (\hat{Y}_s + \hat{Y}_i)/\sqrt{2}$ (black solid curve), as a function of ω (the measurement frequency in the rotating frame). (b) Noise spectra for the single-mode quadratures \hat{X}_s (gray dashed curve) and \hat{Y}_s (black solid curve), as a function of ω . (a),(b) The noise spectra follow the same definition as in Eq. (B.19), and we have $g\alpha_c = 0.3\gamma_a$. (c) Entanglement witness as defined in Eq. (I.90), as a function of the coupling $g\alpha_c$, at $\omega = 0$.

the single-mode quadratures are amplified above the SQL.²⁴ This can be understood by noting that we have an entangled state, and thus looking at single-mode properties amounts to make a partial trace over the bipartite state, which leaves us a mixed single mode state, hence with more noise than the vacuum in every direction in phase-space. Indeed, the full state's entanglement is proven in Figs. I.9(c) and I.9(d), where one can appreciate the violation of the entanglement witness (I.90) as well as the quantification of the entanglement through the logarithmic negativity (I.94).

I.2.10 Some examples of other nonclassical states

Although the non-classical states encountered in rest of the thesis are squeezed states, belonging to the more general category of Gaussian states, we wish at last in this chapter

²⁴Note that here the single-mode properties of mode \hat{b} are exactly the same that those of mode \hat{a} .

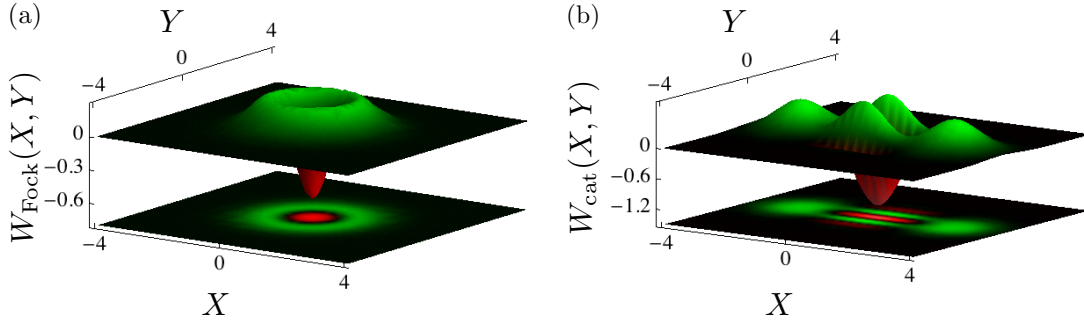


Figure I.10: Wigner functions for two non-Gaussian quantum states displaying negative regions. (a) Single photon Fock state. (b) Schrödinger cat state $|c_{-}\rangle = (|\beta\rangle - |-\beta\rangle)/\sqrt{2}$, with $\beta = \sqrt{3}$.

to mention some non-classical states that are non-Gaussian. Non-Gaussian states are states whose Wigner function is not a Gaussian function of α . For pure states, it goes hand in hand with the presence of negative regions in phase-space for the Wigner function. The simplest type of non-Gaussian states one could think of are Fock states, whose expression was already given in Eq. (I.39). For instance, the Wigner function for a single photon Fock state is [Haroche06]

$$W_{\text{Fock}}(\alpha) = \frac{2}{\pi} (4|\alpha|^2 - 1) e^{-2|\alpha|^2}. \quad (\text{I.96})$$

shown in Fig. I.10(a). Another type of non-Gaussian states are the famous Schrödinger cat states $|c_{\pm}\rangle = (|\beta\rangle \pm |-\beta\rangle)/\sqrt{2}$, whose Wigner function, shown in Fig. I.10(b), is

$$W_{\text{cat}}(\alpha) = \frac{2}{\pi(1 \pm e^{-2|\beta|^2})} \left(e^{-2|\alpha-\beta|^2} + e^{-2|\alpha+\beta|^2} \pm 2e^{-2|\alpha|^2} \cos(4\text{Im}\{\alpha\}\text{Re}\{\beta\}) \right). \quad (\text{I.97})$$

In order to generate both Fock states and Schrödinger cat states, one has to perform non-Gaussian operations on the system. For such operations one needs a high nonlinearity, such as when a two-level system interacts with a cavity mode, or cavity with a high Kerr nonlinearity, which would give a non-linear equation of motion for the cavity, as opposed to the linear equations exposed in Eqs. (B.3) and (C.3). It is a challenge to generate these states in a laboratory, however experimental demonstrations exist, both at microwave [Brune96, Varcoe00] and at optical [Lvovsky01, Ourjoumtsev07] frequencies.

I.3 Conclusion

In this chapter we have seen some important concepts in quantum mechanics, that will be of great help to tackle the topics studied in the next chapters. In particular, we defined the notion of squeezing as the benchmark of the correlations that can arise for photons in Gaussian states. Furthermore, we reviewed the different regimes of light-matter interactions, and focused on the different features of the ultrastrong coupling regime that we will encounter again later in this manuscript.

The following chapters are devoted to present the research carried in this thesis, which as a main goal was focused on the utilization of the USC regime as a resource for the generation of squeezed states of radiation in various experimental set-ups.

II Dispersive ultrastrong coupling regime in intersubband devices

This chapter presents one of the results of this thesis, and is a first step in a broader study of the relation between squeezed states of light and the ultrastrong coupling (USC) regime. It is mainly based on the results reported in [Fedortchenko16]. Although the model presented here could in principle be applied to superconducting circuits architectures (see chapter III), the prime focus of the work is on intersubband devices [Todorov10]. Therefore, the chapter starts with a quick overview of these systems. Then, using the tools at our disposal, we build a model where two important ingredients are added to the standard framework with intersubband transitions in the electrical dipole gauge [Todorov12a], namely a time dependence of the ultrastrong light-matter coupling [De Liberato07], as well as a large detuning between the light and the matter degrees of freedom. We study the consequence of these hypotheses on the noise spectrum of the radiation coming out of the system, as well as the influence of other physical parameters. Furthermore, after reported results for the simplest architecture possible which is a two-level quantum well, we extend our model to the situation where the quantum well has three levels. The prerequisites for the present chapter are the same as for chapter I, as well as the notions seen in the latter.

II.1 Many-body properties of intersubband devices

Building solid-state devices where electrons induce quantum effects is a long standing goal [Capasso90], both for fundamental and practical applications. The most famous such application is the so-called Quantum Cascade Laser, demonstrated for the first time more than twenty years ago [Faist94]. On the fundamental side, great interest has been devoted in studying the interactions between collective excitations of electrons and confined cavity modes of unprecedented strength. Such strength can define new regimes of light-matter interactions (see chapter I), and as a matter of fact, both the strong [Weisbuch92, Rapaport00] and the ultrastrong [Günter09, Todorov09, Anappara09] coupling regimes that have been achieved in those systems. Our interest in those systems specifically lies of the fact that such light-matter coupling regimes can be reached in them with nowadays technology. Specifically, we are interested in semiconducting heterostructures, such as made of GaAs or GaInAs for instance¹. One way to reach quantum effects in those structures is to confine the electrons in discrete levels, called subbands in a quantum well. To obtain a quantum well, the semiconductor in question is imprisoned between two layers of another semiconductor with a wider gap

¹In this chapter we are interested in III-V semiconductors with a direct gap [Pegolotti14a].

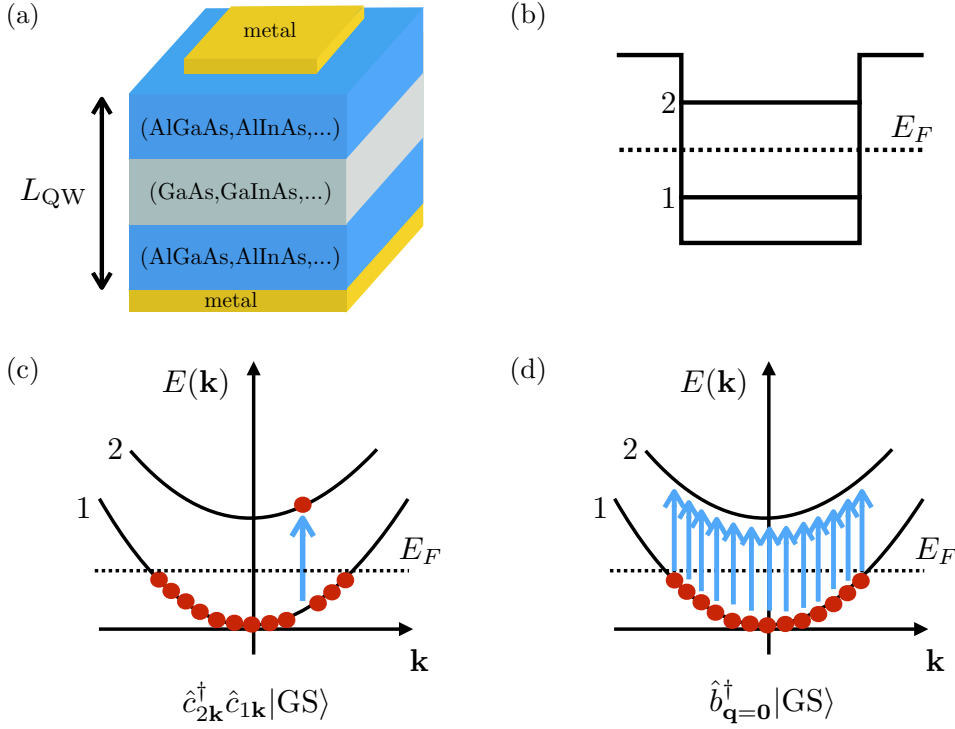


Figure II.1: Various representations of a quantum well. (a) Sketch of a quantum well showing a semiconductor (GaAs or GaInAs for instance), confined between two layers of another semiconductor with a wider gap (accordingly, AlGaAs or AlInAs). The length L_{QW} of one quantum well can range from few nm to tens of nm. The bottom metal layer and the top metal patch (array of patches for the full sample) play the role of cavity and can be engineered to confine light resonant with the intersubband electronic transitions. (b) Schematic of the quantum well in terms of a square potential, where we can see the two subbands labeled 1 and 2. E_F is the Fermi level. (c) Fermionic single-particle excitation $\hat{c}_{2\mathbf{k}}^\dagger \hat{c}_{1\mathbf{k}}$, the jump of an electron from the first to the second subband. (d) Fermionic collective excitation that can be described as a single bosonic one $\hat{b}_{\mathbf{q}=\mathbf{0}}^\dagger = \sqrt{\langle \hat{N}_1 \rangle - \langle \hat{N}_2 \rangle} \sum_{\mathbf{k}} \hat{c}_{2\mathbf{k}+\mathbf{q}}^\dagger \hat{c}_{1\mathbf{k}}$ [Todorov12a]. |GS⟩ stands for the ground state of the system.

(see Fig. II.1(a)). For instance, if this additional semiconductor can be made of AlGaAs or AlInAs for quantum wells respectively made of GaAs or GaInAs. In the simplest scenario, there are only two subbands available to the two-dimensional electron gas contained in the confined semiconductor, and these subbands are separated by the Fermi level (see Fig. II.1(b)). More complex level structures can be engineered with more than two subbands, as well as structures that superimpose many quantum wells [Todorov12b]. Note that in Fig. II.1(a) the interaction with light can only occur between the electrons and free space radiation, which can be mended by putting the sample between metallic patches that will confine light, thus forming a cavity.

II.2 General light-matter Hamiltonian in the Power-Zinau-Wooley representation

Here follows a brief review of the theoretical description of those systems. For a more detailed introduction, see [Todorov12a, Pegolotti14a]. We start by recalling the Hamiltonian describing the interaction light and particles of mass m_i and charge e in the Coulomb gauge [Cohen-Tannoudji89, Pegolotti14a],

$$\hat{H} = \hat{H}_{\text{mat}} + \hat{H}_{\text{ph}} + \hat{H}_{\text{int}}, \quad (\text{II.1})$$

standing, from left to right, for the Hamiltonian describing only the matter, then the Hamiltonian for the photons, and finally the Hamiltonian for their interaction. Their expressions are

$$\hat{H}_{\text{mat}} = \sum_i \frac{\hat{\mathbf{p}}_i^2}{2m_i}, \quad (\text{II.2})$$

$$\hat{H}_{\text{ph}} = \int \left(\frac{\epsilon_0 \epsilon_s \hat{\mathbf{E}}^2}{2} + \frac{\mu_0 \hat{\mathbf{H}}^2}{2} \right) d\mathbf{r}, \quad (\text{II.3})$$

$$\hat{H}_{\text{int}} = - \sum_i \frac{e \hat{\mathbf{p}}_i \cdot \hat{\mathbf{A}}}{m_i} + \sum_i \frac{e^2 \hat{\mathbf{A}}^2}{2m_i} + \hat{V}_{\text{Coulomb}}, \quad (\text{II.4})$$

where as in chapter I, ϵ_0 and μ_0 are respectively the vacuum permittivity and the vacuum permeability as in chapter I, and $\hat{\mathbf{E}}$ is the electric field. ϵ_s is the material permittivity, $\hat{\mathbf{p}}_i$ is the momentum operator for the i -th particle, $\hat{\mathbf{A}}$ is the vector potential, and $\hat{\mathbf{H}}$ is the magnetic field, proportional to the magnetic field $\hat{\mathbf{B}}$ defined in chapter I through the relation $\hat{\mathbf{B}} = \mu_0 \hat{\mathbf{H}}$ if the magnetic interactions are negligible in the material. The Coulomb interactions between the electrons can be expressed as

$$\hat{V}_{\text{Coulomb}} = \sum_{i \neq j} \frac{e^2}{4\pi\epsilon_0 |\hat{\mathbf{r}}_i - \hat{\mathbf{r}}_j|}, \quad (\text{II.5})$$

where $\hat{\mathbf{r}}_i$ is the position operator for the i -th particle. In what follows, we will use a different representation than the one used in Eqs. (II.2) (II.3) and (II.4). It is called the Power-Zinau-Wooley representation (or dipole representation) [Todorov12a, Pegolotti14a], and after one applies the appropriate transformation to the Hamiltonian, (II.3) and (II.4) become [Cohen-Tannoudji89, Pegolotti14a]

$$\hat{H}_{\text{ph}} = \int \left(\frac{\hat{\mathbf{D}}^2}{2\epsilon_0 \epsilon_s} + \frac{\mu_0 \hat{\mathbf{H}}^2}{2} \right) d\mathbf{r}, \quad (\text{II.6})$$

$$\hat{H}_{\text{int}} = - \int \frac{\hat{\mathbf{D}} \cdot \hat{\mathbf{P}}}{\epsilon_0 \epsilon_s} d\mathbf{r} + \int \frac{\hat{\mathbf{P}}^2}{2\epsilon_0 \epsilon_s} d\mathbf{r}, \quad (\text{II.7})$$

where $\hat{\mathbf{D}}$ is the displacement field operator, and $\hat{\mathbf{P}}$ is the polarization density operator. In Eq. (II.7), $- \int \hat{\mathbf{D}} \cdot \hat{\mathbf{P}} d\mathbf{r} / \epsilon_0 \epsilon_s$ is the light-matter interaction, while $\int \hat{\mathbf{P}}^2 d\mathbf{r} / 2\epsilon_0 \epsilon_s$ describes the self-interaction of the electronic polarization and contains the Coulomb interactions.

II.3 From a fermionic to a bosonic description of electronic excitations

We will now rewrite the Hamiltonian (II.1) in second quantization. For the electronic part in Eq. (II.2), the latter can be written

$$\hat{H}_{\text{mat}} = \sum_{i,\mathbf{k}} \hbar\omega_{i\mathbf{k}} \hat{c}_{i\mathbf{k}}^\dagger \hat{c}_{i\mathbf{k}}, \quad (\text{II.8})$$

where $\hat{c}_{i\mathbf{k}}$ ($\hat{c}_{i\mathbf{k}}^\dagger$) is a fermionic annihilation (creation) operator, such that $\{\hat{c}_{i\mathbf{k}}, \hat{c}_{j\mathbf{k}'}^\dagger\} = \delta_{i,j} \delta_{\mathbf{k},\mathbf{k}'}$. $\hbar\omega_{i\mathbf{k}} = \hbar\omega_i + \hbar^2 \mathbf{k}^2 / 2m^*$ is the total energy of the electron in the subband i with in plane wavevector \mathbf{k} (m^* is the effective mass of the electron). Here the simplest single particle excitation that can occur is one electron jumping from its subband to the immediate upper subband. Such an excitation can be described with the operator $\hat{c}_{i+1\mathbf{k}}^\dagger \hat{c}_{i\mathbf{k}}$ and is represented in Fig.II.1(c). However, in highly doped quantum wells where the electron gas is very dense, collective effects can arise, and in that case the electronic Hamiltonian can be rewritten in terms of bosonic excitations

$$\hat{H}_{\text{mat}} = \sum_{\alpha,\mathbf{q}} \hbar\omega_{\alpha\mathbf{q}} \hat{b}_{\alpha\mathbf{q}}^\dagger \hat{b}_{\alpha\mathbf{q}}, \quad (\text{II.9})$$

where α stands for a transition $i \rightarrow j$, and where $\hat{b}_{\alpha\mathbf{q}}$ is defined as a collective fermionic excitation

$$\hat{b}_{\alpha\mathbf{q}}^\dagger = \sqrt{\langle \hat{N}_i \rangle - \langle \hat{N}_j \rangle} \sum_{\mathbf{k}} \hat{c}_{j\mathbf{k}+\mathbf{q}}^\dagger \hat{c}_{i\mathbf{k}}. \quad (\text{II.10})$$

Essentially, it is a coherent excitation that induces the transition of all the electrons one one band to the next upper band, as can be seen in Fig. II.1(d).

II.4 Simplified Hamiltonian in the Power-Zinau-Wooley representation

While it does not removes the generality of the present study, in the rest of the chapter for the sake of simplicity we omit the sum over the in-plane wavevector \mathbf{q} , which amounts to consider the dipole approximation ($\mathbf{q} \ll \mathbf{k}$) [Pegolotti14a]. With this simplification, in the case where the quantum well is confined in a cavity, as represented in Fig. II.1, the total Hamiltonian (II.1) can be written in second quantization as

$$\hat{H} = \sum_{\alpha} \hbar\omega_{\alpha} \hat{b}_{\alpha}^\dagger \hat{b}_{\alpha} + \hbar\omega_a \hat{a}^\dagger \hat{a} + i \sum_{\alpha} \hbar\Omega_{\alpha} (\hat{a}^\dagger - \hat{a}) (\hat{b}_{\alpha}^\dagger + \hat{b}_{\alpha}) + \sum_{\alpha,\beta} \hbar B_{\alpha\beta} (\hat{b}_{\alpha}^\dagger + \hat{b}_{\alpha}) (\hat{b}_{\beta}^\dagger + \hat{b}_{\beta}), \quad (\text{II.11})$$

where ω_a is the cavity frequency, which mode is described by the annihilation (creation) operator \hat{a} (\hat{a}^\dagger). Ω_{α} is the so-called Rabi frequency for the light-matter coupling, while $B_{\alpha\beta}$ is the coupling frequency between intersubband excitations of different transitions. Note that in principle the cavity has also a wavevector dependence, that accordingly the the approximation above does not appear here. As in chapter I, we used the standard quantization of the Eq. (II.6) in terms of quantum harmonic oscillators. For the

explicit definition of the various frequencies shown in Eq. (II.11), we refer the reader to [Todorov12a, Pegolotti14a].

It is worthwhile noting here that one of the advantages of the Power-Zináu-Wooley representation of quantum electrodynamics is that the squared vector potential term, proportional to $(\hat{a}^\dagger + \hat{a})^2$, does not explicatively appear here. However, it is taken into account in Eq. (II.11) due to the Power-Zináu-Wooley transformation. In the standard representation of quantum electrodynamics, the squared vector potential contribution is explicit. One could switch Eq. (II.11) for the standard representation by simply changing the definitions of ω_α , ω_a , Ω_α and $B_{\alpha\beta}$, and adding the squared vector potential term $\hbar D(\hat{a}^\dagger + \hat{a})^2$ to the Hamiltonian [Ciuti05, Ciuti06].

II.5 Renormalization of the many-body excitation frequencies: the intersubband plasmons

Let us now introduce the so-called intersubband plasmons. These excitations are formally defined in the diagonalization of the matter part of the Hamiltonian (II.11), namely the first and the last terms of the right-hand side, but only for the case $\alpha = \beta$. This means that we search the eigenmodes of the system for each transition $i \rightarrow j$ separately. It also means that when the quantum well is only made of two levels, we thus have only one transition, for which we can define an intersubband plasmon. The motivation for defining such modes is that these have a physical origin and consequence. Indeed, when the electron gas has a high density and is submitted to an external electromagnetic radiation, each electron feels a depolarization field, an effective field induced by the excitation of the other electrons. This eventually induces a plasma-like oscillation for the electrons [Pegolotti14a] (and Refs. therein). This oscillation translates in a frequency shift $\omega_{\alpha,P}$ with respect to the electronic excitation frequencies ω_α , such that the resonance observed experimentally is the following renormalized one

$$\tilde{\omega}_\alpha = \sqrt{\omega_\alpha^2 + \omega_{\alpha,P}^2}, \quad (\text{II.12})$$

where $\omega_{\alpha,P}$ is the so-called plasma frequency [Todorov12a]. The diagonalization² thus gives us

$$\sum_\alpha \hbar \tilde{\omega}_\alpha \hat{p}_\alpha^\dagger \hat{p}_\alpha = \sum_\alpha \hbar \omega_\alpha \hat{b}_\alpha^\dagger \hat{b}_\alpha + \sum_{\alpha,\beta} \hbar B_{\alpha\alpha} (\hat{b}_\alpha^\dagger + \hat{b}_\alpha) (\hat{b}_\alpha^\dagger + \hat{b}_\alpha), \quad (\text{II.13})$$

where \hat{p}_α (\hat{p}_α^\dagger) is the annihilation (creation) operator of an intersubband plasmon associated to the transition α . The interaction between intersubband excitations of different subbands can be rewritten as

$$\sum_{\alpha \neq \beta} \hbar \Xi_{\alpha\beta} (\hat{p}_\alpha^\dagger + \hat{p}_\alpha) (\hat{p}_\beta^\dagger + \hat{p}_\beta) = \sum_{\alpha,\beta} \hbar B_{\alpha\beta} (\hat{b}_\alpha^\dagger + \hat{b}_\alpha) (\hat{b}_\beta^\dagger + \hat{b}_\beta). \quad (\text{II.14})$$

The light-matter interaction term in Eq. (II.11) can also be rewritten in terms of the intersubband plasmons operators \hat{p}_α and \hat{p}_α^\dagger , so that the full Hamiltonian can be expressed

²Not detailed here, but can be found in [Todorov12a, Pegolotti14a].

as

$$\hat{H} = \sum_{\alpha} \hbar\tilde{\omega}_{\alpha}\hat{p}_{\alpha}^{\dagger}\hat{p}_{\alpha} + \hbar\omega_a\hat{a}^{\dagger}\hat{a} + i \sum_{\alpha} \hbar\tilde{\Omega}_{\alpha}(\hat{a}^{\dagger} - \hat{a})(\hat{p}_{\alpha}^{\dagger} + \hat{p}_{\alpha}) + \sum_{\alpha \neq \beta} \hbar\Xi_{\alpha\beta}(\hat{p}_{\alpha}^{\dagger} + \hat{p}_{\alpha})(\hat{p}_{\beta}^{\dagger} + \hat{p}_{\beta}). \quad (\text{II.15})$$

For the exact expressions of $\tilde{\Omega}_{\alpha}$ and $\Xi_{\alpha\beta}$, we again refer the reader to [Todorov12a, Pegolotti14a]. In the following we will focus on two particular situations: one where the quantum well has only one transition, which drops the index α , and another situation where a quantum well with two transitions is considered (thus $\alpha = 1, 2$).

II.6 Two-level quantum well

II.6.1 The need for a time-modulated coupling

In a case where the quantum well has only two subbands, as pictured in Figs. II.1(a), II.1(b) and II.1(c), the Hamiltonian (II.15) is simplified to

$$\hat{H} = \hbar\omega_p\hat{p}^{\dagger}\hat{p} + \hbar\omega_a\hat{a}^{\dagger}\hat{a} + i\hbar\Omega(\hat{a}^{\dagger} - \hat{a})(\hat{p}^{\dagger} + \hat{p}), \quad (\text{II.16})$$

which is now simply a model of two coupled bosons, that we already encountered in chapter I. Indeed, we retrieve Eq. (I.16), with $\hat{A} = \hat{p}$. Here there is only one transition, thus we dropped the index α , and replaced $\tilde{\omega}_{\alpha}$ by ω_p , and $\tilde{\Omega}_{\alpha}$ by Ω for the sake of compactness.

In chapter I, we have seen that when the ultrastrong coupling (USC) regime is reached for the Hamiltonian (II.16), quantum correlations arise between the two-bosons even when the system is in the ground state. Our goal here is to study how one could extract these ground state correlations and observe them. In order to do so, the system would need to somehow emit excitations towards its surrounding environment, and these excitations would need to contain the information about these quantum correlations. This precise point is precisely tackled in the next chapter, since here only one side of the light-matter interaction can be observed. Indeed, the cavity mode described by the operator \hat{a} can emit electromagnetic radiation to its environment, that is a priori, observable by a measurement apparatus capable of measuring light from the terahertz to the mid-infrared part of the spectrum [Askenazi14]. However, the intersubband plasmon described by the operator \hat{p} on the other hand, can omit excitations only in a non-radiative way, since its environment, whose nature is more complex to define [Ciuti06], rather comes from non-radiative processes inside the solid-state samples due to phonons for instance [Ferreira89]. For this reason, in the remainder of this chapter we shall focus on the emission of light coming from the cavity. We will study this emission using input-output theory (see appendixes A and B), and seek for a way to obtain an output radiation with nonclassical properties.

However, we can already take a moment to comment on the emission that can occur in the model described by Eq. (II.16). Indeed, the first important element to note here is that even when the USC regime is reached, no squeezed radiation can be emitted from the system, unless the cavity was driven with a squeezed radiation in the first place [Ciuti06]. This comes from the fact that in Eq. (II.16), the coupling frequency Ω is time-independent, and the Hamiltonian itself is only quadratic, meaning that there is

no physical nonlinearity nor any parametric process involved. These last two elements are the key conditions to obtain a squeezed light emission. Note that a recent work proved that squeezing can be found in the output field coming from an ultrastrong light-matter interaction in a time independent case [Stassi16]. However, it was possible because the light was interacting with a qubit, which makes it a nonlinear interaction.

In our case here, for a time independent coupling, no matter how large the coupling Ω , and accordingly, no matter how many virtual photons are contained in the ground state, these photons cannot escape the cavity unless some sort of parametric process occurs in the system. This phenomenon is very much reminiscent of the Dynamical Casimir effect [Moore70, Kardar99], where originally the model concerned a cavity with one of the mirrors shaken in a relativistic fashion, such that the cavity could emit photons from the vacuum. The relativistic motion of the mirror could be a periodic vibration, and the frequency of this vibration would need to be of the same order of magnitude as the resonant frequency of the cavity, namely the frequency at which the photons escape. Translated to our quantum well problem, it means that in Eq. (II.16), we need at least one of the parameters to be modulated in time at some frequency ω_{mod} , of the same order of magnitude as ω_a . Such a direct identification can be made because what matters in the Dynamical Casimir effect is not to specifically relativistically move one of the cavity mirrors, but rather to perturb one or several parameters of the system in a non-adiabatic way [De Liberato09, Johansson09, Wilson11].

Modulating parameters in intersubband devices is an idea suggested [Ciuti05, Ciuti06] and theoretically explored a decade ago [De Liberato07]. In this paper, the authors studied the USC regime between intersubband excitations and cavity photons, with a periodic time dependence for the coupling, such that $\Omega(t) = \Omega_0 + \Omega_{\text{mod}}(t)$. For a non-zero modulation amplitude Ω_{mod} , yet not large enough to be in the USC regime, it was found that photons can be emitted from the vacuum, for modulation frequencies close to twice the bare system frequencies ω_a and ω_p . However, the noise properties of the light escaping the cavity were left unstudied. This is exactly the direction we will take later on, since finding noise reduction beyond the standard quantum limit in this system means that we are generating squeezed radiation in the terahertz band, a important step towards the development of quantum optics at this frequency range.

II.6.2 Model of a dispersive ultrastrong coupling regime

Here we shall explore this yet untouched direction by studying the noise properties of the output radiation in a model that contains a time modulated coupling, where one of the differences with the model studied in [De Liberato07], is that we shall examine the case where the modulated amplitude Ω_{mod} also reaches the USC regime, and therefore is comparable with the time independent coupling Ω_0 . Another difference in our model is that we introduce a new regime, called the dispersive ultrastrong coupling regime, which relies on the fact that here the frequency ω_p of the intersubband plasmon is smaller than both the cavity frequency ω_a and the modulation frequency ω_{mod} . Essentially, our model, based on the Hamiltonian (II.16) is given by the following Hamiltonian

$$\hat{H} = \hbar\omega_p\hat{p}^\dagger\hat{p} + \hbar\omega_a\hat{a}^\dagger\hat{a} + i\hbar\Omega(t)(\hat{a}^\dagger - \hat{a})(\hat{p}^\dagger + \hat{p}), \quad (\text{II.17})$$

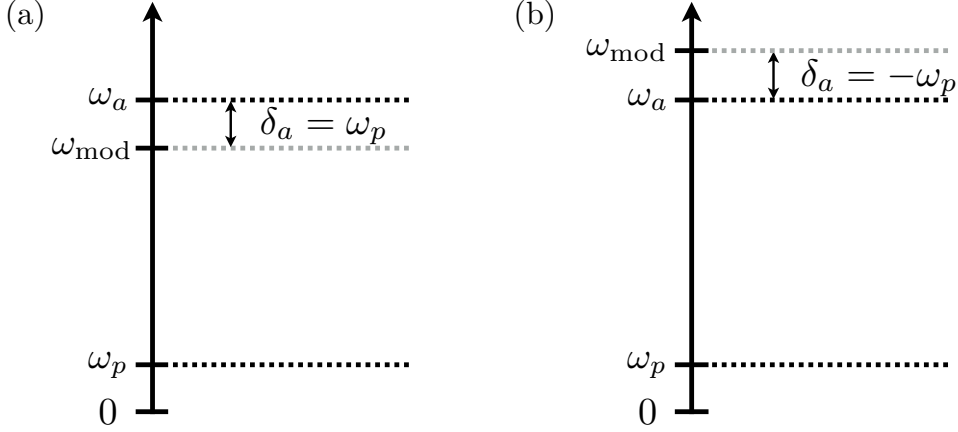


Figure II.2: Vertical representation of the different frequencies in the system for two resonance conditions. (a) $\delta_a = \omega_a - \omega_{\text{mod}} = \omega_p$. (b) $\delta_a = \omega_a - \omega_{\text{mod}} = -\omega_p$.

with

$$\Omega(t) = \Omega_0 + \Omega_{\text{mod}} \cos(\omega_{\text{mod}} t). \quad (\text{II.18})$$

The goal in having $\omega_p < \omega_a, \omega_{\text{mod}}$ is that we can study different kinds resonance conditions. The two main resonance conditions we are interested in are represented in Fig. II.2. Note that such a sinusoidal time-dependent coupling between two bosons was also considered in [Felicetti14] as a means to entangle artificial atoms.

Given the form of Eq. (II.17), an analogy can be made between our model and the nondegenerate optical parametric oscillator reviewed in chapter I. Indeed, the time modulated coupling in Eq. (II.17) plays the role of the pump field in Eq. (I.95).

Using the unitary transformation $\hat{U}(t) = e^{i\omega_{\text{mod}} \hat{a}^\dagger \hat{a} t}$, we can move to a frame rotating at ω_{mod} , with time dependent terms oscillating at ω_{mod} or at $2\omega_{\text{mod}}$

$$\begin{aligned} \hat{H}' &= \hbar \delta_a \hat{a}^\dagger \hat{a} + \hbar \omega_p \hat{p}^\dagger \hat{p} \\ &+ i \hbar \Omega_0 (\hat{a}^\dagger e^{i\omega_{\text{mod}} t} - \hat{a} e^{-i\omega_{\text{mod}} t}) (\hat{p}^\dagger + \hat{p}) \\ &+ i \frac{\hbar \Omega_{\text{mod}}}{2} (\hat{a}^\dagger e^{2i\omega_{\text{mod}} t} - \hat{a} e^{-2i\omega_{\text{mod}} t}) (\hat{p}^\dagger + \hat{p}) \\ &+ i \frac{\hbar \Omega_{\text{mod}}}{2} (\hat{a}^\dagger - \hat{a}) (\hat{p}^\dagger + \hat{p}), \end{aligned} \quad (\text{II.19})$$

where $\delta_a = \omega_a - \omega_{\text{mod}}$. We work in the regime where $\omega_p \sim |\delta_a|$, $\omega_p < \omega_{\text{mod}}$ and $\Omega_0, \Omega_{\text{mod}} \ll \omega_{\text{mod}}$, meaning that the terms oscillating at ω_{mod} and $2\omega_{\text{mod}}$ can be safely neglected using the rotating wave approximation. Consequently, we end up with the effective Hamiltonian

$$\hat{H}_{\text{eff}} = \hbar \delta_a \hat{a}^\dagger \hat{a} + \hbar \omega_p \hat{p}^\dagger \hat{p} + i \frac{\hbar \Omega_{\text{mod}}}{2} (\hat{a}^\dagger - \hat{a}) (\hat{p}^\dagger + \hat{p}). \quad (\text{II.20})$$

Now we have a Hamiltonian in a rotating frame, similar to the Hamiltonian (I.95) of a nondegenerate OPO, also in the rotating frame. As mentioned above, here ω_{mod} is analogous to the pump frequency for the OPO. One difference with the OPO however, is that

the interaction contains not only the two-mode squeezing term $i\hbar\Omega_{\text{mod}}(\hat{a}^\dagger\hat{p}^\dagger - \hat{a}\hat{p})/2$, but also the exchange interaction term $i\hbar\Omega_{\text{mod}}(\hat{a}^\dagger\hat{p} - \hat{a}\hat{p}^\dagger)/2$. Note that the Hamiltonian (II.20) shows great resemblance with a linearized optomechanical Hamiltonian in a rotating frame (see chapter IV).

Since here the intersubband plasmon is not at resonance with the cavity, and that we have $\omega_p < \omega_a$, the dispersive USC regime is achieved when $\Omega(t) \geq 0.1\omega_p$. However, given that in the rotating frame, only the modulation amplitude Ω_{mod} is relevant for our study, we shall consider the USC regime to be reached when $\Omega_{\text{mod}} \geq 0.1\omega_p$. It is now worthwhile to comment on the values that Ω_{mod} can take. In intersubband devices, the value of the total light-matter coupling $\Omega(t)$ is limited by the frequency ω_p , such that $\Omega(t) \leq \omega_p$. Additionally, the modulation amplitude Ω_{mod} cannot exceed the value of the time independent coupling Ω_0 , otherwise for $\cos(\omega_{\text{mod}}t) = -1$ we would get $\Omega(t) = \Omega_0 - \Omega_{\text{mod}} < 0$, and it is not possible to inverse the sign of the total light-matter coupling in intersubband devices. We are thus limited by $\Omega_0 + \Omega_{\text{mod}} < \omega_p$ and by $\Omega_0 \leq \Omega_{\text{mod}}$, therefore

$$\Omega_{\text{mod}} \leq \frac{\omega_p}{2}. \quad (\text{II.21})$$

II.6.3 Noise spectra

With the model being defined, we can now study the output radiation using input-output theory [Gardiner04], as we already used for the degenerate and the nondegenerate OPOs (see appendixes B and C). With this approach, the cavity mode is considered to have only vacuum input or thermal input, with an environment made of harmonic oscillators corresponding to all the modes of the electromagnetic field. For the intersubband plasmon however, defining its environment is less trivial [Ciuti06]. We consider here a model commonly used of an ensemble of harmonic oscillators modeling the non-radiative dissipation of the plasmon. The technical treatment in input-output theory is thus strictly equivalent to the one used for the cavity. This way, one can easily define equations of motions for the operators $\hat{a}(t)$ and $\hat{p}(t)$ and solve them in frequency space to obtain the output radiation $\hat{a}_{\text{out}}(\omega)$, and then the noise spectra for this output field. The equations of motion and the obtainment of the output field noise spectra are given in appendix D.

In Fig. II.3 we show the noise spectra for the output field $\hat{a}_{\text{out}}(\omega)$, as a function of various parameters. For the moment we consider only vacuum inputs, which is equivalent to state that the environment for both the cavity and the plasmon is at zero temperature. In Fig. II.3(a) the spectra for two conjugate quadratures $\hat{X}_{a,\phi=\pi/6}$ and $\hat{X}_{a,\phi=2\pi/3}$ ³ are shown as functions of the measurement frequency ω . It is the frequency at which the signal would be recorded in an experiment. A high degree of squeezing is shown, particularly for the quadrature $\hat{X}_{a,\phi=\pi/6}$ (solid line in Fig. II.3(a)). Note that in this figure the frequency $\omega/\omega_a = 0.1$ correspond to the resonance with the plasmon since here $\omega_p/\omega_a = 0.1$. Note that the value $\omega/\omega_a = -0.1$ simply correspond for the spectra to the symmetric counterpart of the resonance $\omega = \omega_p$. However, no squeezing dips are observed at $\omega = \pm\omega_p$ in Fig. II.3(a). The squeezing dips are in fact observed for frequencies close to $\omega = \pm\omega_p$, which is reminiscent of the vacuum Rabi

³For the definition of a field quadrature with an arbitrary phase ϕ , see Eq. (I.37).

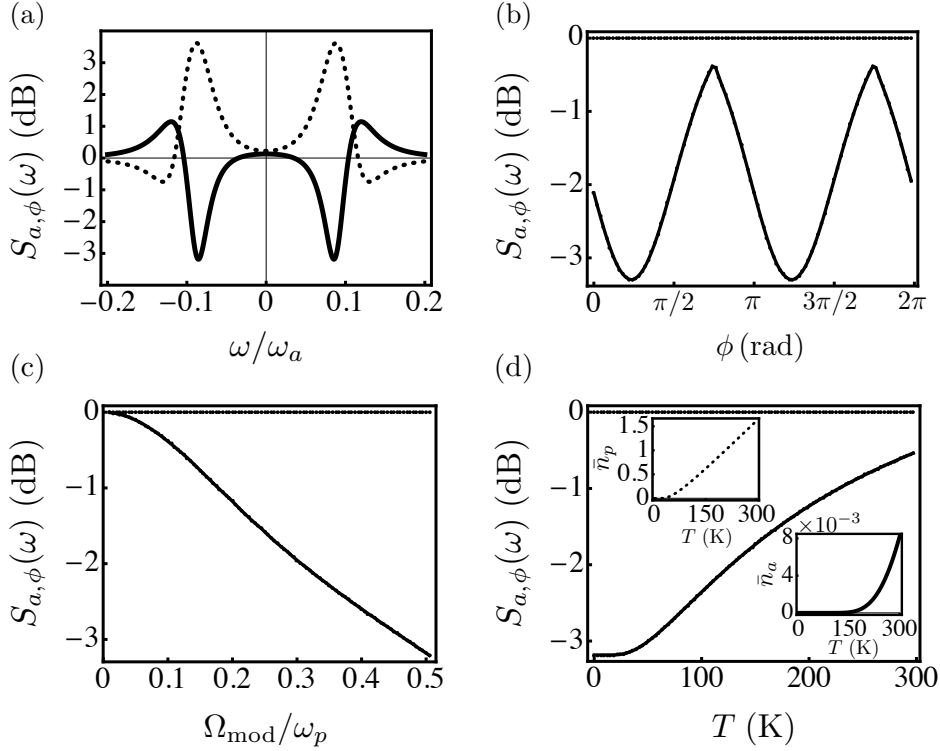


Figure II.3: Noise spectra $S_{a,\phi}(\omega)$ of the radiation emitted by a cavity containing an quantum well with one intersubband plasmon. The parameters are $\omega_p = 0.1\omega_a$, $\omega_{mod} = 0.9\omega_a$, $\gamma_a = \omega_a/10$, $\gamma_p = \omega_p/15$ (a) $S_{a,\phi=\pi/6}(\omega)$ (solid line) and $S_{a,\phi=2\pi/3}(\omega)$ (dotted line), for the conjugate quadratures $\hat{X}_{a,\pi/6}$ and $\hat{X}_{a,2\pi/3}$ (see Eq. (I.37)), as functions of the measurement frequency ω . Here $\Omega_{mod} = 0.5\omega_p$. (b) $S_{a,\phi}(\omega)$ as a function of the phase ϕ , for a fixed frequency ω that minimizes the value of $S_{a,\phi}(\omega)$. Here $\Omega_{mod} = 0.5\omega_p$. (c) $S_{a,\phi=\pi/6}(\omega)$ as a function of the modulation amplitude Ω_{mod} , for a fixed frequency ω that minimizes the value of $S_{a,\phi=\pi/6}(\omega)$. (d) $S_{a,\phi=\pi/6}(\omega)$ as a function of the temperature T for thermal inputs in both the cavity and the intersubband plasmon (see appendix D), again for a fixed frequency ω that minimizes the value of $S_{a,\phi=\pi/6}(\omega)$. Here $\Omega_{mod} = 0.5\omega_p$; $\omega_a = 30$ THz. Insets: thermal occupation numbers \bar{n}_p (dotted line) and \bar{n}_a (solid line) for both the plasmon and the cavity inputs, as functions of the temperature T .

splitting discussed in chapter I, where due to the ultrastrong coupling, the system was not resonant any more at the bare resonance frequency, but since the resonant splits.

Yet, here the situation is slightly different that the one encountered in chapter I. Indeed, in the standard USC regime, we would have

$$\omega_a = \omega_p. \quad (\text{II.22})$$

It means that the cavity is resonant with the intersubband plasmon, which is the regime explored so far in experiments [Günter09, Todorov09, Anappara09, Askenazi14]. In that case the Rabi splitting occurs around the frequency $\omega_a = \omega_p$. In our work however,

we explore a new and original regime where the cavity and the plasmon are far from resonance, and in Fig. II.3(a) we have $\omega_p = 0.1\omega_a$. Therefore, the resonance condition used for our dispersive USC regime is

$$\delta_a = \omega_p, \quad (\text{II.23})$$

where $\delta_a = \omega_a - \omega_{\text{mod}}$. This resonance condition is the key point for obtaining output squeezing from the dispersive USC regime. Indeed, $\delta_a = \omega_p$ means that in the rotating frame we mimic the resonance (II.22) of standard USC regime, and, squeezed photons can escape the cavity from vacuum because we are non-adiabatically perturbing the light-matter coupling in time, thus giving enough energy for the system to release the photons. In other words, we achieve a parametric process very reminiscent to what is achieved in an OPO. Yet the difference with an OPO is that here we see some signatures of the USC regime in the squeezing spectrum, i.e., the splitting observed in Fig. II.3(a) around $\omega = \pm\omega_p$.

In Fig. II.3(b) we study how the squeezing changes with the quadrature phase ϕ , where for each value of ϕ we used a value of ω that was optimized to minimize $S_{a,\phi}(\omega)$. We have used the same optimization to plot $S_{a,\phi=\pi/6}(\omega)$ as a function of the modulation amplitude Ω_{mod} in Fig. II.3(c). There we can notice that the squeezing definitely become more significant after reaching the dispersive USC regime. Indeed, we can see in Fig. II.3(c) that when $\Omega_{\text{mod}}/\omega_p = 0.1$, the squeezing is around -0.5dB .

II.6.4 Influence of the temperature

We also studied the influence of the temperature on the squeezing, that we report in Fig. II.3(d). To include a dependence on the temperature, we consider thermal inputs for both the cavity and the plasmon (see appendix D). This is characterized by the thermal populations $\bar{n}_a = 1/(\exp(\hbar\omega_a/k_B T) - 1)$ and $\bar{n}_p = 1/(\exp(\hbar\omega_p/k_B T) - 1)$. These are shown as functions of the temperature in Fig. II.3(d) as insets. We can see that even at $T = 300\text{ K}$ the cavity thermal population is negligible, with $\bar{n}_a = 8 \times 10^{-3}$, and although the plasmon one is rather small, with $\bar{n}_p = 1.5$, it is enough to decrease the squeezing from $\sim -3.2\text{ dB}$ to $\sim -0.6\text{ dB}$. Note that we have $\bar{n}_p \ll \bar{n}_a$ because of the large detuning between ω_p and ω_a , enough so that the plasmon is more prone to the effects of temperature than the cavity.

II.6.5 Influence of the modulation frequency

Previously we have seen that the resonance condition in Eq. (II.23) allows us to define a dispersive USC regime, and extract squeezed photons from the cavity. Here we study how a change in the value of ω_{mod} could influence the squeezing spectrum $S_{a,\phi}(\omega)$. Note that a change in ω_{mod} thus changes the value of δ_a , and consequently, the condition (II.23) for the dispersive USC would not be verified anymore. In Fig. II.4(a) we show how the squeezing changes with the quadrature phase ϕ , similarly to what we have done in Fig. II.3(b), yet here we have $\omega_{\text{mod}} = 1.1\omega_a$. Thus the resonance condition (II.23) becomes $\delta_a = -\omega_p$ (see Fig. II.2(b)). By comparing Fig. II.3(b) and Fig. II.4(a), we can see that the phase ϕ minimizing $S_{a,\phi}(\omega)$ has been shifted, and more importantly, that the maximal amount of reachable squeezing has been drastically reduced, coming

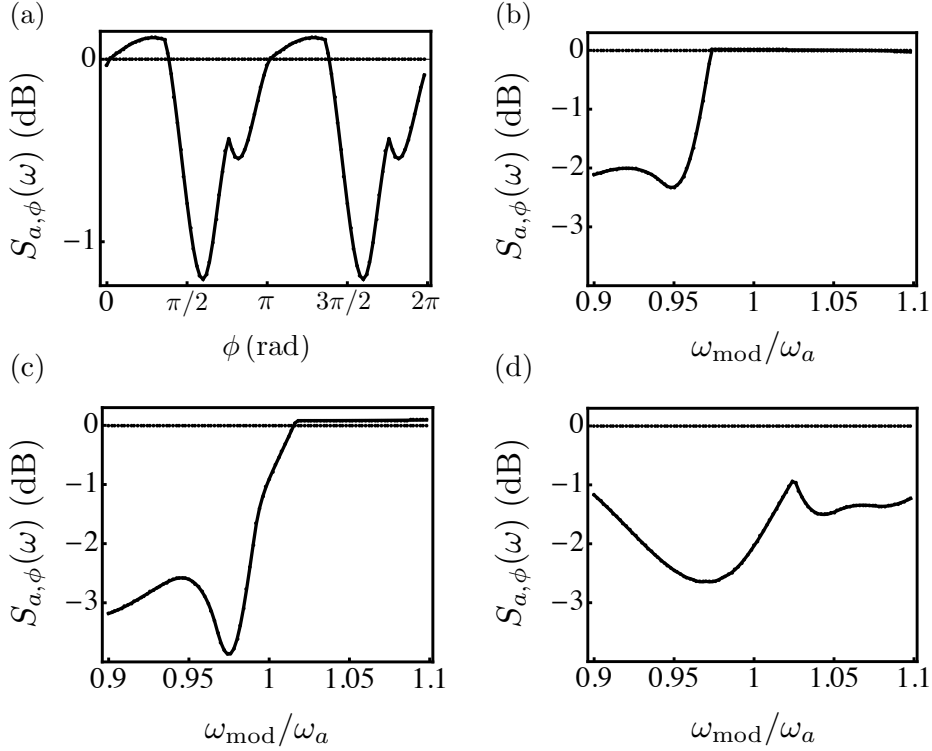


Figure II.4: Noise spectra $S_{a,\phi}(\omega)$ of the radiation emitted by a cavity containing an quantum well with one intersubband plasmon. The parameters are $\omega_p = 0.1\omega_a$, $\gamma_a = \omega_a/10$, $\gamma_p = \omega_p/15$, $\Omega_{\text{mod}} = 0.5\omega_p$, $T = 0$. (a) $S_{a,\phi}(\omega)$ as a function of the phase ϕ , for a fixed frequency ω that minimizes the value of $S_{a,\phi}(\omega)$. Here $\omega_{\text{mod}} = 1.1\omega_a$. (b)-(d) $S_{a,\phi}(\omega)$ as a function of the modulation frequency Ω_{mod} , for a fixed frequency ω that minimizes the value of $S_{a,\phi}(\omega)$. (b) $\phi = 0$. (c) $\phi = \pi/6$. (d) $\phi = 0.6\pi$.

from ~ -3.3 dB in Fig. II.3(b) to ~ -1.2 dB in Fig. II.4(a).

To study this question further, we show in Figs. II.4(b), II.4(c), and II.4(c) the noise spectrum $S_{a,\phi}(\omega)$ as a function of the modulation frequency ω_{mod} , for three values of ϕ . We notice that in general the amount of squeezing is drastically reduced in the region $\omega_{\text{mod}} > \omega_a$, and that the amount of squeezing is maximized (thus $S_{a,\phi}(\omega)$ is minimized) in the region $\omega_{\text{mod}} < \omega_a$. In Figs. II.4(b), II.4(c), and II.4(d) we do not go below $\omega_{\text{mod}} = 0.9\omega_a$ since it may jeopardize the validity of the input-output theory (see appendixes A and D).

Note that both resonance conditions $\delta_a = \omega_p$ (see Fig. II.2(a)) and $\delta_a = -\omega_p$ (see Fig. II.2(b)) are reminiscent of the so-called red-detuned and blue-detuned regimes in optomechanics [Aspelmeyer14]. It is well known that the blue-detuned regime lead to two-mode squeezing [Palomaki13b, Aspelmeyer14], but not to single-mode squeezing. Thus here we have shown that in the red-detuned regime, when the coupling is high enough not to neglect the counter rotating terms, and when this coupling is varied in time in a nonadiabatic way, optimal single-mode squeezing is extracted from the system.

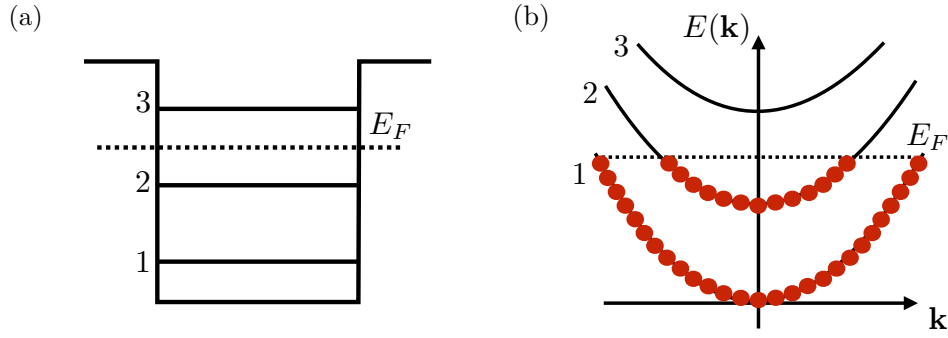


Figure II.5: Quantum well with three subbands. (a) Schematic of the quantum well in terms of a square potential, with the three subbands labeled 1, 2 and 3. (b) Band diagram of the quantum well. E_F stands for the Fermi level.

II.7 Three-level quantum well

II.7.1 An additional diagonalization

Quantum wells can be engineered to have more than two subbands. In what remains of this chapter we are interested in a case where the quantum well has three subbands; although there can be more. Such a system is pictured in Fig. II.5, and using Eq. (II.15), the Hamiltonian can be written as

$$\begin{aligned} \hat{H} = & \hbar\tilde{\omega}_1\hat{p}_1^\dagger\hat{p}_1 + \hbar\tilde{\omega}_2\hat{p}_2^\dagger\hat{p}_2 + \hbar\omega_a\hat{a}^\dagger\hat{a} \\ & + i\hbar\tilde{\Omega}_1(\hat{a}^\dagger - \hat{a})(\hat{p}_1^\dagger + \hat{p}_1) + i\hbar\tilde{\Omega}_2(\hat{a}^\dagger - \hat{a})(\hat{p}_2^\dagger + \hat{p}_2) \\ & + \hbar\Xi_{12}(\hat{p}_1^\dagger + \hat{p}_2)(\hat{p}_1^\dagger + \hat{p}_2). \end{aligned} \quad (\text{II.24})$$

In this Hamiltonian we can see that the electron gas has two collective excitations at two different frequencies. Thus, in principle one should be able to detect these resonances in an experiment. However, lately, surprising results were reported where one single resonance was observed instead, at a frequency different from the intersubband plasmon ones [Delteil12]. No matter how many intersubband resonances are predicted for the system, the single sharp resonance that is observed has a frequency distinguishable from them by a significant shift [Delteil12]. It turns out that this new excitation is a collective mode of the intersubband plasmons, called *multisubband plasmon*, and is essentially a cooperative oscillation of the excitations populations in the different subbands. In fact, it was proven that the multisubband plasmons are described by operators that diagonalize the electronic part of the Hamiltonian [Pegolotti14b, Pegolotti14a]. For our situation with two transitions, this gives

$$\hbar W_1\hat{P}_1^\dagger\hat{P}_1 + \hbar W_2\hat{P}_2^\dagger\hat{P}_2 = \hbar\tilde{\omega}_1\hat{p}_1^\dagger\hat{p}_1 + \hbar\tilde{\omega}_2\hat{p}_2^\dagger\hat{p}_2 + \hbar\Xi_{12}(\hat{p}_1^\dagger + \hat{p}_2)(\hat{p}_1^\dagger + \hat{p}_2), \quad (\text{II.25})$$

where $\hat{P}_{1,2}$ are the annihilation operators describing the multisubband plasmons. Here the diagonalization procedure is rather common. However, when a large number of plasmons is considered, the diagonalization is less straightforward, and for details on the

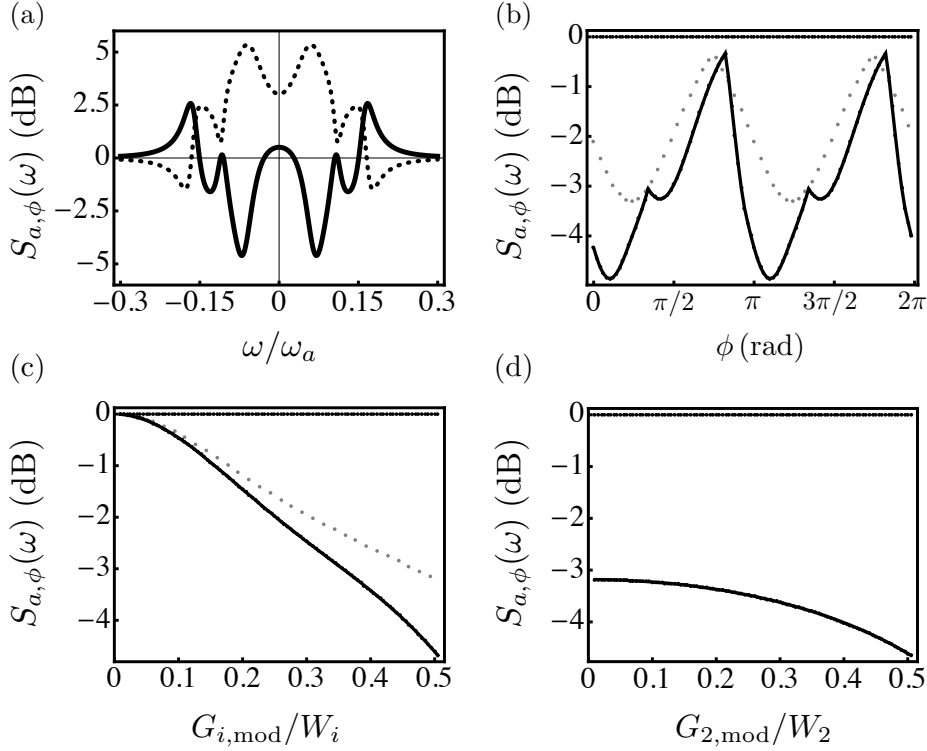


Figure II.6: Noise spectra $S_{a,\phi}(\omega)$ of the radiation emitted by a cavity containing an quantum well with two subbands. The parameters are $W_1 = 0.1\omega_a$, $W_2 = 0.15\omega_a$, $\omega_{\text{mod}} = 0.9\omega_a$, $\gamma_a = \omega_a/10$, $\gamma_1 = W_1/15$, $\gamma_2 = W_2/15$ (a) $S_{a,\phi=\pi/6}(\omega)$ (solid line) and $S_{a,\phi=2\pi/3}(\omega)$ (dotted line), for the conjugate quadratures $\hat{X}_{a,\pi/6}$ and $\hat{X}_{a,2\pi/3}$ (see Eq. (I.37)), as functions of the measurement frequency ω . Here $G_{1,\text{mod}}/W_1 = G_{2,\text{mod}}/W_2 = 0.5$. (b) $S_{a,\phi}(\omega)$ (black solid line) as a function of the phase ϕ , for a fixed frequency ω that minimizes the value of $S_{a,\phi}(\omega)$. Here $G_{1,\text{mod}}/W_1 = G_{2,\text{mod}}/W_2 = 0.5$. (c) $S_{a,\phi=\pi/6}(\omega)$ (black solid line) as a function of the ratio $G_{1,\text{mod}}/W_1 = G_{2,\text{mod}}/W_2$, for a fixed frequency ω that minimizes the value of $S_{a,\phi=\pi/6}(\omega)$. (b),(c) The gray dotted line stands for the results for a quantum well with only two subbands shown already in Fig. II.3(b) and II.3(c). (d) $S_{a,\phi=\pi/6}(\omega)$ as a function of the ratio $G_{2,\text{mod}}/W_2$, for $G_{1,\text{mod}}/W_1 = 0.5$ and a fixed frequency ω that minimizes the value of $S_{a,\phi=\pi/6}(\omega)$.

procedure in the general case, see [Pegolotti14b, Pegolotti14a]. The Hamiltonian (II.24) can be entirely rewritten in terms of the multisubband plasmons and of the cavity mode

$$\begin{aligned} \hat{H} = & \hbar W_1 \hat{P}_1^\dagger \hat{P}_1 + \hbar W_2 \hat{P}_2^\dagger \hat{P}_2 + \hbar \omega_a \hat{a}^\dagger \hat{a} \\ & + i\hbar G_1 (\hat{a}^\dagger - \hat{a}) (\hat{P}_1^\dagger + \hat{P}_1) + i\hbar G_2 (\hat{a}^\dagger - \hat{a}) (\hat{P}_2^\dagger + \hat{P}_2), \end{aligned} \quad (\text{II.26})$$

Where the only interaction explicitly appearing here is the one between between the cavity and each of the plasmons.

II.7.2 Dispersive USC with multisubband plasmons

Now that we have the diagonalized Hamiltonian (II.26), we can use it to study the dispersive USC regime, by introducing time-dependent light-matter couplings $G_1(t)$ ($G_2(t)$) with the modulation amplitudes $G_{1,\text{mod}}$ ($G_{2,\text{mod}}$) and modulation frequency ω_{mod}

$$\begin{aligned} \hat{H} = & \hbar W_1 \hat{P}_1^\dagger \hat{P}_1 + \hbar W_2 \hat{P}_2^\dagger \hat{P}_2 + \hbar \omega_a \hat{a}^\dagger \hat{a} \\ & + i\hbar G_1(t) (\hat{a}^\dagger - \hat{a}) (\hat{P}_1^\dagger + \hat{P}_1) + i\hbar G_2(t) (\hat{a}^\dagger - \hat{a}) (\hat{P}_2^\dagger + \hat{P}_2), \end{aligned} \quad (\text{II.27})$$

with

$$\begin{cases} G_1(t) = G_{1,0} + G_{1,\text{mod}} \cos(\omega_{\text{mod}} t), \\ G_2(t) = G_{2,0} + G_{2,\text{mod}} \cos(\omega_{\text{mod}} t). \end{cases} \quad (\text{II.28})$$

We work in the same regime as in section II.6, namely where $W_{1,2} \sim \delta_a$, $W_{1,2} < \omega_{\text{mod}}$ and $G_{0,1}, G_{0,2}, G_{1,\text{mod}}, G_{2,\text{mod}} \ll \omega_{\text{mod}}$. We can thus use the same unitary transformation $\hat{U}(t) = e^{i\omega_{\text{mod}} \hat{a}^\dagger \hat{a} t}$, and here again discard the fast oscillating terms at ω_{mod} and $2\omega_{\text{mod}}$ in order to obtain an effective Hamiltonian in a rotating frame

$$\begin{aligned} \hat{H}_{\text{eff}} = & \hbar \delta_a \hat{a}^\dagger \hat{a} + \hbar W_1 \hat{P}_1^\dagger \hat{P}_1 + \hbar W_2 \hat{P}_2^\dagger \hat{P}_2 \\ & + i \frac{\hbar G_{1,\text{mod}}}{2} (\hat{a}^\dagger - \hat{a}) (\hat{P}_1^\dagger + \hat{P}_1) + i \frac{\hbar G_{2,\text{mod}}}{2} (\hat{a}^\dagger - \hat{a}) (\hat{P}_2^\dagger + \hat{P}_2). \end{aligned} \quad (\text{II.29})$$

For the study of the dispersive USC regime, we have the same limitation for $G_{1,\text{mod}}$ and $G_{2,\text{mod}}$ as we had for Ω_{mod} in section II.6

$$G_{i,\text{mod}} \leq \frac{W_i}{2}. \quad (\text{II.30})$$

II.7.3 Noise spectra

As we did for the intersubband plasmon case in section II.6, we can also study the output noise spectra of the system by applying the same method as in appendix D, using input-output theory [Gardiner04]. We can thus obtain the output field $\hat{a}_{\text{out}}(\omega)$ in frequency, and compute the noise spectra using vacuum or thermal inputs for $\hat{a}_{\text{in}}(\omega)$, $\hat{P}_{1,\text{in}}(\omega)$ and $\hat{P}_{2,\text{in}}(\omega)$. Here the dissipation rates for \hat{P}_1 and \hat{P}_2 are respectively γ_1 and γ_2 .

In Fig. II.6 we show the noise spectra for the output field $\hat{a}_{\text{out}}(\omega)$, as a function of various parameters. For the moment we consider only vacuum inputs, which is equivalent to state that the environment for both the cavity and the plasmon is at zero temperature. In Fig. II.6(a) the spectra for two conjugate quadratures $\hat{X}_{a,\phi=\pi/6}$ and $\hat{X}_{a,\phi=2\pi/3}$ are shown as functions of the measurement frequency ω . The degree of squeezing that is shown is higher than in Fig. II.3(a). Note that in this figure the first multisubband plasmon is at $W_1/\omega_a = 0.1$ (which is equivalent to having $\omega_p/\omega_a = 0.1$ in Fig. II.3(a)). However, now there is a second matter excitation, \hat{P}_2 , and we consider the case $W_2/\omega_a = 0.15$. Thus, instead of having two resonances on each side of the spectrum as in Fig. II.3(a), now we have three resonances on each side of the spectrum.

In Fig. II.6(b) we study again how the squeezing, optimal with respect to ω , changes

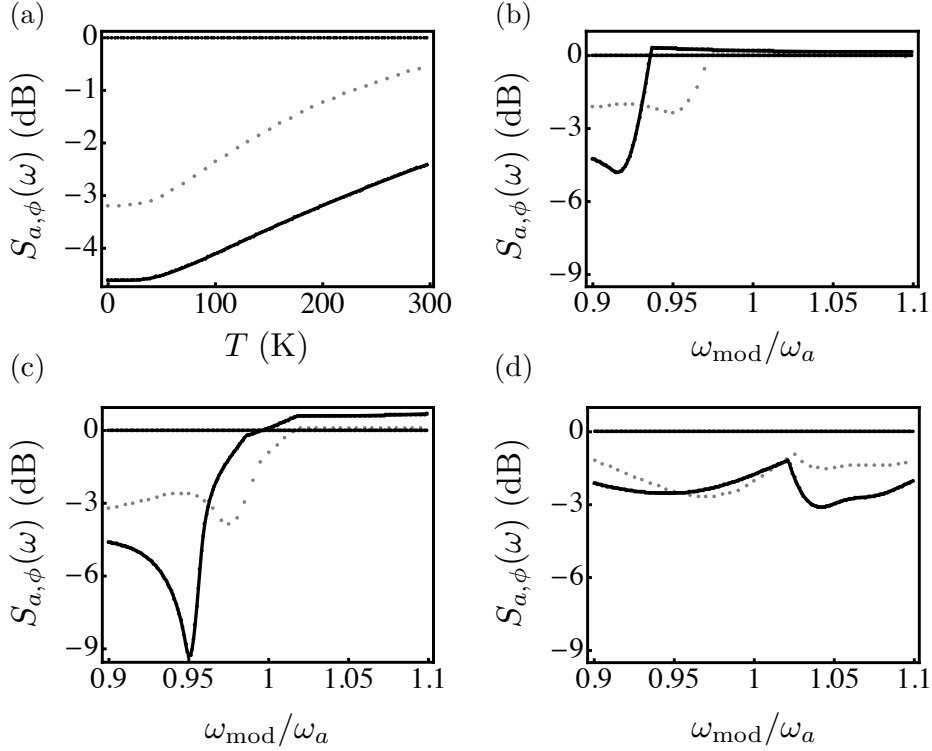


Figure II.7: Noise spectra $S_{a,\phi}(\omega)$ of the radiation emitted by a cavity containing an quantum well with one intersubband plasmon. The parameters are $W_1 = 0.1\omega_a$, $W_2 = 0.15\omega_a$, $\gamma_a = \omega_a/10$, $\gamma_1 = W_1/15$, $\gamma_2 = W_2/15$, $G_{1,\text{mod}}/W_1 = G_{2,\text{mod}}/W_2 = 0.5$. (a) $S_{a,\phi=\pi/6}(\omega)$ as a function of the temperature T for thermal inputs in both the cavity and the intersubband plasmon (see appendix D), again for a fixed frequency ω that minimizes the value of $S_{a,\phi=\pi/6}(\omega)$. Here $\omega_a = 30$ THz. (b)-(d) $S_{a,\phi}(\omega)$ as a function of the modulation frequency Ω_{mod} , for a fixed frequency ω that minimizes the value of $S_{a,\phi}(\omega)$, with $T = 0$. (b) $\phi = 0$. (c) $\phi = \pi/6$. (d) $\phi = 0.6\pi$.

with the quadrature phase ϕ (black solid curve), and we compare it with the case studied in Fig. II.3(b) with only one plasmon (gray dotted curve). We notice again that the amount of squeezing has increased with respect to the situation considered in section II.6. We also show the squeezing for both the three level quantum well (black solid curve) and, for comparison, the two level quantum well (gray dotted curve) in Fig. II.3(c) as functions of the ratios $G_{1,\text{mod}}/W_1 = G_{2,\text{mod}}/W_2$. For the sake on completeness we show in Fig. II.3(d) the noise spectrum $S_{a,\phi=\pi/6}(\omega)$ for a situation where we start from $G_{1,\text{mod}}/W_1 = 0.5$ and increase $G_{2,\text{mod}}/W_2$ from 0 to 0.5, which clearly shows how including a second plasmon has increased the squeezing.

II.7.4 Influence of the temperature

We included the influence of the temperature in the same manner as we did in section II.6.4, by considering thermal inputs for $\hat{a}_{\text{in}}(\omega)$, $\hat{P}_{1,\text{in}}(\omega)$ and $\hat{P}_{2,\text{in}}(\omega)$. The optimal noise spectra $S_{a,\phi=\pi/6}(\omega)$ with respect to ω is shown on Fig. II.7(a) (black solid curve),

as a function of the temperature. For comparison we also added in Fig. II.7(a) the noise spectrum for the two level quantum well case already studied in section II.6.4 (gray dotted curve). We can see that going from the two level quantum well to the three level quantum well the noise spectrum has been shifted by an approximate amount of -1.5 dB. Therefore, even at 300 K we have a large degree of squeezing between -2.5 and -3 dB.

II.7.5 Influence of the modulation frequency

Here we study how a change in the value of ω_{mod} influences the squeezing. We show in Figs. II.7(b), II.7(c) and II.7(d) the noise spectrum $S_{a,\phi}(\omega)$ as a function of the modulation frequency ω_{mod} (black solid curve), for three values of ϕ . For comparison we also added in Figs. II.7(b), II.7(c) and II.7(d) the noise spectrum for the two level quantum well case already studied in section II.6.5 (gray dotted curve). In general, as for the two level quantum well here the squeezing is reduced as we go from $\omega_{\text{mod}} = 0.9\omega_a$ to $\omega_{\text{mod}} = 1.1\omega_a$, except in Fig. II.7(d). In Fig. II.7(b) and II.7(c) the squeezing for the three level quantum well is more significant than for the two level one, in particular in Fig. II.7(c) where it exceeds -9 dB.

II.8 Experimental implementation

Before concluding this chapter, write few words on an experimental implementation of our model. At first sight, without the time dependent coupling, the experimental implementation of both the two level quantum well and the three level quantum well confined in a cavity are straightforward, since it corresponds to the standard USC regime that has already been achieved in cavity embedded semi-conductor quantum wells [Delteil12, Askenazi14]. However, in order to fully implement the model studied in this thesis we need to include a modulation in time of the coupling (or the couplings for the three level quantum well case), which is crucial in order to extract squeezing from the system. For this one needs to change the light-matter interaction on a time scale comparable with the oscillation time of the light. Although such a specific scheme has not been demonstrated yet, first demonstrations of time-dependent light-matter interaction turned on in an ultrafast time scale were observed in [Günter09, Porer12]. Even if this is not the exact time dependency discussed in this manuscript, these realizations indicates the possibility of implementing different time dependent light-matter couplings, which is the essential ingredient to the emergence of the ultrastrong limit as described in our model. In addition, the theoretical study of the generation of squeezed states within the framework of already experimentally observed time dependent couplings is an interesting perspective for a future work, but not in the scope of this thesis. Regarding squeezing detection, although the state of the art of homodyne detection in the THz and mid-IR ranges is not as advanced as the one involving optical frequencies, experimental demonstrations with the retrieving of both amplitude and phase information exist [Riek15]. One can thus be optimistic about the application of that experimental result to the detection of squeezing. We stress that although it is possible to produce THz electromagnetic waves for such frequencies by using regular non-degenerate OPOs, the generation of single mode squeezed states in this frequency range remains unexploited

and unachievable in such experiments [Kawase01, Edwards06, Molter09]. At last, although the chapter is plainly focused on cavity embedded semi-conductor quantum wells, it is worth to mention that the model presented here can be fully implemented in superconducting circuits. We do not detail this implementation here since the next chapter is plainly focused on superconducting circuits.

II.9 Conclusion

In this chapter we have presented how the many-body properties of semi-conductor quantum wells can give rise to bosonic excitations that can be ultrastrongly coupled to the radiation confined in a cavity mode. Using the fact that these devices can reach the USC regime, we have introduced the dispersive USC regime, a new regime of light-matter interactions. In this regime, the free oscillation frequencies of light and matter have a large detuning, instead of being resonant as in the standard USC regime. The second ingredient of this regime is a time-dependent light-matter coupling, modulated at a particular frequency close to the cavity frequency. These two ingredients, the detuning and the time modulated coupling, are crucial in our model as they allow us to find a judicious resonance condition between the matter, light and modulation frequencies, responsible for a parametric process reminiscent of the Dynamical Casimir effect, at the origin of the emission of squeezed light from the system. We analyse in detail this output squeezing, by studying the influence of the modulated coupling strength, the temperature, as well as the modulation frequency. We also considered two distinct cases, where the quantum well has one transition in the first case and two transitions in the second one, which showed that the latter increases the amount of squeezing which respect to the first case. With the perspective of improvement of the detection and of the capability in modulating the light-matter coupling on a very short timescale, squeezed light in these frequencies may be used for spectroscopy [Yasui06], interferometry [Rakić13], or precision measurements [Hoshina08]. One perspective of this work can be a generalization to quantum wells with an arbitrary number of transitions, but was not the scope of our study. Another natural perspective of our results is investigating the possibility of two mode squeezed states generation in the ultrastrong coupling regime, namely extracting not only the one-photon correlations in the ground but also the light-matter correlations. This perspective is thoroughly developed in the next chapter. Finally, we mention that the model developed in this chapter could in principle be realized in a different physical platform, namely superconducting circuits. We did not need to develop this additional implementation here as the next chapter tackles this problem.

III Quantum simulated ultrastrong coupling regime in superconducting circuits

In this chapter we shall continue the subject started in the previous chapter, focused on studying how the ultrastrong coupling (USC) regime can lead to squeezed states. In the previous study, due to the constraints of intersubband devices, we were only able to study one party, among the two, involved in the light-matter interaction (see chapter II). Therefore, the potential entanglement that could occur between the two parties could not be extracted as output to be measured. Here, we will get rid of the previous constraints by considering a different physical platform for the implementation of our model. This platform is a superconducting circuits architecture [Flurin12, Flurin14], where both parties of the light-matter interactions will be played by two microwave resonators. Indeed, instead of having a genuine light-matter USC regime, we will derive a model for a light-light USC regime, that will simulate the Hamiltonian of a true USC regime. Given the characteristics of this device, this quantum simulation will allow us to reach the USC regime in a particular rotating frame, where in the laboratory frame the actual physical interaction is not in the USC regime. Additionally, the coupling between the two modes appears as time independent in the rotating frame while being actually modulated in time in the laboratory frame, which as we saw in the previous chapter will allow us to extract radiation from the system. The work reported here has been published in [Fedortchenko17].

We start by briefly presenting the superconducting circuit architecture using as a platform for our model, that we thoroughly detail afterwards. We then show and describe the results we obtained, and study them under the influence of several physical parameters. The prerequisites for the present chapter are the same as for chapter I, as well as the notions seen in the latter.

III.1 Superconducting circuits as tools for quantum information and quantum optics

After the fruitful development of cavity quantum electrodynamics since the seventies (see chapter I), alternative physical platforms have emerged, capable of contributing to both the fundamental and practical studies of various quantum physics phenomena. One of them is based on superconducting architectures. Hereafter we briefly review the description of those systems in general, and then focus on the specific architecture we studied in this thesis.

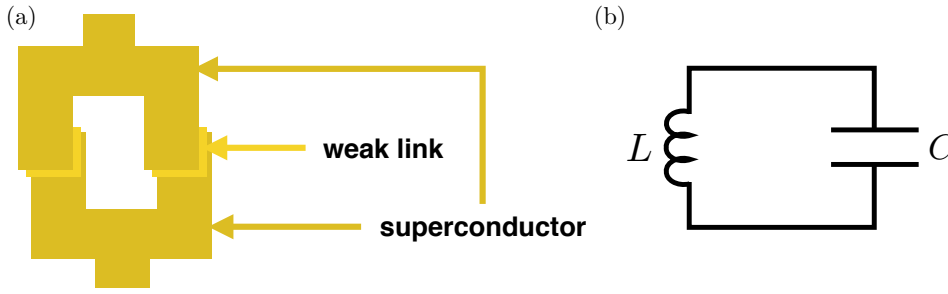


Figure III.1: Schematic of a SQUID (superconducting quantum interference device) containing two Josephson junctions. The weak link refers to a non-superconducting material, and may be an insulator, or a semiconductor for instance. (b) Schematic of an LC circuit made of a capacitor with capacitance C and of an inductive coil with inductance L .

III.1.1 The Josephson junction

In order to understand how superconducting circuits operate, one has to turn to its most basic element, the Josephson junction. It is based on the Josephson effect, predicted in 1962 [Josephson62] and experimentally demonstrated shortly after [Anderson63]. The effect itself consists in a supercurrent flowing through a device made of a superconductor separated by a weak link, a layer of a non-superconducting material (see Fig. III.1(a)). The supercurrent is essentially a tunneling of electrons, Cooper pairs, through the weak link. Since its discovery, this phenomenon has been used in a variety of applications, such as for the development of SQUIDs (superconducting quantum interference devices) for instance [Jaklevic64], useful to measure very small magnetic fields. However, here we are interested in its applications in quantum information and quantum optics, which started when the quantization of a variable describing the electric current in a Josephson junction was demonstrated [Martinis85]. It was an unprecedented result, since it showed that a macroscopic variable, in the sense that it is a variable describing a current made of many electrons, can be quantized and described as a quantum harmonic oscillator [Flurin14].

III.1.2 The quantum LC circuit

The Hamiltonian of a quantum LC circuit, represented in Fig. III.1(b) is

$$\hat{H} = \frac{\hat{Q}^2}{2C} + \frac{\hat{\Phi}^2}{2L}, \quad (\text{III.1})$$

where C is the capacitance in the circuit, that in a simple model corresponds to a capacitor made of two plates, while L is the inductance in the circuit, that would correspond to an inductive coil. \hat{Q} is the charge of the circuit accumulated of the plates, while $\hat{\Phi}$ is the magnetic flux in the coil. The Hamiltonian (III.1) has the same form as the Hamiltonian for a classical LC circuit, but where the two variables \hat{Q} and $\hat{\Phi}$ have been quantized, such that $\hat{\Phi} = \sqrt{\hbar Z/2}(\hat{a} + \hat{a}^\dagger)$ and $\hat{Q} = -i\sqrt{\hbar/2Z}(\hat{a} - \hat{a}^\dagger)$, with $Z = \sqrt{L/C}$ being the characteristic impedance of the circuit. This allows us to retrieve the

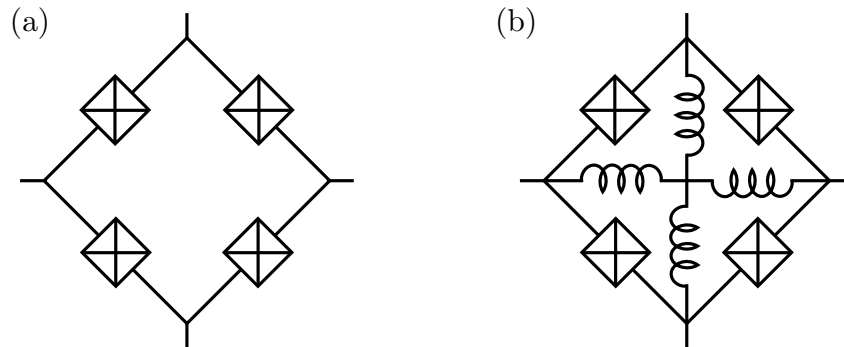


Figure III.2: Circuit representation of two types of Josephson ring modulators. (a) Original Josephson ring modulator made of a loop with four Josephson junctions, first introduced in [Bergeal10b]. (b) The so-called shunted Josephson ring modulator [Flurin14], where four inductances are introduced in the loop to divide it into four sub-loops, first introduced in [Roch12].

Hamiltonian of a quantum harmonic oscillator (see Eq. (I.30)). The Hamiltonian (III.1) is a very useful model in superconducting circuits, as it can describe not only Josephson junctions, but a variety of quantum resonators, such as $\lambda/2$ microwave resonators for instance, that play the roles of cavities.

III.1.3 The Josephson ring modulator

The advantage of superconducting circuits is to be able to engineer systems that are described by quantum mechanics, yet having a size several orders of magnitude larger than the typical platforms reaching the quantum regime. One goal for such systems is to tackle problems typically studied in other physical platforms. For instance, pushing the limits in light-matter interactions, such as reaching the ultrastrong [Niemczyk10, Forn-Díaz10], or even deep strong [Yoshihara17b, Yoshihara17a] coupling regimes. Another example is the capability of reproducing the quantum phenomena studied in quantum optics, such as a three-wave mixing for instance. As a matter of fact, such a non-linear interaction has recently been demonstrated in a device called Josephson ring modulator [Bergeal10a, Bergeal10b]. It is a device made of four Josephson junctions that couples three spatially separated microwave modes [Abdo13a], such that the interaction Hamiltonian is written

$$\hat{H}_{\text{int}} = \chi(\hat{c} + \hat{c}^\dagger)(\hat{a} + \hat{a}^\dagger)(\hat{b} + \hat{b}^\dagger), \quad (\text{III.2})$$

where \hat{a} , \hat{b} , \hat{c} are annihilation operators for the three modes, with frequencies ω_a , ω_b , and ω_c .¹ Typically one works in a regime where one of the modes, say \hat{c} can be treated as a classical signal, and is referred to as the pump. In this way, one can study the interaction between modes \hat{a} and \hat{b} . The simplest representation of such a device is represented in Fig. III.2(a), where four Josephson junctions are embedded in a loop.

¹For a detailed derivation of the Hamiltonian (III.2), see [Flurin14].

The design is very reminiscent of a standard classical component in electronics called the double-balanced mixer, which is a diode ring modulator that is also made of a loop but with diodes instead of Josephson junctions. This device is also nonlinear but cannot reach the quantum regime as the Josephson ring modulator. The Josephson ring modulator has been used as a quantum amplifier near the quantum limit [Bergeal10b], to realize coherent frequency conversion [Abdo13b], and to act as a circulator or directional amplifier [Sliwa15].

The circuit shown in Fig. III.2(a) suffers from an instability issue which limits its frequency tunability. This can be overcome by shunting four inductances in the circuit, such as shown in Fig. III.2(b).² This new design has also been used as a quantum amplifier near the quantum limit [Roch12], as well as to generate a two-mode squeezed vacuum shared between two traveling or stationary microwave modes [Flurin12, Flurin15]. Therefore, it is a platform where the generation of squeezing and its measurement are not only possible but well mastered.

III.2 Basics of a quantum simulation

The idea of quantum simulation dates back the eighties with Feynman, who proposed in 1982 [Feynman82] that if a quantum system A is too hard to be studied experimentally, then one shall find a quantum system B that can be used to reproduce or mimic some quantum process from system A in order to access some wanted degrees of freedom a priori inaccessible in system A. In order for this to work, the system B used as a platform for the quantum simulation needs to be well controlled, in terms of the implementation of the desired dynamics, as well as in terms of the available means to verify the implementation and measure with great accuracy some desired observables. Although the idea is more than thirty years old, this criteria took its time to be actually achievable, while in the mean time much theoretical efforts were devoted to understand quantum simulation, and that for instance a universal quantum computer [Deutsch85] can be used as a universal quantum simulator [Lloyd96]. Recently, the available technology matured enough so that proof of principle experiments were reported [Greiner02, Leibfried02]. Nowadays, various topics benefit from quantum simulation such as physics, chemistry and even biology. Indeed, several physical platforms are advanced enough to attract much attention on their quantum simulation possibilities. One should not be disregarded with respect to another as they all have their advantages and drawbacks depending on the task one wants to simulate. Among the most promising candidates we have cold atoms [Bloch12], trapped ions [Blatt12], photonic devices [Aspuru-Guzik12], as well as superconducting circuits [Houck12]. In this thesis, our attention was devoted to the last one, and before presenting our model let us briefly comment on the different types of quantum simulations. There are two categories, digital and analog quantum simulations [Georgescu14].

In the digital case, the quantum simulation of a system A is implemented by applying to a system B an time evolution corresponding to the one that would be naturally experienced by system A, yet in a stepwise way. Indeed, here system B would not

²For details on the instability issue, as well as on how the new architecture in Fig. III.2(b) solves the problem, see [Flurin14].

experience the wanted dynamics at one, but rather step by step, in the form of the so-called *quantum gates* [Nielsen00]. Each quantum gate is a piece of unitary evolution, but is not necessarily applied on the whole system B. In fact, a digital quantum simulation can consist of a series of quantum gates, where each one is judiciously implemented on some subsystem inside the system B, such that in the big picture the dynamics of system A are effectively reproduced.

In the analog case, a different approach is adopted where the purpose for the system A is to have its Hamiltonian reproduced by the system B used as the simulating platform. In this case, system B directly mimics the dynamics of system A. Sometimes, the two systems A and B have a priori very different Hamiltonians, which can be overcome by cleverly choosing a regime where an effective Hamiltonian can be derived for the system B, such that it mimics the target Hamiltonian. In this thesis, the analog quantum simulation approached has been carried, as presented in the next section.

III.3 Modeling a quantum simulation in a Josephson mixer

III.3.1 Motivation for a quantum simulation of the USC regime

Quantum simulation of ultrastrong coupling, or even deep strong coupling [Casanova10], has recently received a great deal of interest. However, previous theoretical works have focused on simulating in several physical systems the interaction between a qubit and a cavity mode, namely, the quantum Rabi model [Rabi36, Jaynes63]. For instance, proposals were formulated in photonic superlattices [Longhi11], in superconducting circuits [Ballester12, Mezzacapo14, Lamata16], in cavity quantum electrodynamics [Grimsmo13], in trapped ions [Pedernales15], and in ultracold atoms where the first and second Bloch bands in the first Brillouin zone encode the qubit [Felicetti17b]. On the experimental side, quantum simulations of such a regime also solely focused on the Rabi model. Examples of experimental quantum simulations of the ultrastrong and the deep strong coupling regimes have been reported in photonic superlattices [Crespi12], and in superconducting circuits [Langford16, Braumüller16].

Surprisingly, the important case of a quantum simulation of ultrastrongly coupled bosonic modes is still missing. Remarkably, the ultrastrong interaction between two bosonic modes has the particularity of producing a two-mode squeezed vacuum in the ground state [Ciuti05, Ciuti06], as already mentioned in chapter I. However, this squeezed state cannot lead to actual excitations coming out of the system and, thus, cannot be directly observed. In the case of spin-boson ultrastrong coupling, methods to probe the ground-state properties of the system were proposed in Refs. [Lolli15, Peropadre13a, Cirio16]. Nonetheless, in the case of two ultrastrongly coupled bosonic modes, the only studied solution to the problem is to modulate the coupling between the two modes in time [De Liberato07, Fedortchenko16]. However, as stated in chapter II, measuring the corresponding correlations between the two output channels of both bosonic modes seems currently out of reach for physical implementations of light-matter USC regime [Günter09, Anappara09, Todorov09], since matter excitations (for instance the electron gas in a quantum well) decay through a nonradiative channel.

It was shown in chapter II that with an appropriate time-modulation of the light-matter coupling, in the dispersive USC regime, squeezed radiation can be emitted from

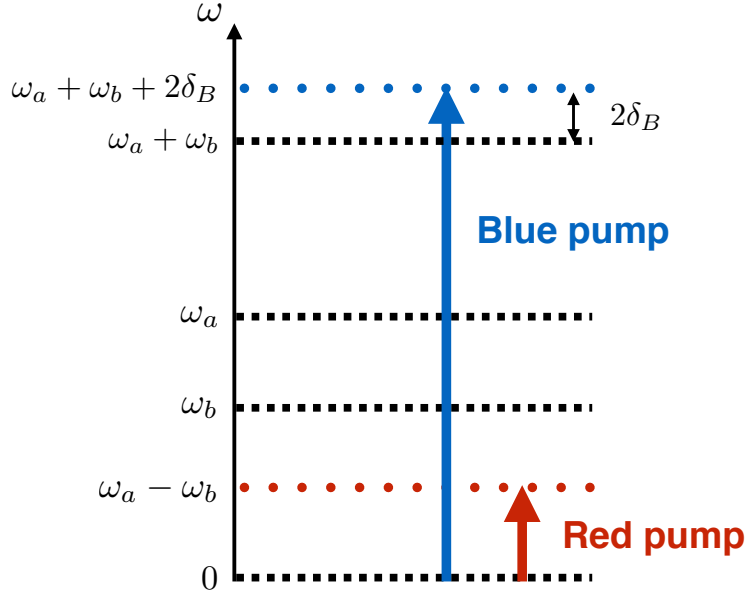


Figure III.3: Representation of the different frequencies scales involved in the model.

the system. A legitimate extension of this previous work is to study what happens if one could discard the main constraint present before: the fact that only the output of the cavity mode could be accessible. Indeed, if one could establish a realistic model where the outputs of both modes could be measurable, one could study the output light-matter correlations and how these are linked with the single mode squeezed already demonstrated, or with the ground state correlations present in a standard USC Hamiltonian.

III.3.2 The model

The constraints mentioned above can be lifted in our model, where we use the Josephson mixer³ to simulate a USC regime between two bosons \hat{a} and \hat{b} . Indeed, in this device, these two bosons correspond to microwave fields inside microwave resonators, and are coupled to transmission lines which allow one to measure both fields and study the possible correlations between them [Flurin12]. In the point of view of the quantum simulation, the first mode, \hat{a} , plays the role of light while the second one, \hat{b} , plays the role of matter. The purpose is thus to have a quantum simulation of light-matter interaction by a light-light interaction platform.

In our model, we want our simulation platform, the Josephson mixer, to be described by the Hamiltonian of the same form as in Eq. (I.22), in order to simulate a USC regime. However, we start from a Hamiltonian where the interaction is rather given by the Eq. (III.2). Therefore, in order to generate an effective Hamiltonian that is formally equivalent to Eq. (I.22), we drive the system with a two-tone radiation. A blue pump drives mode c with an amplitude c_B at frequency $\omega_B = \omega_a + \omega_b + 2\delta_B$, while a red pump

³The Josephson mixer studied here is a device comprising the Josephson ring modulation shown in Fig. III.2(a), as well as the microwave resonators it is coupled to.

drives the same mode c with an amplitude c_R at $\omega_R = \omega_a - \omega_b$. Here ω_a and ω_b are the frequencies of modes a and b , and $2\delta_B$ is a small detuning compared to them. A representation of these frequencies scales is shown in Fig. III.3. Mode c being driven off resonance, we use the stiff pump approximation and describe its amplitude as a complex number instead of an operator. The interaction Hamiltonian now has two three-wave mixing terms, which result in the following effective Hamiltonian in the rotating frame where mode a rotates at $\omega_a + \delta_B$ and mode b at $\omega_b + \delta_B$ (see Appendix E),

$$\hat{H}_{\text{eff}} = \delta_B \hat{a}^\dagger \hat{a} + \delta_B \hat{b}^\dagger \hat{b} + G_B (\hat{a}^\dagger \hat{b}^\dagger + \hat{a} \hat{b}) + G_R (\hat{a}^\dagger \hat{b} + \hat{a} \hat{b}^\dagger), \quad (\text{III.3})$$

where $G_{B,R} = \chi c_{B,R}$ is time-independent (in the rotating frame) and results from the physical time-dependent coupling rate $\tilde{G}_{B,R}(t) = G_{B,R} e^{-i\omega_{B,R}t}$ (in the laboratory frame). The derivation above is valid only for low three-wave mixing rates $|G_{B,R}| \ll \omega_a, \omega_b, |\omega_a - \omega_b|$. In the case when $G_R = 0$, the Hamiltonian describes parametric amplification, which results in two-mode squeezing, while when $G_B = 0$, it describes a beam splitter between modes a and b . Now if $G_B = G_R = G$, Eq. (III.3) has exactly the same form as Eq. (I.22) if $\omega_\alpha = \omega_\beta$. Here, δ_B plays the role of the bosonic mode free oscillation frequency. It is now clear that when the coupling G becomes comparable to δ_B , the doubly pumped Josephson mixer simulates ultrastrongly coupled modes, even if the genuine coupling is much smaller than the genuine free oscillation frequencies of the physical system. It is worthwhile to note that although the simulated coupling rates $G_{B,R}$ are time-independent, as in the case of genuine ultrastrong coupling in semiconductors [Günter09, Todorov09, Anappara09], the actual coupling rate oscillates in the laboratory frame of the output ports of modes a and b . Note that a method to obtain a genuine ultrastrong coupling between two bosonic modes in superconducting circuits was proposed in [Peropadre13b]. There the coupling is mediated not by a third oscillator but by a SQUID. While the physical coupling studied in this article could in principle reach the ultrastrong regime, its predicted coupling-to-frequency ratio does not reach the highest values of the coupling-to-effective frequency ratio that can be reached here, and that lead to the interesting squeezing properties shown hereafter and realistically achievable in our quantum simulation.

III.4 Results

In this section we show the expected results of the quantum simulation, by determining the radiation emitted by the device in the regime where the latter can be described by the effective Hamiltonian (III.3). Each mode \hat{a} or \hat{b} is connected to a transmission line at a rate $\gamma_{a,b}$ and is subjected to internal losses at a rate γ_L . As in chapters I and II, we can use the input-output formalism [Gardiner04]. We are interested in the state of the output modes whose operators are \hat{a}_{out} and \hat{b}_{out} . They are related to the input mode operators by the input-output relations $\hat{a}_{\text{out}} = \hat{a}_{\text{in}} + \sqrt{\gamma_a} \hat{a}$ and $\hat{b}_{\text{out}} = \hat{b}_{\text{in}} + \sqrt{\gamma_b} \hat{b}$. From the known input state, one gets the output state from the above expressions and from

the quantum Langevin equations for the intracavity operators in the case $G_B = G_R = G$

$$\dot{\hat{a}}(t) = -i\delta\hat{a}(t) - \frac{\gamma_a + \gamma_L}{2}\hat{a}(t) - iG(\hat{b}(t) + \hat{b}^\dagger(t)) - \sqrt{\gamma_a}\hat{a}_{\text{in}}(t) - \sqrt{\gamma_L}\hat{f}_a(t) \quad (\text{III.4})$$

$$\dot{\hat{b}}(t) = -i\delta\hat{b}(t) - \frac{\gamma_b + \gamma_L}{2}\hat{b}(t) - iG(\hat{a}(t) + \hat{a}^\dagger(t)) - \sqrt{\gamma_b}\hat{b}_{\text{in}}(t) - \sqrt{\gamma_L}\hat{f}_b(t). \quad (\text{III.5})$$

where \hat{f}_a and \hat{f}_b are noise operators modeling the internal losses of the system. It is straightforward to solve these equations in the frequency domain (see appendixes B and C) to obtain the expressions of $\hat{a}_{\text{out}}(\omega)$ and $\hat{b}_{\text{out}}(\omega)$.

III.4.1 Noise spectra

Once we obtained the output fields $\hat{a}_{\text{out}}(\omega)$ and $\hat{b}_{\text{out}}(\omega)$, we can compute the noise spectra $S_\phi(\omega)$ (as defined in appendix B) for these fields. In particular we can obtain the noise spectra for the single modes quadratures \hat{X}_{a,ϕ_a} and \hat{X}_{b,ϕ_b} ⁴, as well as for any two-mode quadrature $\hat{u}_{\phi_a,\phi_b}^\pm$.⁵ Note that temperature has a dramatic effect on the squeezing, we assumed vacuum inputs for both modes since an actual experiment takes place in a dilution fridge where the temperature is low enough to discard its effect in the theory.

In Figs. III.4(a)-(f) we show the output noise spectra of single-mode quadratures \hat{X}_a and \hat{Y}_a , of two-mode quadratures $\hat{X}_a - \hat{X}_b$ and $\hat{Y}_a + \hat{Y}_b$, and the EPR variance [Duan00, Simon00], as a function of frequency. We work in the case $G_B = G_R = G$, and therefore the Hamiltonian III.3 becomes

$$\hat{H}_{\text{eff}} = \delta_B \hat{a}^\dagger \hat{a} + \delta_B \hat{b}^\dagger \hat{b} + G(\hat{a}^\dagger + \hat{a})(\hat{b}^\dagger + \hat{b}), \quad (\text{III.6})$$

thus simulating the bosonic USC Hamiltonian (I.22). In the rotating frame, a signal at frequency ω corresponds to $\omega_a + \delta - B + \omega$ for mode \hat{a} , and to $\omega_b + \delta_B + \omega$ for mode \hat{b} in the laboratory frame. We do not show the noise spectra of \hat{X}_b and \hat{Y}_b since they are the same as for \hat{X}_a and \hat{Y}_a , both modes having the same effective frequency δ , and the dissipation rates γ_a and γ_b being assumed identical. As expected, and as already shown in chapter II, the output radiation is more squeezed for stronger coupling $G = G_B = G_R$. Furthermore, the squeezing becomes visible in the figures when ultrastrong coupling is reached for $G \gtrsim 0.1\delta_B$. The behavior of the system in the physical implementation picture is illustrated in Fig. III.5. When modes \hat{a} and \hat{b} are in the vacuum state at the input, the output of the system is in an unusual two-mode state, where each mode is squeezed, while the two modes are quantum correlated. Interestingly, the squeezing we predict here occurs between two propagating modes that are separated both in space and frequency.

Let us now comment on the shape of the spectra. In the rotating frame, we show the positive and negative parts of the frequency spectrum, which correspond to measurable noise powers at positive frequencies in the laboratory frame. In Figs. III.4(a)-(c), we can see that for the smallest shown coupling $G = 0.01\delta_B$, the spectra develop a resonance at $\omega = \pm\delta_B$, symmetrically for positive and negative frequencies. This resonance occurs at

⁴For a definition of a general quadrature \hat{X}_ϕ , see Eq. (I.37).

⁵For a definition of a general two-mode quadrature, see Eq. (I.86).

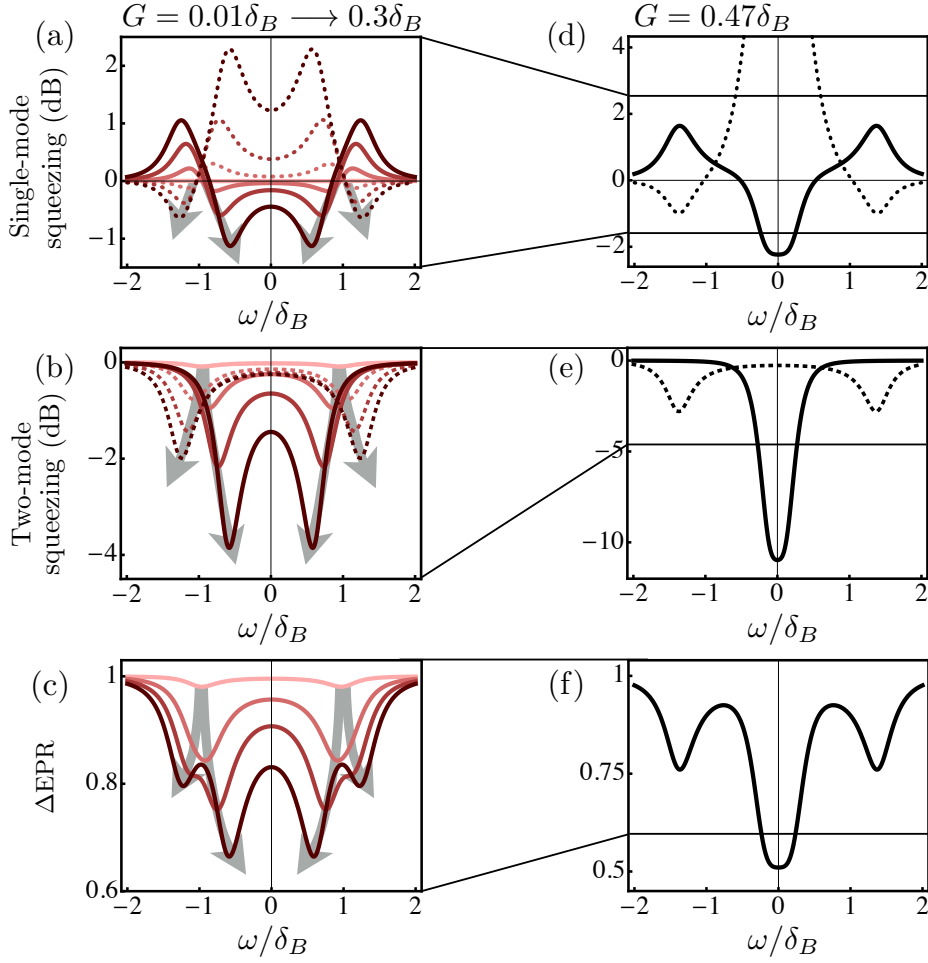


Figure III.4: Noise spectra of the system output for $G_B = G_R = G$, as functions of the measurement frequency ω in units of the blue pump detuning δ_B . (a), (d) Noise spectra of \hat{X}_a (dotted curve) and of \hat{Y}_a (solid curve). (b), (e) Noise spectra of $\hat{X}_a - \hat{X}_b$ (dashed curve) and of $\hat{Y}_a + \hat{Y}_b$ (solid curve). (c), (f) EPR variance $\Delta\text{EPR} = \Delta(X_a - X_b)^2 + \Delta(Y_a + Y_b)^2$. The parameters are: $\omega_a = 2\pi \times 9$ GHz ; $\omega_b = 2\pi \times 6$ GHz ; $\delta_B = 2\pi \times 50$ MHz ; $\gamma_a = \gamma_b = 2\pi \times 25$ MHz ; $\gamma_L = 2\pi \times 0.5$ MHz. (a-c) Color code: each color or shade is associated with a value of G/δ_B : lighter curves represent $G/\delta_B = 0.01$; darker ones, $G/\delta_B = 0.3$. From lightest to darkest curve, G/δ_B takes the values $\{0.01, 0.1, 0.2, 0.3\}$. Arrows follow the splitting of the resonance frequency as G/δ_B increases, simulating Rabi splitting. (d-f) Here we fix $G/\delta_B = 0.47$, for which the two central dips (peaks) predicted in (a-c) merge. The black horizontal lines indicate the plot range in (a-c).

the transition frequency δ_B of the effectively degenerate modes \hat{a} and \hat{b} in the rotating frame (see Eq. (III.3)). As G increases, the resonance splits into two, leading to four dips in the EPR variance Figs. III.4(c). This can be understood as the vacuum Rabi splitting of both effective modes, as already observed in a physically ultrastrongly coupled light-matter system [Günter09].

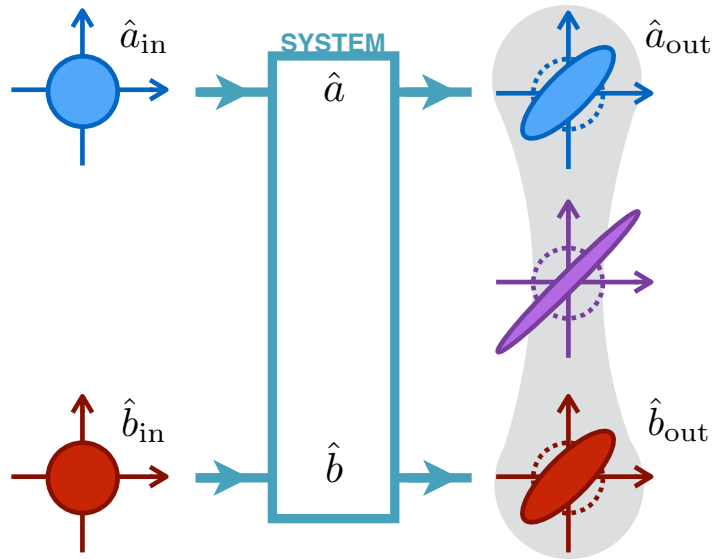


Figure III.5: Summary of the generation of the squeezed output state represented as contours of the marginals of the Wigner function in single- and two-mode quadrature phase spaces.

As the splitting increases with G , one of the two resonance frequencies resulting from the Rabi splitting shifts towards $\omega = 0$. In Figs III.4(a)-(c), this can be seen as two dips getting closer to the origin, corresponding to the resonance frequency and its image on the negative part of the spectrum. When $G \approx 0.5\delta_B$, the dips merge at the origin and the resonance occurs at $\omega = 0$. This is shown in Figs. III.4(d)-(f), where there are no longer four dips but only three, and the one at the origin shows the largest amount of two-mode squeezing. Thereby, the EPR variance almost reaches the lower bound of 0.5, which corresponds to an optimal case where $\hat{Y}_a + \hat{Y}_b$ is infinitely squeezed, while $\hat{X}_a - \hat{X}_b$ is shot noise limited only. Besides, the single mode squeezing in the quadratures \hat{Y}_a and \hat{Y}_b reaches almost -3 dB. This is in fact the maximal expected single-mode squeezing one can hope for. We note that if the two outputs were combined in a 50:50 beam splitter (with frequency conversion on one arm), one of the output modes would be in an infinitely squeezed state while the other would be in the vacuum state [Laurat05]; the reverse has been demonstrated in [Ku15]. This can be done using an extra Josephson mixer as in [Flurin12] but in frequency conversion mode.

The squeezing amplitudes in Fig. III.4(d)-(e) are limited by the realistic internal losses and coupling rates to the transmission lines we use in the model. Their minimal value is set by the need to stay in the regime where the three wave mixing Hamiltonian (III.2) is valid [Flurin14]. The figures stop at $G \approx 0.5\delta_B$ since beyond that point, the Hamiltonian (III.3) has no stable solution and extra terms should be included to make the Hamiltonian physically sound again. For instance, in case of the Dicke model modeling a spin ensemble coupled to a bosonic mode, this value for the coupling is a critical point of a quantum phase transition [Emary03b, Emary03a, Nataf10]. In the proposed simulation using a Josephson mixer, these extra terms arise from a Taylor expansion of the Josephson Hamiltonian beyond second order.

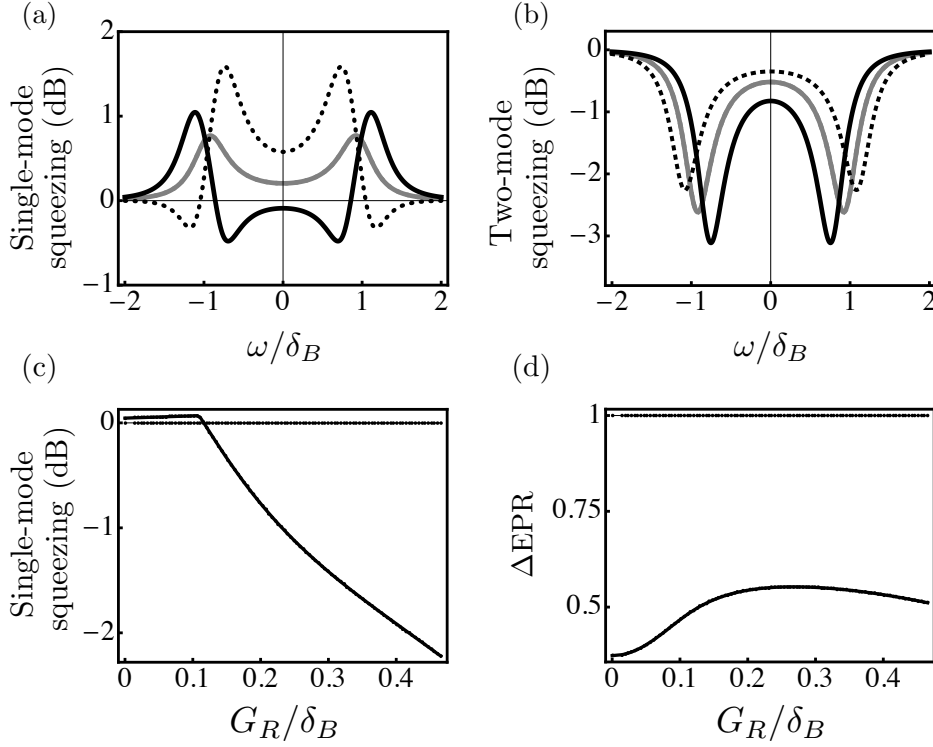


Figure III.6: Noise spectra of the system's output for $G_B = 0.47\delta_B$, as functions of various parameters. (a) Noise spectra of \hat{X}_a (dotted curve) and of \hat{Y}_a (solid curve) as functions the measurement frequency ω in units of the blue pump detuning δ_B . (b) Noise spectra of $\hat{X}_a - \hat{X}_b$ (dashed curve) and of $\hat{Y}_a + \hat{Y}_b$ (solid curve) as functions the measurement frequency ω in units of the blue pump detuning δ_B . (a),(b) Gray curves: $G_R = 0$; black curves: $G_R = 0.15\delta_B$. (c) Optimal single-mode squeezing $S_{a,\phi}(\omega)$ for the quadrature \hat{Y}_a and as a function of G_R . The curve shows the minimal value of $S_{a,\phi}(\omega)$ with respect to ω . (d) Optimal EPR variance $\Delta\text{EPR} = \Delta(X_a - X_b)^2 + \Delta(Y_a + Y_b)^2$ and as a function of G_R . The curve shows the minimal value of $S_{a,\phi}(\omega)$ with respect to ω . The parameters are: $\omega_a = 2\pi \times 9$ GHz ; $\omega_b = 2\pi \times 6$ GHz ; $\delta_B = 2\pi \times 50$ MHz ; $\gamma_a = \gamma_b = 2\pi \times 25$ MHz ; $\gamma_L = 2\pi \times 0.5$ MHz.

III.4.2 Influence of the red pump intensity

So far we have shown that when $G_B = G_R = G$ and $G \gtrsim 0.1\delta_B$, the system eventually emits a two-mode state that shows both single-mode squeezing and entanglement. Furthermore, in line with the work started in chapter II, the single-mode spectra shown in Fig. III.4(a) is resemblant to the one shown in Fig. II.3(a). Here, we study another situation, a rather interesting case where $G_B \neq G_R$. The simplest scenario is when $G_R = 0$, meaning that we apply the blue pump only. Therefore, the effective Hamiltonian (III.3) becomes

$$\hat{H}_{\text{eff}} = \delta_B \hat{a}^\dagger \hat{a} + \delta_B \hat{b}^\dagger \hat{b} + G_B (\hat{a}^\dagger \hat{b}^\dagger + \hat{a} \hat{b}), \quad (\text{III.7})$$

which is the same two-mode squeezing interaction as in Eq. (I.95) achieved in a non-degenerate optical parametric oscillator (OPO), presented in chapter I. The only dif-

ference between Eqs. (III.7) and (I.95) is that here we have a blue pump detuning δ_B , whereas the pump was resonant in chapter I.

It is thus interesting to study the transition between the non-degenerate OPO regime when $G_R = 0$ to the simulated USC regime when $G_B = G_R = G$. Such a study is reported in Fig. III.6. In Fig. III.6(a) are shown the noise spectra $S_{a,\phi}(\omega)$ for the quadratures \hat{X}_a (dotted curves) and \hat{Y}_a (solid curves). In Fig. III.6(b) are shown the noise spectra $S_{a,b,\phi}(\omega)$ for the quadratures $\hat{X}_a - \hat{X}_b$ (dashed curves) and $\hat{Y}_a + \hat{Y}_b$ (solid curves). The curves in gray indicate the case $G_R = 0$ while the black ones indicate the case $G_R = 0.15\delta_B$. We can notice two important features on these plots. The first one is that when G_R increases the single mode noise spectra go from a regime where there are only amplified to a regime with squeezing. The second feature is that we start from only one resonance (and its symmetric counter part) which makes two peaks in the single-mode spectra and two dips in the two-mode spectra, and, and up in a situation where this resonance splits, with each spectra choosing one side for the splitting. It is thus the red pump intensity that triggers the simulation of the Rabi splitting. In Fig. III.6(c), which shows the minimal single-mode noise spectra for \hat{Y}_a with respect to ω , we can notice that the single-mode squeezing really appears after $G_R \gtrsim 0.1\delta_B$.

While the splitting increases along with the single mode squeezing, we can notice that the optimal two-mode squeezing does not occur at the same frequency anymore for the quadratures $\hat{X}_a - \hat{X}_b$ and $\hat{Y}_a + \hat{Y}_b$. Therefore, it should come with less violation of the entanglement criterion ΔEPR , which is shown in Fig. III.6(d). In this figure is shown the minimal value of $\Delta\text{EPR} = \Delta(X_a - X_b)^2 + \Delta(Y_a + Y_b)^2$ with respect to ω , as a function of G_R . Indeed, as G_R increases, as expected the violation of the entanglement criterion, which initially lower than 0.5, then increases, and eventually decreases up the 0.5 because at $G_R = G_B = G \sim 0.5\delta_B$ for $\hat{Y}_a + \hat{Y}_b$ merge at the origin of the rotating frame thus increasing the two-mode squeezing.

III.4.3 Influence of the red pump frequency

Another situation worth studying is the influence of the red pump frequency ω_R . Indeed, so far we have studied only the case where $\omega_R = \omega_a - \omega_b$, but in an experiment one could end up with an imperfect difference between ω_a and ω_b , and for instance include a detuning δ_R such that

$$\omega_R = \omega_a - \omega_b + 2\delta_R. \quad (\text{III.8})$$

Therefore, the effective Hamiltonian is modified, and by using the same procedure as the one detailed in appendix E, one can derive the following effective Hamiltonian

$$\hat{H}_{\text{eff}} = (\delta_B + \delta_R) \hat{a}^\dagger \hat{a} + (\delta_B - \delta_R) \hat{b}^\dagger \hat{b} + G_B(\hat{a}^\dagger \hat{b}^\dagger + \hat{a} \hat{b}) + G_R(\hat{a}^\dagger \hat{b} + \hat{a} \hat{b}^\dagger). \quad (\text{III.9})$$

In Eq. (III.9), we have two coupled bosons whose effective frequencies are not resonant, but detuned. In the following we study the case $G_B = G_R = G$. The effective frequencies for both modes are different, and the frequency for mode \hat{b} is lower than δ_B . Therefore, the simulated USC regime will occur below the value $G \gtrsim 0.1\delta_B$.

In Fig. III.7 we show the influence of δ_R on the single-mode squeezing of both modes, as well as on the violation of the entanglement criterion. We can notice that the quadratures \hat{Y}_a and \hat{Y}_b can be more squeezed for non-vanishing δ_R . In Fig. III.7(a), when

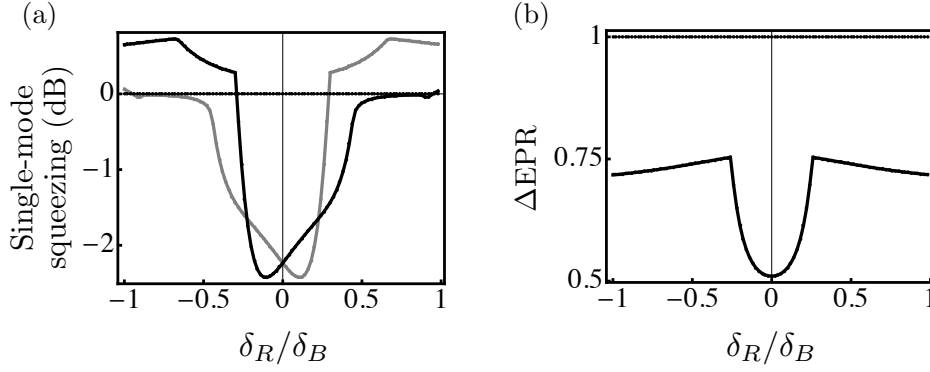


Figure III.7: Noise spectra of the system's output for $G_B = 0.47\delta_B$, as functions of the red pump detuning δ_R . (a) Optimal single-mode squeezing $S_{a,\phi}(\omega)$ for the quadrature \hat{Y}_a and as a function of δ_R . The curve shows the minimal value of $S_{a,\phi}(\omega)$ with respect to ω . (b) Optimal EPR variance $\Delta\text{EPR} = \Delta(X_a - X_b)^2 + \Delta(Y_a + Y_b)^2$ and as a function of δ_R . The curve shows the minimal value of $S_{a,\phi}(\omega)$ with respect to ω . The parameters are: $\omega_a = 2\pi \times 9$ GHz ; $\omega_b = 2\pi \times 6$ GHz ; $\delta_B = 2\pi \times 50$ MHz ; $\gamma_a = \gamma_b = 2\pi \times 25$ MHz ; $\gamma_L = 2\pi \times 0.5$ MHz.

$\delta_R < 0$, \hat{Y}_a (black curve) can be slightly more squeezed than for $\delta_R = 0$, while \hat{Y}_b (gray curve) can be slightly more squeezed when $\delta_R > 0$. The fact that each curve is symmetric with respect to the other is not surprising and simply comes from expressions of the effective frequencies for both modes in Eq. (III.9). This symmetry is also seen in Fig. III.7(b), where the entanglement criterion ΔEPR is symmetric with respect to $\delta_R = 0$. Moreover, as the single-mode squeezing of one mode or the other can be increased by tuning the value of δ_R from 0, the opposite happens with ΔEPR where a non-vanishing red pump detuning can only decrease the entanglement. This of course makes sense, and for an intuitive explanation let us consider a situation without the internal losses. In such case, $\gamma_L = 0$ and the single-mode squeezing for both modes would be -3 dB, which is the limit for having the optimal entanglement with an optimal single-mode squeezing. This means that having the single-mode above -3 dB authorizes a better entanglement, while having a single-mode noise less than -3 dB inevitably decreases the entanglement. Here, tuning δ_R from 0 would make the single-mode squeezing for one mode or the other reach values below -3 dB, and which results in less violation of the entanglement criterion as can be seen in Fig. III.7(b).

III.5 Link with the USC ground state correlations

In this section we wish to push further the understanding of the connection between output squeezed state we can obtain in our quantum simulation presented in the previous section, with the correlations present in the ground state of genuine ultrastrong coupling. Therefore, let us first evaluate such correlations in this ground state.

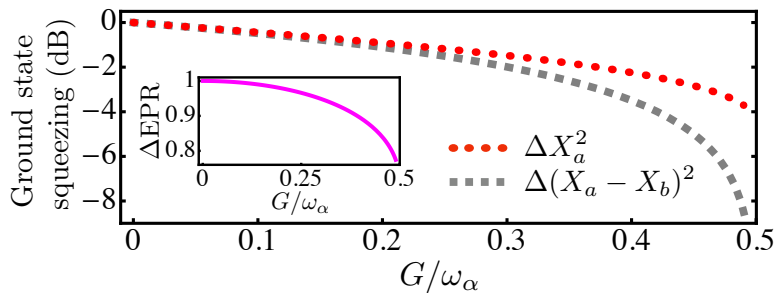


Figure III.8: Squeezing of ultrastrongly coupled a and b modes in the ground state, as a function of the coupling rate G . Red dotted curve: single mode squeezing of the quadrature \hat{X}_a . Here the modes are degenerate $\omega_a = \omega_b$, therefore the squeezing of \hat{X}_b is the same as of \hat{X}_a . Gray dashed curve: two-mode squeezing of the collective quadrature $\hat{X}_a - \hat{X}_b$. Inset: EPR variance $\Delta\text{EPR} = \Delta(X_a - X_b)^2 + \Delta(Y_a + Y_b)^2$.

III.5.1 Ground state squeezing

Let us start by studying the squeezing of a pair of ultrastrongly coupled bosonic modes in their ground state. For this we introduce the light-matter Hamiltonian we want to simulate,

$$\hat{H} = \omega_\alpha \hat{a}^\dagger \hat{a} + \omega_\beta \hat{b}^\dagger \hat{b} + G(\hat{a} + \hat{a}^\dagger)(\hat{b} + \hat{b}^\dagger), \quad (\text{III.10})$$

where \hat{a} (\hat{b}) and ω_α (ω_β) are the annihilation operator and the frequency of the light (matter) mode, and $\hbar = 1$. The two modes are coupled at a rate G . We consider here the Hamiltonian (III.10) in its most elementary form. For instance, we do not include extra terms such as a squared electromagnetic vector potential, as is the case in semiconductors described in the Coulomb gauge [Ciuti05, Ciuti06]. Indeed, while the versatility of superconducting circuits would allow us to simulate extra terms, we choose to restrict the simulation to the simplest form of ultrastrong coupling in the present paper.

In order to identify the ground state of the Hamiltonian (III.10), as in chapter I we first apply the Hopfield method [Hopfield58] to identify the two eigenmodes of the system, which are called polaritons in case of a genuine light-matter interaction (see chapter I for more details). The annihilation operators \hat{p}_1 and \hat{p}_2 of the two eigenmodes are expressed [Ciuti05, Ciuti06] as linear combinations of \hat{a} , \hat{b} , \hat{a}^\dagger and \hat{b}^\dagger (see Eq. (I.24)). Their expressions as well as their eigenvalues determine the validity of this model (see appendix F). We then express \hat{a} and \hat{b} as a function of the eigenmode operators \hat{p}_1 and \hat{p}_2 . The ground state $|\text{GS}\rangle$ being defined as $\hat{p}_1|\text{GS}\rangle = \hat{p}_2|\text{GS}\rangle = 0$, we can fully characterize the squeezing of the original modes \hat{a} and \hat{b} in the ground state $|\text{GS}\rangle$ by computing the covariance matrix $\mathcal{V} = \{\langle x_i x_j + x_j x_i \rangle_{|\text{GS}\rangle} - 2\langle x_i \rangle_{|\text{GS}\rangle} \langle x_j \rangle_{|\text{GS}\rangle}\}_{ij}$ in the basis $\{x_1, x_2, x_3, x_4\} = \{(\hat{a}^\dagger + \hat{a})/\sqrt{2}, (i\hat{a}^\dagger - i\hat{a})/\sqrt{2}, (\hat{b}^\dagger + \hat{b})/\sqrt{2}, (i\hat{b}^\dagger - i\hat{b})/\sqrt{2}\}$ [Serafini04, Adesso05].

In Fig. III.8, we show the single-mode squeezing, the two-mode squeezing, and the EPR variance ΔEPR in the ground state of a pair of ultrastrongly coupled bosonic modes, as a function of the coupling constant G . As usual, we show the squeezing in dB using the following logarithmic scale $S_{X_\theta} = 10 \log_{10} (\langle \Delta \hat{X}_\theta^2 \rangle / \langle \Delta \hat{X}_{\text{vac}}^2 \rangle)$, where $\langle \Delta \hat{X}_{\text{vac}}^2 \rangle = 1/2$ corresponds to the noise of a vacuum state. One can note that the

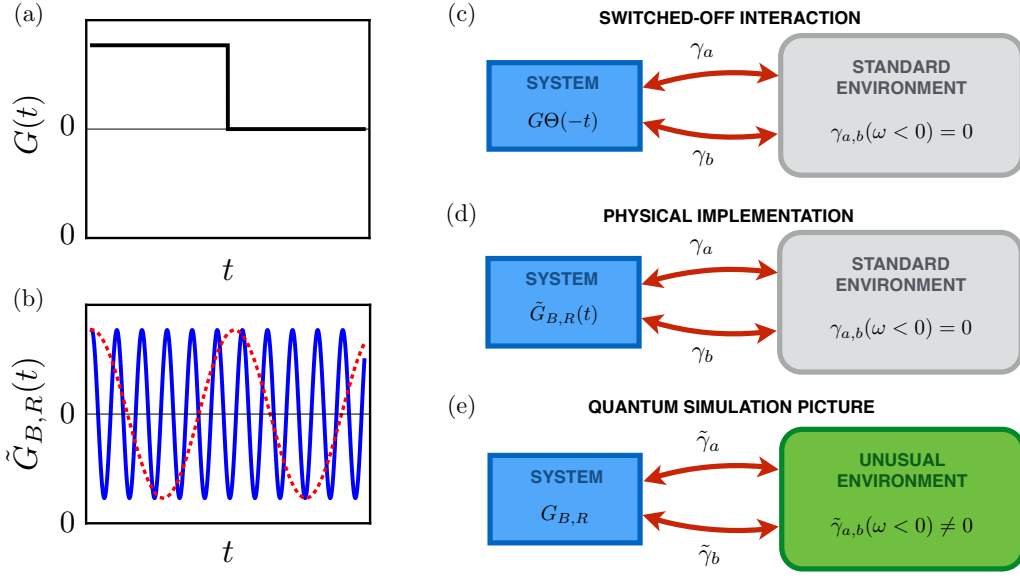


Figure III.9: Comparison between a standard USC and the quantum simulation. (a) Non-adiabatic instantaneous switching-off of the light-matter coupling strength G as proposed in [Ciuti05]. (b) Time modulation of the coupling strength $\tilde{G}_{B,R}(t)$ as occurring in our model in the laboratory frame. (c)-(e) Schemes of three models describing two interacting bosonic modes that are coupled to an environment, in which a squeezed field is emitted. (c) Genuine ultrastrongly interacting bosonic modes whose interaction is abruptly switched-off at time 0 [Ciuti05], and which are coupled to a standard environment. $\Theta(t)$ is the unit step function, introduced to model the switch-off of the interaction. (d) Physical picture with a time-dependent interaction and a standard environment, which is coupled at a rate that vanishes for negative frequencies. (e) Quantum simulated model mapped from (d), where the ultrastrong interaction is time independent and the baths are unusual with a support for $\gamma_{a,b}$ spanning positive and negative frequencies.

ground state shows a significant amount of squeezing in the single-mode picture, as well as in the two-mode picture, enough to be detected by a Gaussian entanglement witness: the EPR variance goes below 1 [Duan00, Simon00]. Note that since here the two modes are at resonance, only $\Delta\hat{X}_a^2$ is shown, because $\Delta\hat{X}_b^2$ has exactly the same amount of squeezing. We thus verified that there is two-mode squeezing in the ground state, and additionally found single-mode squeezing as well.

III.5.2 Discussion

So far, we have focused on the observable squeezing contained in the output modes of the physical system that simulates the ultrastrong coupling Hamiltonian (III.3). In this section, we interpret the nature of the output modes in the simulated picture and how their noise can be related to the ground state squeezing seen in Fig. III.8.

The squeezing in the ground state of a genuinely USC regimes between two bosonic modes comes from the single-mode and the two-mode correlations of the virtual photons

present in the ground state. Indeed, in principle they do not correspond to accessible excitations. However, if one could somehow instantaneously switch-off the coupling strength G appearing in Eq. (III.10), then the photons should be released to the environment as an output [Ciuti05, De Liberato09]. This is represented in Fig. III.9(a), where the coupling is switched-off with the step function $\Theta(t)$.

Similarly, in Fig. III.9(b), we show the time-modulation of the coupling strength $\tilde{G}_{B,R}(t)$ in the laboratory frame. We can see that $\tilde{G}_{B,R}(t)$ is rigorously different from the switching-off in Fig. III.9(a). However, each period of the time-oscillation is essentially a cycle composed of a switching-off followed directly by a switching-on, yet not instantaneous, but still non-adiabatic. Hence, in the quantum simulation set-up correlated photons are released because of non-adiabatic switch-off/switch-on cycles while purely ground state photons are released because of a non-adiabatic and instantaneous switch-off. The process is thus not the same in both cases but is still similar, which is why the output state of the quantum simulation shares the same noise properties with the ground state in a genuine USC regime.

Additionally to the analysis we just developed, we may also compare the two cases by focusing on their interaction to the environment. For a genuine USC regime, the system is coupled to a standard environment, where the dissipation rates are vanishing at negative frequencies, such that $\gamma_{a,b}(\omega < 0) = 0$. This model is shown in Fig. III.9(c). If we look at our model in the laboratory frame, as shown in Fig. III.9(d), we have the coupling between modes \hat{a} and \hat{b} that is modulated in time and each mode is coupled to a zero temperature bath at a rate $\gamma_{a,b}(\omega)$ with vanishing contribution at negative frequencies [Ciuti06]. In contrast, in the simulated picture shown in Fig. III.9(e), the modes are coupled at a fixed rates $G_{B,R}$ but interact with an unusual environment, whose coupling rates $\tilde{\gamma}_{a,b}(\omega)$ are nonzero at negative frequencies. This results from a shift of the zero frequency in the rotating frame of the simulation. The vacuum squeezing of the ultrastrongly coupled modes reminiscent of the ground state in Fig. III.8 can be understood as resulting from the excitations corresponding to the nonzero $\tilde{\gamma}_{a,b}(\omega)$ for $\omega < 0$. It can be seen as a continuous extraction of ground states photons from an ultrastrongly coupled system whose ground state is immediately repopulated along with our extraction, such that the ground state is unchanged at all times. Of course this repopulation can be easily understood in the laboratory frame as the energy continuously provided to the system by the two pump photons.

III.6 Comments on the experimental implementation

At last, let us comment on the experimental realization of our model. As previously mentioned, our model can be straightforwardly implemented in the Josephson mixer, since the tools we require are similar to what has been done already, for the generation of entangled microwave fields for instance [Flurin12]. For this, the Josephson ring modulator shown in Fig. III.2(b) is embedded in a larger device including the microwave resonators for modes \hat{a} , \hat{b} , the pumps, as well as their coupling to transmission lines used for the inputs and for measuring the output state. Precisely, the schematic of the whole electronic circuit for the Josephson mixer is shown in Fig. III.10.

Additionally, it is worthwhile to wonder how realistic are the parameters we chose in Figs. III.4, III.6 and III.7. The phenomena we propose to observe require that

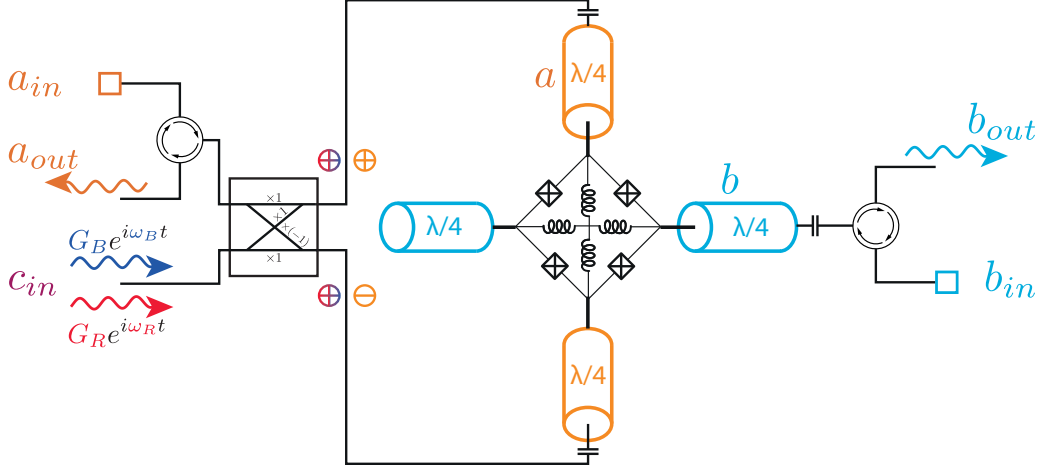


Figure III.10: Scheme of a possible implementation based on a Josephson mixer [Abdo13a]. A ring of four Josephson junctions is shorted by inductors and couples two $\lambda/2$ microwave resonators of frequency ω_a and ω_b . Capacitors couple the resonators to transmission lines leading to decay rates $\gamma_a + \gamma_L$ and $\gamma_b + \gamma_L$, where γ_L corresponds to internal losses of the resonators. This circuit implements three-wave mixing between the nondegenerate modes \hat{a} and \hat{b} and a mode \hat{c} that can be addressed using a signal driven with the same phase on each port of the resonator \hat{a} . One may use a 180° hybrid coupler (box on the left) to selectively couple \hat{a} and \hat{c} modes to two separate transmission lines. Circulators ensure that the input modes a_{in} and b_{in} are prepared in the vacuum state by thermalizing a 50Ω load at $T \ll \hbar\omega_{a,b}/k_B$. When mode \hat{c} is driven off resonance by two tones at frequency $\omega_B = \omega_a + \omega_b + 2\delta$ and $\omega_R = \omega_a - \omega_b$, it reproduces the physics of two ultrastrongly coupled bosonic modes of frequency δ . Signatures of the ultrastrong coupling can be observed in the squeezing properties of the noise in ports a_{out} and b_{out} .

$\gamma_L \ll \gamma_{a,b} < \delta_B$ and that $2G_{B,R} \lesssim \delta_B$. It is shown in [Flurin14] that

$$\frac{2G_{B,R}}{\sqrt{\gamma_a \gamma_b}} \leq \frac{1}{4} \sqrt{\xi_a \xi_b Q_a Q_b}, \quad (\text{III.11})$$

where $\xi < 1$ is the participation ratio of the Josephson junction in the resonator [Flurin14] and Q is the quality factor of the resonator. Therefore, in order to reach $2G_{B,R} \approx \delta_B$, one needs

$$1 < \frac{\delta}{\gamma_{a,b}} \leq \frac{1}{4} \sqrt{\xi_a \xi_b Q_a Q_b}. \quad (\text{III.12})$$

The condition that $\sqrt{\xi_a \xi_b Q_a Q_b} > 4$ sets constraints on the device similar to the ones needed to realize a quantum limited amplifier using the Josephson mixer [Abdo13a, Pillet15] and is perfectly realistic. The parameters we chose in Figs. III.4, III.6 and III.7 are thus within reach in standard devices.

III.7 Conclusion

In this chapter we have presented the Josephson mixer, a well controlled physical platform that enables the study of the interaction between three bosonic fields. We have shown how to use this system to study the interaction between two bosonic fields that is in line with the work started in chapter II. In particular, as a central result we have shown how to use this platform to perform a quantum simulation of the USC regime between two bosonic modes. We have seen that the consequence of the simulation is the emission of particular two-mode state that shows both single-mode squeezing and entanglement, similarly as in the ground state of a genuine USC regime. Using the high level of control of superconducting circuits enables the access of both modes directly, a feat that is not possible with current light-matter systems. Therefore, the model developed in this chapter that is achievable with current technology can be used as a tool to probe the peculiar correlations that also arise between the virtual excitations in the ground state of a genuine USC regime. Thus, we have fully characterized the relation between the USC regime and squeezed states.

Additionally, our proposal will determine the smooth transition from strong to ultrastrong coupling regimes by measuring the squeezing properties of the output modes. Beyond the fundamental interest in observing this transition, the unusual squeezing properties of the proposed device can be used as a resource for bath engineering [Aron14, Aron16] and nonclassical state generation [Felicetti14, Stassi15, Rossatto16] in complex resonator networks.

In the remaining chapter we will show that similar results can be achieved between the coupling of two optical cavities with the mediation of a mechanical resonator, suggesting that a sort of quantum simulation of the USC regime may also take place. Additionally, we will go beyond the initial scope of this thesis by showing that the same optomechanical set-up can be used as a mean for quantum communications.

IV Light-matter interactions and quantum communications in optomechanics

In this last chapter we will conclude our study on the link between the ultrastrong coupling (USC) regime and squeezed states. We focus on a different physical platform, an unusual optomechanical [Aspelmeyer14] set-up where two optical cavities embedded in an interferometer can show a behavior very similar to the one observed in chapter III in the quantum simulation of the USC regime. The two optical cavity modes interaction is indirect and is mediated by a mechanical resonator, which results in the emission of two-mode state from the cavities whose noise spectra are very similar to the ones emitted from the Josephson mixer in the case of a quantum simulation of the USC regime.

Second, we wonder how the interferometric optomechanical system introduced above could not only be used to study light-matter interaction from a fundamental point of view, but could also be of use as a building block in quantum communications. Specifically, switching from the continuous pumping regime used above to a pulsed regime, we will show how one of these building blocks can be used to quantum communicate with two protocols. The first one uses only a classical communication channel between the two building blocks at the expense of requiring an initial entanglement between them. This first protocol is called *quantum teleportation with continuous variables* [Braunstein05]. The second protocol however does not require entanglement for the transfer of information at the expense of using a quantum channel for the communication. This work has been published in [Felicetti17a].

We start by briefly reviewing few basics of quantum optomechanics, followed by a presentation of the interferometric optomechanical set-up considered here. Next, we study this set-up in the continuous driving regime and show the link with the quantum simulation of the USC regime studied in chapter III. Finally, we study the system in the pulsed driving regime and show how to implement the two quantum communication protocols mentioned above. The prerequisites for the present chapter are the same as for chapter I, as well as the notions seen in the latter.

IV.1 Introduction to quantum optomechanics

IV.1.1 Old and recent achievements

The fact that light could in some way act as a force that pushes matter was demonstrated early in the twentieth century [Lebedew01, Nichols01]. Since then, much progress has been made to study and understand this force coming from the radiation pressure of light on the matter, due to the fact that the impinging photons carry momentum. One of the most famous phenomena of this pressure is its use for cooling the motion of

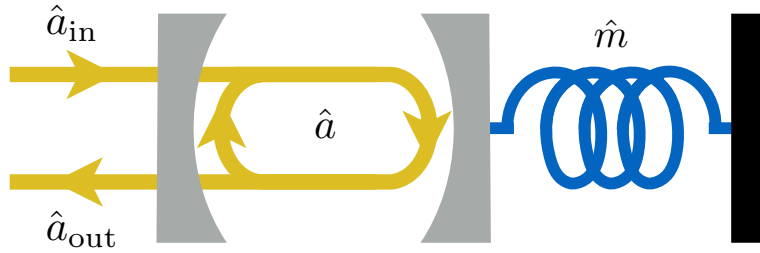


Figure IV.1: Scheme of the most common device involving optomechanical interaction. A pump field is sent to one of the mirrors of an optical cavity (the left mirror). A field establishes inside the cavity, and its photons exert a radiation pressure on the right mirror of the cavity. This right mirror is not fixed in its position but attached to a string, which cause the mirror to oscillate around its equilibrium position, causing a shift in the cavity resonance frequency.

atoms, namely laser cooling, first pointed out in the seventies [Hänsch75, Wineland75] and demonstrated shortly after [Wineland78, Neuhauser78]. One spectacular application of this technique is in the trapping of Bose-Einstein condensates [Anderson95] for instance. Although the interaction of light and matter through the radiation pressure is a vast topic, such as in the laser cooling physics, here we are interested on the specific case where the light is confined in a cavity mode which is coupled to a mechanical degree of freedom, such as represented in Fig. IV.1. This configuration was first considered by Braginsky and co-workers, who predicted [Braginsky67] and showed preliminary experimental proof [Braginsky70] of two important phenomena in such a model. Although these first studies were performed in the realm of classical physics, the phenomena they tackled later became the basics ingredients in modern quantum optomechanics as well. These phenomena correspond to situations where this model is operated in a regime where the mechanical damping is enhanced, or in another regime where the opposite effect occurs allowing self-sustained mechanical oscillations to arise, called also a *mechanical instability* [Aspelmeyer14]. This first experimental demonstration was carried in a microwave cavity, but later on these processes were demonstrated in a variety of platforms. For instance, in the early eighties, bistability in an optomechanical interaction was first reported in the optical domain [Dorsel83].

In the quantum domain, the influence of quantum noise in optomechanical systems has been theoretically explored over the years, as in the measurement of gravitational waves [Caves80], the reduction of noise beyond the standard quantum limit (SQL) [Fabre94, Mancini94], and quantum nondemolition measurements [Jacobs94, Pinard95], the preparation of nonclassical [Bose97] and entangled [Mancini97] states, or feedback cooling of the mechanical motion [Mancini98] for instance. More recently, theoretical interest has been fruitful for proposing light-to-mechanical teleportation [Mancini03, Hofer11], qubit-to-light transduction [Stannigel10], non-Gaussian state swapping [Filip15], thermodynamics [Kolář16], and further investigation of entanglement generation [Pirandola06, Genes08, He13, Hofer15, Vivoli16, Asjad16, Chakraborty16].

Experimentally, great advances were made over the years in quantum optomechan-

ics, such as the first the demonstration of optical feedback cooling [Cohadon99], and cooling at sub-Kelvin temperatures [Kleckner06, Poggio07]. Optomechanical coupling has been recently demonstrated in a variety of new physical platforms, such as membranes [Thompson08b] and nanorods [Favero09] inside Fabry-Pérot cavities, whispering gallery microdisks [Jiang09, Wiederhecker09] and microspheres [Ma07, Park09, Tomes09], photonic crystals [Eichenfield09a, Eichenfield09b], evanescently coupled nanobeams [Anetsberger09], the motion of a cloud of cold atoms [Brennecke08, Murch08], and superconducting microwave resonators capacitively coupled to mechanical elements [Regal08, Teufel11] also labeled *electromechanics*. Additionally, purely quantum features have been recently reported, such as squeezed light due to the optomechanical interaction [Brooks12, Safavi-Naeini13, Purdy13], squeezing of the mechanical degree of freedom [Pirkkalainen15], as well as entanglement between the photons and the mechanical motion [Palomaki13b, Riedinger16].

IV.1.2 Modeling the quantum optomechanical interaction

Let us now briefly introduce a simple model for a quantum optomechanical interaction. The typical set-up for this interaction is shown in Fig. IV.1. An input laser is shined on one of the cavity's mirrors, the mirror on the left, and some of the light enters the cavity, due to the imperfect reflectivity of the mirror, which is modeled by the input-output dissipation rate κ . The photons travel in round-trips inside the cavity, and thereby bounce on the right mirror of the cavity, which is not fixed to the ground, but can move to some extent. This is modeled by the mirror being attached to a spring. The photons create a radiation force when impinging on the right mirror, and therefore this mirror can be physically displaced, which consequently starts a mechanical oscillation of the mirror due to the spring. During this mechanical oscillation, the cavity length is periodically changed, which changes the resonance frequency of the cavity, and thereby modifies the input of the laser photons at the left mirror. Eventually, the mechanical motion stops due to its dissipation rate γ , that is typically several orders of magnitude larger than the photons input-output dissipation rate κ .

In mathematical terms, it means that the cavity frequency is a function depending of the position of the mechanical oscillator, here the right mirror, and vice versa. The Hamiltonian of the system can then simply be expressed as

$$\hat{H} = \omega_a(\mathcal{X}_m)\hat{a}^\dagger\hat{a} + \omega_m\hat{m}^\dagger\hat{m}, \quad (\text{IV.1})$$

where $\hat{a}(\hat{a}^\dagger)$ is the annihilation (creation) operator for the cavity mode, with the position-dependent frequency $\omega_a(\mathcal{X}_m)$, while $\hat{m}(\hat{m}^\dagger)$ is the annihilation (creation) operator for the mechanical resonator, with the frequency ω_m . The position-dependent cavity frequency can be written with a Taylor expansion

$$\omega_a(\mathcal{X}_m) = \omega_a + \mathcal{X}_m \frac{\partial\omega_a(\mathcal{X}_m)}{\partial\mathcal{X}_m} + \dots \quad (\text{IV.2})$$

For a sufficiently small optomechanical coupling, we can keep solely the zeroth and the first order terms in Eq. (IV.2), and rewrite the Hamiltonian as

$$\hat{H} \approx \omega_a\hat{a}^\dagger\hat{a} + \omega_m\hat{m}^\dagger\hat{m} - g_0\hat{a}^\dagger\hat{a}(\hat{m}^\dagger + \hat{m}), \quad (\text{IV.3})$$

where g_0

$$g_0 = -\frac{x_{\text{ZPF}}}{\sqrt{2}} \frac{\partial \omega_a(\mathcal{X}_m)}{\partial \mathcal{X}_m} \quad (\text{IV.4})$$

is the single photon optomechanical coupling, noting that $\mathcal{X}_m = x_{\text{ZPF}}(\hat{m}^\dagger + \hat{m})/\sqrt{2}$ with x_{ZPF} being the zero point fluctuations of the mechanical position.

Note that in most cases g_0 is very weak with respect to the dissipation rates κ , γ and to the frequencies ω_a , ω_m . Therefore, a further approximation can be applied to the Hamiltonian, one that states that the cavity field can be written as the sum of a coherent amplitude $\langle \hat{a} \rangle = \alpha$ which is the average of the field, and the field fluctuations $\delta \hat{a}$ such that

$$\hat{a} = \alpha + \delta \hat{a}. \quad (\text{IV.5})$$

With this approximation, the Hamiltonian (IV.3) can be rewritten

$$\hat{H} \approx \omega_a \hat{a}^\dagger \hat{a} + \omega_m \hat{m}^\dagger \hat{m} - g_0 \alpha (\delta \hat{a}^\dagger + \delta \hat{a}) (\hat{m}^\dagger + \hat{m}), \quad (\text{IV.6})$$

by assuming α real without loss of generality. In Eq. (IV.6) two terms are missing in principle. The first one is $-g_0 |\alpha|^2 (\hat{m}^\dagger + \hat{m})$ that is just a constant displacement in the phase-space of the mechanical resonator, which we omit since it does not impact the physics involving the quantum noise that we are interested in. The second term is $-g_0 \delta \hat{a}^\dagger \delta \hat{a} (\hat{m}^\dagger + \hat{m})$ that we neglect by assuming that $|\alpha|^2 \gg \langle \delta \hat{a}^\dagger \delta \hat{a} \rangle$, namely that the number of photons due to the quantum fluctuations is very small compared to the photons of the average field. The Hamiltonian in Eq. (IV.6) describes the so-called *linearized quantum optomechanics* [Aspelmeyer14]. In Eq. (IV.6), we can see that now we have two bosons coupled with their respective position operator, with an effective coupling strength $g_0 \alpha$. Indeed, the optomechanical coupling strength is in principle g_0 . However, when enough photons are injected in the cavity and the linearized regime is still valid, the optomechanical coupling is enhanced by the cavity field amplitude [Aspelmeyer14].

IV.2 Interferometric model with a double-sided moving mirror

In this section we present the model that we use in this study, consisting of an interferometer embedding a double cavity separated in the middle by a double-sided mirror, whose motion characterizes a mechanical degree of freedom. This scheme has several advantages over the standard scheme see in Fig. IV.1, that we detail hereafter.

Our model is depicted in Fig. IV.2. A monochromatic laser is sent in the bottom port of a 50:50 beams-splitter, represented by the mode \hat{b}_{in} , while in left port, \hat{a}_{in} , is a field in an arbitrary quantum state. After the beam-splitter, both arms of the common-path Sagnac interferometer reach both ends of a double cavity, with modes \hat{c} and \hat{d} separated in the middle by a moving double-sided mirror, represented by mode \hat{m} . We describe each cavity as being a single-mode one, the mirror in the middle, made of a non-transmissive vibrating membrane, is assumed to effectively support a single phononic mode, since intermode couplings are typically negligible. The radiation pressure induces an optomechanical coupling between the optical modes \hat{c} , \hat{d} and the

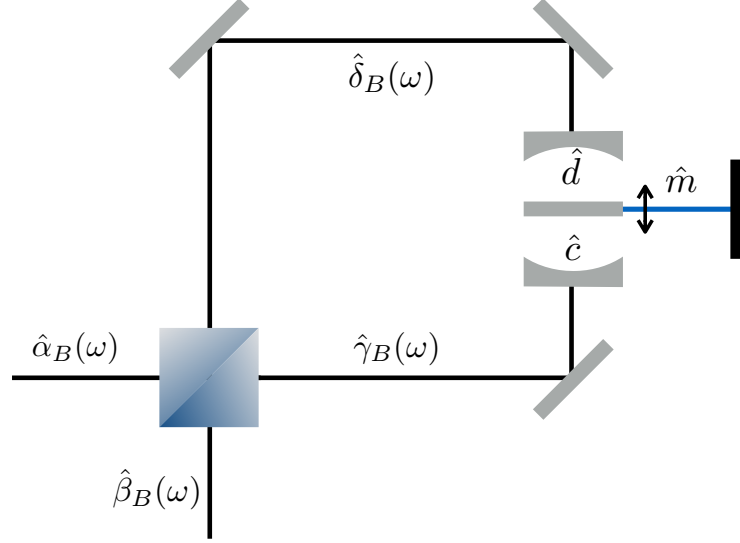


Figure IV.2: Sketch of the interferometric optomechanical scheme. An optomechanical device, composed of two identical optical cavities sharing a vibrating mirror, is embedded in a common-path Sagnac interferometer. A classical drive, sent through the control port $\hat{\beta}_B(\omega)$ modulates the optomechanical interactions with input/output quantum signals $\hat{\alpha}_B(\omega)$.

vibrational mode \hat{m} , such that the system Hamiltonian can be written as

$$\hat{H} = \omega_c \left(\hat{d}^\dagger \hat{d} + \hat{c}^\dagger \hat{c} \right) + \omega_m \hat{m}^\dagger \hat{m} - g_0 \left(\hat{d}^\dagger \hat{d} - \hat{c}^\dagger \hat{c} \right) \left(\hat{m}^\dagger + \hat{m} \right), \quad (\text{IV.7})$$

where $\hat{H}_0 = \omega_c \left(\hat{d}^\dagger \hat{d} + \hat{c}^\dagger \hat{c} \right) + \omega_m \hat{m}^\dagger \hat{m}$. We denote with ω_c and ω_m the frequencies of the optical cavities and mechanical modes, respectively, and with g_0 the optomechanical coupling strength, assumed to be equal for the two modes. To derive input/output relations for our system, we consider a standard Markovian coupling of the intra-cavity fields \hat{c} and \hat{d} with the modes describing the electromagnetic environment, $\hat{\gamma}_B(\omega)$ and $\hat{\delta}_B(\omega)$, respectively. It is straightforward to see that the input modes of the 50:50 beam splitter, $\hat{\alpha}_B(\omega)$ and $\hat{\beta}_B(\omega)$ in Fig. IV.2, interact selectively with the bosonic modes \hat{a} and \hat{b} , defined by the relations $\hat{a} = (\hat{c} - \hat{d})/\sqrt{2}$ and $\hat{b} = (\hat{c} + \hat{d})/\sqrt{2}$. These modes correspond to collective excitations of the two optical intra-cavity modes.

The system Hamiltonian can thus be rewritten as

$$\hat{H} = \omega_c \left(\hat{a}^\dagger \hat{a} + \hat{b}^\dagger \hat{b} \right) + \omega_m \hat{m}^\dagger \hat{m} + g_0 \left(\hat{a}^\dagger \hat{b} + \hat{a} \hat{b}^\dagger \right) \left(\hat{m}^\dagger + \hat{m} \right), \quad (\text{IV.8})$$

where $\hat{H}_0 = \omega_c \left(\hat{a}^\dagger \hat{a} + \hat{b}^\dagger \hat{b} \right) + \omega_m \hat{m}^\dagger \hat{m}$. Let us now assume that an undepleted coherent state at frequency ω_b is sent through the port $\hat{\beta}_B(\omega)$. The spatial mode $\hat{\beta}_B(\omega)$ can be decomposed in two modes propagating in opposite directions, proportional to the Fourier transforms of the \hat{b} mode's input and output respectively [Gardiner85, Gardiner04, Walls08]. We can describe the driven mode b as a classical field, and replace $\hat{b} \rightarrow \beta e^{-i\omega_b t}$

in Eq. (IV.8). In a frame where a is rotating at the drive frequency, the Hamiltonian becomes (see appendix G)

$$\hat{H}_{\text{eff}} = (\omega_c - \omega_b) \hat{a}^\dagger \hat{a} + \omega_m \hat{m}^\dagger \hat{m} + g_0 \beta (\hat{a}^\dagger + \hat{a}) (\hat{m}^\dagger + \hat{m}), \quad (\text{IV.9})$$

where $\hat{H}'_0 = (\omega_c - \omega_b) \hat{a}^\dagger \hat{a} + \omega_m \hat{m}^\dagger \hat{m}$, where we assumed β real. Notice that this derivation leads to a linear optomechanical interaction of tunable strength $g_0 \beta$. In the context of linearized optomechanics [Aspelmeyer14], such coupling is usually obtained considering small quantum fluctuations on top of a classical signal, which enhances the otherwise negligible interaction [Liao15]. In our scheme, the quantum input and the classical pump are given by independent modes, a fundamental difference that presents various advantages. 1) The Hamiltonian in Eq. (IV.9) is valid for large quantum fluctuations of the intra-cavity field, where the standard linear approximation of optomechanics breaks down. 2) The proposed optomechanical device is able to interact with arbitrary quantum inputs, without requiring displacing operations beforehand or additional non-linear elements. 3) The effective coupling strength $g_0 \beta$ and the coupling frequency ω_b depend on a classical drive, which is independent on the state and frequency of the quantum input. This point is essential when a large degree of control of the coupling strength is needed [Moore16]. 4) The quantum and the classical output exit the device via independent optical paths.

IV.3 Results in the continuous regime

In this section we explore the model we introduced (in particular the effective Hamiltonian (IV.9)), and focus on a regime where a continuous monochromatic coherent pump is sent through the port $\hat{\beta}_B(\omega)$.

IV.3.1 Validity of the effective Hamiltonian

The purpose of this section is to verify the validity of the effective Hamiltonian (IV.9). To do so we study the system in the framework of input-output theory [Gardiner04]. This way, as in chapters I, II and III we can access the fields leaving the interferometer by the ports $\hat{a}_B(\omega)$ and $\hat{\beta}_B(\omega)$. These fields are \hat{a}_{out} and \hat{b}_{out} . The approximation $\hat{b} \approx \beta$ in Eq. (IV.9) means that \hat{b}_{out} is only made of reflected classical pump. However, in principle we have $\hat{b} = \beta + \delta\hat{b}$ and $\hat{b}_{\text{out}} = \beta_{\text{out}} + \delta\hat{b}_{\text{out}}$, and one might wonder whether the intracavity fluctuations $\delta\hat{b}$ is negligible or not, and therefore whether it can affect the output fluctuations $\delta\beta_{\text{out}}$ or not. We can check that this is not the case, by solving the input-output problem associated to the Hamiltonian (IV.8), considering \hat{a} and \hat{b} as quantum modes. If we write the Heisenberg equations associated to the Hamiltonian (IV.8), we obtain (see appendix A)

$$\begin{cases} \frac{d}{dt} \hat{a} = -((\omega_c - \omega_b) + \frac{\kappa_{\text{tot}}}{2}) \hat{a} - ig_0 \hat{b} (\hat{m}^\dagger + \hat{m}) - \sqrt{\kappa} \hat{a}_{\text{in}}, \\ \frac{d}{dt} \hat{b} = -((\omega_c - \omega_b) + \frac{\kappa_{\text{tot}}}{2}) \hat{b} - ig_0 \hat{a} (\hat{m}^\dagger + \hat{m}) - \sqrt{\kappa} \hat{b}_{\text{in}}, \\ \frac{d}{dt} \hat{m} = -(\omega_m + \frac{\gamma}{2}) \hat{m} - ig_0 (\hat{a}^\dagger \hat{b} + \hat{a} \hat{b}^\dagger) - \sqrt{\gamma} \hat{m}_{\text{in}}, \end{cases} \quad (\text{IV.10})$$

where the equations for modes \hat{a} and \hat{b} are written in a rotating frame. Here $\kappa_{\text{tot}} = \kappa + \kappa_L$ is the total cavity dissipation rate, taking into account both the input-output dissipation rate κ , as well as the internal losses rate κ_L . One can notice that Eqs. (IV.10) are nonlinear, and therefore not practical for the solving method using the frequency space (see appendixes B and C). This is where the linearization $\hat{a} = \alpha + \delta\hat{a}$, $\hat{b} = \beta + \delta\hat{b}$ and $\hat{m} = \mu + \delta\hat{m}$ is greatly useful as it allow us to reemploy the method we used before. Now, we have two sets of coupled equations, one set for the steady state intracavity complex field amplitudes

$$\begin{cases} 0 = -((\omega_c - \omega_b) + \frac{\kappa_{\text{tot}}}{2})\alpha - ig_0\beta(\mu^* + \mu) - \sqrt{\kappa}\alpha_{\text{in}}, \\ 0 = -((\omega_c - \omega_b) + \frac{\kappa_{\text{tot}}}{2})\beta - ig_0\alpha(\mu^* + \mu) - \sqrt{\kappa}\alpha_{\text{in}}, \\ 0 = -(\omega_m + \frac{\gamma}{2})\mu - ig_0(\alpha^*\beta + \alpha\beta^*) - \sqrt{\gamma}\mu_{\text{in}}, \end{cases} \quad (\text{IV.11})$$

and one for the fluctuations, that also depend on the intracavity steady state

$$\begin{cases} \frac{d}{dt}\delta\hat{a} = -((\omega_c - \omega_b) + \frac{\kappa_{\text{tot}}}{2})\delta\hat{a} - ig_0\beta(\delta\hat{m}^\dagger + \delta\hat{m}) - ig_0\delta\hat{b}(\mu^* + \mu) - \sqrt{\kappa}\delta\hat{a}_{\text{in}}, \\ \frac{d}{dt}\delta\hat{b} = -((\omega_c - \omega_b) + \frac{\kappa_{\text{tot}}}{2})\delta\hat{b} - ig_0\alpha(\delta\hat{m}^\dagger + \delta\hat{m}) - ig_0\delta\hat{a}(\mu^* + \mu) - \sqrt{\kappa}\delta\hat{b}_{\text{in}}, \\ \frac{d}{dt}\delta\hat{m} = -(\omega_m + \frac{\gamma}{2})\delta\hat{m} - ig_0(\alpha^*\delta\hat{b} + \alpha\delta\hat{b}^\dagger) - ig_0(\beta\delta\hat{a}^\dagger + \beta^*\delta\hat{a}) - \sqrt{\gamma}\delta\hat{m}_{\text{in}}, \end{cases} \quad (\text{IV.12})$$

where we neglected second order terms. Before solving the equations for the fluctuations we first need to solve the ones for the steady state fields. In the case where a pump is only sent through the port $\hat{\beta}_B(\omega)$ (see Fig. IV.2), there is no classical field going inside through $\hat{\alpha}_B(\omega)$, and hence $\alpha_{\text{in}} = 0$. Moreover, in a realistic scheme, the mechanical oscillator is at best in its ground state, and at worst in a thermal state, which are both states that give 0 for any first order field moment, hence μ_{in} . With these two simplifications the Eqs. (IV.11) are easily solved analytically, and their solution can be plugged in the Eqs. (IV.12). From there, we apply the method shown in appendixes B and C in order to obtain the output spectra for the radiation fields $\delta\hat{a}_{\text{out}}$ and $\delta\hat{b}_{\text{out}}$.

In Fig. IV.3(a) we show the number of photons escaping through the port $\hat{\beta}_B(\omega)$ and belonging only to the fluctuations $\delta\hat{b}_{\text{out}}$ of the field \hat{b}_{out} . It is a spectrum defined as $n_{b,\text{out}}(\omega) = \int d\omega' \langle \delta\hat{b}_{\text{out}}^\dagger(-\omega)\delta\hat{b}_{\text{out}}(\omega') \rangle$. We can notice that as expected in our approximation, no photons are generated in the quantum fluctuations of the mode \hat{b} , which shows that our approximation leading to the effective Hamiltonian (IV.9) is justified.

IV.3.2 Squeezing generation

So far we have only studied the output $\delta\hat{b}_{\text{out}}$, for the purpose of verifying the stiff pump approximation made for the mode \hat{b} . Here, we study the output leaving at the other port of the interferometer, namely $\delta\hat{a}_{\text{out}}$. In particular, what kind of properties can be found in this quantum noise? We show the answer to this question in Fig. IV.3(b) with the noise spectrum $S_{a,\phi}(\omega)$ for the standard quadratures \hat{X}_a (gray dotted curve) and \hat{Y}_a (black solid curve) respectively defined for the angles $\phi = 0$ and $\phi = \pi/2$. We used parameters typical of optical systems interacting with mechanical resonators. The spectra show squeezing below the standard quantum limit at certain frequencies, reaching the -3 dB limit at $\omega = 0$, which is the origin of the rotating frame. Additionally, we can comment that the resonances at which squeezing occurs remind us of a particular case

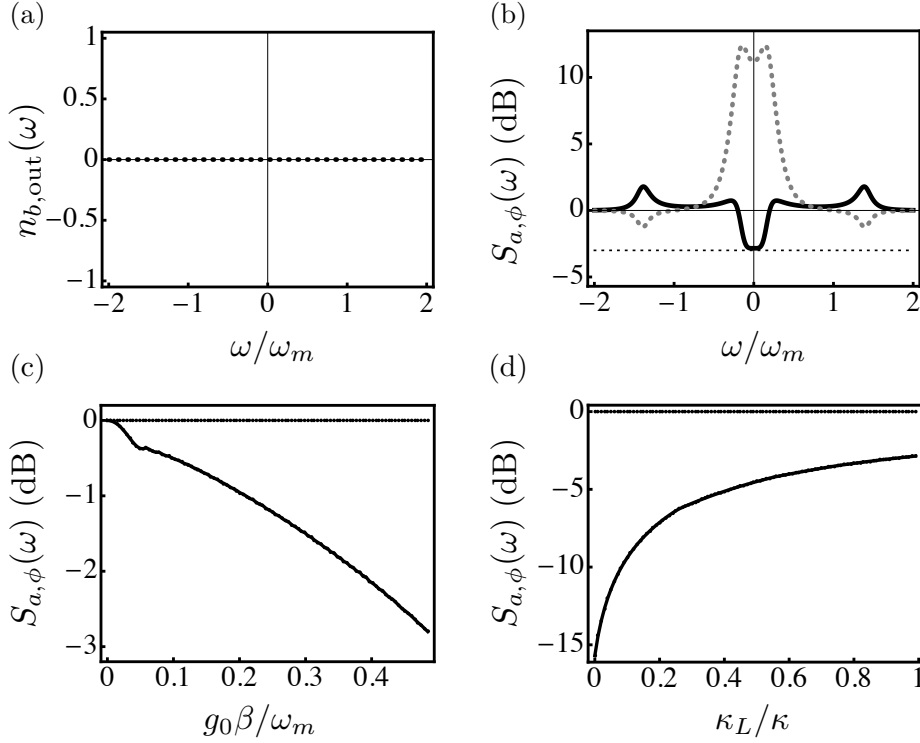


Figure IV.3: Output spectra of various expectation values of the system, as functions of various parameters. The parameters are: $(\omega_c - \omega_b) = \omega_m$; $\kappa = 0.2\omega_m$; $\gamma = 10^{-5}\omega_m$; $\omega_m = 2\pi \times 3$ GHz; mechanical temperature $T_m = 2$ K. (a) Spectrum of the number of photons $n_{b,\text{out}}(\omega) = \int d\omega' \langle \delta \hat{b}_{\text{out}}^\dagger(-\omega) \delta \hat{b}_{\text{out}}(\omega') \rangle$ leaving the system and coming only from the quantum fluctuations of mode \hat{b} . Here $g_0\beta = 0.49\omega_m$; $\kappa_L = \kappa$. (b) Noise spectra $S_{a,\phi}(\omega)$ of \hat{X}_a (gray dotted curve) and of \hat{Y}_a (black solid curve) as functions of the measurement frequency ω in units of the mechanical frequency ω_m , for $g_0\beta = 0.49\omega_m$. Here $\kappa_L = \kappa$. (c) Optimal single-mode squeezing $S_{a,\phi}(\omega)$ for the quadrature \hat{Y}_a and as a function of $g_0\beta$. The curve shows the minimal value of $S_{a,\phi}(\omega)$ with respect to ω . Here $\kappa_L = \kappa$. (d) Optimal single-mode squeezing $S_{a,\phi}(\omega)$ for the quadrature \hat{Y}_a as a function of κ_L , for $g_0\beta = 0.49\omega_m$.

studied in chapter III. In the previous chapter, one consequence of the simulation of the USC regime was squeezing at two resonance frequencies, which symmetrically appear on the both sides of the noise spectra, except in the case where one resonance could meet its negative counterpart, which resulted in spectra whose shape was very similar to the one seen in Fig. IV.3(b).

As in previous chapters, we study the optimal squeezing (optimized with respect to ω) as a function of the coupling strength, which is shown in Fig. IV.3(c). We can see that as expected the squeezing significantly increases with the coupling strength. Note that here, what we call the coupling strength is actually the effective coupling $g_0\beta$ defined in section IV.2, where it is controlled by another mode (\hat{b}) than the one we are interested in (\hat{a}). This means that while we increase the coupling strength by

injecting more photons in the port $\hat{\beta}_B(\omega)$ (see Fig. IV.2), a squeezed vacuum escapes the interferometer through the port $\hat{\alpha}_B(\omega)$.

At last we wish to compare the squeezing we just presented in Figs. IV.3(b) and IV.3(c) with a more favorable situation. So far we considered the case $\kappa_L = \kappa$, which means that on average for each squeezed photon that escape the cavity through the measurable channel, one photon is lost by other means inside the cavity such as absorption for instance. In Fig. IV.3(d) we show the optimal noise spectrum for the quadrature \hat{Y}_a (as in Fig. IV.3(c)), as a function of the loss rate κ_L/κ . We can see that for a sufficiently low internal losses rate the squeezing tends to values lower than -15 dB.

IV.3.3 Comparison with the quantum simulation of the USC regime

In the last part of this section devoted to the study of our model in the continuous regime we report results of a comparison between the properties of the two-mode state of radiation leaving the cavity and the state produced in a Josephson mixer in a quantum simulation of the USC regime (see chapter III). Before doing so, let us specify that contrary to above, we are not interested in the squeezed vacuum leaving the port $\hat{\alpha}_B(\omega)$, but rather the two-mode state leaving the double cavity through the channels $\hat{\gamma}_B(\omega)$ and $\hat{\delta}_B(\omega)$. One important point is that by doing so we abandon the practicability of separating the quantum state \hat{a}_{out} from the classical field $\hat{b}_{\text{out}} \approx \beta_{\text{out}}$, and thus, need to find a way to collect the output states \hat{c}_{out} and \hat{d}_{out} . This can be done by replacing two mirrors by polarizing beam splitter (PBS) and by putting a quarter-wave plate (QWP) right before the each entrance of the double cavity. This allows the input fields in both arms to be reflected through both PBSs and since the inputs and outputs both go twice through the QWPs, the outputs can be transmitted through the PBSs and safely measured. Note however that we still pump this system in the same way as before, with the help of the beam-splitter, since from an experimental point of view it would be the most natural way the drive both cavities at the same time, by using the same laser. Additionally, this driving scheme is particularly practical from the point of view of the input-output resolution, as it allows us to find the mean fields analytically. Indeed, we have seen above that, surprisingly, by using intuitive simplifications ($\alpha_{\text{in}} = \mu_{\text{in}} = 0$), the mean fields α and β and μ can be found analytically in Eq. (IV.11). From there, one just has to apply the beam-splitter relations in order to find the mean fields for \hat{c} and \hat{d} . The same applies for finding the output field fluctuations $\delta\hat{c}_{\text{out}}$ and $\delta\hat{d}_{\text{out}}$.

We show the noise spectra, the single mode ones, as well as the two-mode ones, for the modes $\delta\hat{c}_{\text{out}}$ and $\delta\hat{d}_{\text{out}}$, as functions of the measurement frequency ω in the rotating frame. As one can notice, these spectra show single-mode squeezing, two-mode squeezing and entanglement, in the same fashion as the output state studied in chapter III. Moreover, as in the previous chapter, here we can also witness what resembles a Rabi splitting of the resonance frequency (highlighted with gray arrows). As a matter of fact, to compare the Fig. IV.4 more accurately with Fig. III.4 shown in chapter III, we used the same parameters or the same ratios between parameters in both figures. For instance, the effective frequency δ_B in the previous chapter here becomes the difference $\omega_c - \omega_b = \omega_m$. Similarly, the coupling strength $G = G_B = G_R$ here becomes $g_0\beta$. Concerning the dissipation rates, the ratios $\gamma_{a,b}/\delta_B$ and $\gamma_L/\gamma_{a,b}$ from the previous chapter are here κ/ω_m and κ_L/ω_m . Therefore, it can be noticed in Fig. IV.4 that when the ratio $g_0\beta/\omega_m$ goes beyond 0.1, we have the same spectral

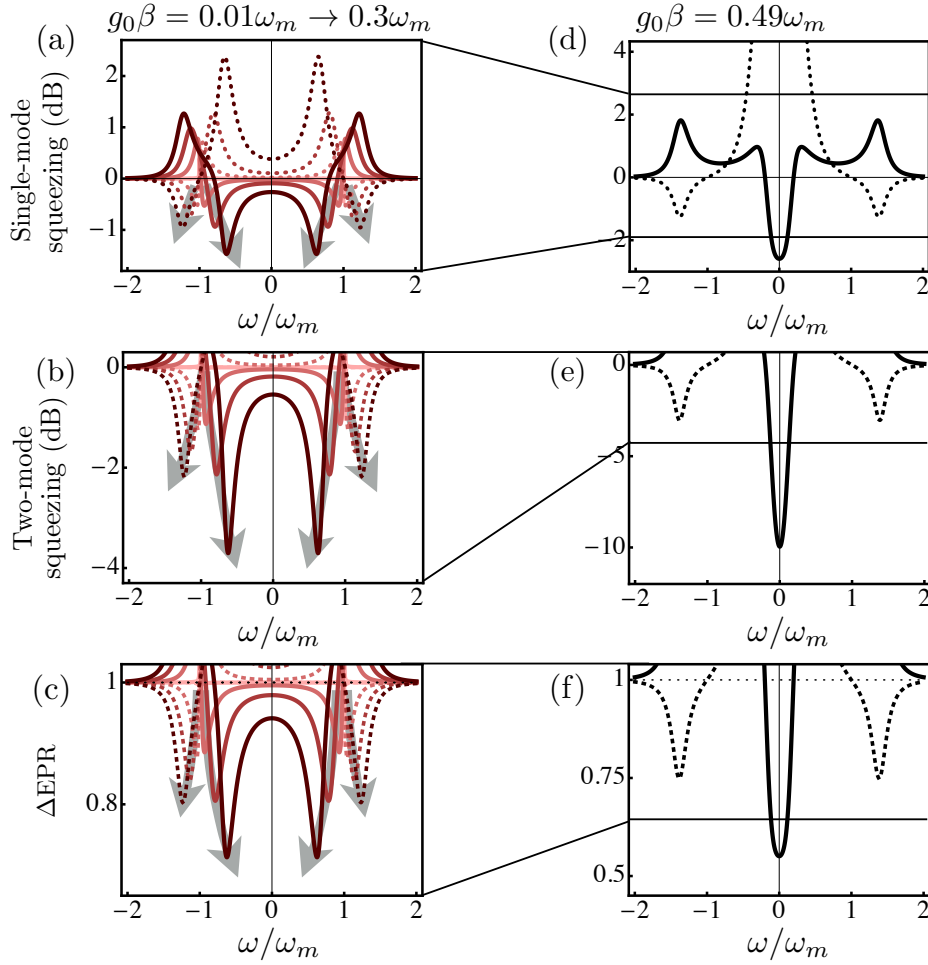


Figure IV.4: Noise spectra of the system's output fields $\delta\hat{c}_{\text{out}}$ and $\delta\hat{d}_{\text{out}}$ as functions of the measurement frequency ω in units of the mechanical δ_B . (a), (d) Single mode noise spectra of \hat{X}_c (dotted curve) and of \hat{Y}_c (solid curve). (b), (e) Two-mode noise spectra of $\hat{X}_c - \hat{X}_d$ (dashed curve) and of $\hat{Y}_c + \hat{Y}_d$ (solid curve). (c), (f) EPR variances $\Delta\text{EPR} = \Delta(X_c - X_d)^2 + \Delta(Y_c + Y_d)^2$ (solid curve) and $\Delta\text{EPR}' = \Delta(X_c + X_d)^2 + \Delta(Y_c - Y_d)^2$. The parameters are: $(\omega_c - \omega_b) = \omega_m$; $\kappa = 0.2\omega_m$; $\kappa_L = 0.02\omega_m$; $\gamma = 10^{-5}\omega_m$; $\omega_m = 2\pi \times 3$ GHz; mechanical temperature $T_m = 2$ K. (a-c) Color code: each color or shade is associated with a value of $g_0\beta/\omega_m$: lighter curves represent $g_0\beta/\omega_m = 0.01$; darker ones, $g_0\beta/\omega_m = 0.3$. From lightest to darkest curve, $g_0\beta/\omega_m$ takes the values $\{0.01, 0.1, 0.2, 0.3\}$. Arrows follow the splitting of the resonance frequency as $g_0\beta/\omega_m$ increases, simulating Rabi splitting. (d-f) Here we fix $g_0\beta/\omega_m = 0.47$, for which the two central dips (peaks) merge at the origin. The black horizontal lines indicate the plot range in (a-c). (c), (f) The thin dotted line indicate the value below which the state is detected as entangled.

features for the output fields fluctuations here, as we had in chapter III. In short, even if the Hamiltonian (IV.7) does not show a direct coupling between modes \hat{c} and \hat{d} , the results are very close to a situation where these modes have an effective frequency

$\omega_c - \omega_b = \omega_m$, and are ultrastrongly coupled in a rotating frame with a coupling strength $g_0\beta$. There however small differences between Figs. IV.4 and III.4. The most noticeable one is the shape of the entanglement witness ΔEPR . Indeed, in Fig. III.4(c) and III.4(f) the entanglement witness $\Delta\text{EPR} = \Delta(X_a - X_b)^2 + \Delta(Y_a + Y_b)^2$ shows four dips with violation, whereas in Fig. IV.4(c) and IV.4(f) $\Delta\text{EPR} = \Delta(X_a - X_b)^2 + \Delta(Y_a + Y_b)^2$ shows only two dips of violation, because the two other dips are violated by the other witness $\Delta\text{EPR}' = \Delta(X_a + X_b)^2 + \Delta(Y_a - Y_b)^2$. This comes from the fact that although the results are surprisingly similar, the Hamiltonians for both models are not the same, which results in these differences.

In chapter III the squeezed vacuum containing the USC regime properties was designed to be generated in the microwave range only, whereas here they could be generated with optical cavities, which opens the way to study the USC regime between optical photons. We note however that here were reported only preliminary results, and a deeper study would be required to fully understand the link between the Hamiltonian (IV.7) and the one of a simulated USC given in Eq. (III.6).

IV.3.4 Stability in the continuous regime

When optomechanics are studied in a regime where the system is driven by a continuous pumping field, a great attention must be devoted to the matter of stability. Indeed, depending on the strength of the drive, on the values of the dissipation rates, an most importantly on the detuning between the pumping field frequency and the cavity frequency. In our case this detuning is $\omega_c - \omega_b = \omega$, which is the so-called red-detuned regime [Aspelmeyer14]. We were solely interested in this regime since it is the one that brings results similar to the quantum simulation of the USC regime. In general this red-detuned regime is of use in schemes when one tries to cool down the mechanical resonator as close as possible to its ground state. This can be understood by simply noting that the resonance condition $\omega_c - \omega_b = \omega$ states that the energy of the pump photons is lower than the energy of the cavity photons by just the energy of a phonon from the mechanical resonator. Therefore, the phonons' energy tends to be transmitted to the cavity in order to generate cavity photons.

Another regime exists, called the blue-detuned regime, where the resonance condition is rather $\omega_c - \omega_b = -\omega$, which basically states that the energy of the photons brought to the system by the pump is higher than the energy of the cavity photons by an amount equal to the energy of a phonon. Therefore, inside the cavity, photons can be generated at the cavity frequency only if that extra energy is transmitted to the mechanical resonator in order to create phonons. This is a rather simple way to summarize the situation, but it gives the idea that in this regime, amplification is involved. When the amplification gain surpasses the effective mechanical damping, self-sustained mechanical oscillations can arise [Aspelmeyer14], such as in a lasing effect. Another name for this effect is *parametric instability*, a matter that was the subject of many studies in optomechanics (see for instance [Marquardt06, Ludwig08]).

In order to avoid the instability in a theoretical model, one can check a stability criterion very reminiscent of the Routh-Hurwitz criterion [DeJesus87]. In quantum optomechanics, it consists in writing the equations of the motions (IV.12) for the quantum

fluctuations as a matrix, such as

$$M(\omega)\hat{\mathbf{A}} - i\hat{\mathbf{A}}_{\text{in}} = 0 \quad (\text{IV.13})$$

where

$$\hat{\mathbf{A}} = \{\delta\hat{a}(\omega), \delta\hat{b}(\omega), \delta\hat{m}(\omega), \delta\hat{a}^\dagger(-\omega), \delta\hat{b}^\dagger(-\omega), \delta\hat{m}^\dagger(-\omega)\}, \quad (\text{IV.14})$$

$$\hat{\mathbf{A}}_{\text{in}} = \{\sqrt{\kappa}\delta\hat{a}_{\text{in}}(\omega), \sqrt{\kappa}\delta\hat{b}_{\text{in}}(\omega), \sqrt{\gamma}\delta\hat{m}_{\text{in}}(\omega), \sqrt{\kappa}\delta\hat{a}_{\text{in}}^\dagger(-\omega), \sqrt{\kappa}\delta\hat{b}_{\text{in}}^\dagger(-\omega), \sqrt{\gamma}\delta\hat{m}_{\text{in}}^\dagger(-\omega)\}, \quad (\text{IV.15})$$

since this criterion does not take into account internal losses. Then, the eigenvalues of the matrix $M(\omega)$ are computed and whose imaginary parts have to be negative in order for the mean fields to be stable [Restrepo14b]. In our model, this criterion has been checked and is valid for the parameters of both Fig. IV.3 and IV.4.

IV.4 Results in the pulsed regime

We now move to our results in the pulsed regime. This means that here, the drive sent through the port $\hat{\beta}_B(\omega)$ in our model presented in Fig. IV.2 is not continuous but made of pulses. Using such a drive in quantum optomechanics can present several advantages over the continuous regime [Hofer11, Vanner11]. For instance, now we are not working in the steady state regime as before, so that the pulsed regime is not subjected to stability requirements, which can limit the amount of achievable optomechanical entanglement in the continuous regime. Additionally, the optomechanical interaction can be activated and verified with two subsequent pulses of light.

In this section we will show that in the pulsed regime, the scheme shown in Fig. IV.2 can be used as a black-box for quantum communication with an internal quantum variable (the mechanical resonator), a quantum input/output port $\alpha_B(\omega)$ and a classical control port $\beta_B(\omega)$ that modulates the interaction between them. Specifically, we will show that two such black boxes can quantum communicate with two quantum protocols, first with the so-called quantum teleportation with continuous variables [Braunstein05], and second with a direct quantum state transfer. Since we showed in the previous section that mode \hat{b} can be safely approximated by a classical amplitude β , we use here the effective Hamiltonian (IV.9). We consider the resolved-sideband regime $\kappa < \omega_m$, where κ is the cavity dissipation rate. Under the requirement that the effective coupling strength is smaller than the mode frequencies $g_0\beta \ll \omega_m, \omega_c$, tuning ω_b enables the selective activation of the red or the blue sideband of the optomechanical interaction. We consider a long-pulsed regime [Hofer11], such that the total interaction time τ is short compared with the timescale γ of mechanical dissipative processes, but long enough to adiabatically eliminate the cavity mode $\kappa^{-1} \ll \tau \ll \gamma^{-1}$. Photon losses with decay rate κ_L are included in the full model (see appendix H).

In this parameter regime, two fundamental processes can be selectively implemented, by tuning the frequency of pump in resonance with the red or the blue sidebands of the optomechanical interaction. In the first case, a state-swap process can be implemented between input/output optical pulses and the state of the mechanical resonator. In the second one, an Einstein-Podolsky-Rosen (EPR)-like state [Einstein35a] is generated

between the output optical pulse and the mechanical resonator.

IV.4.1 State swap

Let us consider first the case in which the red sideband is selected in Eq. (IV.9), *i.e.*, the interaction terms $\hat{a}^\dagger \hat{m} + \hat{a} \hat{m}^\dagger$. The classical drive is a coherent pulse of frequency $\omega_b = \omega_a - \omega_m$, of duration τ . In the interaction picture, the Langevin equations are given by [Gardiner85, Gardiner04, Walls08],

$$\begin{aligned}\dot{\hat{a}}(t) &= -\kappa \hat{a}(t) - ig \hat{m}(t) - \sqrt{2\kappa} \hat{a}_{\text{in}}(t), \\ \dot{\hat{m}}(t) &= -\gamma \hat{m}(t) - ig \hat{a}(t) - \sqrt{2\gamma} \hat{m}_{\text{in}}(t),\end{aligned}\tag{IV.16}$$

where $g = g_0 \beta$. Performing an adiabatic elimination of the cavity mode (see appendix H), one is able to find analytically the input/output relations after a fixed interaction time τ ,

$$\begin{aligned}\hat{A}_{\text{out}}^r &= -e^{-G\tau} \hat{A}_{\text{in}}^r - i\sqrt{1 - e^{-2G\tau}} \hat{M}_{\text{in}}, \\ \hat{M}_{\text{out}} &= e^{-G\tau} \hat{M}_{\text{in}} + i\sqrt{1 - e^{-2G\tau}} \hat{A}_{\text{in}}^r - C^r \hat{M}_B^r,\end{aligned}\tag{IV.17}$$

where $G = \frac{(g_0 \beta)^2}{\kappa}$. $\hat{M}_{\text{in}} = m(0)$ and $\hat{M}_{\text{out}} = \hat{m}(\tau)$ are the states of the mechanical resonator before and after the interaction. The relations of Eq. (IV.17) then describe a state-swap process between the mechanical resonator and the normalized temporal modes $\hat{A}_{\text{in}}^r = Q(\tau, \hat{a}_{\text{in}})$ and $\hat{A}_{\text{out}}^r = P(\tau, \hat{a}_{\text{out}})$, which are defined by the functions,

$$\begin{aligned}P(\tau, \hat{O}) &= \sqrt{\frac{2G}{1 - e^{-2G\tau}}} \int_0^\tau dt e^{-Gt} \hat{O}(t), \\ Q(\tau, \hat{O}) &= \sqrt{\frac{2G}{e^{2G\tau} - 1}} \int_0^\tau dt e^{Gt} \hat{O}(t).\end{aligned}\tag{IV.18}$$

For the state-swap interaction to take place, the input/output pulses must be modulated by a specific exponential envelope given by Eq. (IV.18). The interaction of the mechanical resonator with the thermal environment is included in the model via the term $C^r \hat{M}_B^r$, and it will set the upper bound to the optimal interaction time for the state-swap process. We defined $C^r = \sqrt{\frac{\gamma}{G} (1 - e^{-2G\tau})}$, and $\hat{M}_B^r = Q(\tau, \hat{m}_{\text{in}})$, being \hat{m}_{in} the standard input operator for bosonic bath modes. The impact of the mechanical bath on the optical output is a second-order effect in γ/G , and it is negligible for the interaction times τ considered in this section.

IV.4.2 EPR state generation

On the other hand, when one has $\omega_b = \omega_a + \omega_m$, the blue sideband in Eq. (IV.9) is selected, *i.e.*, the interaction terms $\hat{a}^\dagger \hat{m}^\dagger + \hat{a} \hat{m}$. The corresponding Langevin equations are given by

$$\begin{aligned}\dot{\hat{a}}(t) &= -\kappa \hat{a}(t) - ig \hat{m}(t)^\dagger - \sqrt{2\kappa} \hat{a}_{\text{in}}(t), \\ \dot{\hat{m}}(t) &= -\gamma \hat{m}(t) - ig \hat{a}(t)^\dagger - \sqrt{2\gamma} \hat{m}_{\text{in}}(t).\end{aligned}\tag{IV.19}$$

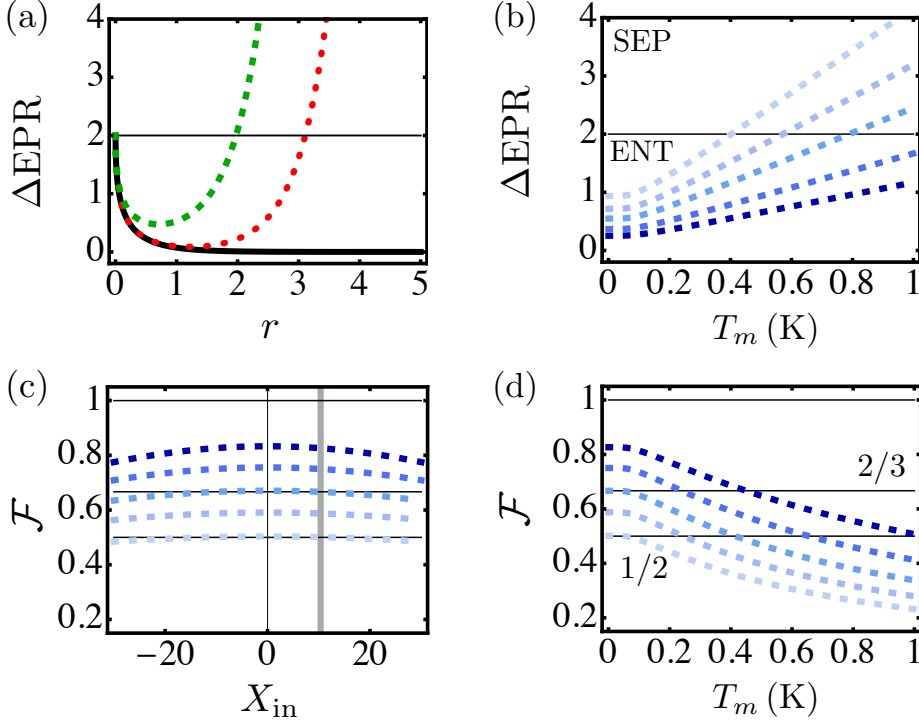


Figure IV.5: Teleportation protocol. Where not specified, here $T_m = 25$ mK, $g = 32.5$ MHz, $\omega_c/2\pi = 194$ THz, $\omega_m/2\pi = 5.3$ GHz, $\gamma/2\pi = 6.5$ kHz, $r = 0.3$, and $\kappa_L/2\pi = 455$ MHz. (a) EPR variance as a function of the squeezing parameter $r = G\tau$. Black full line: no mechanical dissipation γ nor photon losses κ_L ; red dotted line: no photon losses; green dashed line: $\kappa_L/\kappa = 0.3$ and $\kappa/2\pi = 1.52$ GHz. The state is entangled if $\Delta\text{EPR} < 2$. (b) EPR variance as a function of the mechanical bath temperature. (c) Teleportation fidelity \mathcal{F} of a coherent state, as a function of its size X_{in} (here $P_{\text{in}} = 0$) for a displacement efficiency $\eta = 0.99$. The vertical gray line shows the value of $X_{\text{in}} = 10$ used in (d). (d) Teleportation fidelity as a function of the mechanical bath temperature, for $\eta = 0.99$. Color code: from lighter to darker shades of blue: $\kappa_L/\kappa = \{0.7, 0.45, 0.3, 0.18, 0.1\}$ and $r = \{0.2, 0.3, 0.4, 0.58, 0.7\}$. As the κ_L/κ ratio is decreased, the total dissipation rate $\kappa + \kappa_L$ is increased.

Under the same assumptions, analytical solutions for the input/output relations can be found

$$\begin{aligned}\hat{A}_{\text{out}}^b &= -e^{G\tau}\hat{A}_{\text{in}}^b - i\sqrt{e^{2G\tau} - 1} \left(\hat{M}_{\text{in}}\right)^\dagger, \\ \hat{M}_{\text{out}} &= e^{G\tau}\hat{M}_{\text{in}} + i\sqrt{e^{2G\tau} - 1} \left(\hat{A}_{\text{in}}^b\right)^\dagger - C^b\hat{M}_B^b.\end{aligned}\quad (\text{IV.20})$$

This relation corresponds to an EPR state generation between the mechanical resonator and a traveling light mode defined by an exponentially shaped envelope, with central frequency ω_c . In this case, the solutions are found in terms of the normalized temporal modes $A_{\text{in}}^b = P(\tau, \hat{a}_{\text{in}})$ and $A_{\text{out}}^b = Q(\tau, \hat{a}_{\text{out}})$, defined in Eq. (IV.18). Notice that the time-envelope of the input/output pulses of the blue sideband process (en-

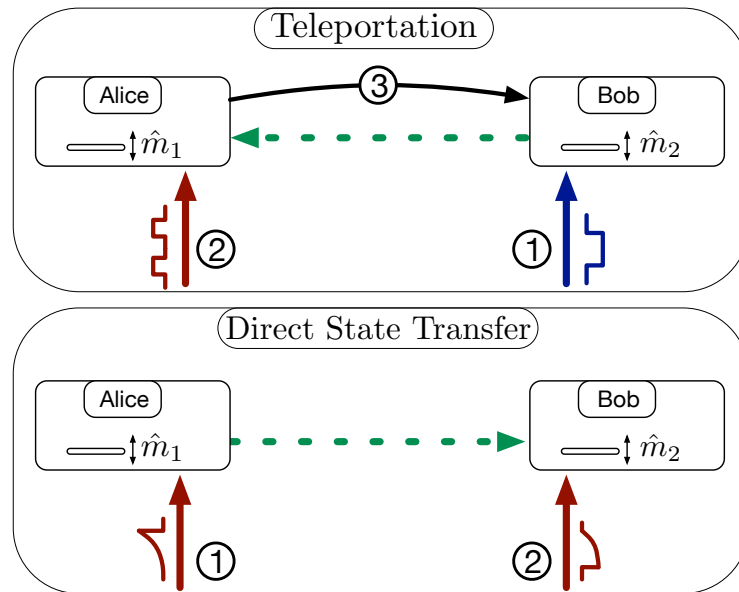


Figure IV.6: Schemes of the teleportation and state transfer protocols. Circled numbers represent different temporal steps. (Top panel) Teleportation protocol. (1) Bob generates an optomechanical EPR state. (2) Alice implements a Beam-Splitter interaction and the required measurements. (3) The results of the measurements are sent over a classical communication channel to Bob. (Bottom panel) State transfer process between remote mechanical oscillators. The classical drive must be time-modulated in order to optimize the time-envelope of the quantum signal.

tanglement generation) are the opposite ones with respect to the red sideband (state-swap). Here, the effect of the thermal environment is given by the term $C^b \hat{M}_B^b$, where $C^b = \sqrt{\frac{\gamma}{G} (e^{2G\tau} - 1)}$, and $\hat{M}_B^b = P(\tau, \hat{m}_{\text{in}})$. To assess the degree of entanglement of the generated state we use the EPR variance [Duan00], shown in Figs. IV.5(a) and IV.5(b), a figure of merit that can be smaller than 2 only for entangled states. The optimal pulse duration is given by a trade-off between entanglement generation and dissipative processes.

IV.4.3 Protocols

In the following, we show how the state-swap and EPR generation processes can be applied to implement quantum communication between remote mechanical resonators. In particular we will consider two protocols shown in Fig IV.6, that is teleportation and remote quantum state transfer. In both cases, the goal is to transmit a quantum state originally encoded on Alice's mechanical resonator onto Bob's, using a quantum-optical channel. In the case of teleportation, an entangled state is initially shared between the two parties, after which only local operations and classical communication are needed. On the other hand, remote quantum state transfer does not require entanglement sharing nor feed-forward operations, at the cost of modulating in time the intensity of the classical driving pulses.

IV.4.3.1 Teleportation

Let us first detail how a standard continuous-variable teleportation protocol [Braunstein98, Pirandola15] can be feasibly applied with the proposed scheme. When the state to be teleported is encoded in Alice's device, the protocol is composed of the following steps, sketched in Fig IV.6. 1) Through the blue sideband process, Bob generates an EPR state between its mechanical device and a light pulse, which is sent to Alice. 2) Alice implements a beam-splitter (BS) interaction between the received pulse and her mechanical oscillator. Such a BS interaction can be obtained with the red sideband process of Eq. (IV.17), setting the effective coupling parameter G so that $e^{-G\tau} = 1/\sqrt{2}$. Notice that the time envelope of the EPR pulse generated in step 1 matches the optimal shape given by the input/output relations of Eq. (IV.17). Then, the output optical pulse is measured via homodyne detection, while the mechanical resonator is measured through red-sideband interaction with a probe field. 3) The results of the two measurements are sent through a classical channel to Bob, who uses this information to choose the phase of a displacement operation to be applied to his mechanical resonator. At the end of the protocol, the state is destroyed in Alice's device and deterministically teleported onto Bob's.

Let us denote the quadratures of Bob's mechanical resonator with $\hat{X}_2(t) = [\hat{m}_2(t)^\dagger + \hat{m}_2(t)]/\sqrt{2}$ and $\hat{P}_2(t) = i[\hat{m}_2(t)^\dagger - \hat{m}_2(t)]/\sqrt{2}$, and Alice's ones with $\hat{X}_1(t)$ and $\hat{P}_1(t)$. At the end of the teleportation protocol, the state of Bob's mechanical resonator is given by (see appendix H)

$$\begin{aligned}\hat{X}_2^{tel} &= \eta\hat{X}_1(0) + R\hat{X}_2(0) + R'\hat{P}_{\text{in}}, \\ \hat{P}_2^{tel} &= \eta\hat{P}_1(0) + R\hat{P}_2(0) + R'\hat{X}_{\text{in}},\end{aligned}\tag{IV.21}$$

where $\hat{X}_{\text{in}} = [(\hat{A}_{\text{in}}^b)^\dagger + \hat{A}_{\text{in}}^b]/\sqrt{2}$ and $\hat{P}_{\text{in}} = i[(\hat{A}_{\text{in}}^b)^\dagger - \hat{A}_{\text{in}}^b]/\sqrt{2}$ are the quadratures of the optical input of Bob's device, as defined in Eq. (IV.20). Here η is the efficiency of the coherent displacement applied by Bob at the end of the protocol, and we defined the parameters $R = e^r - \eta\sqrt{e^{2r} - 1}$ and $R' = \sqrt{e^{2r} - 1} - \eta e^r$. This teleportation protocol is deterministic, the teleportation fidelity tends to 1 for very large squeezing $r \gg 1$ and $\eta = 1$.

In Figs. IV.5(c) and IV.5(d), we show the fidelity of the final state for different sets of feasible parameters [Krause15, Riedinger16, Massel11, Palomaki13b, Wollman15, Guha16], in the special case in which a coherent state is teleported. Notice that in Eq. (IV.21) we neglected for the sake of simplicity the mechanical decoherence and photon losses, yet a full treatment was used in Fig. IV.5 and can be found in appendix H. For uniformly distributed coherent states, it can be shown [Hammerer05] that the optimal classical strategy gives an average fidelity $\mathcal{F} = 1/2$, providing a lower bound for the validation of the implementation of quantum teleportation. Another interesting bound is given by the no-cloning limit [Cerf00, Grosshans01] $\mathcal{F} > 2/3$, which certifies that Bob has the best existing copy of the original state.

IV.4.3.2 Implementation in physical systems

We now verify the possibility to implement the teleportation protocol by applying it to existing experiments [Massel11, Palomaki13b, Wollman15, Krause15, Riedinger16]. If

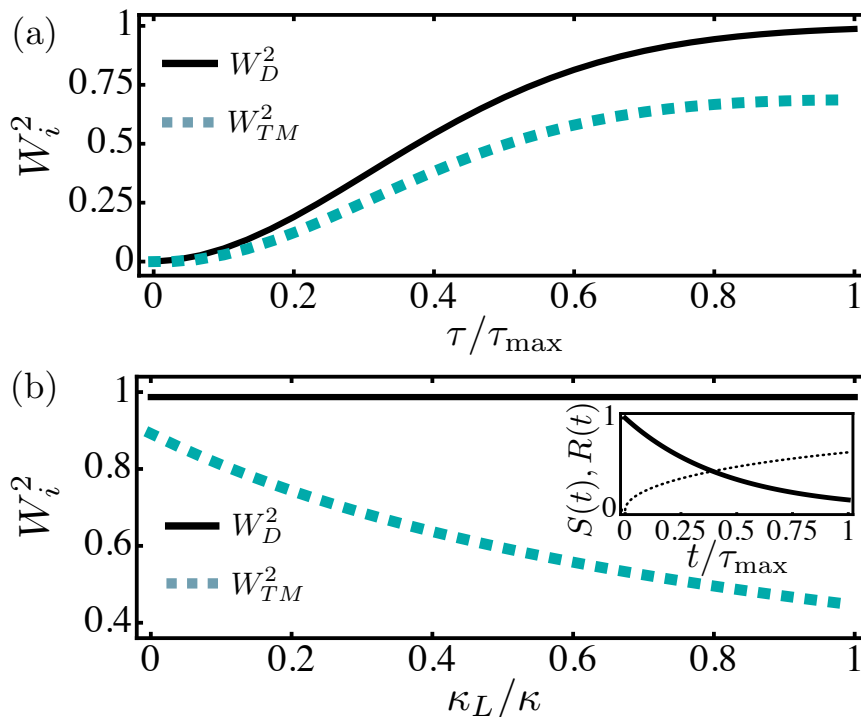


Figure IV.7: State transfer protocol. Fraction of the initial state $\hat{m}(0)$ that have been transferred to the second mechanical oscillator $\hat{m}_2(\tau)$ (W_{TM}^2), and that have been destroyed on the first mechanical oscillator $\hat{m}_1(\tau)$ (W_D^2), as functions of the pulses duration τ (a), and of the ratio κ_L/κ (b). The parameters are $\tau_{\max}/2\pi = 0.04/\gamma$, $g = 32.5$ MHz, $\omega_c/2\pi = 194$ THz, $\omega_m/2\pi = 5.3$ GHz, $\gamma/2\pi = 6.5$ kHz. (a) $\kappa_L/\kappa = 0.3$, $\kappa/2\pi = 1.52$ GHz. (b) $\tau = \tau_{\max}$, and as κ_L/κ goes from 0 to 1, $\kappa/2\pi$ goes from 4.55 GHz to 650 MHz. INSET : optimal temporal shapes of the control pulses for the sender (solid curve) and the receiver (dotted curve). Note that in (b), even when κ_L/κ goes to 0, we still have $W_{TM}^2 < 1$ due to the mechanical dissipation.

our scheme shown in Fig. IV.2 is adapted to the architecture of each of these experiments, it becomes relevant to study whether the state of the art parameters achieved in these references allow or not to perform a quantum teleportation. Therefore, we will use the parameters from these articles to show what are the typical teleportation fidelities for one can obtain. Note however that if the values of the parameters are different from the needed values, it may not only due to the current technological and technical limits, but also to the fact that these experiments have not been optimized for quantum teleportation. In order to verify this, in the following we show the computed fidelity for each of these references, by starting with experiments performed with telecom wavelength photons [Krause15, Riedinger16].

Implementation with telecom wavelength photons In Fig. IV.8 we show the fidelity for the parameters from [Krause15, Riedinger16], as a function of the temperature T_m of the mechanical oscillator, as well as a function of the output coupling rate κ of the cavity and the ratio between the photon losses rate κ_L and the output coupling

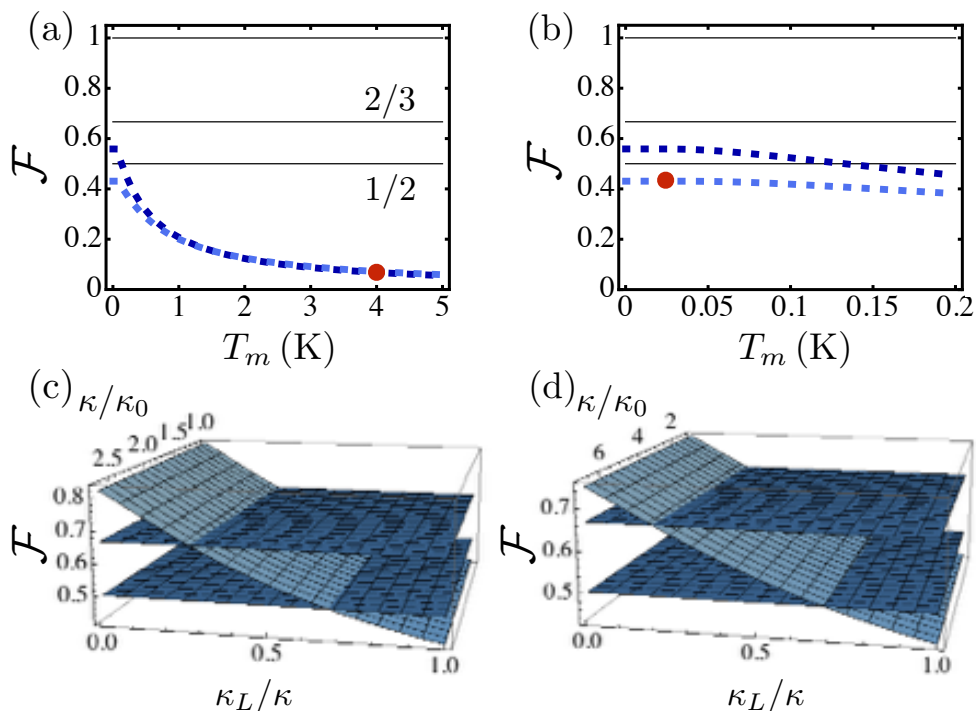


Figure IV.8: Teleportation fidelity from Eq. (H.41) for a coherent state using the parameters from [Krause15] (darker blue dashed line in (a) and (b)) and [Riedinger16] (lighter blue dashed line in (a) and (b)). The red dots correspond to the temperature from each experiment. From lighter to darker shades of blue: $r = 0.25$; $r = 0.1$. (c) Experiment from [Krause15], with the temperature as in line five, *i.e.*, $T_m = 25$ mK. (d) Experiment from [Riedinger16]. κ_0 correspond to the original value from [Krause15, Riedinger16]. Note that in (c) and (d) the maximum values for κ/κ_0 that are considered are limited by the resolved sideband regime where $\kappa < \omega_m$.

rate. The study as a function of T_m in Figs. IV.8(a) and IV.8(b) shows how much the system needs to be cooled down to beat the classical limit of $\mathcal{F} = 0.5$, or the limit $\mathcal{F} = 2/3$. Note that the actual temperature in each experiment is indicated by a dot. We can notice in Fig. IV.8(b) that even with a very low temperature of 25 mK, it is only enough to achieve a 0.4 fidelity with the parameters from [Riedinger16] because the photon losses rate κ_L is equal to the output coupling rate κ . It is thus intuitive that in order to achieve a teleportation fidelity of at least 0.5, one needs the photon losses rate to be smaller than the output coupling rate.

Let us remark that the high ratios κ_L/κ in these experiments are not the best achievable values. Indeed, this ratio can be decreased at the expense of an increase of the total cavity linewidth $\kappa + \kappa_L$. For this reason, we show in Figs. IV.8(c) and IV.8(d) the fidelity as a function of κ_L/κ and of κ , which allows us to study the effect of a decrease of the photon losses ratio, while taking into account the overall increase in the cavity linewidth. Here we remark that we can reach values of \mathcal{F} above $2/3$ when $\kappa_L/\kappa \lesssim 0.15$, even when κ is increased by more than one order of magnitude. Furthermore, the classical limit can be beaten with larger ratio κ_L/κ . Note however that for Fig. IV.8(c), we

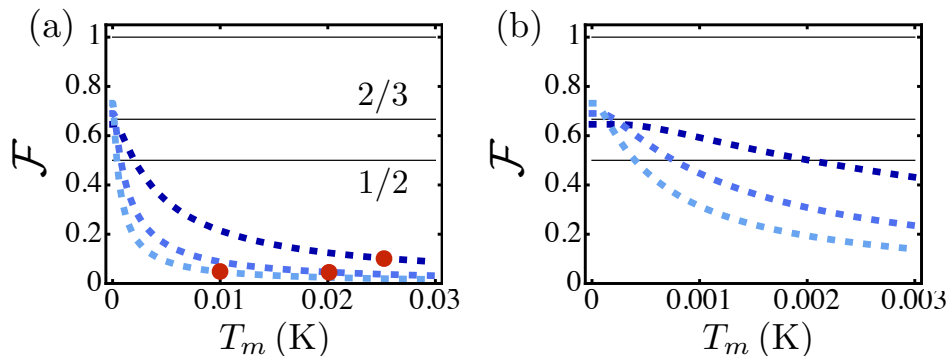


Figure IV.9: Teleportation fidelity from Eq. (H.41) for a coherent state using the parameters from [Massel11, Palomaki13b, Wollman15] (respectively from darker to lighter shades of blue in (a) and (b)). The red dots correspond to the temperature from each experiment. Note that for the experiment from [Wollman15] we used the same ratio $\kappa_L/\kappa = 0.2$ as in line 2. From lighter to darker shades of blue: $r = 0.35$; $r = 0.5$; $r = 0.5$.

consider the same temperature as in IV.8(d), $T_m = 25$ mK.

Implementation with microwave photons Let us now verify the feasibility of our protocol in electromechanical systems, working at microwave frequency. In Fig. IV.9 we show the fidelity for the parameters from [Massel11, Palomaki13b, Wollman15], as a function of the temperature T_m of the mechanical oscillator. We can see again how much the three systems must be cooled down in order to achieve a fidelity of 0.5 or $2/3$. One can notice here that when the temperature tends to 0 K, the three fidelities overcome the $2/3$ limit. However, in Figs. IV.8(a) and IV.8(b), only one of the fidelities overcomes the 0.5 classical limit when the temperature tends to 0 K. It can be understood by noticing that the κ_L/κ ratio is lower for the microwave systems in Fig. IV.9 than for the optical systems in IV.8.

IV.4.3.3 Remote state transfer

Let us now consider the case in which a quantum state is directly exchanged between two remote mechanical resonators, as in the lower panel of Fig IV.6. The protocol is organised as follows: a red detuned driving pulse $\beta_S(t) = \beta S(t)$ of duration τ is sent through Alice's control port, mapping the state of her mechanical resonator onto a propagating light pulse $\hat{a}_{\text{out}}(t)$. The quantum signal is sent to Bob, who modulates the optomechanical interaction in his device via a red-detuned control pulse $\beta_R(t) = \beta R(t)$. The interaction within Bob's toolbox completes the transfer between Alice's $\hat{m}_1(0)$ and Bob's $\hat{m}_2(\tau)$ mechanical resonators. Time-modulated classical drivings are needed to overcome a fundamental issue, absent in the teleportation protocol presented above. The photon emission and absorption processes are the time-reversal of each other, when flat drivings are considered. Hence, the emitted pulse sent by Alice would not have the right

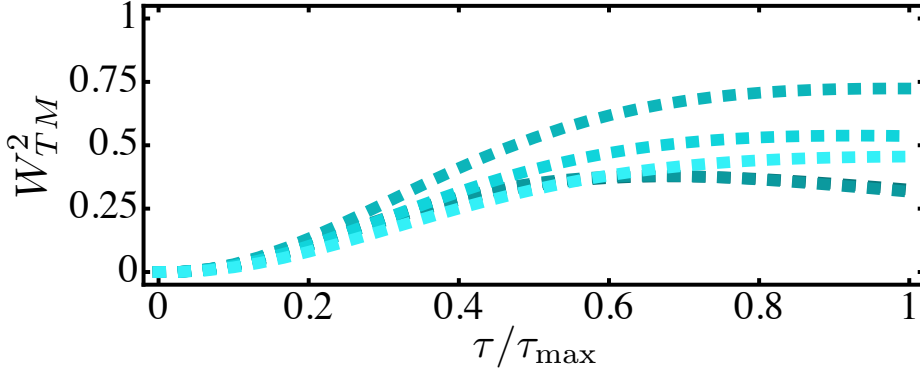


Figure IV.10: Direct state transfer efficiency W_{TM}^2 defined in Eq.(IV.22) (and the detailed expression is specified in the appendix I), as a function of the pulses duration τ , using parameters from [Massel11, Palomaki13b, Wollman15, Krause15, Riedinger16](respectively from darker to lighter shades of green). From darker to lighter shades of green: $\tau_{\max}/2\pi = 0.417/\gamma$; $\tau_{\max}/2\pi = 0.467/\gamma$; $\tau_{\max}/2\pi = 0.0533/\gamma$; $\tau_{\max}/2\pi = 0.0857/\gamma$; $\tau_{\max}/2\pi = 0.0295/\gamma$. The two darkest dashed lines using parameters from [Massel11, Palomaki13b] are superimposed, due to the fact that for these references, the ratio γ/κ is similar.

time-envelope to be efficiently absorbed by Bob. Designing the time-envelopes is crucial if one wants to avoid any undesirable signal reflections between two nodes of a quantum network [Cirac97]. The temporal shapes have been optimized for the pumps used by the sender $S(t)$ and by the receiver $R(t)$, for arbitrary states, in order to maximize the transfer efficiency. The inset in Fig. IV.7(b) shows the optimal functions $S(t)$ and $R(t)$ for the state-of-the-art parameters considered in our work (see appendix I).

At the end of the protocol, the states of Alice's mechanical resonator and Bob's mechanical resonator are

$$\begin{aligned}\hat{m}_1(\tau) &= \sqrt{1 - W_D^2} \hat{m}_1(0) + N_1(\hat{a}_{\text{in}}, \hat{m}_{\text{in}}, \tau), \\ \hat{m}_2(\tau) &= W_{TM} \hat{m}_1(0) + N_2(\hat{a}_{\text{in}}, \hat{m}'_{\text{in}}, \hat{m}_{\text{in}}, \tau),\end{aligned}\quad (\text{IV.22})$$

where for the sake of clarity we gathered all the contributions due to the optical and thermal environment in N_1 and N_2 . The parameter W_{TM} establishes how significant is the transfer of $\hat{m}_1(0)$ to $\hat{m}_2(\tau)$, optimal state transfer corresponds to $W_{TM} = 1$. The parameter W_D shows how the state $\hat{m}_1(\tau)$ of the sender (Alice) is destroyed throughout the protocol.

In Fig. IV.7 we show the results for state-of-the-art experimental parameters, and details of the calculations leading to these results can be found in appendix I. We consider the square of these quantities since it establishes the efficiency of the transfer for the second order moments. We stress out that the pulse sequence is optimal, i.e., there are no losses of information due to the time-envelope mismatch between the emission and absorption processes. Notice that, depending on the duration of the pump pulses, the state $\hat{m}_1(0)$ can be partially transferred to Bob, and only partially destroyed in Alice's device. Hence, arbitrary quantum states can be transferred in a tunable and

non-destructive way.

IV.4.4 Implementation in physical systems

Just as we did in for the teleportation protocol above, here we wish to verify the feasibility of the direct state transfer protocol considering the physical parameters of five previous experiments [Massel11, Palomaki13b, Wollman15, Krause15, Riedinger16]. These parameters are used to compute the quantity defined in Eq.(IV.22) (and whose detailed expression is specified in the appendix I), which is the figure of merit of the protocol. We report the results in Fig. IV.10, where we can see that even for experiments which have not been optimized for our protocol, their parameters give a good efficiency W_{TM}^2 . Note that here again, the success of the protocol is limited by the ratio κ_L/κ . To increase the efficiency, one would need to decrease this ratio, at the expense of increasing the total dissipation rate $\kappa + \kappa_L$.

IV.5 Conclusion

In this last chapter we presented another fruitful platform for the study of fundamental as well as practical applications of quantum mechanics and light-matter interactions. We have shown that in quantum systems where optomechanical interactions can be found, it is possible to design a particular interferometric scheme that can be used as a black-box for different tasks, with the advantage of naturally emitting the quantum output of interest already separated from the pumping field. We have shown that for sufficiently larger effective optomechanical coupling with respect to the mechanical frequency, one can reach a regime where the system emits a highly squeezed state, with spectral features reminiscent of the ones found in the quantum simulation of the USC regime studied in chapter III. Additionally, on a more opening note, we slightly shifted from the main focus of the thesis, namely the link between the USC regimes and squeezed states, to explore broader perspectives regarding the optomechanical scheme we designed. Indeed, we have shown how this interferometric scheme could be used as a node in a quantum communication network, by proposing two protocol, feasible with current technology.

As a first perspective, we wish to point out that the link between this optomechanical device studied in this chapter and the quantum simulation of the USC regime between two bosonic fields should be the topic of a deeper study, as the preliminary results presented here seem to only scrape the surface of richer physics. As a second perspective, the versatility of the optomechanical devices could be explored further by working towards a model where mechanical resonators are not only coupled to telecom wavelength photons, but also the microwave systems for instance such as qubits in order to perform to totality of quantum information tasks.

General conclusion

Light-matter interactions at the quantum level is a prominent field of research encompassing both fundamental and applied questions. In this thesis we have explored a new facet of the ultrastrong coupling (USC) regime in light-matter interactions, mainly related to its link with nonclassical states of light.

Namely, we have shown the conditions needed in a USC regime such that the system can generate nonclassical states of light, motivated by the idea that similar conditions have already been proven to trigger the emission of quantum vacuum radiation [De Liberato07]. Thus, we showed that when a system is ultrastrongly coupled, and this coupling is ruled by a non-adiabatic time modulation such as in a dynamical Casimir effect [Moore70, Kardar99], the photons that are generated from vacuum are actually less noisy than the vacuum itself. This result is not only of fundamental interest, but is also pertinent for applications. For instance, if this model is realized in solid-state resonators made of semiconducting quantum wells inside microcavities, these systems would emit squeezed radiation at terahertz or at mid-infrared frequency ranges. As a matter of fact, up to now quantum optics phenomena have only been fully explored at the optical and the microwave frequencies ranges, leaving the frequency range in between mainly untouched. Therefore, demonstrating squeezed radiation for this new frequency band would be a major step towards helping to close the so-called *terahertz gap* [Sirtori02, Kleiner07].

Additionally, we proposed a scheme to explore the ground state properties of the USC regime. By devising a model based on a physical platform with a high degree of experimental control, we have shown how this system could emit a two-tone microwave radiation with quantum noise properties very similar to the ones in a ground state of the USC between two bosonic fields. Using in our model only tools available with current technology, we demonstrated the efficiency of quantum simulation, namely, when a problem cannot be tackled directly in its genuine physical platform. Indeed, in the USC regime between two bosonic fields experimentally achieved so far, it is not possible yet for the system to emit a radiation with such quantum properties. Therefore, studying these ground state properties and in particular demonstrating them experimentally is very difficult, and for the coupling between two bosonic fields no solution was ever proposed. We bypassed this difficulty by designing a quantum simulation of the USC regime using current technology, which allow one to experimentally access quantum noise properties similar to the ones in the ground state.

Furthermore, we designed a model featuring optomechanical interaction and found that such a system can generate a two-mode radiation at optical frequencies showing noise properties similar to the ones achievable in a quantum simulation of the USC regime. However, in this new optomechanical model, the USC regime is not explicitly achieved nor simulated, which indicate that a non-trivial link may exist between the USC regime and this optomechanical model. Therefore, these preliminary results call

for a deeper study in order to fundamentally understand this link.

Finally, having this optomechanical model at our disposal, we further explored its physics and slightly deviated from our initial scope concerned with the USC regime. Consequently, we presented, as an outlook, means to use this model as a base ground for quantum communication tasks, such as a quantum teleportation with continuous variables and a direct quantum state transfer. Although several physical platforms are good candidates for acting as nodes of a quantum networks, our contribution is in line with a logic of diversification and thus the development of alternate candidates to host a potential quantum Internet [Pirandola16].

In short, this thesis has been an excellent opportunity to explore the consequences of various kinds of light-matter interactions and to study how, on the one hand, these impact our understanding of some fundamental questions, and how, on the other hand, these can be used as a resource for useful applications in quantum technologies, a field of research more useful than ever nowadays.

A Deriving the equations of motion with input-output theory

Here we show how to derive the equation of motion, or Langevin equation, for a quantum harmonic oscillator described by annihilation and creation operators \hat{a} and \hat{a}^\dagger . We will follow the steps of the input-output theory proposed in [Gardiner85]. We want an equation of motion that takes into account dissipation in the time evolution, and for that reason we need to model the environment of the oscillator in the Hamiltonian. We will model it by a continuum of quantum harmonic oscillators described by $\hat{A}(\omega)$ and $\hat{A}^\dagger(\omega)$. In the framework, the full Hamiltonian for our system is

$$\hat{H}_{\text{full}} = \hat{H}_{\text{sys}} + \hat{H}_{\text{bath}} + \hat{H}_{\text{sb}}, \quad (\text{A.1})$$

$$\text{where } \hat{H}_{\text{bath}} = \hbar \int_{-\infty}^{+\infty} d\omega \omega \hat{A}^\dagger(\omega) \hat{A}(\omega), \quad (\text{A.2})$$

$$\text{and } \hat{H}_{\text{sb}} = i\hbar \int_{-\infty}^{+\infty} d\omega \kappa_a(\omega) (\hat{A}^\dagger(\omega) \hat{a} - \hat{A}(\omega) \hat{a}^\dagger). \quad (\text{A.3})$$

\hat{H}_{sys} is the system Hamiltonian that solely involves \hat{a} and \hat{a}^\dagger . \hat{H}_{bath} is the bath free evolution Hamiltonian, while \hat{H}_{sb} is the system-bath coupling. The fact that both integrals are between $-\infty$ and $+\infty$ may appear unphysical at first sight. Indeed, if \hat{a} correspond to a mode of the electromagnetic field, then modes $\hat{A}(\omega)$ do so as well, and thus all must be defined only for positive frequencies. However, input-output theory was originally defined to treat quantum optics problems, that are usually considered in a rotating frame at some frequency Ω . Indeed, in a frame rotating at Ω , the frequency origin has been shifted from 0 to Ω . Thus, in Eqs. (A.2) and (A.3) the terms with negative ω s inside the integrals would still correspond to physical positive frequencies as long as $\Omega + \omega > 0$. Furthermore, if the physics of the studied problem occur on a frequency band $\Delta\omega$ around Ω , with $\Delta\omega \ll \Omega$, for \hat{H}_{bath} the integration can be performed between $-\infty$ and $+\infty$. Regarding \hat{H}_{sb} however, an additional approximation must be made in order to extend the integration range, as the system-bath coupling must be written in the rotating wave approximation, which is the case here. Indeed, in \hat{H}_{sb} we already dropped the terms $\hat{A}^\dagger(\omega) \hat{a}^\dagger$ and $\hat{A}(\omega) \hat{a}$ [Gardiner04].

For any operator \hat{S} , the Heisenberg equation of motion is expressed as [Cohen-Tannoudji77]

$$i\hbar \frac{d}{dt} \hat{S} = [\hat{S}, \hat{H}_{\text{full}}]. \quad (\text{A.4})$$

In order to obtain such an equation for \hat{a} , we first need to obtain it for \hat{A}

$$\begin{aligned}\frac{d}{dt}\hat{A}(\omega) &= -\frac{i}{\hbar}[\hat{A}(\omega), \hat{H}_{\text{full}}] \\ &= -i \int_{-\infty}^{+\infty} d\omega' \omega' [\hat{A}(\omega), \hat{A}^\dagger(\omega')] \hat{A}(\omega') + \int_{-\infty}^{+\infty} d\omega' \kappa_a(\omega') [\hat{A}(\omega), \hat{A}^\dagger(\omega')] \hat{a} \\ &= -i\omega \hat{A}(\omega) + \kappa_a(\omega) \hat{a},\end{aligned}\tag{A.5}$$

simplified by using $[\hat{A}(\omega), \hat{A}^\dagger(\omega')] = \delta(\omega - \omega')$ and $\int_{-\infty}^{+\infty} d\omega' f(\omega') \delta(\omega - \omega') = f(\omega)$. Eq. (A.5) can easily be solved and its solution is

$$\hat{A}(\omega) = e^{-i\omega(t-t_i)} \hat{A}_i(\omega) + \kappa_a(\omega) \int_{t_i}^t dt' e^{-i\omega(t-t')} \hat{a}(t')\tag{A.6}$$

where $\hat{A}_i(\omega)$ stands for the bath operator prior to its interaction with the system, at a time t_i . For \hat{a} , such an equation writes

$$\begin{aligned}\frac{d}{dt}\hat{a} &= -\frac{i}{\hbar}[\hat{a}, \hat{H}_{\text{full}}] \\ &= -\frac{i}{\hbar}[\hat{a}, \hat{H}_{\text{sys}}] - \int_{-\infty}^{+\infty} d\omega \kappa_a(\omega) \hat{A}(\omega),\end{aligned}\tag{A.7}$$

where we can inject Eq. (A.5) in order to obtain

$$\begin{aligned}\frac{d}{dt}\hat{a}(t) &= -\frac{i}{\hbar}[\hat{a}(t), \hat{H}_{\text{sys}}] - \int_{-\infty}^{+\infty} d\omega \kappa_a(\omega) e^{-i\omega(t-t_i)} \hat{A}_i(\omega) \\ &\quad - \int_{-\infty}^{+\infty} d\omega \kappa_a^2(\omega) \int_{t_i}^t dt' e^{-i\omega(t-t')} \hat{a}(t').\end{aligned}\tag{A.8}$$

At this stage, additional approximations must be made in order to obtain an equation of motion that is convenient to handle. We use the *first Markov approximation* [Gardiner85, Gardiner04],

$$\kappa_a(\omega) = \sqrt{\frac{\gamma_a}{2\pi}},\tag{A.9}$$

which amounts to say that the system-bath coupling is the same regardless of the frequency ω . By defining an input annihilation operator as

$$\hat{a}_{\text{in}}(t) = \frac{1}{\sqrt{2\pi}} \int_{-\infty}^{+\infty} d\omega e^{-i\omega(t-t_i)} \hat{A}_i(\omega),\tag{A.10}$$

and injecting both Eqs. (A.9) and (A.10) in Eq. (A.8), we obtain

$$\frac{d}{dt}\hat{a}(t) = -\frac{i}{\hbar}[\hat{a}(t), \hat{H}_{\text{sys}}] - \sqrt{\gamma_a} \hat{a}_{\text{in}}(t) - \gamma_a \int_{t_i}^t dt' \delta(t-t') \hat{a}(t').\tag{A.11}$$

One last approximation consists in writing

$$\int_{t_i}^t dt' \delta(t-t') \hat{a}(t') = \frac{1}{2} \hat{a}(t), \quad (\text{A.12})$$

where the factor of 1/2 arises because the delta function is peaked at the end of the integration range [Gardiner04]. Finally, one obtains the following equation of motion

$$\frac{d}{dt} \hat{a}(t) = -\frac{i}{\hbar} [\hat{a}(t), \hat{H}_{\text{sys}}] - \sqrt{\gamma_a} \hat{a}_{\text{in}}(t) - \frac{\gamma_a}{2} \hat{a}(t). \quad (\text{A.13})$$

Note that as we defined the input operator \hat{a}_{in} , we can define an output operator

$$\hat{a}_{\text{out}}(t) = \frac{1}{\sqrt{2\pi}} \int_{-\infty}^{+\infty} d\omega e^{-i\omega(t-t_i)} \hat{A}_f(\omega), \quad (\text{A.14})$$

where analogously to \hat{A}_i , here \hat{A}_f stands for the bath operator after its interaction with the system, at a time t_f . An equation for the solution of $\hat{A}(\omega)$, analogous to the Eq. (A.6) can be found and is written as

$$\hat{A}(\omega) = e^{-i\omega(t-t_f)} \hat{A}_f(\omega) - \kappa_a(\omega) \int_{t_f}^t dt' e^{-i\omega(t-t')} \hat{a}(t'). \quad (\text{A.15})$$

Then, by integrating both Eqs. (A.6) and (A.15), we obtain

$$\frac{1}{\sqrt{2\pi}} \int_{-\infty}^{+\infty} d\omega \hat{A}(\omega) = \hat{a}_{\text{in}}(t) + \frac{\sqrt{\gamma_a}}{2} \hat{a}(t) = \hat{a}_{\text{out}}(t) - \frac{\sqrt{\gamma_a}}{2} \hat{a}(t), \quad (\text{A.16})$$

thus giving

$$\hat{a}_{\text{out}} = \hat{a}_{\text{in}} + \sqrt{\gamma_a} \hat{a}. \quad (\text{A.17})$$

The procedure to obtain the output of the system is then to solve the Eq. (A.13) and then inject it in the Eq. (A.17).

B Evaluating the output squeezing from a degenerate optical parametric oscillator with input-output theory

Here we are interested in the calculation of the squeezed radiation that can escape an optical parametric oscillator (OPO). In the laboratory frame, the Hamiltonian describing this parametric process is

$$\hat{H}_{\text{lab}} = \omega_a \hat{a}^\dagger \hat{a} + i \frac{\hbar g \alpha_c}{2} ((\hat{a}^\dagger)^2 e^{-i\omega_c t} - \hat{a}^2 e^{i\omega_c t}), \quad (\text{B.1})$$

where $\omega_a = \omega_c/2$ is the frequency of the mode \hat{a} and ω_c is the frequency of the pump. We already assumed the pump to be a classical field described by its complex amplitude, assumed real here, as addressed in section I.2.9.1.¹ In a frame rotating at $\omega_c/2$, Eq. (B.1) becomes

$$\hat{H}_{\text{dOPO}} = i \frac{\hbar g \alpha_c}{2} ((\hat{a}^\dagger)^2 - \hat{a}^2). \quad (\text{B.2})$$

By using eq. (A.13) with $\hat{H}_{\text{sys}} = \hat{H}_{\text{dOPO}}$, we obtain

$$\frac{d}{dt} \hat{a}(t) = g \alpha_c \hat{a}^\dagger(t) - \sqrt{\gamma_a} \hat{a}_{\text{in}}(t) - \frac{\gamma_a}{2} \hat{a}(t). \quad (\text{B.3})$$

As usual in input-output theory, we will solve this equation in frequency space

$$-i\omega \hat{a}(\omega) = g \alpha_c \hat{a}^\dagger(-\omega) - \sqrt{\gamma_a} \hat{a}_{\text{in}}(\omega) - \frac{\gamma_a}{2} \hat{a}(\omega), \quad (\text{B.4})$$

where the Fourier transform is defined as

$$\hat{a}(\omega) = \frac{1}{\sqrt{2\pi}} \int dt e^{i\omega t} \hat{a}(t), \quad (\text{B.5})$$

and where we used the definition $(\hat{a}(\omega))^\dagger = \hat{a}^\dagger(-\omega)$. Eq. (B.4) can be rewritten as the following system

$$\begin{pmatrix} \hat{a}_{\text{in}}(\omega) \\ \hat{a}_{\text{in}}^\dagger(\omega) \end{pmatrix} = \begin{pmatrix} i\omega - \gamma_a/2 & g\alpha_c \\ g\alpha_c & i\omega - \gamma_a/2 \end{pmatrix} \begin{pmatrix} \hat{a}(\omega) \\ \hat{a}^\dagger(\omega) \end{pmatrix}, \quad (\text{B.6})$$

¹Note that in Eq. (B.1), we retrieve the fact that in the laboratory frame, we have $\langle \hat{c} \rangle = \alpha_c e^{-i\omega_c t}$ (\hat{c} being the quantum mode describing the pump), whereas in section I.2.9.1, the equality $\langle \hat{c} \rangle = \alpha_c$ is valid in the rotating frame.

which can be inverted to give

$$\begin{pmatrix} \hat{a}(\omega) \\ \hat{a}^\dagger(\omega) \end{pmatrix} = \begin{pmatrix} A_{1,\text{cav}}(\omega) & A_{2,\text{cav}}(\omega) \\ A_{2,\text{cav}}^*(-\omega) & A_{1,\text{cav}}^*(-\omega) \end{pmatrix} \begin{pmatrix} \hat{a}_{\text{in}}(\omega) \\ \hat{a}_{\text{in}}^\dagger(\omega) \end{pmatrix}, \quad (\text{B.7})$$

where

$$A_{1,\text{cav}}(\omega) = \frac{\sqrt{\gamma_a}(\gamma_a/2 - i\omega)}{g^2\alpha_c^2 - (\gamma_a/2 - i\omega)^2}, \quad (\text{B.8})$$

$$A_{2,\text{cav}}(\omega) = \frac{\sqrt{\gamma_a}g\alpha_c}{g^2\alpha_c^2 - (\gamma_a/2 - i\omega)^2}. \quad (\text{B.9})$$

Then, using the Eq. (A.17), one finally obtains the input-output relation

$$\hat{a}_{\text{out}}(\omega) = A_1(\omega)\hat{a}_{\text{in}}(\omega) + A_1(\omega)\hat{a}_{\text{in}}^\dagger(\omega), \quad (\text{B.10})$$

with

$$A_1(\omega) = 1 + \sqrt{\gamma_a}A_{1,\text{cav}}(\omega) = \frac{g^2\alpha_c^2 + (\gamma_a/2)^2 + \omega^2}{g^2\alpha_c^2 - (\gamma_a/2 - i\omega)^2}, \quad (\text{B.11})$$

$$A_2(\omega) = \sqrt{\gamma_a}A_{2,\text{cav}}(\omega) = \frac{\gamma_a g \alpha_c}{g^2\alpha_c^2 - (\gamma_a/2 - i\omega)^2}. \quad (\text{B.12})$$

As we will see hereafter, with the Eqs. (B.10), (B.11) and (B.12) we have everything we need to evaluate the output squeezing from the degenerate OPO. For the quadrature \hat{X} , the noise spectrum is defined as [Clerk10]

$$\mathcal{S}_{XX}(\omega) = \int dt e^{i\omega t} \langle \hat{X}(t) \hat{X}(0) \rangle. \quad (\text{B.13})$$

Note that the Eq. (B.13) is the quantum analog of a spectral density used in classical physics. Here it is a quantum noise spectral density, related to the autocorrelation function $\langle \hat{X}(t) \hat{X}(0) \rangle$. Eq. (B.13) in its current form is a measurable quantity, but not very useful in our theoretical calculation. In fact, by using Eq. (B.5) and Eq. (B.13), we can write

$$\begin{aligned} \mathcal{S}_{XX}(\omega) &= \int dt e^{i\omega t} \frac{1}{\sqrt{2\pi}} \int d\omega'' e^{-i\omega'' t} \frac{1}{\sqrt{2\pi}} \int d\omega' \langle \hat{X}(\omega'') \hat{X}(\omega') \rangle \\ &= \frac{1}{2\pi} \int d\omega'' \int dt e^{i(\omega - \omega'')t} \int d\omega' \langle \hat{X}(\omega'') \hat{X}(\omega') \rangle \\ &= \int d\omega' \int d\omega'' \delta(\omega - \omega'') \langle \hat{X}(\omega'') \hat{X}(\omega') \rangle \\ &= \int d\omega' \langle \hat{X}(\omega) \hat{X}(\omega') \rangle, \end{aligned} \quad (\text{B.14})$$

where we have used $\int dt e^{i(\omega - \omega'')t} = 2\pi\delta(\omega - \omega'')$. According to Eq. (I.37), we have $\hat{X}_\phi \hat{X}_\phi = (\hat{a}_{\text{out}} \hat{a}_{\text{out}}^\dagger + \hat{a}_{\text{out}}^\dagger \hat{a}_{\text{out}} + \hat{a}_{\text{out}} \hat{a}_{\text{out}} e^{-2i\phi} + \hat{a}_{\text{out}}^\dagger \hat{a}_{\text{out}}^\dagger e^{2i\phi})/2$.² Thus, for a quadrature

²Note that having \hat{X}_ϕ^2 is enough for getting the variance $\langle \Delta \hat{X}_\phi \rangle$, since here $\langle \Delta \hat{X}_\phi \rangle^2 = \langle \hat{X}_\phi^2 \rangle$. Indeed, $\langle \hat{X}_\phi \rangle = 0$ because we will always consider an input vacuum.

with an arbitrary angle ϕ , the noise spectrum is

$$\begin{aligned} \mathcal{S}_{X_\phi X_\phi}(\omega) = & \int d\omega' \left(\langle \hat{a}_{\text{out}}(\omega) \hat{a}_{\text{out}}^\dagger(-\omega') \rangle + \langle \hat{a}_{\text{out}}^\dagger(-\omega) \hat{a}_{\text{out}}(\omega') \rangle \right. \\ & \left. + \langle \hat{a}_{\text{out}}(\omega) \hat{a}_{\text{out}}(\omega') \rangle e^{-2i\phi} + \langle \hat{a}_{\text{out}}^\dagger(-\omega) \hat{a}_{\text{out}}^\dagger(-\omega') \rangle e^{2i\phi} \right). \end{aligned} \quad (\text{B.15})$$

Note how the sign in front of ω and ω' changes depending on whether it is the Fourier transform of the annihilation or the creation operator that is considered [Gardiner84].

We consider that only the mode at ω_c is pumped, and that no energy is directly brought to the mode \hat{a} from the environment. Thus, the input \hat{a}_{in} is the vacuum. Therefore, we have [Gardiner85]

$$\begin{cases} \langle \hat{a}_{\text{in}}(\omega) \hat{a}_{\text{in}}^\dagger(-\omega') \rangle = \delta(\omega + \omega'), \\ \langle \hat{a}_{\text{in}}^\dagger(-\omega) \hat{a}_{\text{in}}(\omega') \rangle = 0, \\ \langle \hat{a}_{\text{in}}(\omega) \hat{a}_{\text{in}}(\omega') \rangle = 0, \\ \langle \hat{a}_{\text{in}}^\dagger(-\omega) \hat{a}_{\text{in}}^\dagger(-\omega') \rangle = 0, \end{cases} \quad (\text{B.16})$$

which comes from the commutation relations in time $[\hat{a}_{\text{in}}(t), \hat{a}_{\text{in}}^\dagger(t')] = \delta(t - t')$, which gives in frequency space $[\hat{a}_{\text{in}}(\omega), \hat{a}_{\text{in}}^\dagger(-\omega')] = \delta(\omega + \omega')$. With these equations, one can obtain

$$\begin{cases} \int d\omega' \langle \hat{a}_{\text{out}}(\omega) \hat{a}_{\text{out}}^\dagger(-\omega') \rangle = A_1(\omega) A_1^*(\omega), \\ \int d\omega' \langle \hat{a}_{\text{out}}^\dagger(-\omega) \hat{a}_{\text{out}}(\omega') \rangle = A_2^*(-\omega) A_2(-\omega), \\ \int d\omega' \langle \hat{a}_{\text{out}}(\omega) \hat{a}_{\text{out}}(\omega') \rangle = A_1(\omega) A_2(-\omega), \\ \int d\omega' \langle \hat{a}_{\text{out}}^\dagger(-\omega) \hat{a}_{\text{out}}^\dagger(-\omega') \rangle = A_2^*(-\omega) A_1^*(\omega), \end{cases} \quad (\text{B.17})$$

which can be directly used to retrieve the full spectrum in Eq. (B.15). Instead of giving the full cumbersome expression of $\mathcal{S}_{X_\phi X_\phi}(\omega)$ for arbitrary ϕ , let us give it for the standard quadratures defined by $\phi = 0$ and $\phi = \pi/2$ that have the compact expressions [Walls08]

$$\mathcal{S}_{XX}(\omega) = \frac{1}{2} + \frac{g\alpha_c\gamma_a}{(\gamma/2 - g\alpha_c)^2 + \omega^2}, \quad (\text{B.18})$$

$$\mathcal{S}_{YY}(\omega) = \frac{1}{2} - \frac{g\alpha_c\gamma_a}{(\gamma/2 + g\alpha_c)^2 + \omega^2}, \quad (\text{B.19})$$

also called squeezing spectra. Note that these last two equations are not only theoretical tools but are measurable quantities. In particular, these quantities are shown in the experimental plots in Fig. B.19, yet in different scales. If one wants to study these spectra in a logarithmic scale, one can use the Eq. (I.80), which in the present case will be

$$S_{\phi=0}(\omega) = 10 \log_{10} \left(\frac{\mathcal{S}_{XX}(\omega)}{\mathcal{S}_{XX}^{\text{vac}}(\omega)} \right) = 10 \log_{10} \left(2\mathcal{S}_{XX}(\omega) \right), \quad (\text{B.20})$$

$$S_{\phi=\pi/2}(\omega) = 10 \log_{10} \left(\frac{\mathcal{S}_{YY}(\omega)}{\mathcal{S}_{YY}^{\text{vac}}(\omega)} \right) = 10 \log_{10} \left(2\mathcal{S}_{YY}(\omega) \right), \quad (\text{B.21})$$

since the spectra for vacuum are $\mathcal{S}_{XX}^{\text{vac}}(\omega) = \mathcal{S}_{YY}^{\text{vac}}(\omega) = 1/2$.

C Evaluating the output two-squeezing and logarithmic negativity from a non-degenerate optical parametric oscillator with input-output theory

Here we are interested in the calculation of the two-squeezing and logarithmic negativity of the radiation that can escape an non-degenerate optical parametric oscillator (OPO). In the laboratory frame, the Hamiltonian describing this parametric process is

$$\hat{H}_{\text{lab}} = \omega_s \hat{a}_s^\dagger \hat{a}_s + \omega_i \hat{a}_i^\dagger \hat{a}_i + i \frac{\hbar g \alpha_c}{2} (\hat{a}_s^\dagger \hat{a}_i^\dagger e^{-i\omega_c t} - \hat{a}_s \hat{a}_i e^{i\omega_c t}), \quad (\text{C.1})$$

ω_s being the frequency of the signal \hat{a}_s , ω_i being the frequency of the idler \hat{a}_i . ω_c is the frequency of the pump such that $\omega_c = \omega_s + \omega_i$. We already assumed the pump to be a classical field described by its complex amplitude, assumed real here, as addressed in section I.2.9.1.¹ In a frame where the signal rotates at ω_s and the idler rotates at ω_i , Eq. (C.1) becomes

$$\hat{H}_{\text{OPO}} = i \frac{\hbar g \alpha_c}{2} (\hat{a}_s^\dagger \hat{a}_i^\dagger - \hat{a}_s \hat{a}_i). \quad (\text{C.2})$$

By using eq. (A.13) with $\hat{H}_{\text{sys}} = \hat{H}_{\text{OPO}}$, we obtain the following coupled equations

$$\begin{cases} \frac{d}{dt} \hat{a}_s(t) = g \alpha_c \hat{a}_i^\dagger(t) - \sqrt{\gamma_a} \hat{a}_{s,\text{in}}(t) - \frac{\gamma_a}{2} \hat{a}_s(t), \\ \frac{d}{dt} \hat{a}_i(t) = g \alpha_c \hat{a}_s^\dagger(t) - \sqrt{\gamma_a} \hat{a}_{i,\text{in}}(t) - \frac{\gamma_a}{2} \hat{a}_i(t), \end{cases} \quad (\text{C.3})$$

which in frequency space gives

$$\begin{cases} -i\omega \hat{a}_s(\omega) = g \alpha_c \hat{a}_i^\dagger(-\omega) - \sqrt{\gamma_a} \hat{a}_{s,\text{in}}(\omega) - \frac{\gamma_a}{2} \hat{a}_s(\omega), \\ -i\omega \hat{a}_i(\omega) = g \alpha_c \hat{a}_s^\dagger(-\omega) - \sqrt{\gamma_a} \hat{a}_{i,\text{in}}(\omega) - \frac{\gamma_a}{2} \hat{a}_i(\omega), \end{cases} \quad (\text{C.4})$$

where both modes are considered to have the same dissipation rate γ_a since the photons from both modes escape from the same cavity. We can solve the system of Eqs. C.4,

¹Note that as in appendix B, in Eq. (C.1) we retrieve the fact that in the laboratory frame, we have $\langle \hat{c} \rangle = \alpha_c e^{-i\omega_c t}$ (\hat{c} being the quantum mode describing the pump), whereas in section I.2.9.2, the equality $\langle \hat{c} \rangle = \alpha_c$ is valid in the rotating frame.

and by using Eq. A.17 we obtain

$$\begin{pmatrix} \hat{a}_{s,\text{out}}(\omega) \\ \hat{a}_{i,\text{out}}(\omega) \\ \hat{a}_{s,\text{out}}^\dagger(-\omega) \\ \hat{a}_{i,\text{out}}^\dagger(-\omega) \end{pmatrix} = \begin{pmatrix} A_1(\omega) & A_2(\omega) & A_3(\omega) & A_4(\omega) \\ B_1(\omega) & B_2(\omega) & B_3(\omega) & B_4(\omega) \\ A_3^*(-\omega) & A_4^*(-\omega) & A_1^*(-\omega) & A_2^*(-\omega) \\ B_3^*(-\omega) & B_4^*(-\omega) & B_1^*(-\omega) & B_2^*(-\omega) \end{pmatrix} \begin{pmatrix} \hat{a}_{s,\text{in}}(\omega) \\ \hat{a}_{i,\text{in}}(\omega) \\ \hat{a}_{s,\text{in}}^\dagger(-\omega) \\ \hat{a}_{i,\text{in}}^\dagger(-\omega) \end{pmatrix}. \quad (\text{C.5})$$

The input-output relations given in Eq. (C.5) are all we need in order to construct the covariance matrix that will allow us to obtain the two-mode squeezing spectrum, to test the entanglement witness given in Eq. (I.90), and to compute of the logarithmic negativity. To do all this we need the spectra of sixteen expectation values, that we can compute in the same manner as in appendix B, by again assuming vacuum inputs for the signal and the idler. The first ones are for the signal mode

$$\begin{cases} \int d\omega' \langle \hat{a}_{s,\text{out}}(\omega) \hat{a}_{s,\text{out}}^\dagger(-\omega') \rangle = A_1(\omega)A_1^*(\omega) + A_2(\omega)A_2^*(\omega), \\ \int d\omega' \langle \hat{a}_{s,\text{out}}^\dagger(-\omega) \hat{a}_{s,\text{out}}(\omega') \rangle = A_3^*(-\omega)A_3(-\omega) + A_4^*(-\omega)A_4(-\omega), \\ \int d\omega' \langle \hat{a}_{s,\text{out}}(\omega) \hat{a}_{s,\text{out}}(\omega') \rangle = A_1(\omega)A_3(-\omega) + A_2(\omega)A_4(-\omega), \\ \int d\omega' \langle \hat{a}_{s,\text{out}}^\dagger(-\omega) \hat{a}_{s,\text{out}}^\dagger(-\omega') \rangle = A_3^*(-\omega)A_1^*(\omega) + A_4^*(-\omega)A_2^*(\omega). \end{cases} \quad (\text{C.6})$$

Accordingly, we have the ones for the idler mode

$$\begin{cases} \int d\omega' \langle \hat{a}_{i,\text{out}}(\omega) \hat{a}_{i,\text{out}}^\dagger(-\omega') \rangle = B_1(\omega)B_1^*(\omega) + B_2(\omega)B_2^*(\omega), \\ \int d\omega' \langle \hat{a}_{i,\text{out}}^\dagger(-\omega) \hat{a}_{i,\text{out}}(\omega') \rangle = B_3^*(-\omega)B_3(-\omega) + B_4^*(-\omega)B_4(-\omega), \\ \int d\omega' \langle \hat{a}_{i,\text{out}}(\omega) \hat{a}_{i,\text{out}}(\omega') \rangle = B_1(\omega)B_3(-\omega) + B_2(\omega)B_4(-\omega), \\ \int d\omega' \langle \hat{a}_{i,\text{out}}^\dagger(-\omega) \hat{a}_{i,\text{out}}^\dagger(-\omega') \rangle = B_3^*(-\omega)B_1^*(\omega) + B_4^*(-\omega)B_2^*(\omega). \end{cases} \quad (\text{C.7})$$

Finally we have the cross terms, attesting for the correlations between signal and idler

$$\begin{cases} \int d\omega' \langle \hat{a}_{s,\text{out}}(\omega) \hat{a}_{i,\text{out}}^\dagger(-\omega') \rangle = A_1(\omega)B_1^*(\omega) + A_2(\omega)B_2^*(\omega), \\ \int d\omega' \langle \hat{a}_{i,\text{out}}(\omega) \hat{a}_{s,\text{out}}^\dagger(-\omega') \rangle = B_1(\omega)A_1^*(\omega) + B_2(\omega)A_2^*(\omega), \\ \int d\omega' \langle \hat{a}_{s,\text{out}}^\dagger(-\omega) \hat{a}_{i,\text{out}}(\omega') \rangle = A_3^*(-\omega)B_3(-\omega) + A_4^*(-\omega)B_4(-\omega), \\ \int d\omega' \langle \hat{a}_{i,\text{out}}^\dagger(-\omega) \hat{a}_{s,\text{out}}(\omega') \rangle = B_3^*(-\omega)A_3(-\omega) + B_4^*(-\omega)A_4(-\omega), \\ \int d\omega' \langle \hat{a}_{s,\text{out}}(\omega) \hat{a}_{i,\text{out}}(\omega') \rangle = A_1(\omega)B_3(-\omega) + A_2(\omega)B_4(-\omega), \\ \int d\omega' \langle \hat{a}_{i,\text{out}}(\omega) \hat{a}_{s,\text{out}}(\omega') \rangle = B_1(\omega)A_3(-\omega) + B_2(\omega)A_4(-\omega), \\ \int d\omega' \langle \hat{a}_{s,\text{out}}^\dagger(-\omega) \hat{a}_{i,\text{out}}^\dagger(-\omega') \rangle = A_3^*(-\omega)B_1^*(\omega) + A_4^*(-\omega)B_2^*(\omega), \\ \int d\omega' \langle \hat{a}_{i,\text{out}}^\dagger(-\omega) \hat{a}_{s,\text{out}}^\dagger(-\omega') \rangle = B_3^*(-\omega)A_1^*(\omega) + B_4^*(-\omega)A_2^*(\omega), \end{cases} \quad (\text{C.8})$$

where

$$A_1(\omega) = \frac{g^2\alpha^2 + (\gamma_a/2)^2 + \omega^2}{g^2\alpha_c^2 - (\gamma_a/2 - i\omega)^2}, \quad (\text{C.9})$$

$$A_2(\omega) = 0, \quad (\text{C.10})$$

$$A_3(\omega) = 0, \quad (\text{C.11})$$

$$A_4(\omega) = \frac{\gamma_a g \alpha_c}{g^2\alpha_c^2 - (\gamma_a/2 - i\omega)^2}, \quad (\text{C.12})$$

and

$$B_1(\omega) = 0, \quad (\text{C.13})$$

$$B_2(\omega) = \frac{g^2\alpha^2 + (\gamma_a/2)^2 + \omega^2}{g^2\alpha_c^2 - (\gamma_a/2 - i\omega)^2}, \quad (\text{C.14})$$

$$B_3(\omega) = \frac{\gamma_a g \alpha_c}{g^2\alpha_c^2 - (\gamma_a/2 - i\omega)^2}, \quad (\text{C.15})$$

$$B_4(\omega) = 0, \quad (\text{C.16})$$

Following the definition (I.91), one can construct the covariance matrix by replacing the theoretical variances $\langle \hat{X}_\phi \hat{X}_{\phi'} \rangle$ by the corresponding and measurable noise spectra $\mathcal{S}_{X_\phi X_{\phi'}}(\omega) = \int d\omega' \langle \hat{X}_\phi(\omega) \hat{X}_{\phi'}(\omega') \rangle$

$$\mathcal{V}(\omega) = \begin{pmatrix} \mathcal{S}_{X_a X_a}(\omega) & 0 & \frac{\mathcal{S}_{X_a X_b}(\omega) + \mathcal{S}_{X_b X_a}(\omega)}{2} & \frac{\mathcal{S}_{X_a Y_b}(\omega) + \mathcal{S}_{Y_b X_a}(\omega)}{2} \\ 0 & \mathcal{S}_{Y_a Y_a}(\omega) & \frac{\mathcal{S}_{Y_a X_b}(\omega) + \mathcal{S}_{X_b Y_a}(\omega)}{2} & \frac{\mathcal{S}_{Y_a Y_b}(\omega) + \mathcal{S}_{Y_b Y_a}(\omega)}{2} \\ \frac{\mathcal{S}_{X_b X_a}(\omega) + \mathcal{S}_{X_a X_b}(\omega)}{2} & \frac{\mathcal{S}_{X_b Y_a}(\omega) + \mathcal{S}_{Y_a X_b}(\omega)}{2} & \mathcal{S}_{X_b X_b}(\omega) & 0 \\ \frac{\mathcal{S}_{Y_b X_a}(\omega) + \mathcal{S}_{X_a Y_b}(\omega)}{2} & \frac{\mathcal{S}_{Y_b Y_a}(\omega) + \mathcal{S}_{Y_a Y_b}(\omega)}{2} & 0 & \mathcal{S}_{Y_b Y_b}(\omega) \end{pmatrix}, \quad (\text{C.17})$$

Using this covariance matrix, now one can easily apply the entanglement witness defined in Eq. (I.90) and the logarithmic negativity defined in Eqs. (I.93) and (I.94).

D Evaluating the output squeezing in the dispersive ultrastrong coupling regime

In this appendix we investigate the squeezing of the radiation coming out of the inter-subband devices in the dispersive USC regime, studied in chapter II, section II.6. We recall the Hamiltonian of the system

$$\hat{H} = \hbar\omega_p\hat{p}^\dagger\hat{p} + \hbar\omega_a\hat{a}^\dagger\hat{a} + i\hbar\Omega_{\text{mod}}(\hat{a}^\dagger - \hat{a})(\hat{p}^\dagger + \hat{p}). \quad (\text{D.1})$$

Since this Hamiltonian is in a rotating frame, we can apply the tools of input-output theory already used in appendix A, in order to derive the following equations of motion

$$\begin{cases} \frac{d}{dt}\hat{a}(t) = -i\delta_a\hat{a}(t) + \Omega_{\text{mod}}(\hat{p}^\dagger(t) + \hat{p}(t))/2 - \sqrt{\gamma_a}\hat{a}_{\text{in}}(t) - \frac{\gamma_a}{2}\hat{a}(t), \\ \frac{d}{dt}\hat{p}(t) = -i\omega_p\hat{p}(t) + \Omega_{\text{mod}}(\hat{a}^\dagger(t) - \hat{a}(t))/2 - \sqrt{\gamma_p}\hat{p}_{\text{in}}(t) - \frac{\gamma_p}{2}\hat{p}(t), \end{cases} \quad (\text{D.2})$$

where $\delta_a = \omega_a - \omega_{\text{mod}}$. In frequency space, the equations become

$$\begin{cases} (i(\delta - \omega) + \frac{\gamma_a}{2})\hat{a}(\omega) = \Omega_{\text{mod}}(\hat{p}^\dagger(-\omega) + \hat{p}(\omega))/2 - \sqrt{\gamma_a}\hat{a}_{\text{in}}(\omega), \\ (i(\omega_p - \omega) + \frac{\gamma_p}{2})\hat{p}(\omega) = \Omega_{\text{mod}}(\hat{a}^\dagger(-\omega) - \hat{a}(\omega))/2 - \sqrt{\gamma_p}\hat{p}_{\text{in}}(\omega). \end{cases} \quad (\text{D.3})$$

These equations are easily solved and as in appendixes B and C, and since we only interested in the output radiation, we compute the cavity input-output relation in frequency space,¹

$$\hat{a}_{\text{out}}(\omega) = A_1(\omega)\hat{a}_{\text{in}}(\omega) + A_2(\omega)\hat{p}_{\text{in}}(\omega) + A_3(\omega)\hat{a}_{\text{in}}^\dagger(-\omega) + A_4(-\omega)\hat{p}_{\text{in}}^\dagger(-\omega). \quad (\text{D.4})$$

This time, we consider thermal inputs for both the cavity and the plasmon, since it is not certain that the squeezing will be independent of the temperature for a radiation in the terahertz range. Therefore, the inputs are [Gardiner85]

$$\begin{cases} \langle \hat{a}_{\text{in}}(\omega)\hat{a}_{\text{in}}^\dagger(-\omega') \rangle = (\bar{n}_a(T) + 1)\delta(\omega + \omega'), \\ \langle \hat{a}_{\text{in}}^\dagger(-\omega)\hat{a}_{\text{in}}(\omega') \rangle = \bar{n}_a(T)\delta(\omega + \omega'), \\ \langle \hat{a}_{\text{in}}(\omega)\hat{a}_{\text{in}}(\omega') \rangle = 0, \\ \langle \hat{a}_{\text{in}}^\dagger(-\omega)\hat{a}_{\text{in}}^\dagger(-\omega') \rangle = 0, \end{cases} \quad (\text{D.5})$$

¹Here we do not give the explicit expressions for the coefficients $A_i(\omega)$, since they are quite lengthy compared to the ones in appendixes B and C.

and

$$\begin{cases} \langle \hat{p}_{\text{in}}(\omega) \hat{p}_{\text{in}}^\dagger(-\omega') \rangle = (\bar{n}_p(T) + 1) \delta(\omega + \omega'), \\ \langle \hat{p}_{\text{in}}^\dagger(-\omega) \hat{p}_{\text{in}}(\omega') \rangle = \bar{n}_p(T) \delta(\omega + \omega'), \\ \langle \hat{p}_{\text{in}}(\omega) \hat{p}_{\text{in}}(\omega') \rangle = 0, \\ \langle \hat{p}_{\text{in}}^\dagger(-\omega) \hat{p}_{\text{in}}^\dagger(-\omega') \rangle = 0, \end{cases} \quad (\text{D.6})$$

where $\bar{n}_a(T) = 1/(\exp(\hbar\omega_a/k_B T) - 1)$ and $\bar{n}_p(T) = 1/(\exp(\hbar\omega_p/k_B T) - 1)$ are the thermal occupation numbers for the cavity and the plasmon. We can then compute the noise spectra for the quadratures of $\hat{a}_{\text{out}}(\omega)$ in a similar fashion as in appendixes B and C.

In Eqs. (D.3) we can note that for $\hat{a}(\omega)$, we have $\delta - \omega = \omega_a - (\omega_{\text{mod}} + \omega)$ whereas for $\hat{p}(\omega)$ we have $\omega_p - \omega$. The sum $\omega_{\text{mod}} + \omega$ shows us that the cavity mode is in a frame rotating at ω_{mod} . As mentioned in appendix A, as long as $\omega_{\text{mod}} + \omega > 0$ even for negative ω , then in the laboratory frame we are still studying positive frequencies. Accordingly, the cavity bath Hamiltonian and the bath-system coupling shown in Eqs. (A.2) and (A.3) are integrals over ω between $-\infty$ and $+\infty$, which is then a valid approximation. However, the situation is not that simple for the intersubband plasmon $\hat{p}(\omega)$. Indeed, the plasmon is not in a rotating frame, therefore, strictly speaking the plasmon bath Hamiltonian, and the coupling between the plasmon and its bath should only be integrated between 0 and $+\infty$. However, it is not in the scope of this thesis to provide a new input-output theory that would somehow be more consistent on this point, but rather investigate the output from the cavity for which the standard input-output theory is well applicable. Therefore we do not attempt to compute and interpret the output of the plasmon. Note that the standard input-output theory is often used in a situation where as here one boson is in a rotating frame, while a second boson, coupled to the first one, is still in the laboratory frame. It is the case in linearized optomechanics, where the Hamiltonian has exactly the same form as in Eq. (D.1). Additionally, the equations of motion in linearized optomechanics are usually in same form as Eqs. (D.2), since they are derived using the same procedure as the one used here [Hofer11, Aspelmeyer14].

E Derivation of the effective Hamiltonian

Here we show the derivation of the effective Hamiltonian (REF). As mentioned in section III.3, the interaction in the physical system is a three-wave mixing process between a pump mode c and two microwave modes a and b , described by Eq. (III.2). However, since we drive the pump mode by a two-tone radiation, the interaction Hamiltonian now includes two three-wave mixing terms, and the full system Hamiltonian reads

$$\begin{aligned}\hat{H} &= \omega_a \hat{a}^\dagger \hat{a} + \omega_b \hat{b}^\dagger \hat{b} + \omega_B \hat{c}_B^\dagger \hat{c}_B + \omega_R \hat{c}_R^\dagger \hat{c}_R \\ &+ \chi(\hat{c}_B + \hat{c}_B^\dagger)(\hat{a} + \hat{a}^\dagger)(\hat{b} + \hat{b}^\dagger) \\ &+ \chi(\hat{c}_R + \hat{c}_R^\dagger)(\hat{a} + \hat{a}^\dagger)(\hat{b} + \hat{b}^\dagger),\end{aligned}\quad (\text{E.1})$$

In the interaction picture, this Hamiltonian reads

$$\begin{aligned}\hat{H}_{\text{IP}} &= \chi(\hat{c}_B e^{-i\omega_B t} + \hat{c}_R e^{-i\omega_R t})(\hat{a} \hat{b} e^{-i(\omega_a + \omega_b)t} \\ &+ \hat{a} \hat{b}^\dagger e^{-i(\omega_a - \omega_b)t} + \hat{a}^\dagger \hat{b} e^{i(\omega_a - \omega_b)t} \\ &+ \hat{a}^\dagger \hat{b}^\dagger e^{i(\omega_a + \omega_b)t}) + \text{h.c.},\end{aligned}\quad (\text{E.2})$$

where the frequencies of the two-tone driving are

$$\omega_B = \omega_a + \omega_b + 2\delta_B, \quad (\text{E.3})$$

$$\omega_R = \omega_a - \omega_b, \quad (\text{E.4})$$

where $|\delta_B| \ll \omega_a, \omega_b, |\omega_a - \omega_b|$. Mode c being driven off resonance, we use the stiff pump approximation and describe its amplitude as a complex number instead of an operator. Let us call $G_{B,R} = \chi c_{B,R}$ as the time independent parts of the coupling rates $\tilde{G}_{B,R}(t) = G_{B,R} e^{-i\omega_{B,R}t}$. Using Eqs. (E.2),(E.3) and (E.4), we obtain

$$\begin{aligned}\hat{H}_{\text{IP}} &= G_B(\hat{a} \hat{b} e^{-2i(\omega_a + \omega_b + \delta_B)t} + \hat{a} \hat{b}^\dagger e^{-2i(\omega_a + \delta_B)t} \\ &+ \hat{a}^\dagger \hat{b} e^{-2i(\omega_b + \delta_B)t} + \hat{a}^\dagger \hat{b}^\dagger e^{-2i\delta_B t}) + \\ &+ G_R(\hat{a} \hat{b} e^{-2i\omega_a t} + \hat{a} \hat{b}^\dagger e^{-2i(\omega_a - \omega_b)t} \\ &+ \hat{a}^\dagger \hat{b} + \hat{a}^\dagger \hat{b}^\dagger e^{2i\omega_b t}) + \text{h.c.},\end{aligned}\quad (\text{E.5})$$

We work in a regime where $|G_{B,R}| \ll \omega_a, \omega_b, |\omega_a - \omega_b|$ and $|G_{B,R}| \lesssim |\delta_B|$, which allows us to perform a rotating wave approximation. Thus, in the interaction picture, the important terms that contribute to the evolution of the system are resonant in this

rotating frame, or oscillate at $2\delta_B$, and all the other terms can be fairly neglected,

$$\hat{H}_{\text{IP}} \approx G_B(\hat{a}^\dagger \hat{b}^\dagger e^{-2i\delta_B t} + \hat{a} \hat{b} e^{2i\delta_B t}) + G_R(\hat{a}^\dagger \hat{b} + \hat{a} \hat{b}^\dagger). \quad (\text{E.6})$$

With a rather simple, yet judiciously chosen unitary transformation we obtain the effective Hamiltonian

$$\hat{H}_{\text{eff}} = \delta_B \hat{a}^\dagger \hat{a} + \delta_B \hat{b}^\dagger \hat{b} + G_B(\hat{a}^\dagger \hat{b}^\dagger + \hat{a} \hat{b}) + G_R(\hat{a}^\dagger \hat{b} + \hat{a} \hat{b}^\dagger). \quad (\text{E.7})$$

We are now in a rotating frame where mode a oscillates at $\omega_a + \delta_B$ and mode b oscillates at $\omega_b + \delta_B$. Any single mode squeezing or correlations observed in this frame at a frequency ω would correspond in the laboratory frame to $\omega_a + \delta_B + \omega$ and $\omega_b + \delta_B + \omega$ for modes \hat{a} and \hat{b} respectively.

F Validity of the diagonalization

In this Appendix we briefly discuss the validity region of our model used to compute the ground state squeezing shown in Fig. III.8. To understand it we need the expressions of $\hat{p}_{1,2}$, the eigenmodes of the Hamiltonian (III.10). These operators are linear combinations of \hat{a} and \hat{b} ,

$$\hat{p}_{1,2} = t_{1,2}\hat{a} + u_{1,2}\hat{b} + v_{1,2}\hat{a}^\dagger + w_{1,2}\hat{b}^\dagger, \quad (\text{F.1})$$

where the coefficients $\vec{p}_{1,2} = \{t_{1,2}, u_{1,2}, v_{1,2}, w_{1,2}\}$ are obtained by diagonalizing the Hopfield matrix [Hopfield58] for the Hamiltonian (III.10). These coefficients are

$$\vec{p}_1 = \frac{1}{\sqrt{N_1}} \begin{pmatrix} \frac{\sqrt{(\delta-2G)\delta+\delta}}{G} - 1 \\ -\frac{\sqrt{(\delta-2G)\delta+\delta}}{G} + 1 \\ -1 \\ 1 \end{pmatrix} \quad (\text{F.2})$$

$$\vec{p}_2 = \frac{1}{\sqrt{N_2}} \begin{pmatrix} \frac{\sqrt{(\delta+2G)\delta+\delta}}{G} + 1 \\ \frac{\sqrt{(\delta+2G)\delta+\delta}}{G} + 1 \\ 1 \\ 1 \end{pmatrix} \quad (\text{F.3})$$

with eigenvalues

$$\omega_{1,2} = \sqrt{(\delta \mp 2G)\delta}. \quad (\text{F.4})$$

$N_{1,2}$ are the normalization coefficients, such that the condition $|t_{1,2}|^2 + |u_{1,2}|^2 - |v_{1,2}|^2 - |w_{1,2}|^2 = 1$ is satisfied, imposed by the Bose commutation rule. With Eqs. (F.2) and (F.4) one can see that when $G > \delta/2$, the model is not valid anymore.

G Derivation of the system's Hamiltonian and coupling to the baths

In this appendix, we detail the steps to obtain the Hamiltonian of Eq. (IV.9), by showing how the intracavity modes are coupled to the environment modes. The full model is obtained extending Eq. (IV.7) to include the coupling between the system and the environment,

$$\begin{aligned}\hat{H}_{SE} = & i \int_{-\infty}^{\infty} d\omega \kappa_c(\omega) \left(\hat{\gamma}_B^\dagger(\omega) \hat{c}(t) - \hat{\gamma}_B(\omega) \hat{c}^\dagger(t) \right) + \\ & i \int_{-\infty}^{\infty} d\omega \kappa_c(\omega) \left(\hat{\delta}_B^\dagger(\omega) \hat{d}(t) - \hat{\delta}_B(\omega) \hat{d}^\dagger(t) \right) + \\ & + i \int_{-\infty}^{\infty} d\omega \kappa_m(\omega) \left(\hat{\mu}_B^\dagger(\omega) \hat{m}(t) - \hat{\mu}_B(\omega) \hat{m}^\dagger(t) \right),\end{aligned}\quad (\text{G.1})$$

and the free Hamiltonian of the baths

$$\begin{aligned}\hat{H}_E = & \int_{-\infty}^{\infty} d\omega \omega \left(\hat{\gamma}_B^\dagger(\omega) \hat{\gamma}_B(\omega) \right. \\ & \left. + \hat{\delta}_B^\dagger(\omega) \hat{\delta}_B(\omega) + \hat{\mu}_B^\dagger(\omega) \hat{\mu}_B(\omega) \right).\end{aligned}\quad (\text{G.2})$$

The global Hamiltonian of the system and the baths is thus $\hat{H}_{TOT} = \hat{H} + \hat{H}_{SE} + \hat{H}_E$. Note that we used the Markov approximation, neglecting the frequency dependence of the system-baths coupling and using the notations $\kappa_c(\omega) = \sqrt{\kappa/\pi}$ and $\kappa_m(\omega) = \sqrt{\gamma/\pi}$.

The physical inputs of the interferometer of Fig. IV.2 correspond to the modes $\hat{\alpha}_B(\omega)$ and $\hat{\beta}_B(\omega)$. They can be related to the modes inside the interferometer $\hat{\gamma}_B(\omega)$ and $\hat{\delta}_B(\omega)$ through the relations $\hat{\alpha}_B(\omega) = \left(\hat{\gamma}_B(\omega) - \hat{\delta}_B(\omega) \right) / \sqrt{2}$ and $\hat{\beta}_B(\omega) = \left(\hat{\gamma}_B(\omega) + \hat{\delta}_B(\omega) \right) / \sqrt{2}$. It is then meaningful to rewrite Eq. (G.1) in terms of the operators $\hat{\alpha}_B(\omega)$ and $\hat{\beta}_B(\omega)$,

$$\begin{aligned}\hat{H}_{SE} = & i \int_{-\infty}^{\infty} d\omega \kappa_c(\omega) \left(\hat{\alpha}_B^\dagger(\omega) \frac{\left(\hat{c}(t) - \hat{d}(t) \right)}{\sqrt{2}} - \hat{\alpha}_B(\omega) \frac{\left(\hat{c}^\dagger(t) - \hat{d}^\dagger(t) \right)}{\sqrt{2}} \right) + \\ & + i \int_{-\infty}^{\infty} d\omega \kappa_c(\omega) \left(\hat{\beta}_B^\dagger(\omega) \frac{\left(\hat{c}(t) + \hat{d}(t) \right)}{\sqrt{2}} - \hat{\beta}_B(\omega) \frac{\left(\hat{c}^\dagger(t) + \hat{d}^\dagger(t) \right)}{\sqrt{2}} \right) + \\ & + i \int_{-\infty}^{\infty} d\omega \kappa_m(\omega) \left(\hat{\mu}_B^\dagger(\omega) \hat{m}(t) - \hat{\mu}_B(\omega) \hat{m}^\dagger(t) \right),\end{aligned}\quad (\text{G.3})$$

where we can naturally define two collective intracavity modes $\hat{a} = (\hat{c} - \hat{d})/\sqrt{2}$ and $\hat{b} = (\hat{c} + \hat{d})/\sqrt{2}$, coupled to $\hat{\alpha}_B(\omega)$ and $\hat{\beta}_B(\omega)$ respectively. By rewriting Eq. (IV.7) in terms of the new defined collective optical modes, we obtain

$$\hat{H} = \omega_c (\hat{a}^\dagger \hat{a} + \hat{b}^\dagger \hat{b}) + \omega_m \hat{m}^\dagger \hat{m} + g_0 (\hat{a}^\dagger \hat{b} + \hat{a} \hat{b}^\dagger) (\hat{m}^\dagger + \hat{m}). \quad (\text{G.4})$$

We now consider that an undepleted coherent state at frequency ω_b is sent through the port $\hat{\beta}_B(\omega)$, which is essentially the input of the intracavity mode \hat{b} . Assuming that such classical driving dominates the dynamics, the state of the driven mode \hat{b} can be approximated by a coherent state. We can then make the following replacement $\hat{b} \rightarrow \beta e^{-i\omega_b t}$, where β is the size of the coherent state inside the cavity. Finally, in order to obtain a time-independent Hamiltonian we define the unitary transformation $\hat{U}(t) = e^{i\omega_b \hat{a}^\dagger \hat{a} t}$ and we move in a picture where the Hamiltonian is $\hat{H}_{\text{eff}} = \hat{U} \hat{H} \hat{U}^\dagger + i \frac{d\hat{U}}{dt} \hat{U}^\dagger$, which gives us the final expression of the effective Hamiltonian of Eq. (IV.9).

H Teleportation between two distant mechanical resonators

The teleportation protocol described here consists of three steps. First, an optomechanical entangled state is generated by Bob, who keeps one party of the state (a mechanical resonator), and sends the other party (an optical pulse) to Alice. The generation of this entangled EPR state is detailed in section H.0.1. Subsequently, Alice implements a state-swap process, *i.e.*, a beam splitter-type interaction between the light pulse coming from Bob and her own mechanical resonator, which is initially in the state to teleport. This part of the protocol is detailed in section H.0.2. Finally, Alice performs a Bell measurement of an optical quadrature and a mechanical quadrature, sends the outcomes through a classical channel to Bob, who implements a phase-space displacement on the state of his mechanical resonator, which concludes the teleportation protocol. This last step is described in section H.0.3.

H.0.1 EPR state generation

The first step of the teleportation protocol is the generation of an EPR state by Bob, between his own mechanical resonator, a double sided moving mirror, and a light pulse, which is sent to Alice after the entangling interaction. This requires to send a blue detuned pump pulse β with a frequency $\omega_b = \omega_c + \omega_m$ to the bottom input port of Bob's interferometer, that enhances a two-mode squeezing interaction, thus reducing the system Hamiltonian, in a frame rotating with ω_m , to

$$\hat{H}_I^b = g_0\beta \left(\hat{a}^\dagger \hat{m}_2^\dagger + \hat{a} \hat{m}_2 \right), \quad (\text{H.1})$$

where \hat{m}_2 represents Bob's mechanical resonator, the one towards which the initial state of a distant mechanical resonator \hat{m}_1 will be teleported.

With the standard Input-Output theory [Gardiner85, Gardiner04, Walls08], we first take into account the mechanical dissipation and the output coupling of the cavity, and derive the following Langevin equations

$$\dot{\hat{a}}(t) = -\kappa\hat{a}(t) - ig_0\beta \hat{m}_2^\dagger(t) - \sqrt{2\kappa} \hat{a}_{\text{in}}(t), \quad (\text{H.2})$$

$$\dot{\hat{m}}_2(t) = -\gamma\hat{m}_2(t) - ig_0\beta \hat{a}^\dagger(t) - \sqrt{2\gamma} \hat{m}_{\text{in}}(t). \quad (\text{H.3})$$

The condition $g_0\beta \ll \kappa$ allows us to adiabatically eliminate the optical mode \hat{a} , by setting $\dot{\hat{a}}(t) = 0$, thus imposing

$$\hat{a}(t) \approx -i\frac{g_0\beta}{\kappa}\hat{m}_2^\dagger(t) - \sqrt{\frac{2}{\kappa}} \hat{a}_{\text{in}}(t). \quad (\text{H.4})$$

To obtain the expression for the quantum optical output $\hat{a}_{\text{out}}(t)$ of the interferometer,

we use the input-output relation $\hat{a}_{\text{out}}^{\text{lossless}}(t) = \hat{a}_{\text{in}}(t) + \sqrt{2\kappa}\hat{a}(t)$. However, this relation gives the output field in the lossless case, *i.e.*, where no losses have occurred inside the cavities. In the following, we take into account the photon losses of the cavities by adding a virtual beam-splitter at the output of the lossless interferometric scheme. This additional beam-splitter is of high transmission, and its reflectivity models the losses. The beam-splitter relation giving the output field in the presence of photon losses is

$$\hat{a}_{\text{out}}(t) = \sqrt{\mu}\hat{a}_{\text{out}}^{\text{lossless}}(t) + \sqrt{1-\mu}\hat{f}_{\text{in}}(t), \quad (\text{H.5})$$

where $\hat{f}_{\text{in}}(t)$ is a mode introduced to take into account photon losses, and where μ is the transmission coefficient of the beam-splitter. It is defined as $\mu = \kappa/(\kappa + \kappa_L)$, where κ_L is the dissipation rate for the photon losses. In the lossless case, the output field is

$$\begin{aligned} \hat{a}_{\text{out}}^{\text{lossless}}(t) &= -\hat{a}_{\text{in}}(t) - i\sqrt{2G}e^{(G-\gamma)t}\hat{m}_2^\dagger(0) \\ &- \sqrt{2G}e^{(G-\gamma)t} \int_0^t dt' e^{-(G-\gamma)t'} \left(\sqrt{2G}\hat{a}_{\text{in}}(t') - i\sqrt{2\gamma}\hat{m}_{\text{in}}^\dagger(t') \right). \end{aligned} \quad (\text{H.6})$$

By using Eq.(H.5) we can write the equations of $\hat{a}_{\text{out}}(t)$, the field propagating between the two nodes, and $\hat{m}_2(t)$, the time evolved annihilation operator of Bob's mechanical resonator

$$\begin{aligned} \hat{a}_{\text{out}}(t) &= \sqrt{\frac{\kappa}{\kappa_{\text{tot}}}} \left(-\hat{a}_{\text{in}}(t) - i\sqrt{2G}e^{(G-\gamma)t}\hat{m}_2^\dagger(0) \right. \\ &- \left. \sqrt{2G}e^{(G-\gamma)t} \int_0^t dt' e^{-(G-\gamma)t'} \left(\sqrt{2G}\hat{a}_{\text{in}}(t') \right. \right. \\ &- \left. \left. i\sqrt{2\gamma}\hat{m}_{\text{in}}^\dagger(t') \right) \right) + \sqrt{\frac{\kappa_L}{\kappa_{\text{tot}}}}\hat{f}_{\text{in}}(t), \end{aligned} \quad (\text{H.7})$$

$$\begin{aligned} \hat{m}_2(t) &= e^{(G-\gamma)t}\hat{m}_2(0) + e^{(G-\gamma)t} \int_0^t dt' e^{-(G-\gamma)t'} \left(i\sqrt{2G}\hat{a}_{\text{in}}^\dagger(t') \right. \\ &- \left. \sqrt{2\gamma}\hat{m}_{\text{in}}(t') \right), \end{aligned} \quad (\text{H.8})$$

with $G = (g_0\beta)^2/\kappa$ and $\kappa_{\text{tot}} = \kappa + \kappa_L$. We will now make two important approximations in Eqs. (H.7) and (H.8). We use the fact that in our model $\gamma \ll G$, and first, take $G - \gamma \approx G$, and second, neglect the effect of the mechanical bath on the optical mode, which gives us

$$\begin{aligned} \hat{a}_{\text{out}}(t) &\approx \sqrt{\frac{\kappa}{\kappa_{\text{tot}}}} \left(-\hat{a}_{\text{in}}(t) - i\sqrt{2G}e^{Gt}\hat{m}_2^\dagger(0) \right. \\ &- \left. 2Ge^{Gt} \int_0^t dt' e^{-Gt'}\hat{a}_{\text{in}}(t') \right) + \sqrt{\frac{\kappa_L}{\kappa_{\text{tot}}}}\hat{f}_{\text{in}}(t), \end{aligned} \quad (\text{H.9})$$

$$\begin{aligned} \hat{m}_2(t) &\approx e^{Gt}\hat{m}_2(0) + i\sqrt{2G}e^{Gt} \int_0^t dt' e^{-Gt'}\hat{a}_{\text{in}}^\dagger(t') \\ &- \sqrt{2\gamma}e^{Gt} \int_0^t dt' e^{-Gt'}\hat{m}_{\text{in}}(t'). \end{aligned} \quad (\text{H.10})$$

We now use the definitions for normalized temporal field modes of Eq. (IV.18), in order to rewrite Eqs. (H.9) and (H.10) into the convenient forms,

$$\begin{aligned}\hat{A}_{\text{out}}^b &= -\sqrt{\frac{\kappa}{\kappa_{\text{tot}}}}e^{G\tau}\hat{A}_{\text{in}}^b \\ &\quad -i\sqrt{\frac{\kappa}{\kappa_{\text{tot}}}(e^{2G\tau}-1)}\left(\hat{M}_{\text{in}}\right)^\dagger + \sqrt{\frac{\kappa L}{\kappa_{\text{tot}}}}\hat{F}_{\text{in}}^b,\end{aligned}\quad (\text{H.11})$$

$$\hat{M}_{\text{out}} = e^{G\tau}\hat{M}_{\text{in}} + i\sqrt{e^{2G\tau}-1}\left(\hat{A}_{\text{in}}^b\right)^\dagger - C^b\hat{M}_B^b, \quad (\text{H.12})$$

where $\hat{A}_{\text{out}}^b = Q(\tau, \hat{a}_{\text{out}})$, $\hat{A}_{\text{in}}^b = P(\tau, \hat{a}_{\text{in}})$, $\hat{F}_{\text{in}}^b = Q(\tau, \hat{f}_{\text{in}})$, $\hat{M}_{\text{in}} = \hat{m}_2(0)$, $\hat{M}_{\text{out}} = \hat{m}_2(\tau)$, $\hat{M}_B^b = P(\tau, \hat{m}_{\text{in}})$ and $C^b = \sqrt{(e^{2G\tau}-1)\gamma}/G$. Using the Eqs. (H.11) and (H.12), the quadratures of these modes are

$$\hat{X}_{\text{out}} = -\sqrt{\frac{\kappa}{\kappa_{\text{tot}}}}e^r\hat{X}_{\text{in}} - \sqrt{\frac{\kappa}{\kappa_{\text{tot}}}(e^{2r}-1)}\hat{P}_2(0) + \sqrt{\frac{\kappa L}{\kappa_{\text{tot}}}}\hat{X}_f, \quad (\text{H.13})$$

$$\hat{P}_{\text{out}} = -\sqrt{\frac{\kappa}{\kappa_{\text{tot}}}}e^r\hat{P}_{\text{in}} - \sqrt{\frac{\kappa}{\kappa_{\text{tot}}}(e^{2r}-1)}\hat{X}_2(0) + \sqrt{\frac{\kappa L}{\kappa_{\text{tot}}}}\hat{P}_f, \quad (\text{H.14})$$

$$\hat{X}_2 = e^r\hat{X}_2(0) + \sqrt{e^{2r}-1}\hat{P}_{\text{in}} - C^bX_B^b, \quad (\text{H.15})$$

$$\hat{P}_2 = e^r\hat{P}_2(0) + \sqrt{e^{2r}-1}\hat{X}_{\text{in}} - C^bP_B^b, \quad (\text{H.16})$$

where $r = G\tau$, $X_{\text{in}} = [(\hat{A}_{\text{in}}^b)^\dagger + \hat{A}_{\text{in}}^b]/\sqrt{2}$ and $P_{\text{in}} = i[(\hat{A}_{\text{in}}^b)^\dagger - \hat{A}_{\text{in}}^b]/\sqrt{2}$ are the quadrature of the optical input of Bob's device, and where $X_2(0) = [\hat{m}_2^\dagger(0) + \hat{m}_2(0)]/\sqrt{2}$, $X_2 = [\hat{m}_2^\dagger(\tau) + \hat{m}_2(\tau)]/\sqrt{2}$, $P_2(0) = i[\hat{m}_2^\dagger(0) - \hat{m}_2(0)]/\sqrt{2}$, $P_2 = i[\hat{m}_2^\dagger(\tau) - \hat{m}_2(\tau)]/\sqrt{2}$, $X_f = [(\hat{F}_{\text{in}}^b)^\dagger + \hat{F}_{\text{in}}^b]/\sqrt{2}$ and $P_f = i[(\hat{F}_{\text{in}}^b)^\dagger - \hat{F}_{\text{in}}^b]/\sqrt{2}$.

Eqs. (H.13)-(H.16) are similar to those of a standard optical two-mode squeezed state with a squeezing parameter r [Braunstein05], except for the fact that here photon losses are taken into account, and we have terms containing X_B^b , P_B^b , *i.e.*, the thermal noise of Bob's mechanical resonator. In the limit $r \rightarrow \infty$, the term C^b eventually kills the entanglement, as shown in Fig. IV.5(a). It is thus important to find the optimal point r_{opt} , for which the amount of entanglement is sufficient to carry out the teleportation protocol, without a significant thermal disturbance.

Assuming Bob's mechanical oscillator is initially in a thermal state $\langle \hat{X}_2(0) \rangle = \langle \hat{P}_2(0) \rangle = (n_T + 1/2)$, with n_T being the thermal occupation number, and taking the vacuum state for Bob's optical quantum input $\langle \hat{X}_{\text{in}} \rangle = \langle \hat{P}_{\text{in}} \rangle = 1/2$, the EPR entanglement criterion is written as

$$\begin{aligned}\Delta_{\text{EPR}} &= \left[\Delta\left(\hat{X}_{\text{in}} + \hat{P}_2\right)\right]^2 + \left[\Delta\left(\hat{P}_{\text{in}} + \hat{X}_2\right)\right]^2 \\ &= 2(n_T + 1)\left(e^r - \sqrt{\frac{\kappa}{\kappa_{\text{tot}}}(e^{2r}-1)}\right)^2 + \frac{\gamma}{G}\left(e^{2r}-1\right)(2n_T + 1).\end{aligned}\quad (\text{H.17})$$

H.0.2 State-swap, or beam splitter-type interaction

After Bob sent the pulse entangled with his mechanical resonator, Alice must implement a beam splitter-type interaction between this pulse and her mechanical resonator. This operation is carried out by pumping Alice's optomechanical toolbox with a red detuned drive pulse with amplitude β and frequency $\omega_b = \omega_c - \omega_m$, which activates a beam splitter type interaction. In this case, the system Hamiltonian is given by, in a frame rotating with ω_m ,

$$\hat{H}_I^r = g_0\beta \left(\hat{a}'^\dagger \hat{m}_1 + \hat{a}' \hat{m}_1^\dagger \right), \quad (\text{H.18})$$

where \hat{m}_1 describes Alice's mechanical resonator, the state of which is to be teleported to Bob.

Using the same method as before, we derive the Langevin equations for Alice's toolbox

$$\dot{\hat{a}}'(t) = -\kappa\hat{a}'(t) - ig_0\beta\hat{m}_1(t) - \sqrt{2\kappa}\hat{a}'_{\text{in}}(t), \quad (\text{H.19})$$

$$\dot{\hat{m}}_1(t) = -\gamma\hat{m}_1(t) - ig_0\beta\hat{a}'(t) - \sqrt{2\gamma}\hat{m}'_{\text{in}}(t). \quad (\text{H.20})$$

We again adiabatically eliminate the optical mode and include photon losses to obtain the evolution for $\hat{a}'_{\text{out}}(t)$ and $\hat{m}_1(t)$

$$\begin{aligned} \hat{a}'_{\text{out}}(t) &= \sqrt{\frac{\kappa}{\kappa_{\text{tot}}}} \left(-\hat{a}'_{\text{in}}(t) - i\sqrt{2G}e^{-(G+\gamma)t}\hat{m}_1(0) \right. \\ &\quad \left. + \sqrt{2G}e^{-(G+\gamma)t} \int_0^t dt' e^{(G+\gamma)t'} \left(\sqrt{2G}\hat{a}'_{\text{in}}(t') + i\sqrt{2\gamma}\hat{m}'_{\text{in}}(t') \right) \right) \\ &\quad + \sqrt{\frac{\kappa_L}{\kappa_{\text{tot}}}} \hat{f}'_{\text{in}}(t), \end{aligned} \quad (\text{H.21})$$

$$\begin{aligned} \hat{m}_1(t) &= e^{-(G+\gamma)t}\hat{m}_1(0) + e^{-(G+\gamma)t} \int_0^t dt' e^{(G+\gamma)t'} \left(i\sqrt{2G}\hat{a}'_{\text{in}}(t') \right. \\ &\quad \left. - \sqrt{2\gamma}\hat{m}'_{\text{in}}(t') \right), \end{aligned} \quad (\text{H.22})$$

where $\hat{f}'_{\text{in}}(t)$ is the mode introduced to take into account photon losses. We use again the fact that $\gamma \ll G$, take $G - \gamma \approx G$, and neglect the effect of the mechanical bath on the optical mode,

$$\begin{aligned} \hat{a}'_{\text{out}}(t) &\approx \sqrt{\frac{\kappa}{\kappa_{\text{tot}}}} \left(-\hat{a}'_{\text{in}}(t) - i\sqrt{2G}e^{-Gt}\hat{m}_1(0) \right. \\ &\quad \left. + 2Ge^{-Gt} \int_0^t dt' e^{Gt'} \hat{a}'_{\text{in}}(t') \right) + \sqrt{\frac{\kappa_L}{\kappa_{\text{tot}}}} \hat{f}'_{\text{in}}(t), \end{aligned} \quad (\text{H.23})$$

$$\begin{aligned} \hat{m}_1(t) &\approx e^{-Gt}\hat{m}_1(0) + i\sqrt{2G}e^{-Gt} \int_0^t dt' e^{Gt'} \hat{a}'_{\text{in}}(t') \\ &\quad - \sqrt{2\gamma}e^{-Gt} \int_0^t dt' e^{Gt'} \hat{m}'_{\text{in}}(t'). \end{aligned} \quad (\text{H.24})$$

We write Eqs. (H.23) and (H.24) into the convenient forms

$$\hat{A}_{\text{out}}^r = -\sqrt{\frac{\kappa}{\kappa_{\text{tot}}}} e^{-Gt} \hat{A}_{\text{in}}^r - i\sqrt{\frac{\kappa}{\kappa_{\text{tot}}}} (1 - e^{-2Gt}) \hat{M}'_{\text{in}} + \sqrt{\frac{\kappa_L}{\kappa_{\text{tot}}}} \hat{F}_{\text{in}}^r, \quad (\text{H.25})$$

$$\hat{M}'_{\text{out}} = e^{-Gt} \hat{M}'_{\text{in}} + i\sqrt{1 - e^{-2Gt}} \hat{A}_{\text{in}}^r - C^r \hat{M}_B^r, \quad (\text{H.26})$$

where $\hat{A}_{\text{out}}^r = P(\tau, \hat{a}'_{\text{out}})$, $\hat{A}_{\text{in}}^r = Q(\tau, \hat{a}'_{\text{in}})$, $\hat{F}_{\text{in}}^r = Q(\tau, \hat{f}'_{\text{in}})$, $\hat{M}'_{\text{in}} = \hat{m}_1(0)$, $\hat{M}'_{\text{out}} = \hat{m}_1(\tau)$, $\hat{M}_B^r = Q(\tau, \hat{m}_{\text{in}})$ and $C^r = \sqrt{(1 - e^{-2G\tau})\gamma}/G$. Note that here $\hat{a}'_{\text{in}} = \hat{a}_{\text{out}}$ hence, in this case, the quantum optical output of Bob's toolbox is the quantum optical input of Alice's toolbox. Hence, we have $\hat{A}_{\text{in}}^r = \hat{A}_{\text{out}}^b$, meaning that Bob's output pulse shape perfectly matches Alice's optical input shape. Using the Eqs. (H.25) and (H.26), the quadratures of these modes are

$$\hat{X}_u = -\sqrt{\frac{\kappa}{\kappa_{\text{tot}}}} e^{-r'} \hat{X}_{\text{out}} + \sqrt{\frac{\kappa}{\kappa_{\text{tot}}}} (1 - e^{-2r'}) \hat{P}_1(0) + \sqrt{\frac{\kappa_L}{\kappa_{\text{tot}}}} \hat{X}_{f'}, \quad (\text{H.27})$$

$$\hat{P}_u = -\sqrt{\frac{\kappa}{\kappa_{\text{tot}}}} e^{-r'} \hat{P}_{\text{out}} - \sqrt{\frac{\kappa}{\kappa_{\text{tot}}}} (1 - e^{-2r'}) \hat{X}_1(0) + \sqrt{\frac{\kappa_L}{\kappa_{\text{tot}}}} \hat{P}_{f'}, \quad (\text{H.28})$$

$$\hat{X}_v = e^{-r'} \hat{X}_1(0) - \sqrt{1 - e^{-2r'}} \hat{P}_{\text{out}} - C^r X_B^r, \quad (\text{H.29})$$

$$\hat{P}_v = e^{-r'} \hat{P}_2(0) + \sqrt{e^{-2r} - 1} \hat{X}_{\text{out}} - C^r P_B^r, \quad (\text{H.30})$$

where $r' = G\tau'$, $X_{\text{out}} = [(\hat{A}_{\text{out}}^b)^\dagger + \hat{A}_{\text{out}}^b]/\sqrt{2}$ and $P_{\text{out}} = i[(\hat{A}_{\text{out}}^b)^\dagger - \hat{A}_{\text{out}}^b]/\sqrt{2}$, where $X_u = [(\hat{A}_{\text{out}}^r)^\dagger + \hat{A}_{\text{out}}^r]/\sqrt{2}$ and $P_u = i[(\hat{A}_{\text{out}}^r)^\dagger - \hat{A}_{\text{out}}^r]/\sqrt{2}$, and where $X_1(0) = [\hat{m}_1^\dagger(0) + \hat{m}_1(0)]/\sqrt{2}$, $X_v = [\hat{m}_1^\dagger(\tau') + \hat{m}_1(\tau')]/\sqrt{2}$, $P_1(0) = i[\hat{m}_1^\dagger(0) - \hat{m}_1(0)]/\sqrt{2}$, and $P_v = i[\hat{m}_1^\dagger(\tau') - \hat{m}_1(\tau')]/\sqrt{2}$. One can see that in Eqs. (H.27)-(H.30), a judicious choice of τ' can lead to a 50-50 beam splitter-type interaction. Indeed, by choosing τ' such that $e^{-r'} = 1/\sqrt{2}$, Eqs. (H.27)-(H.30) become

$$\hat{X}_u = \sqrt{\frac{\kappa}{\kappa_{\text{tot}}}} \frac{\hat{P}_1(0) - \hat{X}_{\text{out}}}{\sqrt{2}} + \sqrt{\frac{\kappa_L}{\kappa_{\text{tot}}}} \hat{X}_{f'}, \quad (\text{H.31})$$

$$\hat{P}_u = \sqrt{\frac{\kappa}{\kappa_{\text{tot}}}} \frac{-\hat{X}_1(0) - \hat{P}_{\text{out}}}{\sqrt{2}} + \sqrt{\frac{\kappa_L}{\kappa_{\text{tot}}}} \hat{P}_{f'}, \quad (\text{H.32})$$

$$\hat{X}_v = \frac{\hat{X}_1(0) - \hat{P}_{\text{out}}}{\sqrt{2}} - \sqrt{\frac{\gamma}{2G}} X_B^r, \quad (\text{H.33})$$

$$\hat{P}_v = \frac{\hat{P}_1(0) + \hat{X}_{\text{out}}}{\sqrt{2}} - \sqrt{\frac{\gamma}{2G}} P_B^r. \quad (\text{H.34})$$

We now use Eqs. (H.15) and (H.32) to write Bob's mechanical resonator \hat{X}_2 quadrature

as

$$\begin{aligned}
\hat{X}_2 &= (\hat{X}_2 + \hat{P}_{\text{out}}) + \sqrt{\frac{2\kappa_{\text{tot}}}{\kappa}} \hat{P}_u + \hat{X}_1(0) - \sqrt{\frac{2\kappa_L}{\kappa}} \hat{P}_{f'}, \\
&= \hat{X}_1(0) + \left(e^r - \sqrt{\frac{\kappa}{\kappa_{\text{tot}}}} (e^{2r} - 1) \right) \hat{X}_2(0) + \left(\sqrt{e^{2r} - 1} - \sqrt{\frac{\kappa}{\kappa_{\text{tot}}}} e^r \right) \hat{P}_{\text{in}} \\
&+ \sqrt{\frac{2\kappa_{\text{tot}}}{\kappa}} \hat{P}_u - C^b X_B^b - \sqrt{\frac{2\kappa_L}{\kappa}} \hat{P}_{f'} + \sqrt{\frac{\kappa_L}{\kappa_{\text{tot}}}} \hat{P}_f.
\end{aligned} \tag{H.35}$$

By using Eqs. (H.16) and (H.34) we can finally write Bob's mechanical resonator \hat{P}_2 quadrature as

$$\begin{aligned}
\hat{P}_2 &= (\hat{P}_2 + \hat{X}_{\text{out}}) - \sqrt{2} \hat{P}_v + \hat{P}_1(0) - \sqrt{\frac{\gamma}{G}} P_B^r, \\
&= \hat{P}_1(0) + \left(e^r - \sqrt{\frac{\kappa}{\kappa_{\text{tot}}}} (e^{2r} - 1) \right) \hat{P}_2(0) + \left(\sqrt{e^{2r} - 1} - \sqrt{\frac{\kappa}{\kappa_{\text{tot}}}} e^r \right) \hat{X}_{\text{in}} \\
&- \sqrt{2} \hat{P}_v - C^b P_B^b - \sqrt{\frac{\gamma}{G}} P_B^r + \sqrt{\frac{\kappa_L}{\kappa_{\text{tot}}}} \hat{X}_f.
\end{aligned} \tag{H.36}$$

H.0.3 Measurement and classical channel

The next step of the protocol is Alice's measurement of both \hat{P}_u and \hat{P}_v , which become classical random variables P_u and P_v after the measurement. Notice that, in the simplified case where one neglect both the mechanical bath effects and the photon losses, and takes $r \rightarrow \infty$, Bob's mechanical resonator state collapses into a state which differs from the initial Alice's mechanical resonator state by a phase-space displacement.

Through a classical communication channel, Bob receives Alice's outcomes P_u and P_v and performs the needed phase-space displacement,

$$\hat{X}_2 \longrightarrow \hat{X}_2^{\text{tel}} = \hat{X}_2 - \eta \sqrt{\frac{2\kappa_{\text{tot}}}{\kappa}} \hat{P}_u, \tag{H.37}$$

$$\hat{P}_2 \longrightarrow \hat{P}_2^{\text{tel}} = \hat{P}_2 + \eta \sqrt{2} \hat{P}_v, \tag{H.38}$$

where the parameter η describes both the efficiency of the measurement and of the displacement. We can rewrite the teleported state quadratures from Eqs. (H.37) and (H.38) as

$$\begin{aligned}
\hat{X}_2^{\text{tel}} &= \eta \hat{X}_1(0) + \left(e^r - \eta \sqrt{\frac{\kappa}{\kappa_{\text{tot}}}} (e^{2r} - 1) \right) \hat{X}_2(0) + \left(\sqrt{e^{2r} - 1} \right. \\
&- \left. \eta \sqrt{\frac{\kappa}{\kappa_{\text{tot}}}} e^r \right) \hat{P}_{\text{in}} - C^b X_B^b - \eta \sqrt{\frac{2\kappa_L}{\kappa}} \hat{P}_{f'} + \sqrt{\frac{\kappa_L}{\kappa_{\text{tot}}}} \hat{P}_f,
\end{aligned} \tag{H.39}$$

$$\begin{aligned}
\hat{P}_2^{\text{tel}} &= \eta \hat{P}_1(0) + \left(e^r - \eta \sqrt{\frac{\kappa}{\kappa_{\text{tot}}}} (e^{2r} - 1) \right) \hat{P}_2(0) + \left(\sqrt{e^{2r} - 1} \right. \\
&- \left. \eta \sqrt{\frac{\kappa}{\kappa_{\text{tot}}}} e^r \right) \hat{X}_{\text{in}} - C^b P_B^b - \eta \sqrt{\frac{\gamma}{G}} P_B^r + \sqrt{\frac{\kappa_L}{\kappa_{\text{tot}}}} \hat{X}_f.
\end{aligned} \tag{H.40}$$

One can see that without mechanical dissipation and photon losses, *i.e.*, $\gamma = \kappa_L = 0$, and with the limits $r \rightarrow \infty$ and $\eta \rightarrow 1$, perfect teleportation $X_2^{tel} = X_1(0)$ and $P_2^{tel} = P_1(0)$ is deterministically obtained.

In order to check how successful the protocol is, we use the teleportation fidelity $\mathcal{F} = \langle \psi_1 | \hat{\rho}_2^{tel} | \psi_1 \rangle$, where $|\psi_1\rangle$ is the state to teleport, *i.e.*, the initial state of Alice's double sided moving mirror, and where $\hat{\rho}_2^{tel}$ is the density matrix of the teleported state, *i.e.*, the final state of Bob's double sided moving mirror. We consider the initial state of Alice's mechanical resonator to be a coherent state with a displacement $\alpha_1 = (X_1(0) + iP_1(0))/\sqrt{2}$. In that case, $\mathcal{F} = \pi Q_{tel}(\alpha_1)$, where Q_{tel} is the Q function of the teleported state [Braunstein05],

$$\mathcal{F} = \frac{1}{2\sqrt{\sigma_X\sigma_P}} \exp \left[- (1 - \eta)^2 \left(\frac{X_1^2(0)}{2\sigma_X} + \frac{P_1^2(0)}{2\sigma_P} \right) \right]. \quad (\text{H.41})$$

σ_X and σ_P are the variances of the Q function,

$$\begin{aligned} \sigma_P &= \sigma_X + \eta^2 \frac{\gamma}{2G} \left(n_T + \frac{1}{2} \right) - \eta^2 \frac{\kappa_L}{2\kappa}, \\ &= \frac{1}{4}(1 + \eta^2) + \left[\frac{1}{2} \left(e^r - \eta \sqrt{\frac{\kappa}{\kappa_{tot}}} (e^{2r} - 1) \right)^2 \right. \\ &\quad \left. + \frac{(C^b)^2}{2} + \eta^2 \frac{\gamma}{2G} \right] \left(n_T + \frac{1}{2} \right) \\ &\quad + \frac{1}{4} \left(\sqrt{e^{2r} - 1} - \sqrt{\frac{\kappa}{\kappa_{tot}}} \eta e^r \right)^2 + \frac{\kappa_L}{2\kappa_{tot}}, \end{aligned} \quad (\text{H.42})$$

where we used the fact that initially, Bob's double sided moving mirror, and the mechanical baths of both mechanical resonators are all at thermal equilibrium.

Let us us briefly comment the measurements needed to perform the operation shown in Eqs. (H.37) and (H.38). For these two measurements, Alice proceeds as follows: the optical quadrature \hat{P}_u is measured with a homodyne scheme applied to Alice's output pulse, which concludes this first measurement. Subsequently, an additional red detuned pulse β with a duration τ'' is sent through the pumping port of Alice's toolbox, in order to transfer the mechanical quadrature \hat{P}_v to a second output light pulse, whose quadratures will be measured again with a homodyne measurement. To clarify this point, let us write the expressions of Alice's optical output quadratures, after the second pulse of duration τ''

$$\begin{aligned} \hat{X}_{meas} &= -\sqrt{\frac{\kappa}{\kappa_{tot}}} e^{-r''} \hat{X}_{OVN} \\ &\quad + \sqrt{\frac{\kappa}{\kappa_{tot}}} (1 - e^{-2r''}) \hat{P}_v + \sqrt{\frac{\kappa_L}{\kappa_{tot}}} \hat{X}_{f''}, \end{aligned} \quad (\text{H.43})$$

$$\begin{aligned} \hat{P}_{meas} &= -\sqrt{\frac{\kappa}{\kappa_{tot}}} e^{-r''} \hat{P}_{OVN} \\ &\quad - \sqrt{\frac{\kappa}{\kappa_{tot}}} (1 - e^{-2r''}) \hat{X}_v + \sqrt{\frac{\kappa_L}{\kappa_{tot}}} \hat{P}_{f''}, \end{aligned} \quad (\text{H.44})$$

where \hat{X}_{meas} and \hat{P}_{meas} are the quadratures of the second quantum optical output, and where \hat{X}_{OVN} and \hat{P}_{OVN} are the quadratures of the quantum optical vacuum noise (OVN) involved as an input in the interaction process caused by the second red detuned pulse. $\hat{X}_{f''}$ and $\hat{P}_{f''}$ are the quadratures of the mode for the photon loss channel.

By choosing τ'' such that $e^{-r''} \rightarrow 0$, and using Eqs. (H.43) and (H.44), the result of the measurement is

$$\langle \hat{X}_{meas} \rangle = \sqrt{\frac{\kappa}{\kappa_{tot}}} \langle \hat{P}_v \rangle. \quad (\text{H.45})$$

I Remote quantum state transfer between two distant mechanical resonators

The protocol to implement remote quantum state transfer is the following: the first interferometer, containing the state to transfer, is pumped by a classical driving pulse at the classical port. This results in the generation of a quantum output pulse, which is sent to the receiver. While this flying pulse enters the second interferometer, the latter is pumped by a classical driving pulse that completes the transfer.

There are two major differences in these two steps, with respect to the teleportation protocol. The first difference is that both devices are pumped with red detuned classical driving pulses. The second major difference is that the use of the same temporal pulse shapes as before does not lead to a significant transfer efficiency. Indeed, in the teleportation protocol the fact that Bob's toolbox was pumped by a blue detuned drive made its quantum output pulse shape perfect to be absorbed by Alice's toolbox, which was pumped at the same time by a red detuned drive. When both devices are in the red-sideband regime, the temporal-shape mismatch of input-output pulses prevent the receiver from absorbing the communication signal.

To overcome this issue, the temporal shapes of both red detuned pumps must be optimized. The driving-pulse shapes will have duration τ and they will have the following amplitudes $\beta_S(t) = \beta S(t)$ and $\beta_R(t) = \beta R(t)$ for the sender and receiver devices, respectively. We defined the functions

$$S(t) = \sqrt{1 - e^{-\mu_S G t}}, \quad (\text{I.1})$$

$$R(t) = e^{-\mu_R G t}, \quad (\text{I.2})$$

which specify the pulse shapes (see inset in Fig. IV.7). We also defined $G = (g_0\beta)^2/\kappa$, while μ_S and μ_R are parameters that must be optimized to maximize the transfer efficiency. For $g_0\beta = 0.05\kappa$, we have $\mu_S = 0.05$ and $\mu_R = 0.22$.

Both pumps enhance a state-swap process, described by the Hamiltonian (H.18), which gives the following Langevin equations for the sender, similar to Eqs. (H.19) and (H.20),

$$\dot{\hat{a}}(t) = -\kappa\hat{a}(t) - ig_0\beta S(t)\hat{m}_1(t) - \sqrt{2\kappa}\hat{a}_{\text{in}}(t), \quad (\text{I.3})$$

$$\dot{\hat{m}}_1(t) = -\gamma\hat{m}_1(t) - ig_0\beta S(t)\hat{a}(t) - \sqrt{2\gamma}\hat{m}_{\text{in}}(t). \quad (\text{I.4})$$

As in the previous section, we adiabatically eliminate the optical mode and obtain the

evolution for $\hat{a}_{\text{out}}(t)$ and $\hat{m}_1(t)$

$$\begin{aligned} \hat{a}_{\text{out}}(t) &= \sqrt{\frac{\kappa}{\kappa_{\text{tot}}}} \left(-\hat{a}_{\text{in}}(t) - i\sqrt{2}GS(t)e^{-\gamma t-G\int_0^t dt' S^2(t')} \hat{m}_1(0) \right. \\ &+ \sqrt{2}GS(t)e^{-\gamma t-G\int_0^t dt' S^2(t')} \int_0^t dt' e^{\gamma t'+G\int_0^{t'} dt'' S^2(t'')} \left(\sqrt{2}GS(t') \hat{a}_{\text{in}}(t') \right. \\ &\left. \left. + i\sqrt{2}\gamma \hat{m}_{\text{in}}(t') \right) \right) + \sqrt{\frac{\kappa_L}{\kappa_{\text{tot}}}} \hat{f}_{\text{in}}(t), \end{aligned} \quad (\text{I.5})$$

$$\begin{aligned} \hat{m}_1(t) &= e^{-\gamma t-G\int_0^t dt' S^2(t')} \hat{m}_1(0) \\ &+ e^{-\gamma t-G\int_0^t dt' S^2(t')} \int_0^t dt' e^{\gamma t'+G\int_0^{t'} dt'' S^2(t'')} \left(i\sqrt{2}GS(t') \hat{a}_{\text{in}}(t') \right. \\ &\left. - \sqrt{2}\gamma \hat{m}_{\text{in}}(t') \right), \end{aligned} \quad (\text{I.6})$$

where $\hat{f}_{\text{in}}(t)$ is the mode introduced to take into account photon losses. We now need the Langevin equations for the process occurring for the receiver, not very different from Eqs. (I.3) and (I.4),

$$\dot{\hat{a}}'(t) = -\kappa \hat{a}'(t) - ig_0 \beta R(t) \hat{m}_2(t) - \sqrt{2\kappa} \hat{a}'_{\text{in}}(t), \quad (\text{I.7})$$

$$\dot{\hat{m}}_2(t) = -\gamma \hat{m}_2(t) - ig_0 \beta R(t) \hat{a}'(t) - \sqrt{2\gamma} \hat{m}'_{\text{in}}(t). \quad (\text{I.8})$$

Accordingly, the expressions for $\hat{a}'_{\text{out}}(t)$ and $\hat{m}_2(t)$ are similar to the Eqs. (I.5) and (I.6),

$$\begin{aligned} \hat{a}'_{\text{out}}(t) &= \sqrt{\frac{\kappa}{\kappa_{\text{tot}}}} \left(-\hat{a}'_{\text{in}}(t) - i\sqrt{2}GR(t)e^{-\gamma t-G\int_0^t dt' R^2(t')} \hat{m}_2(0) + \right. \\ &+ \sqrt{2}GR(t)e^{-\gamma t-G\int_0^t dt' R^2(t')} \int_0^t dt' e^{\gamma t'+G\int_0^{t'} dt'' R^2(t'')} \left(\sqrt{2}GR(t') \hat{a}'_{\text{in}}(t') \right. \\ &\left. \left. + i\sqrt{2}\gamma \hat{m}'_{\text{in}}(t') \right) \right) + \sqrt{\frac{\kappa_L}{\kappa_{\text{tot}}}} \hat{f}'_{\text{in}}(t), \end{aligned} \quad (\text{I.9})$$

$$\begin{aligned} \hat{m}_2(t) &= e^{-\gamma t-G\int_0^t dt' R^2(t')} \hat{m}_2(0) + \\ &+ e^{-\gamma t-G\int_0^t dt' R^2(t')} \int_0^t dt' e^{\gamma t'+G\int_0^{t'} dt'' R^2(t'')} \left(i\sqrt{2}GR(t') \hat{a}'_{\text{in}}(t') \right. \\ &\left. - \sqrt{2}\gamma \hat{m}'_{\text{in}}(t') \right), \end{aligned} \quad (\text{I.10})$$

where the quantum input pulse of the sender is the quantum output pulse of the receiver, *i.e.*, $\hat{a}'_{\text{in}}(t) = \hat{a}_{\text{out}}(t)$. Using Eqs. (I.10) and (I.5) we obtain

$$\begin{aligned} \hat{m}_2(t) &= e^{-\gamma t-G\int_0^t dt' R^2(t')} \hat{m}_2(0) + \sqrt{\frac{\kappa}{\kappa_{\text{tot}}}} 2Ge^{-\gamma t-G\int_0^t dt' R^2(t')} \\ &\times \int_0^t dt' R(t') S(t') e^{G\int_0^{t'} dt'' (R^2(t'') - S^2(t''))} \hat{m}_1(0) \\ &+ N(\hat{a}_{\text{in}}, \hat{m}_{\text{in}}, \hat{m}'_{\text{in}}, \hat{f}_{\text{in}}, \hat{f}'_{\text{in}}, t), \end{aligned} \quad (\text{I.11})$$

where $N(\hat{a}_{\text{in}}, \hat{m}_{\text{in}}, \hat{m}'_{\text{in}}, \hat{f}_{\text{in}}, \hat{f}'_{\text{in}}, t)$ encodes the dependence on the vacuum noise of the quantum optical input of the sender, the thermal noises and the photon loss modes noises of both the sender and the receiver.

We can rewrite the final states of Eqs. (I.5), (I.6), and (I.11), *i.e.*, after the end of the interaction time τ , into the useful forms

$$\hat{m}_1(\tau) = \sqrt{1 - W_D^2} \hat{m}_1(0) + \dots, \quad (\text{I.12})$$

$$\hat{m}_2(\tau) = W_{TM} \hat{m}_1(0) + \dots, \quad (\text{I.13})$$

where we omitted for clarity all the other contributions different than those of the initial state intended for the transfer, $\hat{m}_1(0)$. The two quantities defined in Eqs. (I.12) and (I.13) give us the following information: W_D shows how the state $\hat{m}_1(\tau)$ of the sender is destroyed by the transfer of its initial state $\hat{m}_1(0)$ to the receiver's state $\hat{m}_2(\tau)$; W_{TM} shows how significant is the transfer of $\hat{m}_1(0)$ to $\hat{m}_2(\tau)$, thus defining a benchmark for the protocol. We show the square of these quantities in Fig. IV.7 since it demonstrates the efficiency of the transfer for the second order moments of the initial state.

Bibliography

- [Abdo13a] B. Abdo, A. Kamal, and M. Devoret. *Nondegenerate three-wave mixing with the josephson ring modulator*. Phys. Rev. B **87**, 014508, 2013.
- [Abdo13b] B. Abdo, K. Sliwa, F. Schackert, N. Bergeal, M. Hatridge, L. Frunzio, A. D. Stone, and M. Devoret. *Full coherent frequency conversion between two propagating microwave modes*. Phys. Rev. Lett. **110**, 173902, 2013.
- [Adesso05] G. Adesso and F. Illuminati. *Gaussian measures of entanglement versus negativities: Ordering of two-mode gaussian states*. Phys. Rev. A **72**, 032334, 2005.
- [Agarwal84] G. S. Agarwal. *Vacuum-field rabi splittings in microwave absorption by rydberg atoms in a cavity*. Phys. Rev. Lett. **53**, 1732–1734, 1984.
- [Anappara09] A. A. Anappara, S. De Liberato, A. Tredicucci, C. Ciuti, G. Biasiol, L. Sorba, and F. Beltram. *Signatures of the ultrastrong light-matter coupling regime*. Phys. Rev. B **79**, 201303, 2009.
- [Anderson63] P. W. Anderson and J. M. Rowell. *Probable observation of the josephson superconducting tunneling effect*. Phys. Rev. Lett. **10**, 230–232, 1963.
- [Anderson95] M. H. Anderson, J. R. Ensher, M. R. Matthews, C. E. Wieman, and E. A. Cornell. *Observation of bose-einstein condensation in a dilute atomic vapor*. Science **269**, 5221, 198–201, 1995.
- [Anetsberger09] G. Anetsberger, O. Arcizet, Q. P. Unterreithmeier, R. Rivière, A. Schliesser, E. M. Weig, J. P. Kotthaus, and T. J. Kippenberg. *Near-field cavity optomechanics with nanomechanical oscillators*. Nature Physics **5**, 909–914, 2009.
- [Aron14] C. Aron, M. Kulkarni, and H. E. Türeci. *Steady-state entanglement of spatially separated qubits via quantum bath engineering*. Phys. Rev. A **90**, 062305, 2014.
- [Aron16] C. Aron, M. Kulkarni, and H. E. Türeci. *Photon-mediated interactions: A scalable tool to create and sustain entangled states of n atoms*. Phys. Rev. X **6**, 011032, 2016.
- [Arons65] A. B. Arons and M. B. Peppard. *Einstein’s proposal of the photon concept—a translation of the annalen der physik paper of 1905*. American Journal of Physics **33**, 5, 367–374, 1965.

- [Arthurs65] E. Arthurs and J. L. Kelly. *B.s.t.j. briefs: On the simultaneous measurement of a pair of conjugate observables*. The Bell System Technical Journal **44**, 4, 725–729, 1965.
- [Ashhab10] S. Ashhab and F. Nori. *Qubit-oscillator systems in the ultrastrong-coupling regime and their potential for preparing nonclassical states*. Phys. Rev. A **81**, 042311, 2010.
- [Asjad16] M. Asjad, S. Zippilli, and D. Vitali. *Mechanical einstein-podolsky-rosen entanglement with a finite-bandwidth squeezed reservoir*. Phys. Rev. A **93**, 062307, 2016.
- [Askenazi14] B. Askenazi, A. Vasanelli, A. Delteil, Y. Todorov, L. C. Andreani, G. Beaudoin, I. Sagnes, and C. Sirtori. *Ultra-strong light-matter coupling for designer reststrahlen band*. New Journal of Physics **16**, 4, 043029, 2014.
- [Aspelmeyer14] M. Aspelmeyer, T. J. Kippenberg, and F. Marquardt. *Cavity optomechanics*. Rev. Mod. Phys. **86**, 1391–1452, 2014.
- [Aspuru-Guzik12] A. Aspuru-Guzik and P. Walther. *Photonic quantum simulators*. Nature Physics **8**, 285–291, 2012.
- [Ballester12] D. Ballester, G. Romero, J. J. García-Ripoll, F. Deppe, and E. Solano. *Quantum simulation of the ultrastrong-coupling dynamics in circuit quantum electrodynamics*. Phys. Rev. X **2**, 021007, 2012.
- [Barberena17] D. Barberena, L. Lamata, and E. Solano. *Dispersive regimes of the multiqubit quantum rabi model*. arXiv:1703.03377, 2017.
- [Bennett96] C. H. Bennett, H. J. Bernstein, S. Popescu, and B. Schumacher. *Concentrating partial entanglement by local operations*. Phys. Rev. A **53**, 2046–2052, 1996.
- [Bergeal10a] N. Bergeal, F. Schackert, M. Metcalfe, R. Vijay, V. E. Manucharyan, L. Frunzio, D. E. Prober, R. J. Schoelkopf, S. M. Girvin, and M. H. Devoret. *Phase-preserving amplification near the quantum limit with a josephson ring modulator*. Nature **465**, 64–68, 2010.
- [Bergeal10b] N. Bergeal, R. Vijay, V. E. Manucharyan, I. Siddiqi, R. J. Schoelkopf, S. M. Girvin, and M. H. Devoret. *Analog information processing at the quantum limit with a josephson ring modulator*. Nature Physics **6**, 296–302, 2010.
- [Bertet01] P. Bertet, S. Osnaghi, A. Rauschenbeutel, G. Nogues, A. Auffeves, M. Brune, J. M. Raimond, and S. Haroche. *A complementarity experiment with an interferometer at the quantum-classical boundary*. Nature **411**, 166–170, 2001.
- [Bertet02] P. Bertet, A. Auffeves, P. Maioli, S. Osnaghi, T. Meunier, M. Brune, J. M. Raimond, and S. Haroche. *Direct measurement of the wigner function of a one-photon fock state in a cavity*. Phys. Rev. Lett. **89**, 200402, 2002.

- [Blais04] A. Blais, R.-S. Huang, A. Wallraff, S. M. Girvin, and R. J. Schoelkopf. *Cavity quantum electrodynamics for superconducting electrical circuits: An architecture for quantum computation*. Phys. Rev. A **69**, 062320, 2004.
- [Blatt12] R. Blatt and C. F. Roos. *Quantum simulations with trapped ions*. Nature Physics **8**, 277–284, 2012.
- [Bloch40] F. Bloch and A. Siegert. *Magnetic resonance for nonrotating fields*. Phys. Rev. **57**, 522–527, 1940.
- [Bloch12] I. Bloch, J. Dalibard, and S. Nascimbène. *Quantum simulations with ultracold quantum gases*. Nature Physics **8**, 267–276, 2012.
- [Bohm52] D. Bohm. *A Suggested Interpretation of the Quantum Theory in Terms of "Hidden" Variables. I*. Phys. Rev. **85**, 166–179, 1952.
- [Bose97] S. Bose, K. Jacobs, and P. L. Knight. *Preparation of nonclassical states in cavities with a moving mirror*. Phys. Rev. A **56**, 4175–4186, 1997.
- [Bowen02] W. P. Bowen, N. Treps, R. Schnabel, and P. K. Lam. *Experimental demonstration of continuous variable polarization entanglement*. Phys. Rev. Lett. **89**, 253601, 2002.
- [Braginsky67] V. B. Braginsky and A. B. Manukin. *Ponderomotive effects of electromagnetic radiation*. Sov. Phys. JETP **25**, 653, 1967.
- [Braginsky70] V. B. Braginsky, A. B. Manukin, and M. Y. Tikhonov. *Investigation of dissipative ponderomotive effects of electromagnetic radiation*. Sov. Phys. JETP **31**, 829, 1970.
- [Braumüller16] J. Braumüller, M. Marthaler, A. Schneider, A. Stehli, H. Rotzinger, M. Weides, and A. V. Ustinov. *Analog quantum simulation of the rabi model in the ultra-strong coupling regime*. arXiv:1611.08404, 2016.
- [Braunstein91] S. L. Braunstein, C. M. Caves, and G. J. Milburn. *Interpretation for a positive P representation*. Phys. Rev. A **43**, 1153–1159, 1991.
- [Braunstein98] S. L. Braunstein and H. J. Kimble. *Teleportation of continuous quantum variables*. Phys. Rev. Lett. **80**, 869–872, 1998.
- [Braunstein05] S. L. Braunstein and P. van Loock. *Quantum information with continuous variables*. Rev. Mod. Phys. **77**, 513–577, 2005.
- [Brecha95] R. J. Brecha, L. A. Orozco, M. G. Raizen, M. Xiao, and H. J. Kimble. *Observation of oscillatory energy exchange in a coupled-atom-cavity system*. J. Opt. Soc. Am. B **12**, 12, 2329–2339, 1995.
- [Brennecke08] F. Brennecke, S. Ritter, T. Donner, and T. Esslinger. *Cavity optomechanics with a bose-einstein condensate*. Science **322**, 5899, 235–238, 2008.

- [Brooks12] D. W. C. Brooks, T. Botter, S. Schreppler, T. P. Purdy, N. Brahms, and D. M. Stamper-Kurn. *Non-classical light generated by quantum-noise-driven cavity optomechanics*. *Nature* **488**, 476–480, 2012.
- [Brune96] M. Brune, E. Hagley, J. Dreyer, X. Maître, A. Maali, C. Wunderlich, J. M. Raimond, and S. Haroche. *Observing the progressive decoherence of the "meter" in a quantum measurement*. *Phys. Rev. Lett.* **77**, 4887–4890, 1996.
- [Capasso90] F. Capasso and S. Datta. *Quantum electron devices*. *Physics Today* **43**, 74–82, 1990.
- [Carmichael99] H. Carmichael. *Statistical Methods in Quantum Optics 1: Master Equations and Fokker-Planck Equations*, (Springer, 1999).
- [Casanova10] J. Casanova, G. Romero, I. Lizuain, J. J. García-Ripoll, and E. Solano. *Deep strong coupling regime of the jaynes-cummings model*. *Phys. Rev. Lett.* **105**, 263603, 2010.
- [Castellanos-Beltran08] M. A. Castellanos-Beltran, K. D. Irwin, G. C. Hilton, L. R. Vale, and K. W. Lehnert. *Amplification and squeezing of quantum noise with a tunable josephson metamaterial*. *Nature Phys.* **4**, 929–931, 2008.
- [Caves80] C. M. Caves. *Quantum-mechanical radiation-pressure fluctuations in an interferometer*. *Phys. Rev. Lett.* **45**, 75–79, 1980.
- [Caves81] C. M. Caves. *Quantum-mechanical noise in an interferometer*. *Phys. Rev. D* **23**, 1693–1708, 1981.
- [Cerf00] N. J. Cerf, A. Ipe, and X. Rottenberg. *Cloning of continuous quantum variables*. *Phys. Rev. Lett.* **85**, 1754–1757, 2000.
- [Cerf01] N. J. Cerf, M. Lévy, and G. V. Assche. *Quantum distribution of gaussian keys using squeezed states*. *Phys. Rev. A* **63**, 052311, 2001.
- [Chakraborty16] S. Chakraborty and A. K. Sarma. *Generation of enhanced and robust bipartite optomechanical entanglement via an auxiliary qubit induced quadratic mechanical nonlinearity*. arXiv:1606.06419, 2016.
- [Chen02] Z.-B. Chen, J.-W. Pan, G. Hou, and Y.-D. Zhang. *Maximal violation of bell's inequalities for continuous variable systems*. *Phys. Rev. Lett.* **88**, 040406, 2002.
- [Chiorescu04] I. Chiorescu, P. Bertet, K. Semba, Y. Nakamura, C. J. P. M. Harmans, and J. E. Mooij. *Coherent dynamics of a flux qubit coupled to a harmonic oscillator*. *Nature* **431**, 159–162, 2004.
- [Cirac97] J. I. Cirac, P. Zoller, H. J. Kimble, and H. Mabuchi. *Quantum state transfer and entanglement distribution among distant nodes in a quantum network*. *Phys. Rev. Lett.* **78**, 3221–3224, 1997.
- [Cirio16] M. Cirio, K. Debnath, N. Lambert, and F. Nori. *Amplified opto-mechanical transduction of virtual radiation pressure*. arXiv:1612.02953, 2016.

- [Ciuti05] C. Ciuti, G. Bastard, and I. Carusotto. *Quantum vacuum properties of the intersubband cavity polariton field*. Phys. Rev. B **72**, 115303, 2005.
- [Ciuti06] C. Ciuti and I. Carusotto. *Input-output theory of cavities in the ultrastrong coupling regime: The case of time-independent cavity parameters*. Phys. Rev. A **74**, 033811, 2006.
- [Clerk10] A. A. Clerk, M. H. Devoret, S. M. Girvin, F. Marquardt, and R. J. Schoelkopf. *Introduction to quantum noise, measurement, and amplification*. Rev. Mod. Phys. **82**, 1155–1208, 2010.
- [Cohadon99] P. F. Cohadon, A. Heidmann, and M. Pinard. *Cooling of a mirror by radiation pressure*. Phys. Rev. Lett. **83**, 3174–3177, 1999.
- [Cohen-Tannoudji77] C. Cohen-Tannoudji, B. Diu, and F. Laloë. *Quantum mechanics*, (Wiley, New York, 1977).
- [Cohen-Tannoudji89] C. Cohen-Tannoudji, J. Dupont-Roc, and G. Grynberg. *Photons and atoms : introduction to quantum electrodynamics*, (Wiley, 1989).
- [Collett87] M. Collett, R. Loudon, and C. Gardiner. *Quantum theory of optical homodyne and heterodyne detection*. Journal of Modern Optics **34**, 6-7, 881–902, 1987.
- [Crespi12] A. Crespi, S. Longhi, and R. Osellame. *Photonic realization of the quantum rabi model*. Phys. Rev. Lett. **108**, 163601, 2012.
- [De Liberato07] S. De Liberato, C. Ciuti, and I. Carusotto. *Quantum vacuum radiation spectra from a semiconductor microcavity with a time-modulated vacuum rabi frequency*. Phys. Rev. Lett. **98**, 103602, 2007.
- [De Liberato09] S. De Liberato. *Cavity quantum electrodynamics and intersubband polaritonics of a two dimensional electron gas*. Theses, Université Paris-Diderot - Paris VII, 2009.
- [De Liberato14] S. De Liberato. *Light-matter decoupling in the deep strong coupling regime: The breakdown of the purcell effect*. Phys. Rev. Lett. **112**, 016401, 2014.
- [DeJesus87] E. X. DeJesus and C. Kaufman. *Routh-hurwitz criterion in the examination of eigenvalues of a system of nonlinear ordinary differential equations*. Phys. Rev. A **35**, 5288–5290, 1987.
- [Deléglise08] S. Deléglise, I. Dotsenko, C. Sayrin, J. Bernu, M. Brune, J.-M. Raimond, and S. Haroche. *Reconstruction of non-classical cavity field states with snapshots of their decoherence*. Nature **455**, 510–514, 2008.
- [Delteil12] A. Delteil, A. Vasanelli, Y. Todorov, C. Feuillet Palma, M. Renaudat St-Jean, G. Beaudoin, I. Sagnes, and C. Sirtori. *Charge-induced coherence between intersubband plasmons in a quantum structure*. Phys. Rev. Lett. **109**, 246808, 2012.

- [Deutsch85] D. Deutsch. *Quantum theory, the church-turing principle and the universal quantum computer*. Proceedings of the Royal Society of London A: Mathematical, Physical and Engineering Sciences **400**, 1818, 97–117, 1985.
- [Devoret13] M. H. Devoret and R. J. Schoelkopf. *Superconducting circuits for quantum information: An outlook*. Science **339**, 6124, 1169–1174, 2013.
- [Dicke54] R. H. Dicke. *Coherence in spontaneous radiation processes*. Phys. Rev. **93**, 99–110, 1954.
- [Dirac27] P. A. M. Dirac. *The quantum theory of the emission and absorption of radiation*. Proceedings of the Royal Society of London A: Mathematical, Physical and Engineering Sciences **114**, 767, 243–265, 1927.
- [Dorsel83] A. Dorsel, J. D. McCullen, P. Meystre, E. Vignes, and H. Walther. *Optical bistability and mirror confinement induced by radiation pressure*. Phys. Rev. Lett. **51**, 1550–1553, 1983.
- [Drexhage74] K. H. Drexhage. Progress in Optics **12**, 163–232, 1974.
- [Drummond80] P. D. Drummond and C. W. Gardiner. *Generalised p-representations in quantum optics*. Journal of Physics A: Mathematical and General **13**, 7, 2353, 1980.
- [Duan00] L.-M. Duan, G. Giedke, J. I. Cirac, and P. Zoller. *Inseparability criterion for continuous variable systems*. Phys. Rev. Lett. **84**, 2722–2725, 2000.
- [Edwards06] T. J. Edwards, D. Walsh, M. B. Spurr, C. F. Rae, M. H. Dunn, and P. G. Browne. *Compact source of continuously and widely-tunable terahertz radiation*. Opt. Express **14**, 4, 1582–1589, 2006.
- [Eichenfield09a] M. Eichenfield, R. Camacho, J. Chan, K. J. Vahala, and O. Painter. *A picogram- and nanometre-scale photonic-crystal optomechanical cavity*. Nature **459**, 550–555, 2009.
- [Eichenfield09b] M. Eichenfield, J. Chan, R. M. Camacho, K. J. Vahala, and O. Painter. *Optomechanical crystals*. Nature **462**, 78–82, 2009.
- [Eichler11] C. Eichler, D. Bozyigit, C. Lang, M. Baur, L. Steffen, J. M. Fink, S. Filipp, and A. Wallraff. *Observation of two-mode squeezing in the microwave frequency domain*. Phys. Rev. Lett. **107**, 113601, 2011.
- [Einstein05] A. Einstein. *Über einen die erzeugung und verwandlung des lichtes betreffenden heuristischen gesichtspunkt*. Annalen der Physik **322**, 6, 132–148, 1905. For a translation in English, see [Arons65].
- [Einstein16] A. Einstein. *Strahlungs-emission und absorption nach der quantentheorie*. Deutsche Physikalische Gesellschaft **18**, 1916. For a translation in English, see [Einstein97].
- [Einstein17] A. Einstein. *Zur quantentheorie der strahlung*. Physikalische Zeitschrift **18**, 1917. For a translation in English, see [Einstein97].

- [Einstein35a] A. Einstein, B. Podolsky, and N. Rosen. *Can quantum-mechanical description of physical reality be considered complete?* Phys. Rev. **47**, 777–780, 1935.
- [Einstein35b] A. Einstein, B. Podolsky, and N. Rosen. *Can quantum-mechanical description of physical reality be considered complete?* Phys. Rev. **47**, 777–780, 1935.
- [Einstein97] A. Einstein. *The Collected Papers of Albert Einstein, Volume 6 (English): The Berlin Years: Writings, 1914-1917*, (Princeton University Press, 1997). (English translation supplement), translated by Alfred Engel.
- [Emary03a] C. Emary and T. Brandes. *Chaos and the quantum phase transition in the dicke model*. Phys. Rev. E **67**, 066203, 2003.
- [Emary03b] C. Emary and T. Brandes. *Quantum chaos triggered by precursors of a quantum phase transition: The dicke model*. Phys. Rev. Lett. **90**, 044101, 2003.
- [Fabre94] C. Fabre, M. Pinard, S. Bourzeix, A. Heidmann, E. Giacobino, and S. Reynaud. *Quantum-noise reduction using a cavity with a movable mirror*. Phys. Rev. A **49**, 1337–1343, 1994.
- [Faist94] J. Faist, F. Capasso, D. L. Sivco, C. Sirtori, A. L. Hutchinson, and A. Y. Cho. *Quantum cascade laser*. Science **264**, 5158, 553–556, 1994.
- [Favero09] I. Favero, S. Stapfner, D. Hunger, P. Paulitschke, J. Reichel, H. Lorenz, E. M. Weig, and K. Karrai. *Fluctuating nanomechanical system in a high finesse optical microcavity*. Opt. Express **17**, 15, 12813–12820, 2009.
- [Fedortchenko16] S. Fedortchenko, S. Huppert, A. Vasanelli, Y. Todorov, C. Sirtori, C. Ciuti, A. Keller, T. Coudreau, and P. Milman. *Output squeezed radiation from dispersive ultrastrong light-matter coupling*. Phys. Rev. A **94**, 013821, 2016.
- [Fedortchenko17] S. Fedortchenko, S. Felicetti, D. Marković, S. Jezouin, A. Keller, T. Coudreau, B. Huard, and P. Milman. *Quantum simulation of ultrastrongly coupled bosonic modes using superconducting circuits*. Phys. Rev. A **95**, 042313, 2017.
- [Felicetti14] S. Felicetti, M. Sanz, L. Lamata, G. Romero, G. Johansson, P. Delsing, and E. Solano. *Dynamical casimir effect entangles artificial atoms*. Phys. Rev. Lett. **113**, 093602, 2014.
- [Felicetti15] S. Felicetti, T. Douce, G. Romero, P. Milman, and E. Solano. *Parity-dependent state engineering and tomography in the ultrastrong coupling regime*. Sci. Rep. **5**, 11818, 2015.
- [Felicetti17a] S. Felicetti, S. Fedortchenko, R. Rossi, S. Ducci, I. Favero, T. Coudreau, and P. Milman. *Quantum communication between remote mechanical resonators*. Phys. Rev. A **95**, 022322, 2017.

- [Felicetti17b] S. Felicetti, E. Rico, C. Sabin, T. Ockenfels, J. Koch, M. Leder, C. Grossert, M. Weitz, and E. Solano. *Quantum rabi model in the brillouin zone with ultracold atoms*. Phys. Rev. A **95**, 013827, 2017.
- [Fermi32] E. Fermi. *Quantum theory of radiation*. Rev. Mod. Phys. **4**, 87–132, 1932.
- [Ferreira89] R. Ferreira and G. Bastard. *Evaluation of some scattering times for electrons in unbiased and biased single- and multiple-quantum-well structures*. Phys. Rev. B **40**, 1074–1086, 1989.
- [Feynman82] R. P. Feynman. *Simulating physics with computers*. International Journal of Theoretical Physics **21**, 6, 467–488, 1982.
- [Filip15] R. Filip and A. A. Rakhubovsky. *Transfer of non-gaussian quantum states of mechanical oscillator to light*. Phys. Rev. A **92**, 053804, 2015.
- [Flurin12] E. Flurin, N. Roch, F. Mallet, M. H. Devoret, and B. Huard. *Generating entangled microwave radiation over two transmission lines*. Phys. Rev. Lett. **109**, 183901, 2012.
- [Flurin14] E. Flurin. *The Josephson Mixer, a Swiss army knife for microwave quantum optics*. Ph.D. thesis, École Normale Supérieure, Paris, 2014.
- [Flurin15] E. Flurin, N. Roch, J. D. Pillet, F. Mallet, and B. Huard. *Superconducting quantum node for entanglement and storage of microwave radiation*. Phys. Rev. Lett. **114**, 090503, 2015.
- [Forn-Díaz10] P. Forn-Díaz, J. Lisenfeld, D. Marcos, J. J. García-Ripoll, E. Solano, C. J. P. M. Harmans, and J. E. Mooij. *Observation of the bloch-siegert shift in a qubit-oscillator system in the ultrastrong coupling regime*. Phys. Rev. Lett. **105**, 237001, 2010.
- [Furusawa98] A. Furusawa, J. L. Sørensen, S. L. Braunstein, C. A. Fuchs, H. J. Kimble, and E. S. Polzik. *Unconditional quantum teleportation*. Science **282**, 5389, 706–709, 1998.
- [Gabrielse85] G. Gabrielse and H. Dehmelt. *Observation of inhibited spontaneous emission*. Phys. Rev. Lett. **55**, 67–70, 1985.
- [Gardiner84] C. Gardiner and C. Savage. *A multimode quantum theory of a degenerate parametric amplifier in a cavity*. Optics Communications **50**, 3, 173 – 178, 1984.
- [Gardiner85] C. W. Gardiner and M. J. Collett. *Input and output in damped quantum systems: Quantum stochastic differential equations and the master equation*. Phys. Rev. A **31**, 3761–3774, 1985.
- [Gardiner04] C. W. Gardiner and P. Zoller. *Quantum noise : a handbook of Markovian and non-Markovian quantum stochastic methods with applications to quantum optics*, (Springer, 2004).

- [Genes08] C. Genes, A. Mari, P. Tombesi, and D. Vitali. *Robust entanglement of a micromechanical resonator with output optical fields*. Phys. Rev. A **78**, 032316, 2008.
- [George16] J. George, T. Chervy, A. Shalabney, E. Devaux, H. Hiura, C. Genet, and T. W. Ebbesen. *Multiple rabi splittings under ultrastrong vibrational coupling*. Phys. Rev. Lett. **117**, 153601, 2016.
- [Georgescu14] I. M. Georgescu, S. Ashhab, and F. Nori. *Quantum simulation*. Rev. Mod. Phys. **86**, 153–185, 2014.
- [Giordmaine65] J. A. Giordmaine and R. C. Miller. *Tunable coherent parametric oscillation in linbo_3 at optical frequencies*. Phys. Rev. Lett. **14**, 973–976, 1965.
- [Giovannetti04] V. Giovannetti, S. Lloyd, and L. Maccone. *Quantum-enhanced measurements: Beating the standard quantum limit*. Science **306**, 5700, 1330–1336, 2004.
- [Glauber63a] R. J. Glauber. *Photon correlations*. Phys. Rev. Lett. **10**, 84–86, 1963.
- [Glauber63b] R. J. Glauber. *The quantum theory of optical coherence*. Phys. Rev. **130**, 2529–2539, 1963.
- [Glauber63c] R. J. Glauber. *Coherent and incoherent states of the radiation field*. Phys. Rev. **131**, 2766–2788, 1963.
- [Gordon54] J. P. Gordon, H. J. Zeiger, and C. H. Townes. *Molecular microwave oscillator and new hyperfine structure in the microwave spectrum of NH_3* . Phys. Rev. **95**, 282–284, 1954.
- [Gordon55] J. P. Gordon, H. J. Zeiger, and C. H. Townes. *The maser—new type of microwave amplifier, frequency standard, and spectrometer*. Phys. Rev. **99**, 1264–1274, 1955.
- [Goy83] P. Goy, J. M. Raimond, M. Gross, and S. Haroche. *Observation of cavity-enhanced single-atom spontaneous emission*. Phys. Rev. Lett. **50**, 1903–1906, 1983.
- [Greiner02] M. Greiner, O. Mandel, T. Esslinger, T. W. Hänsch, and I. Bloch. *Quantum phase transition from a superfluid to a mott insulator in a gas of ultracold atoms*. Nature **415**, 39–44, 2002.
- [Grimsmo13] A. L. Grimsmo and S. Parkins. *Cavity-qed simulation of qubit-oscillator dynamics in the ultrastrong-coupling regime*. Phys. Rev. A **87**, 033814, 2013.
- [Grosshans01] F. Grosshans and P. Grangier. *Quantum cloning and teleportation criteria for continuous quantum variables*. Phys. Rev. A **64**, 010301, 2001.
- [Grote13] H. Grote, K. Danzmann, K. L. Dooley, R. Schnabel, J. Slutsky, and H. Vahlbruch. *First long-term application of squeezed states of light in a gravitational-wave observatory*. Phys. Rev. Lett. **110**, 181101, 2013.

- [Grynberg10] G. Grynberg, A. Aspect, and C. Fabre. *Introduction to Quantum Optics: From the Semi-classical Approach to Quantized Light*, (Cambridge University Press, 2010).
- [Guha16] B. Guha, F. Marsault, F. Cadiz, L. Morgenroth, V. Ulin, V. Berkovitz, A. Lemaître, C. Gomez, A. Amo, S. Combrié, B. Gérard, G. Leo, and I. Favero. *Surface-enhanced gallium arsenide photonic resonator with a quality factor of six million*. arXiv:1605.00477, 2016.
- [Günter09] G. Günter, A. A. Anappara, J. Hees, A. Sell, G. Biasiol, L. Sorba, S. D. Liberato, C. Ciuti, A. Tredicucci, A. Leitenstorfer, and R. Huber. *Sub-cycle switch-on of ultrastrong light-matter interaction*. Nature **458**, 178–181, 2009.
- [Hammerer05] K. Hammerer, M. M. Wolf, E. S. Polzik, and J. I. Cirac. *Quantum benchmark for storage and transmission of coherent states*. Phys. Rev. Lett. **94**, 150503, 2005.
- [Hänsch75] T. Hänsch and A. Schawlow. *Cooling of gases by laser radiation*. Optics Communications **13**, 1, 68–69, 1975.
- [Haroche06] S. Haroche and J.-M. Raimond. *Exploring the quantum : atoms, cavities and photons*, (Oxford University Press, 2006).
- [He13] Q. Y. He and M. D. Reid. *Einstein-podolsky-rosen paradox and quantum steering in pulsed optomechanics*. Phys. Rev. A **88**, 052121, 2013.
- [Heinzen87] D. J. Heinzen, J. J. Childs, J. E. Thomas, and M. S. Feld. *Enhanced and inhibited visible spontaneous emission by atoms in a confocal resonator*. Phys. Rev. Lett. **58**, 1320–1323, 1987.
- [Heisenberg27] W. Heisenberg. *Über den anschaulichen inhalt der quantentheoretischen kinematik und mechanik*. Zeitschrift für Physik **43**, 3, 172–198, 1927. For a translation in English, see[NASA83].
- [Herskind09] P. F. Herskind, A. Dantan, J. P. Marler, M. Albert, and M. Drewsen. *Realization of collective strong coupling with ion coulomb crystals in an optical cavity*. Nature **471**, 494–498, 2009.
- [Hofer11] S. G. Hofer, W. Wieczorek, M. Aspelmeyer, and K. Hammerer. *Quantum entanglement and teleportation in pulsed cavity optomechanics*. Phys. Rev. A **84**, 052327, 2011.
- [Hofer15] S. G. Hofer and K. Hammerer. *Entanglement-enhanced time-continuous quantum control in optomechanics*. Phys. Rev. A **91**, 033822, 2015.
- [Hofheinz08] M. Hofheinz, E. M. Weig, M. Ansmann, R. C. Bialczak, E. Lucero, M. Neeley, A. D. O’Connell, H. Wang, J. M. Martinis, and A. N. Cleland. *Generation of fock states in a superconducting quantum circuit*. Nature **454**, 310–314, 2008.

- [Hopfield58] J. J. Hopfield. *Theory of the contribution of excitons to the complex dielectric constant of crystals*. Phys. Rev. **112**, 1555–1567, 1958.
- [Horodecki96] M. Horodecki, P. Horodecki, and R. Horodecki. *Separability of mixed states: necessary and sufficient conditions*. Physics Letters A **223**, 1, 1–8, 1996.
- [Horodecki97] P. Horodecki. *Separability criterion and inseparable mixed states with positive partial transposition*. Physics Letters A **232**, 5, 333–339, 1997.
- [Hoshina08] H. Hoshina, T. Seta, T. Iwamoto, I. Hosako, C. Otani, and Y. Kasai. *Precise measurement of pressure broadening parameters for water vapor with a terahertz time-domain spectrometer*". Journal of Quantitative Spectroscopy and Radiative Transfer **109**, 12, 2303–2314, 2008.
- [Houck08] A. A. Houck, J. A. Schreier, B. R. Johnson, J. M. Chow, J. Koch, J. M. Gambetta, D. I. Schuster, L. Frunzio, M. H. Devoret, S. M. Girvin, and R. J. Schoelkopf. *Controlling the spontaneous emission of a superconducting transmon qubit*. Phys. Rev. Lett. **101**, 080502, 2008.
- [Houck12] A. A. Houck, H. E. Türeci, and J. Koch. *On-chip quantum simulation with superconducting circuits*. Nature Physics **8**, 292–299, 2012.
- [Husimi40] K. Husimi. *Some formal properties of the density matrix*. Proceedings of the Physico-Mathematical Society of Japan. 3rd Series **22**, 4, 264–314, 1940.
- [Jacobs94] K. Jacobs, P. Tombesi, M. J. Collett, and D. F. Walls. *Quantum-nondemolition measurement of photon number using radiation pressure*. Phys. Rev. A **49**, 1961–1966, 1994.
- [Jaklevic64] R. C. Jaklevic, J. Lambe, A. H. Silver, and J. E. Mercereau. *Quantum interference effects in josephson tunneling*. Phys. Rev. Lett. **12**, 159–160, 1964.
- [Jaynes63] E. T. Jaynes and F. W. Cummings. *Comparison of quantum and semiclassical radiation theories with application to the beam maser*. Proceedings of the IEEE **51**, 1, 89–109, 1963.
- [Jiang09] X. Jiang, Q. Lin, J. Rosenberg, K. Vahala, and O. Painter. *High-q double-disk microcavities for cavity optomechanics*. Opt. Express **17**, 23, 20911–20919, 2009.
- [Johansson09] J. R. Johansson, G. Johansson, C. M. Wilson, and F. Nori. *Dynamical casimir effect in a superconducting coplanar waveguide*. Phys. Rev. Lett. **103**, 147003, 2009.
- [Josephson62] B. Josephson. *Possible new effects in superconductive tunnelling*. Physics Letters **1**, 7, 251–253, 1962.
- [Josse04] V. Josse, A. Dantan, A. Bramati, M. Pinard, and E. Giacobino. *Continuous variable entanglement using cold atoms*. Phys. Rev. Lett. **92**, 123601, 2004.

- [Kaluzny83] Y. Kaluzny, P. Goy, M. Gross, J. M. Raimond, and S. Haroche. *Observation of self-induced rabi oscillations in two-level atoms excited inside a resonant cavity: The ringing regime of superradiance*. Phys. Rev. Lett. **51**, 1175–1178, 1983.
- [Kardar99] M. Kardar and R. Golestanian. *The "friction" of vacuum, and other fluctuation-induced forces*. Rev. Mod. Phys. **71**, 1233–1245, 1999.
- [Kastler50] A. Kastler. *Quelques suggestions concernant la production optique et la détection optique d'une inégalité de population des niveaux de quantification spatiale des atomes. Application à l'expérience de Stern et Gerlach et à la résonance magnétique*. J. Phys. Radium **11**, 6, 255–265, 1950.
- [Kawase01] K. Kawase, J. ichi Shikata, H. Minamide, K. Imai, and H. Ito. *Arrayed silicon prism coupler for a terahertz-wave parametric oscillator*. Appl. Opt. **40**, 9, 1423–1426, 2001.
- [Kéna-Cohen13] S. Kéna-Cohen, S. A. Maier, and D. D. C. Bradley. *Ultrastrongly coupled exciton-polaritons in metal-clad organic semiconductor microcavities*. Advanced Optical Materials **1**, 11, 827–833, 2013.
- [Kennard27] E. H. Kennard. *Zur quantenmechanik einfacher bewegungstypen*. Zeitschrift für Physik **44**, 4, 326–352, 1927. For a summary in english, see [Nieto97].
- [Kimble77] H. J. Kimble, M. Dagenais, and L. Mandel. *Photon antibunching in resonance fluorescence*. Phys. Rev. Lett. **39**, 691–695, 1977.
- [Kirchmair13] G. Kirchmair, B. Vlastakis, Z. Leghtas, S. E. Nigg, H. Paik, E. Ginossar, M. Mirrahimi, L. Frunzio, S. M. Girvin, and R. J. Schoelkopf. *Observation of quantum state collapse and revival due to the single-photon kerr effect*. Nature **495**, 205–209, 2013.
- [Kleckner06] D. Kleckner and D. Bouwmeester. *Sub-kelvin optical cooling of a micromechanical resonator*. Nature **444**, 75–78, 2006.
- [Kleiner07] R. Kleiner. *Filling the terahertz gap*. Science **318**, 5854, 1254–1255, 2007.
- [Kolář16] M. Kolář, A. Ryabov, and R. Filip. *Extracting work from quantum states of radiation*. Phys. Rev. A **93**, 063822, 2016.
- [Krause15] A. G. Krause, J. T. Hill, M. Ludwig, A. H. Safavi-Naeini, J. Chan, F. Marquardt, and O. Painter. *Nonlinear radiation pressure dynamics in an optomechanical crystal*. Phys. Rev. Lett. **115**, 233601, 2015.
- [Ku15] H. S. Ku, W. F. Kindel, F. Mallet, S. Glancy, K. D. Irwin, G. C. Hilton, L. R. Vale, and K. W. Lehnert. *Generating and verifying entangled itinerant microwave fields with efficient and independent measurements*. Phys. Rev. A **91**, 042305, 2015.

- [Kyaw15] T. H. Kyaw, S. Felicetti, G. Romero, E. Solano, and L.-C. Kwek. *Scalable quantum memory in the ultrastrong coupling regime*. *Sci. Rep.* **5**, 8621, 2015.
- [Ladd10] T. D. Ladd, F. Jelezko, R. Laflamme, Y. Nakamura, C. Monroe, and J. L. O’Brien. *Quantum computers*. *Nature* **464**, 45–53, 2010.
- [Lamata16] L. Lamata. *Digital-analog quantum simulation of generalized dicke models with superconducting circuits*. *Scientific Reports* **7**, 43768, 2016.
- [Landau76] L. D. Landau and E. M. Lifshitz. *Mechanics. Vol. 1 (3rd ed.)*, (Butterworth-Heinemann, 1976).
- [Langford16] N. K. Langford, R. Sagastizabal, M. Kounalakis, C. Dickel, A. Bruno, F. Luthi, D. J. Thoen, A. Endo, and L. DiCarlo. *Experimentally simulating the dynamics of quantum light and matter at ultrastrong coupling*. arXiv:1610.10065, 2016.
- [Laurat05] J. Laurat, G. Keller, J. A. Oliveira-Huguenin, C. Fabre, T. Coudreau, A. Serafini, G. Adesso, and F. Illuminati. *Entanglement of two-mode gaussian states: characterization and experimental production and manipulation*. *Journal of Optics B: Quantum and Semiclassical Optics* **7**, 12, S577, 2005.
- [Lebedew01] P. Lebedew. *Untersuchungen über die druckkräfte des lichtes*. *Annalen der Physik* **311**, 11, 433–458, 1901.
- [Leibfried02] D. Leibfried, B. DeMarco, V. Meyer, M. Rowe, A. Ben-Kish, J. Britton, W. M. Itano, B. Jelenković, C. Langer, T. Rosenband, and D. J. Wineland. *Trapped-ion quantum simulator: Experimental application to nonlinear interferometers*. *Phys. Rev. Lett.* **89**, 247901, 2002.
- [Liao15] J.-Q. Liao, C. K. Law, L.-M. Kuang, and F. Nori. *Enhancement of mechanical effects of single photons in modulated two-mode optomechanics*. *Phys. Rev. A* **92**, 013822, 2015.
- [Lloyd96] S. Lloyd. *Universal quantum simulators*. *Science* **273**, 5278, 1073–1078, 1996.
- [Lolli15] J. Lolli, A. Baksic, D. Nagy, V. E. Manucharyan, and C. Ciuti. *Ancillary qubit spectroscopy of vacua in cavity and circuit quantum electrodynamics*. *Phys. Rev. Lett.* **114**, 183601, 2015.
- [Longhi11] S. Longhi. *Jaynes–cummings photonic superlattices*. *Opt. Lett.* **36**, 17, 3407–3409, 2011.
- [Lu71] E. Y. C. Lu. *New coherent states of the electromagnetic field*. *Nuovo Cimento Lett.* **2**, 24, 1241–1244, 1971.
- [Ludwig08] M. Ludwig, B. Kubala, and F. Marquardt. *The optomechanical instability in the quantum regime*. *New Journal of Physics* **10**, 9, 095013, 2008.
- [Lvovsky01] A. I. Lvovsky, H. Hansen, T. Aichele, O. Benson, J. Mlynek, and S. Schiller. *Quantum state reconstruction of the single-photon fock state*. *Phys. Rev. Lett.* **87**, 050402, 2001.

- [Lvovsky09] A. I. Lvovsky and M. G. Raymer. *Continuous-variable optical quantum-state tomography*. Rev. Mod. Phys. **81**, 299–332, 2009.
- [Ma07] R. Ma, A. Schliesser, P. Del’Haye, A. Dabirian, G. Anetsberger, and T. J. Kippenberg. *Radiation-pressure-driven vibrational modes in ultrahigh- q silica microspheres*. Opt. Lett. **32**, 15, 2200–2202, 2007.
- [Maiman60] T. H. Maiman. *Stimulated optical radiation in ruby*. Nature **187**, 493–494, 1960.
- [Mallet11] F. Mallet, M. A. Castellanos-Beltran, H. S. Ku, S. Glancy, E. Knill, K. D. Irwin, G. C. Hilton, L. R. Vale, and K. W. Lehnert. *Quantum state tomography of an itinerant squeezed microwave field*. Phys. Rev. Lett. **106**, 220502, 2011.
- [Mancini94] S. Mancini and P. Tombesi. *Quantum noise reduction by radiation pressure*. Phys. Rev. A **49**, 4055–4065, 1994.
- [Mancini97] S. Mancini, V. I. Man’ko, and P. Tombesi. *Ponderomotive control of quantum macroscopic coherence*. Phys. Rev. A **55**, 3042–3050, 1997.
- [Mancini98] S. Mancini, D. Vitali, and P. Tombesi. *Optomechanical cooling of a macroscopic oscillator by homodyne feedback*. Phys. Rev. Lett. **80**, 688–691, 1998.
- [Mancini03] S. Mancini, D. Vitali, and P. Tombesi. *Scheme for teleportation of quantum states onto a mechanical resonator*. Phys. Rev. Lett. **90**, 137901, 2003.
- [Mandel95] L. Mandel and E. Wolf. *Optical coherence and quantum optics*, (Cambridge University Press, 1995).
- [Marquardt06] F. Marquardt, J. G. E. Harris, and S. M. Girvin. *Dynamical multistability induced by radiation pressure in high-finesse micromechanical optical cavities*. Phys. Rev. Lett. **96**, 103901, 2006.
- [Martinis85] J. M. Martinis, M. H. Devoret, and J. Clarke. *Energy-level quantization in the zero-voltage state of a current-biased josephson junction*. Phys. Rev. Lett. **55**, 1543–1546, 1985.
- [Massel11] F. Massel, T. T. Heikkilä, J.-M. Pirkkalainen, S. U. Cho, H. Saloniemi, P. J. Hakonen, and M. A. Sillanpää. *Microwave amplification with nanomechanical resonators*. Nature **480**, 351–354, 2011.
- [McNeil83] K. J. McNeil and C. W. Gardiner. *Quantum statistics of parametric oscillation*. Phys. Rev. A **28**, 1560–1566, 1983.
- [Meschede85] D. Meschede, H. Walther, and G. Müller. *One-atom maser*. Phys. Rev. Lett. **54**, 551–554, 1985.
- [Mezzacapo14] A. Mezzacapo, U. L. Heras, J. S. Pedernales, L. DiCarlo, E. Solano, and L. Lamata. *Digital quantum rabi and dicke models in superconducting circuits*. Scientific Reports **4**, 7482, 2014.

- [Milburn81] G. Milburn and D. Walls. *Production of squeezed states in a degenerate parametric amplifier*. Optics Communications **39**, 6, 401–404, 1981.
- [Molter09] D. Molter, M. Theuer, and R. Beigang. *Nanosecond terahertz optical parametric oscillator with a novel quasi phase matching scheme in lithium niobate*. Opt. Express **17**, 8, 6623–6628, 2009.
- [Moore70] G. T. Moore. *Quantum theory of the electromagnetic field in a variable-length one-dimensional cavity*. Journal of Mathematical Physics **11**, 9, 2679–2691, 1970.
- [Moore16] D. W. Moore, T. Tufarelli, M. Paternostro, and A. Ferraro. *Quantum state reconstruction of an oscillator network in an optomechanical setting*. Phys. Rev. A **94**, 053811, 2016.
- [Müller16] C. R. Müller, C. Peuntinger, T. Dirmeier, I. Khan, U. Vogl, C. Marquardt, G. Leuchs, L. L. Sánchez-Soto, Y. S. Teo, Z. Hradil, and J. Řeháček. *Evading vacuum noise: Wigner projections or husimi samples?* Phys. Rev. Lett. **117**, 070801, 2016.
- [Murch08] K. W. Murch, K. L. Moore, S. Gupta, and D. M. Stamper-Kurn. *Observation of quantum-measurement backaction with an ultracold atomic gas*. Nature Physics **4**, 561–564, 2008.
- [NASA83] NASA. *The actual content of quantum theoretical kinematics and mechanics*. NASA Technical Reports Server, 1983.
- [Nataf10] P. Nataf and C. Ciuti. *No-go theorem for superradiant quantum phase transitions in cavity qed and counter-example in circuit qed*. Nature Comm. **1**, 1–6, 2010.
- [Negele98] J. W. Negele and H. Orland. *Quantum Many-particle Systems*, (Perseus Books, 1998).
- [Neuhauser78] W. Neuhauser, M. Hohenstatt, P. Toschek, and H. Dehmelt. *Optical-sideband cooling of visible atom cloud confined in parabolic well*. Phys. Rev. Lett. **41**, 233–236, 1978.
- [Nichols01] E. F. Nichols and G. F. Hull. *A preliminary communication on the pressure of heat and light radiation*. Phys. Rev. (Series I) **13**, 307–320, 1901.
- [Nielsen00] M. A. Nielsen and I. L. Chuang. *Quantum computation and quantum information*, (Cambridge University Press, New York, 2000).
- [Niemczyk10] T. Niemczyk, F. Deppe, H. Huebl, E. P. Menzel, F. Hocke, M. J. Schwarz, J. J. Garcia-Ripoll, D. Zueco, T. Hummer, E. Solano, A. Marx, and R. Gross. *Circuit quantum electrodynamics in the ultrastrong-coupling regime*. Nature Phys. **6**, 10, 772–776, 2010.
- [Nieto97] M. M. Nieto. *The discovery of squeezed states in 1927*. In *5th International Conference on Squeezed States and Uncertainty Relations (ICSSUR 97) Budapest, Hungary, May 27-31, 1997* (1997). Preprint: quant-ph/9708012.

- [Nogues99] G. Nogues, A. Rauschenbeutel, S. Osnaghi, M. Brune, J. M. Raimond, and S. Haroche. *Seeing a single photon without destroying it*. Nature **400**, 239–242, 1999.
- [Nogues00] G. Nogues, A. Rauschenbeutel, S. Osnaghi, P. Bertet, M. Brune, J. M. Raimond, S. Haroche, L. G. Lutterbach, and L. Davidovich. *Measurement of a negative value for the wigner function of radiation*. Phys. Rev. A **62**, 054101, 2000.
- [Ou92] Z. Y. Ou, S. F. Pereira, H. J. Kimble, and K. C. Peng. *Realization of the einstein-podolsky-rosen paradox for continuous variables*. Phys. Rev. Lett. **68**, 3663–3666, 1992.
- [Ourjoumtsev07] A. Ourjoumtsev, H. Jeong, R. Tualle-Brouri, and P. Grangier. *Generation of optical 'Schrödinger cats' from photon number states*. Nature **448**, 784–786, 2007.
- [Palomaki13a] T. A. Palomaki, J. W. Harlow, J. D. Teufel, R. W. Simmonds, and K. W. Lehnert. *Coherent state transfer between itinerant microwave fields and a mechanical oscillator*. Nature **495**, 210–214, 2013.
- [Palomaki13b] T. A. Palomaki, J. D. Teufel, R. W. Simmonds, and K. W. Lehnert. *Entangling mechanical motion with microwave fields*. Science **342**, 6159, 710–713, 2013.
- [Park09] Y.-S. Park and H. Wang. *Resolved-sideband and cryogenic cooling of an optomechanical resonator*. Nature Physics **5**, 489–493, 2009.
- [Pauli27] W. Pauli. *Zur quantenmechanik des magnetischen elektrons*. Zeitschrift für Physik **43**, 601–623, 1927.
- [Pedernales15] J. S. Pedernales, I. Lizuain, S. Felicetti, G. Romero, L. Lamata, and E. Solano. *Quantum rabi model with trapped ions*. Scientific Reports **5**, 15472, 2015.
- [Pegolotti14a] G. Pegolotti. *Quantum engineering of collective states in semiconductor nanostructures*. Theses, Université Paris Diderot-Paris VII, 2014.
- [Pegolotti14b] G. Pegolotti, A. Vasanelli, Y. Todorov, and C. Sirtori. *Quantum model of coupled intersubband plasmons*. Phys. Rev. B **90**, 035305, 2014.
- [Peres96] A. Peres. *Separability criterion for density matrices*. Phys. Rev. Lett. **77**, 1413–1415, 1996.
- [Peropadre13a] B. Peropadre, D. Zueco, D. Porras, and J. J. García-Ripoll. *Nonequilibrium and nonperturbative dynamics of ultrastrong coupling in open lines*. Phys. Rev. Lett. **111**, 243602, 2013.
- [Peropadre13b] B. Peropadre, D. Zueco, F. Wulchner, F. Deppe, A. Marx, R. Gross, and J. J. García-Ripoll. *Tunable coupling engineering between superconducting resonators: From sidebands to effective gauge fields*. Phys. Rev. B **87**, 134504, 2013.

- [Peter05] E. Peter, P. Senellart, D. Martrou, A. Lemaître, J. Hours, J. M. Gérard, and J. Bloch. *Exciton-photon strong-coupling regime for a single quantum dot embedded in a microcavity*. Phys. Rev. Lett. **95**, 067401, 2005.
- [Pillet15] J.-D. Pillet, E. Flurin, F. Mallet, and B. Huard. *A compact design for the josephson mixer: The lumped element circuit*. Applied Physics Letters **106**, 22, 222603, 2015.
- [Pinard95] M. Pinard, C. Fabre, and A. Heidmann. *Quantum-nondemolition measurement of light by a piezoelectric crystal*. Phys. Rev. A **51**, 2443–2449, 1995.
- [Pirandola06] S. Pirandola, D. Vitali, P. Tombesi, and S. Lloyd. *Macroscopic entanglement by entanglement swapping*. Phys. Rev. Lett. **97**, 150403, 2006.
- [Pirandola15] S. Pirandola, J. Eisert, C. Weedbrook, A. Furusawa, and S. L. Braunstein. *Advances in quantum teleportation*. Nature Photonics **9**, 641–652, 2015.
- [Pirandola16] S. Pirandola and S. L. Braunstein. *Physics: Unite to build a quantum internet*. Nature **532**, 169–171, 2016.
- [Pirkkalainen15] J.-M. Pirkkalainen, E. Damskägg, M. Brandt, F. Massel, and M. A. Sillanpää. *Squeezing of quantum noise of motion in a micromechanical resonator*. Phys. Rev. Lett. **115**, 243601, 2015.
- [Planck01] M. Planck. *Ueber das gesetz der energieverteilung im normalspectrum*. Annalen der Physik **309**, 3, 553–563, 1901. For a translation in English, see [Planck72].
- [Planck72] M. Planck and H. Kangro. *Planck’s original papers in quantum physics: German and English edition*. Classic papers in physics, (Taylor and Francis, 1972).
- [Poggio07] M. Poggio, C. L. Degen, H. J. Mamin, and D. Rugar. *Feedback cooling of a cantilever’s fundamental mode below 5 mk*. Phys. Rev. Lett. **99**, 017201, 2007.
- [Porer12] M. Porer, J.-M. Ménard, A. Leitenstorfer, R. Huber, R. Degl’Innocenti, S. Zanutto, G. Biasiol, L. Sorba, and A. Tredicucci. *Nonadiabatic switching of a photonic band structure: Ultrastrong light-matter coupling and slow-down of light*. Phys. Rev. B **85**, 081302, 2012.
- [Purcell46] E. M. Purcell, H. C. Torrey, and R. V. Pound. *Resonance absorption by nuclear magnetic moments in a solid*. Phys. Rev. **69**, 37–38, 1946.
- [Purdy13] T. P. Purdy, P.-L. Yu, R. W. Peterson, N. S. Kampel, and C. A. Regal. *Strong optomechanical squeezing of light*. Phys. Rev. X **3**, 031012, 2013.
- [Rabi36] I. I. Rabi. *On the process of space quantization*. Phys. Rev. **49**, 324–328, 1936.

- [Raimond01] J. M. Raimond, M. Brune, and S. Haroche. *Manipulating quantum entanglement with atoms and photons in a cavity*. Rev. Mod. Phys. **73**, 565–582, 2001.
- [Raizen89] M. G. Raizen, R. J. Thompson, R. J. Brecha, H. J. Kimble, and H. J. Carmichael. *Normal-mode splitting and linewidth averaging for two-state atoms in an optical cavity*. Phys. Rev. Lett. **63**, 240–243, 1989.
- [Rakić13] A. D. Rakić, T. Taimre, K. Bertling, Y. L. Lim, P. Dean, D. Indjin, Z. Ikonić, P. Harrison, A. Valavanis, S. P. Khanna, M. Lachab, S. J. Wilson, E. H. Linfield, and A. G. Davies. *Swept-frequency feedback interferometry using terahertz frequency qcls: a method for imaging and materials analysis*. Opt. Express **21**, 19, 22194–22205, 2013.
- [Rapaport00] R. Rapaport, R. Harel, E. Cohen, A. Ron, E. Linder, and L. N. Pfeiffer. *Negatively charged quantum well polaritons in a GaAs/AlAs microcavity: An analog of atoms in a cavity*. Phys. Rev. Lett. **84**, 1607–1610, 2000.
- [Regal08] C. A. Regal, J. D. Teufel, and K. W. Lehnert. *Measuring nanomechanical motion with a microwave cavity interferometer*. Nature Physics **4**, 555–560, 2008.
- [Reid88] M. D. Reid and P. D. Drummond. *Quantum correlations of phase in nondegenerate parametric oscillation*. Phys. Rev. Lett. **60**, 2731–2733, 1988.
- [Reid89] M. D. Reid. *Demonstration of the einstein-podolsky-rosen paradox using nondegenerate parametric amplification*. Phys. Rev. A **40**, 913–923, 1989.
- [Reithmaier04] J. P. Reithmaier, G. Sęk, A. Löffler, C. Hofmann, S. Kuhn, S. Reitzenstein, L. V. Keldysh, V. D. Kulakovskii, T. L. Reinecke, and A. Forchel. *Strong coupling in a single quantum dot-semiconductor microcavity system*. Nature **432**, 197–200, 2004.
- [Restrepo14a] J. Restrepo, C. Ciuti, and I. Favero. *Single-polariton optomechanics*. Phys. Rev. Lett. **112**, 013601, 2014.
- [Restrepo14b] J. S. Restrepo. *Theory of quantum optomechanics with unconventional nonlinear coupling schemes*. Theses, Université Paris 7, Sorbonne Paris Cité, 2014.
- [Reynaud87] S. Reynaud, C. Fabre, and E. Giacobino. *Quantum fluctuations in a two-mode parametric oscillator*. J. Opt. Soc. Am. B **4**, 10, 1520–1524, 1987.
- [Ridolfo12] A. Ridolfo, M. Leib, S. Savasta, and M. J. Hartmann. *Photon blockade in the ultrastrong coupling regime*. Phys. Rev. Lett. **109**, 193602, 2012.
- [Riedinger16] R. Riedinger, S. Hong, R. A. Norte, J. A. Slater, J. Shang, A. G. Krause, V. Anant, M. Aspelmeyer, and S. Gröblacher. *Non-classical correlations between single photons and phonons from a mechanical oscillator*. Nature **530**, 313–316, 2016.

- [Riek15] C. Riek, D. V. Seletskiy, A. S. Moskalenko, J. F. Schmidt, P. Krauspe, S. Eckart, S. Eggert, G. Burkard, and A. Leitenstorfer. *Direct sampling of electric-field vacuum fluctuations*. Science **350**, 6259, 420–423, 2015.
- [Roch12] N. Roch, E. Flurin, F. Nguyen, P. Morfin, P. Campagne-Ibarcq, M. H. Devoret, and B. Huard. *Widely tunable, nondegenerate three-wave mixing microwave device operating near the quantum limit*. Phys. Rev. Lett. **108**, 147701, 2012.
- [Rossatto16] D. Z. Rossatto, S. Felicetti, H. Eneriz, E. Rico, M. Sanz, and E. Solano. *Entangling polaritons via dynamical casimir effect in circuit quantum electrodynamics*. Phys. Rev. B **93**, 094514, 2016.
- [Safavi-Naeini13] A. H. Safavi-Naeini, S. Gröblacher, J. T. Hill, J. Chan, M. Aspelmeyer, and O. Painter. *Squeezed light from a silicon micromechanical resonator*. Nature **500**, 185–189, 2013.
- [Schawlow58] A. L. Schawlow and C. H. Townes. *Infrared and optical masers*. Phys. Rev. **112**, 1940–1949, 1958.
- [Schoelkopf08] R. J. Schoelkopf and S. M. Girvin. *Wiring up quantum systems*. Nature **451**, 664–669, 2008.
- [Schrödinger35] E. Schrödinger. *Die gegenwärtige situation in der quantenmechanik*. Naturwissenschaften **23**, 48, 807–812, 1935. For a translation in English, see [Trimmer80].
- [Schwartz11] T. Schwartz, J. A. Hutchison, C. Genet, and T. W. Ebbesen. *Reversible switching of ultrastrong light-molecule coupling*. Phys. Rev. Lett. **106**, 196405, 2011.
- [Scully97] M. O. Scully and M. S. Zubairy. *Quantum Optics*, (Cambridge University Press, 1997).
- [Serafini04] A. Serafini, F. Illuminati, and S. D. Siena. *Symplectic invariants, entropic measures and correlations of gaussian states*. Journal of Physics B: Atomic, Molecular and Optical Physics **37**, 2, L21, 2004.
- [Shelby86] R. M. Shelby, M. D. Levenson, S. H. Perlmuter, R. G. DeVoe, and D. F. Walls. *Broad-band parametric deamplification of quantum noise in an optical fiber*. Phys. Rev. Lett. **57**, 691–694, 1986.
- [Short83] R. Short and L. Mandel. *Observation of sub-poissonian photon statistics*. Phys. Rev. Lett. **51**, 384–387, 1983.
- [Silberhorn01] C. Silberhorn, P. K. Lam, O. Weiß, F. König, N. Korolkova, and G. Leuchs. *Generation of continuous variable einstein-podolsky-rosen entanglement via the kerr nonlinearity in an optical fiber*. Phys. Rev. Lett. **86**, 4267–4270, 2001.

- [Simon00] R. Simon. *Peres-horodecki separability criterion for continuous variable systems*. Phys. Rev. Lett. **84**, 2726–2729, 2000.
- [Sirtori02] C. Sirtori. *Applied physics: Bridge for the terahertz gap*. Nature **417**, 132–133, 2002.
- [Sliwa15] K. M. Sliwa, M. Hatridge, A. Narla, S. Shankar, L. Frunzio, R. J. Schoelkopf, and M. H. Devoret. *Reconfigurable josephson circulator/directional amplifier*. Phys. Rev. X **5**, 041020, 2015.
- [Slusher85] R. E. Slusher, L. W. Hollberg, B. Yurke, J. C. Mertz, and J. F. Valley. *Observation of squeezed states generated by four-wave mixing in an optical cavity*. Phys. Rev. Lett. **55**, 2409–2412, 1985.
- [Smithey93] D. T. Smithey, M. Beck, M. G. Raymer, and A. Faridani. *Measurement of the wigner distribution and the density matrix of a light mode using optical homodyne tomography: Application to squeezed states and the vacuum*. Phys. Rev. Lett. **70**, 1244–1247, 1993.
- [Stannigel10] K. Stannigel, P. Rabl, A. S. Sørensen, P. Zoller, and M. D. Lukin. *Optomechanical transducers for long-distance quantum communication*. Phys. Rev. Lett. **105**, 220501, 2010.
- [Stassi15] R. Stassi, S. De Liberato, L. Garziano, B. Spagnolo, and S. Savasta. *Quantum control and long-range quantum correlations in dynamical casimir arrays*. Phys. Rev. A **92**, 013830, 2015.
- [Stassi16] R. Stassi, S. Savasta, L. Garziano, B. Spagnolo, and F. Nori. *Output field-quadrature measurements and squeezing in ultrastrong cavity-qed*. New Journal of Physics **18**, 12, 123005, 2016.
- [Stenholm92] S. Stenholm. *Simultaneous measurement of conjugate variables*. Annals of Physics **218**, 2, 233–254, 1992.
- [Stoler70] D. Stoler. *Equivalence Classes of Minimum Uncertainty Packets*. Phys. Rev. D **1**, 3217–3219, 1970.
- [Stoler71] D. Stoler. *Equivalence Classes of Minimum-Uncertainty Packets. II*. Phys. Rev. D **4**, 1925–1926, 1971.
- [Stoler74] D. Stoler. *Photon antibunching and possible ways to observe it*. Phys. Rev. Lett. **33**, 1397–1400, 1974.
- [Sudarshan63] E. C. G. Sudarshan. *Equivalence of semiclassical and quantum mechanical descriptions of statistical light beams*. Phys. Rev. Lett. **10**, 277–279, 1963.
- [Teich85] M. C. Teich and B. E. A. Saleh. *Observation of sub-poisson franck-hertz light at 253.7 nm*. J. Opt. Soc. Am. B **2**, 2, 275–282, 1985.
- [Teufel11] J. D. Teufel, D. Li, M. S. Allman, K. Cicak, A. J. Sirois, J. D. Whittaker, and R. W. Simmonds. *Circuit cavity electromechanics in the strong-coupling regime*. Nature **471**, 204–208, 2011.

- [Thompson08a] J. D. Thompson, B. M. Zwickl, A. M. Jayich, F. Marquardt, S. M. Girvin, and J. G. E. Harris. *Strong dispersive coupling of a high-finesse cavity to a micromechanical membrane*. *Nature* **452**, 72–75, 2008.
- [Thompson08b] J. D. Thompson, B. M. Zwickl, A. M. Jayich, F. Marquardt, S. M. Girvin, and J. G. E. Harris. *Strong dispersive coupling of a high-finesse cavity to a micromechanical membrane*. *Nature* **452**, 72–75, 2008.
- [Todorov09] Y. Todorov, A. M. Andrews, I. Sagnes, R. Colombelli, P. Klang, G. Strasser, and C. Sirtori. *Strong light-matter coupling in subwavelength metal-dielectric microcavities at terahertz frequencies*. *Phys. Rev. Lett.* **102**, 186402, 2009.
- [Todorov10] Y. Todorov, A. M. Andrews, R. Colombelli, S. De Liberato, C. Ciuti, P. Klang, G. Strasser, and C. Sirtori. *Ultrastrong light-matter coupling regime with polariton dots*. *Phys. Rev. Lett.* **105**, 196402, 2010.
- [Todorov12a] Y. Todorov and C. Sirtori. *Intersubband polaritons in the electrical dipole gauge*. *Phys. Rev. B* **85**, 045304, 2012.
- [Todorov12b] Y. Todorov, L. Toso, A. Delteil, A. Vasanelli, C. Sirtori, A. M. Andrews, and G. Strasser. *Polaritonic spectroscopy of intersubband transitions*. *Phys. Rev. B* **86**, 125314, 2012.
- [Tomes09] M. Tomes and T. Carmon. *Photonic Micro-Electromechanical Systems Vibrating at X-band (11-GHz) Rates*. *Phys. Rev. Lett.* **102**, 113601, 2009.
- [Trimmer80] J. D. Trimmer. *The present situation in quantum mechanics: a translation of Schrödinger's "cat paradox paper"*. *Proceedings of the American Philosophical Society* **124**, 323–338, 1980. Reprinted in [Wheeler83].
- [Vanner11] M. R. Vanner, I. Pikovski, G. D. Cole, M. S. Kim, Č. Brukner, K. Hammerer, G. J. Milburn, and M. Aspelmeyer. *Pulsed quantum optomechanics*. *Proceedings of the National Academy of Sciences* **108**, 39, 16182–16187, 2011.
- [Varcoe00] B. T. H. Varcoe, S. Brattke, M. Weidinger, and H. Walther. *Preparing pure photon number states of the radiation field*. *Nature* **403**, 743–746, 2000.
- [Vivoli16] V. C. Vivoli, T. Barnea, C. Galland, and N. Sangouard. *Proposal for an optomechanical bell test*. *Phys. Rev. Lett.* **116**, 070405, 2016.
- [Vogel89] K. Vogel and H. Risken. *Determination of quasiprobability distributions in terms of probability distributions for the rotated quadrature phase*. *Phys. Rev. A* **40**, 2847–2849, 1989.
- [Wallraff04] A. Wallraff, D. I. Schuster, A. Blais, L. Frunzio, R.-S. Huang, J. Majer, S. Kumar, S. M. Girvin, and R. J. Schoelkopf. *Strong coupling of a single photon to a superconducting qubit using circuit quantum electrodynamics*. *Nature* **431**, 162–167, 2004.
- [Walls08] D. F. Walls and G. J. Milburn. *Quantum Optics*, (Springer, 2008).

- [Wang65] C. C. Wang and G. W. Racette. *Measurement of parametric gain accompanying optical difference frequency generation*. Applied Physics Letters **6**, 8, 169–171, 1965.
- [Wang16] C. Wang, Y. Y. Gao, P. Reinhold, R. W. Heeres, N. Ofek, K. Chou, C. Axline, M. Reagor, J. Blumoff, K. M. Sliwa, L. Frunzio, S. M. Girvin, L. Jiang, M. Mirrahimi, M. H. Devoret, and R. J. Schoelkopf. *A Schrödinger cat living in two boxes*. Science **352**, 6289, 1087–1091, 2016.
- [Weisbuch92] C. Weisbuch, M. Nishioka, A. Ishikawa, and Y. Arakawa. *Observation of the coupled exciton-photon mode splitting in a semiconductor quantum microcavity*. Phys. Rev. Lett. **69**, 3314–3317, 1992.
- [Wheeler83] J. A. Wheeler and W. H. Zurek. *Quantum theory and measurement*, (Princeton University Press, 1983).
- [Wiederhecker09] G. S. Wiederhecker, L. Chen, A. Gondarenko, and M. Lipson. *Controlling photonic structures using optical forces*. Nature **462**, 633–636, 2009.
- [Wigner32] E. Wigner. *On the quantum correction for thermodynamic equilibrium*. Phys. Rev. **40**, 749–759, 1932.
- [Wilson11] C. M. Wilson, G. Johansson, A. Pourkabirian, M. Simoen, J. R. Johansson, T. Duty, F. Nori, and P. Delsing. *Observation of the dynamical casimir effect in a superconducting circuit*. Nature **479**, 376–379, 2011.
- [Wineland75] D. Wineland and H. Dehmelt. *Proposed $10^{14}\delta\nu/\nu$ laser fluorescence spectroscopy on Tl^+ mono-ion oscillator III (sideband cooling)*. Bull. Am. Phys. Soc. **20**, 637, 1975.
- [Wineland78] D. J. Wineland, R. E. Drullinger, and F. L. Walls. *Radiation-pressure cooling of bound resonant absorbers*. Phys. Rev. Lett. **40**, 1639–1642, 1978.
- [Wollman15] E. E. Wollman, C. U. Lei, A. J. Weinstein, J. Suh, A. Kronwald, F. Marquardt, A. A. Clerk, and K. C. Schwab. *Quantum squeezing of motion in a mechanical resonator*. Science **349**, 6251, 952–955, 2015.
- [Wu86] L.-A. Wu, H. J. Kimble, J. L. Hall, and H. Wu. *Generation of squeezed states by parametric down conversion*. Phys. Rev. Lett. **57**, 2520–2523, 1986.
- [Yablonovitch88] E. Yablonovitch, T. J. Gmitter, and R. Bhat. *Inhibited and enhanced spontaneous emission from optically thin algaas/gaas double heterostructures*. Phys. Rev. Lett. **61**, 2546–2549, 1988.
- [Yamamoto86] Y. Yamamoto and H. A. Haus. *Preparation, measurement and information capacity of optical quantum states*. Rev. Mod. Phys. **58**, 1001–1020, 1986.
- [Yasui06] T. Yasui, Y. Kabetani, E. Saneyoshi, S. Yokoyama, and T. Araki. *Terahertz frequency comb by multifrequency-heterodyning photoconductive detection for high-accuracy, high-resolution terahertz spectroscopy*. Applied Physics Letters **88**, 24, 241104, 2006.

- [Yoshie04] T. Yoshie, A. Scherer, J. Hendrickson, G. Khitrova, H. M. Gibbs, G. Rupper, C. Ell, O. B. Shchekin, and D. G. Deppe. *Vacuum rabi splitting with a single quantum dot in a photonic crystal nanocavity*. Nature **432**, 200–203, 2004.
- [Yoshihara17a] F. Yoshihara, T. Fuse, S. Ashhab, K. Kakuyanagi, S. Saito, and K. Semba. *Characteristic spectra of circuit quantum electrodynamics systems from the ultrastrong- to the deep-strong-coupling regime*. Phys. Rev. A **95**, 053824, 2017.
- [Yoshihara17b] F. Yoshihara, T. Fuse, S. Ashhab, K. Kakuyanagi, S. Saito, and K. Semba. *Superconducting qubit-oscillator circuit beyond the ultrastrong-coupling regime*. Nature Phys. **13**, 44–47, 2017.
- [You11] J. Q. You and F. Nori. *Atomic physics and quantum optics using superconducting circuits*. Nature **474**, 589–597, 2011.
- [Yuen75] H. Yuen. *Generalized coherent states and the statistics of two-photon lasers*. Physics Letters A **51**, 1, 1–2, 1975.
- [Yurke84] B. Yurke and J. S. Denker. *Quantum network theory*. Phys. Rev. A **29**, 1419–1437, 1984.
- [Yurke88] B. Yurke, P. G. Kaminsky, R. E. Miller, E. A. Whittaker, A. D. Smith, A. H. Silver, and R. W. Simon. *Observation of 4.2-k equilibrium-noise squeezing via a josephson-parametric amplifier*. Phys. Rev. Lett. **60**, 764–767, 1988.